



THÈSE

En vue de l'obtention du

DOCTORAT DE L'UNIVERSITÉ DE TOULOUSE

Délivré par *l'Université Toulouse III - Paul Sabatier*

Discipline ou spécialité : *Chimie Moléculaire*

Présentée et soutenue par *Thanh-Tuan BUI*

Le 21 Juillet 2010

Titre :

Synthèse et étude de complexes neutres de nickel bisdithiolènes pour application photovoltaïque organique

JURY

Mme B. Martin-Vaca, Professeur à l'Université Paul Sabatier de Toulouse

M M. Fourmigué, Directeur de Recherche au CNRS à Rennes

Mme C. Dagron-Lartigau, Maître de Conférence à l'Université de Pau

M E. Grelet, Chargé de Recherche au CNRS à Bordeaux

M P. Sutra, Maître de conférence à l'Université Paul Sabatier

Mme K. Moineau-Chane Ching, Directrice de Recherche au CNRS à Toulouse

Mme B. Garreau-de Bonneval, Maître de Conférence à l'Université Paul Sabatier

Présidente du Jury

Rapporteur

Rapporteur

Examineur

Examineur

Directrice de Thèse

Membre invitée

Ecole doctorale : *Sciences de la matière*

Unité de recherche : *Laboratoire de Chimie de Coordination du CNRS à Toulouse*

Directeur(s) de Thèse : *Mme K. Moineau-Chane Ching & Mme B. Garreau-de Bonneval*

Rapporteurs : *M M. Fourmigué & Mme C. Dagron-Lartigau*

Remerciements

Ce travail a été réalisé et soutenu publiquement le 21 Juillet 2010 au Laboratoire de Chimie et de Coordination du CNRS à Toulouse devant le jury composé de :

- ✚ Madame Blanca Martin-Vaca, Professeur à l'Université Paul Sabatier de Toulouse, Présidente du Jury
- ✚ Madame Christine Dagrón-Lartigau, Maître de conférences à l'Université de Pau et des Pays de l'Adour, Rapporteur
- ✚ Monsieur Marc Fourmigué, Directeur de Recherche au CNRS à Rennes, Rapporteur
- ✚ Monsieur Eric Grelet, Chargé de Recherche au CNRS à Bordeaux, Examineur
- ✚ Monsieur Pierre Sutra, Maître de Conférences à l'Université Paul Sabatier de Toulouse, Examineur
- ✚ Kathleen Moineau-Chane Ching, Directrice de Recherche au CNRS à Toulouse, directrice de thèse
- ✚ Bénédicte Garreau-de Bonneval, Maître de Conférences à l'Université Paul Sabatier de Toulouse, co-directrice de thèse.

Je tiens vivement à remercier tous les membres du jury pour avoir accepté de juger mon travail. Pendant mes trois années au sein de l'Équipe B " Molécules et Matériaux " du LCC, j'ai eu beaucoup de souvenirs. Je voudrais adresser mes remerciements à la direction du LCC et, spécialement à Lydie Valade, la responsable de l'équipe B pour m'avoir accueilli pour ce travail de thèse.

Je remercie chaleureusement tous les membres de l'équipe : les séniors, les jeunes, les « moins jeunes », les permanents, les non permanents, les chefs. J'adresse un grand merci à tous pour votre gentillesse : Lydie, Jean-Pierre, Isabelle, Dominique, Bénédicte, Kathleen, Christophe (le surveillant des jeunes), Minh Ha, Ju, Kane (le responsable de la propreté des matériels), Joe, Matthieu, Benoît et tous les stagiaires de l'équipe. C'est avec un grand plaisir que j'ai vécu mes trois années avec vous. Vous allez me manquer.

Mon travail a été réalisé sous la codirection de Kathleen Moineau-Chane Ching et Bénédicte Garreau-de Bonneval. Je vous remercie profondément pour m'avoir suivi et m'avoir encadré tout au long de ce travail avec beaucoup de patience et de bonne humeur. Je vous remercie également pour m'avoir permis de participer à une dizaine de congrès scientifiques nationaux et internationaux. Mais vous ne m'avez pas limité à la frontière de l'Hexagone et vous m'avez permis de réaliser deux stages, un en Pologne et un au Japon où je n'ai pas seulement découvert la chimie polonaise et japonaise mais également d'autres cultures et une autre cuisine. Je profite de cette occasion pour remercier les professeurs J. Ulanski (Lodz) et K. Hashimoto (Tokyo) pour m'avoir accueilli dans leurs laboratoires.

Pendant ce travail, j'ai reçu beaucoup d'aide des services scientifiques du LCC, en particulier du service d'électrochimie, je les en remercie.

Ce travail ne pourrait pas être fait sans les supports financiers. Je remercie dans un premier temps l'Agence Nationale de la Recherche d'avoir financé le Projet CPA FALOIR dont ma thèse fait partie. L'Université Paul Sabatier est remerciée pour la bourse ATUPS qui a permis mon séjour de stage en Pologne. Je remercie également le professeur K. Hashimoto qui a financé partiellement mon séjour au Japon.

Je remercie toute ma grande famille qui est très loin de moi mais leur soutien est permanent et vital.

Thanh-Tuan Bui

Phu Tho – Vietnam, le 22 août 2010

Sommaire

1. Organic photovoltaics, columnar liquid crystals and discotic nickel bisdithiolene complexes: an overview	5
1.1. Introduction générale et objectifs de thèse	6
1.2. Les cellules photovoltaïques organiques	11
1.2.1. L'énergie solaire	11
1.2.2. Histoire des cellules photovoltaïques	11
1.2.3. Les cellules solaires organiques	12
1.3. Cristaux liquides colonnaires.....	21
1.3.1. Introduction aux cristaux liquides	21
1.3.2. Cristaux liquides colonnaires	22
1.4. Neutral nickel bisdithiolene complexes	31
1.4.1. Introduction.....	31
1.4.2. Synthesis of discotic nickel bisdithiolenes.....	31
1.4.3. Properties and Optoelectronic applications.....	34
2. Design and synthesis of new discotic nickel bisdithiolene complexes	41
2.1. Design of new discotic nickel bisdithiolene complexes	42
2.1.1. Bibliographical survey	42
2.1.2. The design of new discotic nickel bisdithiolene complexes	47
2.2. Synthesis of new nickel bisdithiolene complexes.....	51
2.2.1. Synthesis of precursors of dithiolene ligands	51
2.2.2. Synthesis of nickel bisdithiolene complexes	61
3. Physical properties and electronic applications	69
3.1. Physical properties of new neutral [Ni(dpdt) ₂] derivatives.....	70
3.1.1. Electrochemical properties	70
3.1.2. Optical properties	84
3.1.3. Comparisation of electrochemical and optical data.....	90
3.1.4. Thermal stability.....	90
3.1.5. Liquid crystalline properties	91
3.1.6. Octalkoxy-substituted [Ni(dpdt) ₂] mixtures	104
3.2. Preliminary applications of discotic nickel bisdithiolene complexes in electronic devices.....	110
3.2.1. Zone-Casting studies	110
3.2.2. Organic field-effect transistor application.....	119
4. General conclusion and perspectives	122
4.1. General conclusion.....	123
4.1.1. Synthesis of new complexes.....	123
4.1.2. Characterization of the synthesized complexes	125
4.1.3. Device application	126
4.2. Perspectives.....	126
5. Experimental section and References	130
5.1. Experimental section.....	131
5.1.1. General remarks.....	131
5.1.2. Material Synthesis	133
5.2. References	160

1. Organic photovoltaics, columnar liquid crystals and discotic nickel bisdithiolene complexes: an overview

1.1. Introduction générale et objectifs de thèse

Ce travail de recherche a porté sur la conception, la synthèse et la caractérisation de nouveaux matériaux moléculaires conçus pour une utilisation dans des cellules photovoltaïques organiques. Il faisait partie du projet « Cellules Photovoltaïques Auto-structurées à Forte Absorption aux Longueurs d'Onde Infra Rouges » (CPA FALLOIR) dans le cadre du Programme Solaire Photovoltaïque de l'Agence Nationale de la Recherche (ANR). Il a été réalisé dans l'équipe « Molécules et Matériaux » (Responsable de l'équipe : Madame Lydie Valade, Directrice de Recherche au CNRS) du Laboratoire de Chimie de Coordination du Centre National de la Recherche Scientifique (LCC-CNRS UPR 8241) à Toulouse. Ce travail a été codirigé par Madame Kathleen I. Moineau-Chane Ching, Directrice de Recherche au CNRS, et Madame Bénédicte Garreau-de Bonneval, Maître de Conférences à l'Université Paul Sabatier de Toulouse. Le projet CPA FALLOIR s'inscrit dans le cadre des recherches entreprises par la communauté scientifique française pour relever les défis énergétiques majeurs de notre temps, et préserver notre environnement des menaces graves qui pèsent sur lui. Les scénarii énergétiques prévoient en effet une augmentation de 50 à 300% de la consommation mondiale d'énergie d'ici à 2050. Un tel besoin ne pouvant être satisfait par les énergies fossiles, l'humanité doit s'orienter vers des sources d'énergie "propres" et renouvelables parmi lesquelles se situe l'énergie solaire.^[1-3]

Les cellules photovoltaïques commerciales qui permettent de convertir directement le rayonnement solaire en énergie électrique sont aujourd'hui essentiellement constituées de semi-conducteurs inorganiques à base de silicium. L'utilisation de ce matériau entraîne un coût de production très élevé, notamment à cause des différents processus de purification nécessaires pour la fabrication du silicium de grade solaire. Ceci réduit considérablement la compétitivité de ces cellules par rapport aux sources d'énergie traditionnelles pour les applications terrestres. Les recherches aujourd'hui s'orientent vers la conception de cellules photovoltaïques à base de matériaux inorganiques autres que le silicium (arséniure de gallium, diséléniure de cuivre indium, ou nanomatériaux de TiO_2 par exemple) ou encore de matériaux organiques. Les derniers sont des polymères ou des petites molécules. Les semi-conducteurs organiques, faciles à mettre en œuvre et avec un coût de production potentiellement plus bas, constituent une opportunité pour la fabrication de cellules photovoltaïques compétitives.^[4, 5] Les cellules photovoltaïques organiques représentent un enjeu technologique majeur car elles offrent des performances complémentaires à celles des cellules à base de silicium et autres inorganiques, par exemple :

- Leur flexibilité potentielle : leur souplesse mécanique peut permettre leur incorporation dans des structures pliables (comme voiles, vêtements et revêtements), leur variabilité en forme peut permettre leur emplacement sur des supports non plans (formes architecturales variées, carrosseries de véhicules) et l'adaptabilité à des formes de production variées (fabrication sur rouleau plastique en continu, dépôt depuis une solution – par exemple par jet d'encre).
- Le caractère modulable de leur spectre d'absorption qui peut être par exemple centré sur l'infrarouge pour permettre ainsi leur incorporation dans des éléments transparents ou semi-transparentes (fenêtres, pare-brises).

Les enjeux scientifiques portent en particulier sur les rendements de conversion énergétique encore faibles, et sur les durées de vie de ces dispositifs organiques (les meilleures performances rapportées aujourd'hui concernant des rendements énergétiques autour de 8% et des durées de vie inférieures à 5000 h). Ils sont intimement liés aux défis de structuration et d'absorption qui se posent à l'intérieur des couches organiques car :

- *Structuration* : les cellules organiques sont en général des dispositifs à jonction $p-n$ entre un matériau donneur d'électrons (matériau de type p) et un matériau accepteur d'électrons (matériau de type n) (Figure 1).^[6] Le champ électrique intrinsèque présent à cette interface permet de dissocier les excitons en charges libres. Les matériaux organiques sont en général utilisés sous forme amorphe ou microcristalline, les mobilités des excitons et des charges y sont tellement faibles que la désexcitation des excitons et le piégeage des charges deviennent des processus dominants. Pour minimiser le chemin entre le lieu de la création de l'exciton par absorption et l'interface $p-n$, une des stratégies adoptées est de développer des structures interdigitées plutôt qu'une surface plane (Figure 1). On tente d'obtenir une jonction dont la surface est maximale par interpénétration des deux matériaux donneur et accepteur. Les mélanges polymère-fullerène sont les plus utilisés dans ce type de structure mais sont souvent sujets à des problèmes de ségrégation, ce qui conduit à des mélanges peu percolants donnant lieu à des rendements photovoltaïques plus bas que prévus. Une autre stratégie consiste à former des structures bicouches d'épaisseur très mince, de sorte que la distance à parcourir par l'exciton entre le lieu de sa création et l'interface donneur-accepteur soit inférieure à sa longueur de diffusion. Cette condition peut être atteinte par l'utilisation de cristaux liquides colonnaires (Figure 1).

➤ *Absorption* : le spectre d'absorption du silicium, qui couvre essentiellement le domaine visible et l'infrarouge jusqu'à 1150 nm, est bien adapté à des cellules solaires de bon rendement. Une cellule organique performante doit donc absorber une plage similaire de longueurs d'ondes. Toutefois, les matériaux moléculaires à petite bande interdite, absorbant dans le domaine proche infrarouge du spectre solaire, sont très souvent photo-chimiquement et électro-chimiquement instables (pentacènes et autres acènes supérieurs, phthalo- et naphthalocyanines), ou bien leurs coefficients d'extinction sont très faibles (fullerènes, nanotubes de carbone). L'utilisation de matériaux thermiquement et chimiquement stables et absorbant dans le domaine proche infrarouge du spectre solaire peut surmonter ce handicap. Dans ce contexte, les complexes neutres de métaux bisdithiolenes sont des candidats prometteurs.

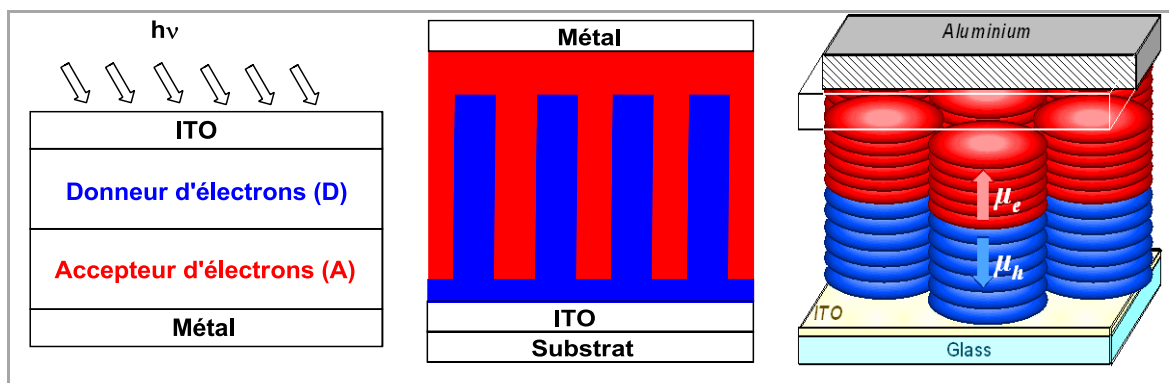


Figure 1. Présentation schématique d'une cellule photovoltaïque bicouche (à gauche), structure interdigitée (au centre) et bicouche à base de matériaux cristaux liquides colonnaires (à droite)

L'objectif du projet CPA FALLOIR est de lever les deux verrous principaux identifiés dans l'approche technologique vers des cellules organiques performantes : 1) la faible organisation des couches organiques, donnant lieu à une mauvaise propagation de charges et d'états excités dans ces couches, et 2) leur faible absorption dans le domaine du proche infrarouge (800 à 1200 nm) du spectre solaire, conduisant à une faible conversion de photons en états excités moléculaires (excitons). Pour atteindre cet objectif, nous utiliserons d'une part une structuration contrôlée de couches optoélectroniques organiques en tentant de maîtriser l'auto-organisation des matériaux en films minces, et d'autre part l'incorporation dans de tels films d'une classe de matériaux particulièrement absorbants dans l'infrarouge et connus pour leur bonne propriété de conduction. Ainsi ce projet est conçu pour ouvrir la voie vers des cellules organiques présentant des rendements énergétiques élevés (comparés aux performances actuelles).

Une classe de matériaux qui laisse espérer des très bonnes performances en matière de transport de charges et d'excitons sans nécessiter une cristallisation macroscopique parfaite concerne les analogues organométalliques du tétrathiafulvalène, notamment les complexes neutres métaux bis-dithiolènes, qui sont connus pour leurs interactions intermoléculaires exceptionnellement fortes qui donnent lieu à de la supraconductivité à basses températures (Figure 2).^[7]

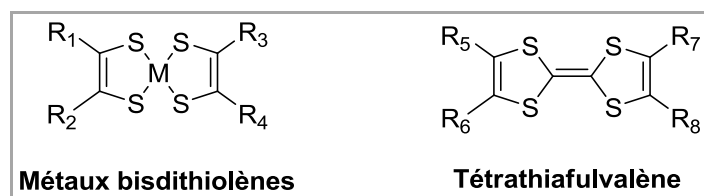


Figure 2. Structures générales des complexes métaux bisdithiolènes et du tétrathiafulvalène

Ce mémoire de thèse décrit la synthèse et la caractérisation de nouveaux matériaux moléculaires accepteurs basés sur les complexes neutres métaux bisdithiolènes dont la finalité est de combiner plusieurs propriétés : stabilité en température et à l'air, capacité à s'auto-organiser en cristaux liquides colonnaires, absorption forte dans le domaine proche infrarouge. Le choix s'est porté sur des complexes de nickel bisdithiolènes avec des ligands de type 1,2-diphényl-1,2-éthylènedithiolène (dpedt) (Figure 3).

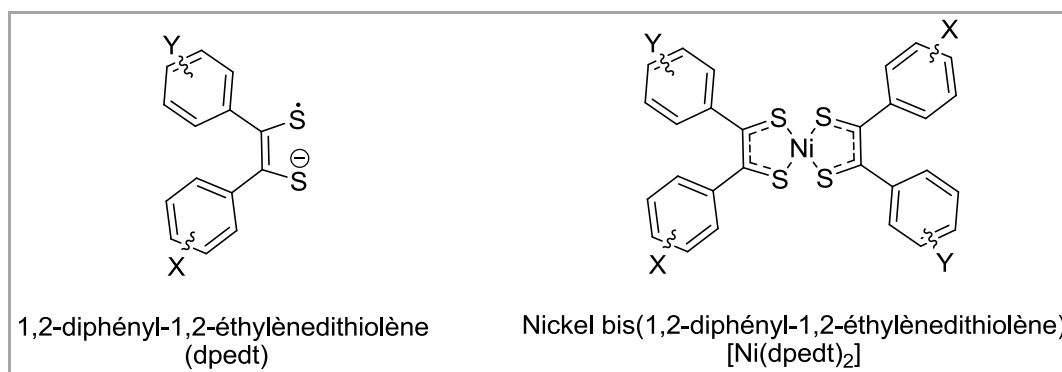


Figure 3. Structures des ligands diphényléthylènedithiolènes et des complexes de nickel correspondants

Le mémoire de thèse est organisé en cinq parties :

- i.** La première est une introduction générale aux cellules solaires organiques, matériaux cristaux liquides colonnaires et complexes discotiques neutres de nickel bisdithiolenes et leurs applications.^[8]
- ii.** La deuxième est consacrée à la conception et aux synthèses de nouveaux complexes discotiques neutres de nickel bisdithiolènes. Nous avons réalisé plusieurs modifications sur les chaînes alkyles latérales et les cycles benzéniques des ligands 1,2-diphénylène-1,2-dithiolène (dpedt).^[9]
- iii.** La troisième est consacrée aux caractérisations des propriétés physiques de nouveaux composés synthétisés et à leurs applications préliminaires dans des dispositifs organiques. Les propriétés physico-chimiques et thermiques ont été étudiées par différentes techniques : analyse thermique différentielle et thermogravimétrie, microscopie optique en lumière polarisée, voltammétrie cyclique et voltammétrie à vague carrée, spectrométrie d'absorption, diffraction des rayons-X sur poudre, zone-casting.
- iv.** La quatrième partie présente la conclusion générale et les perspectives de ce travail au niveau de la synthèse, de la caractérisation et des futures applications et collaborations scientifiques envisagées.
- v.** Ce manuscrit présente en dernière partie les sections expérimentales et références bibliographiques

1.2. Les cellules photovoltaïques organiques

1.2.1. L'énergie solaire

Le Soleil, une immense sphère de gaz de 1,4 millions de kilomètres de diamètre et une masse de 2×10^{27} tonnes, se compose principalement d'hydrogène (78%), d'hélium (28%) et 2% d'autres atomes différents. Dans le centre du soleil, une sphère de 250 000 km de rayon, la matière est comprimée au point de parvenir à une température de 15 millions de degrés. Les atomes d'hydrogène entrent en collision et fusionnent pour former de l'hélium. Au cours de cette réaction thermonucléaire, une partie de la masse du soleil est transformée en énergie sous forme de photons et de neutrinos. Chaque seconde, le soleil consomme 700 millions de tonnes d'hydrogène dans sa réaction de fusion nucléaire et il produit une énorme quantité d'énergie égale à 386 milliards de milliards de mégawatts ($3,86 \times 10^{26}$ W).^[10] Sous la forme de rayonnement électromagnétique, une partie de cette énergie atteint la surface de la terre. Chaque jour, notre planète reçoit une quantité d'énergie 15 000 fois plus élevée que le besoin de toute l'humanité.^[11] Comme les autres sources d'énergie renouvelables, l'énergie solaire est gratuite et disponible partout sur la Terre.

1.2.2. Histoire des cellules photovoltaïques

La cellule photovoltaïque est un dispositif qui permet de produire l'électricité à partir de l'énergie solaire. L'effet photovoltaïque,^[12] qui transforme directement l'énergie solaire en électricité, a été découvert par Becquerel en 1839.^[13] Après cette importante découverte, il a fallu plus de trente ans pour découvrir la photoconductivité du sélénium sous illumination^[14] et en 1877, la première photopile de rendement de conversion de 1% a été décrite.^[15] En 1905, A. Einstein donnait l'explication de la nature physique de ce phénomène : l'extraction de charge électrique de la matière sous l'effet lumineux et l'effet photoélectrique. Par la suite, l'effet photovoltaïque a été observé avec plusieurs autres matériaux tels que l'anthracène, le premier matériau organique photoconducteur.^[16, 17]

En 1953, les chercheurs de « Bell Laboratories » ont découvert au travers de leurs études sur les transistors au silicium,^[18] que ce matériau présentait de nouveaux intérêts pour les cellules solaires. Après un an de recherche et développement, ils ont préparé les premières cellules solaires

capables de produire des quantités utiles de puissance.^[19] Le rendement de conversion était d'environ 6% (60 watts par mètre carré). Cet événement a fait la première page du magazine New York Times. En effet, les travaux de trois chercheurs Chapin, Fuller et Pearson étaient présentés comme suit : "may mark the beginning of a new era, leading eventually to the realization of one of mankind's most cherished dreams—the harnessing of the almost limitless energy of the sun for the uses of civilization."^[18] Toutefois, la commercialisation de cellules photovoltaïques pour la vie quotidienne a échoué en raison de leur coût prohibitif. À cette époque, les cellules solaires au silicium ont attiré l'attention du Pentagone. En 1955, le gouvernement américain a annoncé son projet de lancer un satellite spécial : son prototype comportait des cellules solaires au silicium pour ses centrales électriques. Jusque là, les satellites étaient équipés de piles, dont la puissance décroissante dans le temps rendait les coûts excessifs. En avril 1958, le satellite Vanguard-1 fut le premier équipé de cellules solaires, source d'électricité autonome et fiable à long terme, preuve de leur valeur exceptionnelle. Aujourd'hui, la technologie la plus répandue dans le domaine du photovoltaïque utilise le silicium comme matériau actif. Les cellules produites industriellement donnent des rendements de conversion de 15% en moyenne (11-12% pour les modules).^[20] En laboratoire, les meilleurs prototypes atteignent environ 25% de rendement avec du silicium monocristallin.^[20] Toutefois, la purification du silicium et l'utilisation de produits hautement toxiques constituent aujourd'hui un obstacle majeur au développement de l'énergie photovoltaïque.^[10]

1.2.3. Les cellules solaires organiques

Le secteur photovoltaïque organique remonte à 1959 lorsque Kallmann et Pope ont découvert que l'anthracène pouvait être utilisé pour fabriquer une cellule solaire.^[21] Leur appareil produisit une photo-tension de seulement 0,2 V avec un rendement très faible. En 1978, Merritt avait prévu que l'efficacité du dispositif solaire organique pourrait dépasser 1%.^[22] Mais cet objectif n'a été atteint qu'en 1986, lorsque Tang a décrit les premières cellules solaires organiques bicouches avec un rendement de conversion de 0,95% à base des petites molécules (phthalocyanine de cuivre, donneur d'électrons, et un dérivé de pérylène tétracarboxylique, accepteur d'électrons).^[23] Cependant, la recherche dans ce domaine ne s'est intensifiée qu'au début du vingt et unième siècle. En 2001, les cellules solaires organiques à base de phthalocyanine de cuivre et fullerène ont été décrites avec une efficacité de conversion de 3,6%.^[24] Trois ans plus tard, les rendements ont atteint 4,2%.^[25] En 2007, un rendement 6,5% a été revendiqué lors de la fabrication de cellules solaires tandem à base de polymères (2 cellules en tandem).^[26] En 2009, des chercheurs américains ont signalé des rendements approchant 7% (Yang *et al.*,^[27] Heeger *et al.*^[28]). À l'heure

actuelle (Mai 2010), les meilleurs rendements sont de l'ordre de 8%. Solarmer Energy Inc a communiqué un rendement de 7,9 % pour les cellules à base de polymères avec une surface de 0,1 cm² fabriquée par la technique d'impression. Récemment, Heliatek a annoncé le rendement de 7,7 % pour les cellules de grande surface (1,1 cm²) à base des petites molécules déposées par évaporation sous vide. Cependant, la stabilité de ces dispositifs n'a pas encore été étudiée.

Du point de vue industriel, afin d'atteindre une proportion raisonnable entre le coût et la performance d'une cellule solaire, de nouvelles technologies basées sur des matériaux organiques semi-conducteurs sont maintenant étudiées et développées.^[4, 5] Ces matériaux organiques présentent de nombreux avantages tels que la production à faible coût, la fabrication de grande surface et une facilité de dépôt par des techniques d'impression.^[29] En outre, ce secteur pourrait conduire à l'élaboration de cellules sur des substrats flexibles ouvrant ainsi la voie pour de nouvelles applications. Un facteur important qui limite le développement de tels dispositifs est la stabilité des matières organiques. D'autre part, le rendement de conversion de dispositifs solaires organiques est encore faible. L'ingénierie moléculaire de matériaux organiques et des procédés de fabrication devraient fournir de nouveaux dispositifs plus performants tout en maintenant la stabilité des cellules solaires. Un avantage important des matières organiques est leur grande adaptabilité en fonction de leur composition chimique.

Différentes technologies de cellules solaires organiques font actuellement l'objet de développement intensif :

- ✓ Les cellules solaires à base de colorant (les cellules Grätzel^[30, 31]) : ces dispositifs contiennent un matériau absorbant la lumière (dit colorant^[32-36]), un oxyde métallique nanostructuré permettant le transport d'électrons (en général TiO₂^[37-39] ou ZnO^[40, 41]), et un électrolyte assurant le transport des charges positives.
- ✓ Les cellules solaires hybrides : elles sont constituées de composites organiques-inorganiques. Les nanocristaux de séléniure de cadmium (CdSe) ou tellure de cadmium (CdTe), par exemple, sont dispersés dans une matrice organique. Elles combinent les avantages des semi-conducteurs organiques et inorganiques.^[42-46] Les cellules hybrides contiennent des matériaux organiques semi-conducteurs π -conjugués absorbant la lumière et qui jouent le rôle de donneur d'électrons et transporteur de trous. Les matériaux inorganiques dans la cellule hybride sont utilisés comme accepteur d'électrons et comme transporteur de charges négatives. Les dispositifs hybrides photovoltaïques ont un potentiel important puisqu'ils peuvent être mis en forme par un procédé dit « roll-to-roll » à faible coût.

- ✓ Les cellules solaires organiques : elles sont composées de deux semi-conducteurs organiques, soit des matériaux polymères^[47] soit des matériaux moléculaires^[48, 49] qui constituent la couche photo-active.

Dans ce travail, nous nous intéressons à la conception et au développement de nouveaux matériaux moléculaires constitués de petites molécules organisées en structure bicouche comme représentée ci-dessous (Figure 4). Généralement, une cellule solaire organique bicouche est composée de deux couches très fines de matériaux organiques déposées en sandwich entre deux électrodes, une anode transparente et une cathode métallique sur l'autre côté.

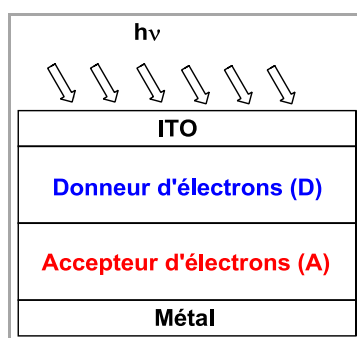


Figure 4. Architecture générale d'une cellule solaire organique bicouche

Quelques exemples de matériaux utilisés dans des cellules photovoltaïques organiques sont présentés dans la Figure 5.

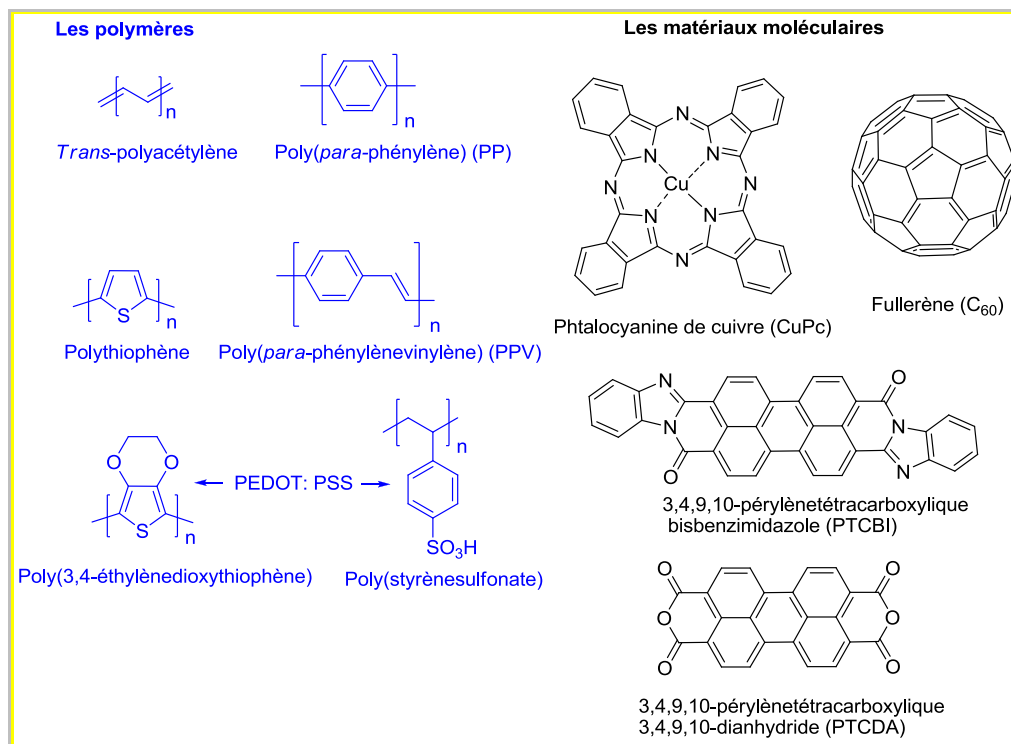


Figure 5. Exemples de matériaux utilisés dans les cellules photovoltaïques organiques

En général, une cellule solaire transforme la lumière du soleil en électricité à travers cinq grandes étapes.

◆ **Étape 1 : absorption de la lumière**

La première étape du processus est l'absorption de lumière dans un solide. Elle se traduit par l'apport d'énergie aux électrons du niveau de l'orbitale HOMO du matériau.

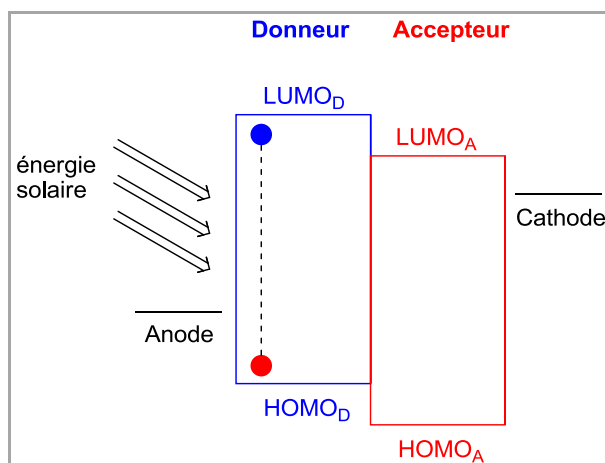


Figure 6. Absorption de la lumière et création d'excitons

Si cette énergie est suffisante, elle permet de faire passer un électron de l'orbitale HOMO vers l'orbitale LUMO. Cette transition vers le niveau de l'orbitale LUMO entraîne l'apparition d'un trou au niveau de l'orbitale HOMO et qui est lié à l'électron par l'interaction électrostatique. Ce couple « électron-trou », électroniquement neutre, est appelée « exciton ». L'exciton peut être formé dans la couche du donneur (D) ou de l'accepteur (A). La Figure 6 présente le cas d'un exciton formé dans le matériau donneur. Cette étape est affectée par les propriétés de surface macroscopique et elle est directement déterminée par la structure de bande du matériau. L'énergie minimale requise est égale à la différence entre les énergies des niveaux des orbitales LUMO et HOMO du matériau (Figure 6). Il y a deux types d'exciton classés en fonction de leurs énergies de liaison. Si les deux charges (electron et trou) sont localisées sur la même molécule ou sur la même unité monomère, l'énergie de liaison est grande et l'exciton est appelé exciton de Frenkel. Dans ce cas, la distance entre l'électron et le trou est typiquement de quelques angströms. Ce type d'exciton est le plus souvent rencontré dans les matériaux organiques. Au contraire, si la distance entre deux charges correspond à plusieurs unités monomères (quelques dizaines d'angströms), leur énergie de liaison est faible et l'exciton est appelé exciton de Wannier. Dans les semiconducteurs inorganiques, la valeur de l'énergie de liaison de l'exciton est faible (par exemple : 14,7 meV pour le silicium) et l'énergie thermique à température ambiante est suffisante pour séparer les deux charges. Dans le cas des semiconducteurs organiques, cette énergie est de

l'ordre de plusieurs centaines de meV et il en résulte une difficulté à dissocier des charges à température ambiante. Dans ce cas, la présence d'un champ électrique local est requise pour surpasser l'attraction coulombienne. En général, la durée de vie des excitons est de l'ordre de quelques nanosecondes (par exemple : 22 ns pour le tris(8-hydroxyquinoline) d'aluminium^[50]). Si la dissociation n'a pas lieu, l'électron rejoint le niveau de l'orbitale HOMO en cédant son énergie de manière radiative (photoluminescence) ou non-radiative sous forme de chaleur.

◆ Etape 2 : diffusion des excitons

Après leur création dans les couches actives, les excitons peuvent diffuser à travers le solide sur une distance appelée la « longueur de diffusion » (L_D , Figure 7). Cette distance, plus ou moins grande, dépend de la nature du matériau. Par exemple, la longueur de diffusion des fils quantiques d'arséniure de gallium peut atteindre 4 μm .^[51]

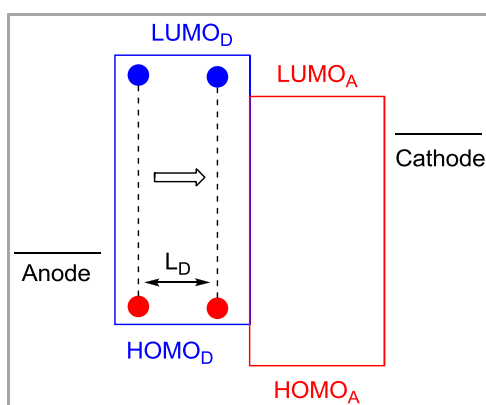


Figure 7. Diffusion des excitons à l'interface donneur-accepteur

Ces distances sont beaucoup plus courtes dans les semiconducteurs organiques, de l'ordre de 10 nm pour les polymères π -conjugués et de 12 nm pour le tris(8-hydroxyquinoline) d'aluminium.^[52] En particulier, une longueur de diffusion de 225 nm a été mesurée pour la molécule discotique dérivée de pérylène tétracarboxilic dianhydride (Figure 5) régulièrement organisée en colonnes.^[53]

◆ Etape 3 : séparation des charges

Pour que la séparation des charges puisse avoir lieu, les excitons doivent rejoindre un site où le champ électrique est suffisamment élevé. Dans un dispositif utilisant deux matériaux de type donneur et accepteur, les excitons doivent être formés dans la zone dit « zone active », située au niveau de la jonction donneur-accepteur. Les excitons générés au-delà de la distance L_D se recombinent avant d'arriver à l'interface donneur-accepteur. A l'interface donneur-accepteur,

l'exciton subit une réaction de dissociation, formant un trou et un électron respectivement dans la couche du donneur et de l'accepteur (Figure 8).

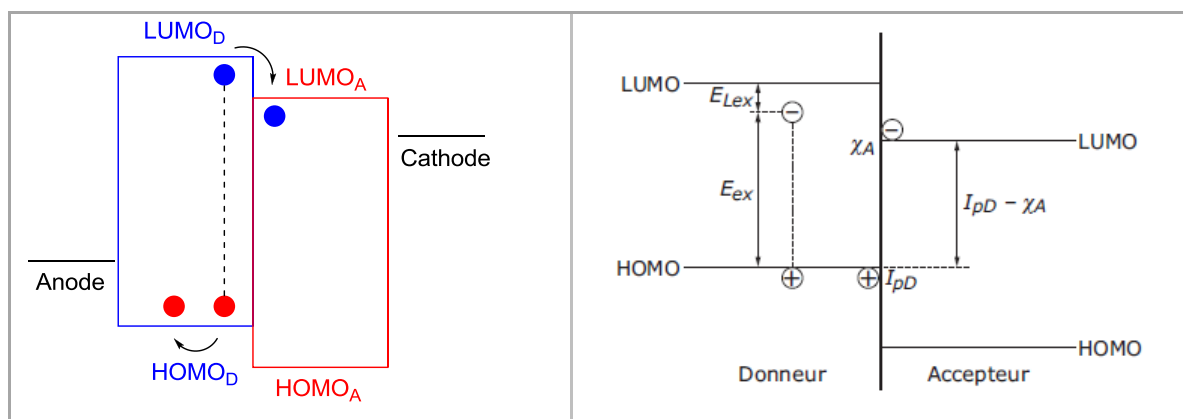


Figure 8. Transfert de charge à l'interface donneur-accepteur (gauche) et conditions de dissociation des excitons : $E_{ex} > I_{pD} - \chi_A$ ^[10]

La force motrice de cette dissociation est la différence d'énergie entre les orbitales moléculaires du donneur et de l'accepteur. La Figure 8 présente également les conditions de dissociation des excitons à partir du diagramme énergétique des matériaux utilisés dans des cellules solaires organiques. La Figure 8 présente le cas où l'exciton est créé dans le matériau donneur. Cet exciton a une énergie E_{ex} inférieure à la différence entre les orbitales LUMO et HOMO du donneur d'une valeur égale à l'énergie de liaison de l'exciton $E_{L_{ex}}$ (Figure 8) : $E_{ex} = E_{L_{LUMO}} - E_{H_{HOMO}} - E_{L_{ex}}$. Après la dissociation, l'électron passe dans l'accepteur tandis que le trou reste dans le donneur (Figure 8). L'énergie de l'ensemble [électron + trou] dissocié est égale à la différence entre les niveaux énergétiques de chaque charge, c'est-à-dire $I_{pD} - \chi_A$ (Figure 8). Pour que la dissociation puisse avoir lieu, ce processus ne doit pas consommer d'énergie, donc E_{ex} doit être supérieure à $I_{pD} - \chi_A$.^[54] Un raisonnement analogue montre que la même condition prévaut pour les excitons générés dans la couche du matériau accepteur. Pour une dissociation efficace, il est donc indispensable de contrôler les niveaux énergétiques des matériaux. Cela peut être réalisé, dans certaines limites, par l'ingénierie de structures moléculaires.

◆ Etape 4 : transport des charges

Une fois générés, les trous et les électrons sont transportés par les matériaux donneur (trous) et accepteur (électrons) vers les électrodes (Figure 9). Pour que ce transport des charges soit aisé, les matériaux organiques dans le dispositif doivent posséder des mobilités de trous (μ_h) et d'électrons (μ_e) les plus grandes possibles. Ces valeurs (par exemple, pour tris(8-hydroxyquinolinolato) aluminum^[55] : $\mu_e = 1,4 \times 10^{-6} \text{ cm}^2 \text{V}^{-1} \text{s}^{-1}$ et $\mu_h = 2 \times 10^{-8} \text{ cm}^2 \text{V}^{-1} \text{s}^{-1}$ mesurée par le technique temps de

vol) dépendent fortement de la méthode de mesure utilisée et sont de plusieurs ordres de grandeur au-dessous de celles qui caractérisent des matériaux inorganiques (par exemple, pour le silicium monocristallin: $\mu_e = 1500 \text{ cm}^2\text{V}^{-1}\text{s}^{-1}$, $\mu_h = 450 \text{ cm}^2\text{V}^{-1}\text{s}^{-1}$).

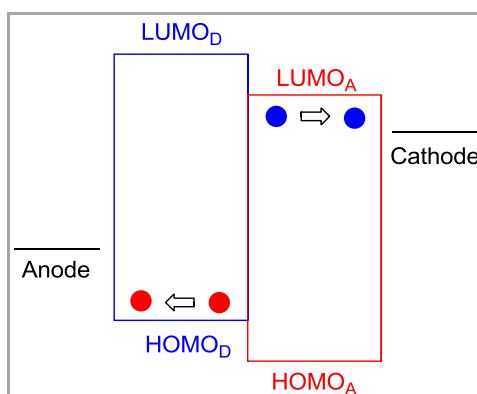


Figure 9. Transport de charge dans les couches actives

Pour les valeurs les plus grandes, on peut citer celles exceptionnelles du pentacène monocristallin ($\mu_h = 35 \text{ cm}^2\text{V}^{-1}\text{s}^{-1}$ à température ambiante et $\mu_h = 58 \text{ cm}^2\text{V}^{-1}\text{s}^{-1}$ à 225K),^[56] des dérivés d'acène,^[57, 58] des oligomères,^[59-61] et des molécules discotiques organisées en réseau colonnaire.^[62] De manière générale, le transport des charges électriques est amélioré lorsque l'ordre moléculaire augmente (il dépend fortement des conditions de dépôt), mais également par la purification des matériaux.^[56] Une grande mobilité des porteurs de charge est essentielle pour une cellule solaire organique efficace. Une faible mobilité (haute résistance) laissera les charges piégées près de l'interface donneur-accepteur et augmentera la recombinaison électron-trou à l'interface. Cela conduira à la diminution du photo-courant et une diminution marquée dans le facteur de forme, contribuant ainsi à diminuer la puissance disponible pour le dispositif.

◆ Etape 5 : collection des charges

Une fois que les charges atteignent les électrodes, elles sont extraites et transférées vers le circuit extérieur, l'électron est transféré à la cathode et le trou à l'anode (Figure 10).

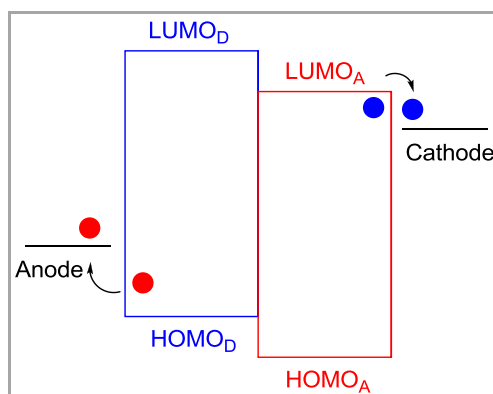


Figure 10. Collection des charges aux électrodes

L'anode est généralement un oxyde semi-conducteur transparent (ITO), qui permet à la lumière de pénétrer dans les couches organiques, tandis que la cathode est généralement une couche métallique (aluminium par exemple) déposée par vaporisation.^[63] L'interface organique-électrode doit présenter un bon contact ohmique pour assurer un transfert de charge efficace.^[63]

Stratégies générales pour améliorer les performances des cellules photovoltaïques organiques

Optimisation du spectre d'absorption des cellules : un des paramètres cruciaux pour optimiser les performances des cellules est l'augmentation de l'absorption des photons pour augmenter le photo-courant. Ceci peut être obtenu :

- En augmentant l'épaisseur de la couche active ; cette solution est cependant limitée par la mobilité réduite des porteurs de charge et leur de temps de vie court.
- En étendant la gamme spectrale d'absorption des matériaux et donc en diminuant leurs gaps entre les niveaux des orbitales HOMO et LUMO.

Pourquoi étendons-nous les réponses spectrales des cellules vers le proche infrarouge ? L'absorption d'une couche active d'une cellule photovoltaïque, à base de P3HT et de PCBM, absorbe dans la zone UV-visible jusqu'à environ 650 nm. Dans ce cas, seulement 22,4 % des photons peuvent être absorbés et transformés en électricité.^[64] Cependant, le spectre solaire (Figure 11) est maximal autour de 700 nm et s'étend jusqu'au proche infrarouge. Une amélioration des performances est espérée par l'ingénierie et l'utilisation de matériaux qui absorbent jusqu'au proche infrarouge.

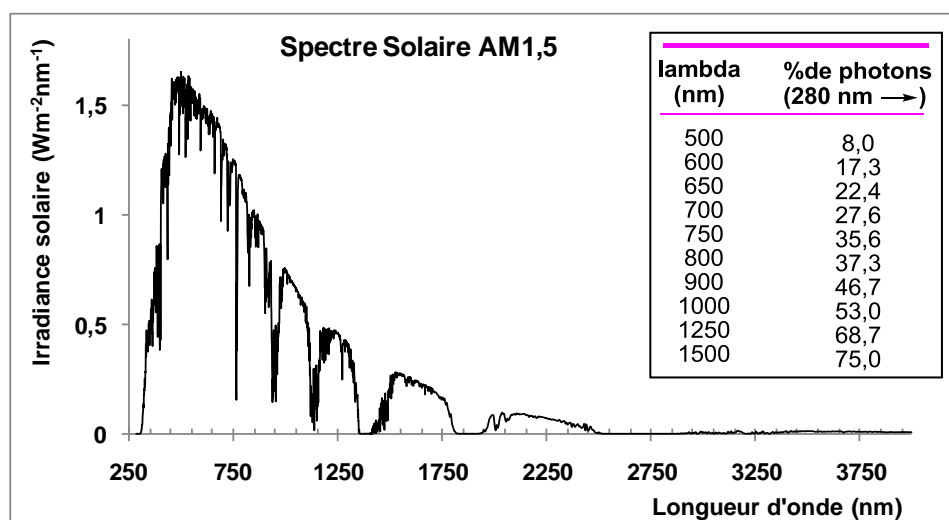


Figure 11. Spectre solaire et intégration du nombre de photons disponibles pour une cellule absorbant de 280 nm à la longueur citée dans le tableau

Actuellement, les recherches en nouveaux matériaux sont consacrées principalement au développement de molécules et de polymères donneurs d'électrons permettant d'étendre l'exploitation du rayonnement solaire au-delà de 650 nm et jusqu'au proche infrarouge,^[64-67] mais sont restées trop restreintes en ce qui concerne les accepteurs d'électrons. A ce jour, très peu de publications se consacrent à de tels matériaux, la dernière en date concerne des composés tout organique dérivés du 9,9'-bifluorenylidene menant à des efficacités de l'ordre de 2%.^[68] C'est dans ce contexte que s'inscrit ce travail qui est dédié à la synthèse de nouveaux matériaux accepteurs de type nickel bisdithiolènes capables d'absorber la lumière dans le domaine du proche infrarouge (de 700 à 1000 nm) et compatibles avec les matériaux donneurs les plus performants. Les complexes neutres de métal bisdithiolènes^[7] qui sont thermiquement stables et stables à l'air sont des candidats prometteurs.

Optimisation de la diffusion des excitons et du transport de charges : une fois les excitons créés sur chacun des matériaux, ils doivent migrer au maximum vers l'interface de donneur-accepteur où ils se dissocient pour créer des charges. Ensuite, les charges doivent être transportées et extraites à chacune des électrodes. Pour cela il faut que chacun des matériaux ait une bonne mobilité des charges positives pour l'un et négatives pour l'autre. Dans cet esprit, les matériaux moléculaires de type cristaux liquides colonnaires sont des candidats très intéressants.^[69-71] Par exemple, la valeur de la mobilité de $2,8 \text{ cm}^2\text{V}^{-1}\text{s}^{-1}$ a été mesurée pour un complexe cristallin liquide colonnaire de nickel bisdithiolènes.^[72] En utilisant des matériaux cristaux liquides colonnaires, les cellules organiques à haute performance peuvent être formées.^[73]

L'objectif de ce travail est donc la conception et la synthèse de nouveaux matériaux moléculaires cristaux liquides colonnaires à base de complexes neutres de nickel bisdithiolènes qui absorbent fortement dans le proche infrarouge.

Dans les paragraphes suivants, les introductions générales concernant les matériaux cristallins liquides colonnaires ainsi que les complexes neutres de nickel bis(1,2-diphényl-1,2-éthylènedithiolène) sont abordées et discutées.

1.3. Cristaux liquides colonnaires

1.3.1. Introduction aux cristaux liquides

Les cristaux liquides sont un état de la matière qui possède des propriétés intermédiaires entre celles d'un liquide isotrope conventionnel et celles d'un cristal solide.^[74-76] Par exemple, un cristal liquide peut couler comme un liquide, mais ses molécules peuvent être orientées comme dans un cristal conventionnel. Historiquement, l'étude des cristaux liquides a commencé en 1888 lorsque F. Reinitzer a observé que le benzoate de cholestérol avait deux points de fusion distincts.^[77] En raison de ces premiers travaux, F. Reinitzer est souvent cité comme le découvreur d'une nouvelle phase de la matière : la phase cristal liquide. La caractéristique distincte de l'état cristal liquide est la tendance des molécules à pointer le long d'un axe commun, appelé la direction. Ceci est contraire à des molécules en phase liquide, qui n'ont pas d'ordre intrinsèque. Dans l'état solide, les molécules sont très ordonnées et ont peu de liberté de translation. L'ordre d'orientation caractéristique de l'état cristal liquide est entre les phases solides et liquides traditionnelles, ce qui est à l'origine du terme « état mésogène », utilisé comme synonyme de cristal liquide. L'alignement moyen des molécules de chaque phase est présenté dans le diagramme suivant (Figure 12).

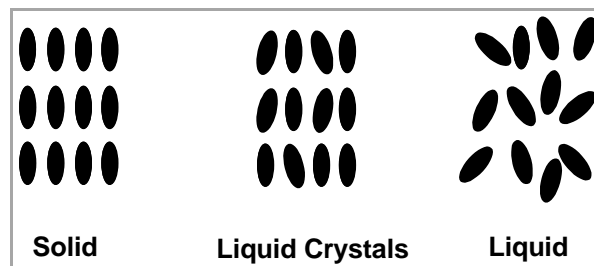


Figure 12. Présentation générale des phases solide, liquide et liquide cristallin

Il est parfois difficile de déterminer si un matériau est sous la forme d'un cristal ou d'un état mésogène. Les matériaux mésogènes sont divisés en deux catégories, les *thermotropes* et les *lyotropes*. Quand une substance passe entre le solide, le mésogène et l'état liquide et *vice versa* en fonction de la température et en l'absence de solvant, les phases mésogènes sont classées comme thermotropes, tandis que les phases lyotropes se forment en présence d'un solvant approprié. Ainsi les mésophases lyotropes se trouvent en abondance dans les systèmes biologiques et sont toujours des mélanges, alors que cristaux liquides thermotropes peuvent être constitués d'un seul composant ou d'un mélange de nombreux composés.

Les états mésogènes thermotropes sont généralement classés par la forme moléculaire des molécules constituantes. La majorité des composés purs montrant des mésophases thermotropes ont une particularité commune: les molécules ont une forme de bâtonnet. Le terme calamitique a été utilisé pour décrire les phases mésogènes des molécules en forme de bâtonnet afin de les distinguer des mésophases composées de molécules discotiques.^[69-71, 78-82] Récemment, les mésophases de molécules sous forme «banane» ont été ajoutés à la famille des cristaux liquides.^[83]

1.3.2. Cristaux liquides colonnaires

La première phase cristalline liquide discotique a été découverte en 1977 par S. Chandrasekhar *et al.*^[84] Cette mésophase est caractérisée par des colonnes empilées de molécules de type benzène-hexa-*n*-alcanoate, l'une au-dessus de l'autre. Les colonnes sont alignées pour former les réseaux cristallins à deux dimensions. L'arrangement des molécules dans les colonnes et la disposition des colonnes elles-mêmes conduit à de nouvelles mésophases.

La majorité des phases cristallines liquides colonnaires est formée grâce à l'interaction intermoléculaire de type π - π de noyaux polyaromatiques.^[71] La distance entre deux noyaux aromatiques voisins dans la même colonne est généralement de l'ordre de 3,5 Å pour qu'il y ait un recouvrement suffisant des orbitales π (Figure 13).

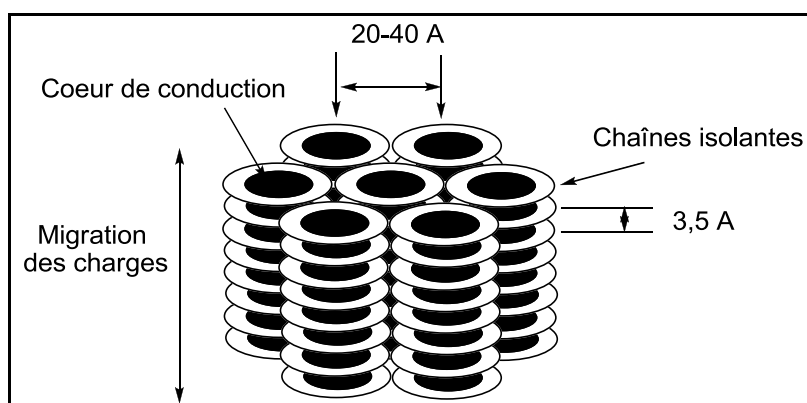


Figure 13. Vue schématique de la migration de charge dans la phase colonnaire

La distance intercolonnaire est généralement de 20 à 40 Å en fonction de la longueur des chaînes aliphatiques latérales greffées sur le noyau. Par conséquent, les interactions intracolonnaires entre deux molécules voisines seraient beaucoup plus fortes que les interactions intercolonnaires entre les colonnes voisines. En conséquence, la conduction des charges dans ces matières devrait être quasi-monodimensionnelle.^[85] la conductivité le long des colonnes dans les mésophases

colonnaires est de plusieurs ordres de grandeur plus grande que dans la direction perpendiculaire. Ainsi, les colonnes peuvent être décrites comme des fils moléculaires (Figure 13). Par exemple, dans le complexe bis[octakis(alkylthio)phthalocyaninato]lutetium(III) la mobilité des porteurs de charges le long des colonnes est élevée ($0,71 \text{ cm}^2\text{V}^{-1}\text{s}^{-1}$).^[86]

1.3.2.1. Les différentes mésophases discotiques

Bien que la plupart des molécules discotiques se présentent sous un seul type de mésophase, des exemples de composés polymorphes sont également connus. Les mésophases formées par des molécules discotiques sont principalement divisées en deux types : *nématique* et *colonnaire*.^[71]

1.3.2.1.1. Les phases nématiques

Les phases nématiques de molécules discotiques (Figure 14)^[79] peuvent être subdivisées en trois types : discotique, colonnaire et chirale.

Dans la phase nématique discotique, les molécules restent plus ou moins parallèles, ayant un ordre orientationnel mais aucun ordre positionnel à longue distance. La phase nématique chirale est rencontrée dans le cas de mélanges des molécules nématiques discotiques avec des composés chiraux (mésomorphes ou non) dopants, ainsi qu'avec des molécules discotiques chirales pures.^[87] Si une molécule chirale est incorporée en concentration appropriée dans une phase nématique, la structure devient hélicoïdale (Figure 14).

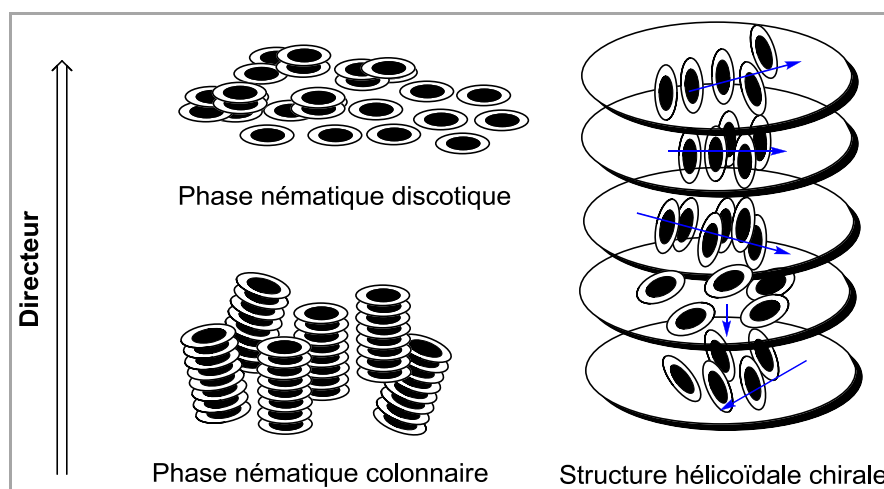


Figure 14. Représentation schématique des phases nématiques : discotique, colonnaire, et structure hélicoïdale chirale

La phase nématique colonnaire, quant à elle, est caractérisée par l'empilement des molécules l'une au dessus de l'autre pour former des colonnes (Figure 14). Toutefois, ces colonnes ne forment pas de structures à deux dimensions. Les molécules affichent un ordre positionnel à courte distance et un ordre orientationnel à longue distance.

1.3.2.1.2. Les phases colonnaires

En mésophases colonnaires, les molécules s'assemblent les unes sur les autres dans les colonnes et sont arrangées parallèlement dans un réseau à deux dimensions. Les molécules peuvent être organisées de manière régulière, ordonnée ou désordonnée. En fonction de l'ordre de l'empilement moléculaire dans les colonnes et de la symétrie du réseau à deux dimensions, les phases colonnaires peuvent être classées en six sous-classes (Figure 15): rectangulaire, oblique, hexagonale, plastique, hélicoïdale et lamellaire.

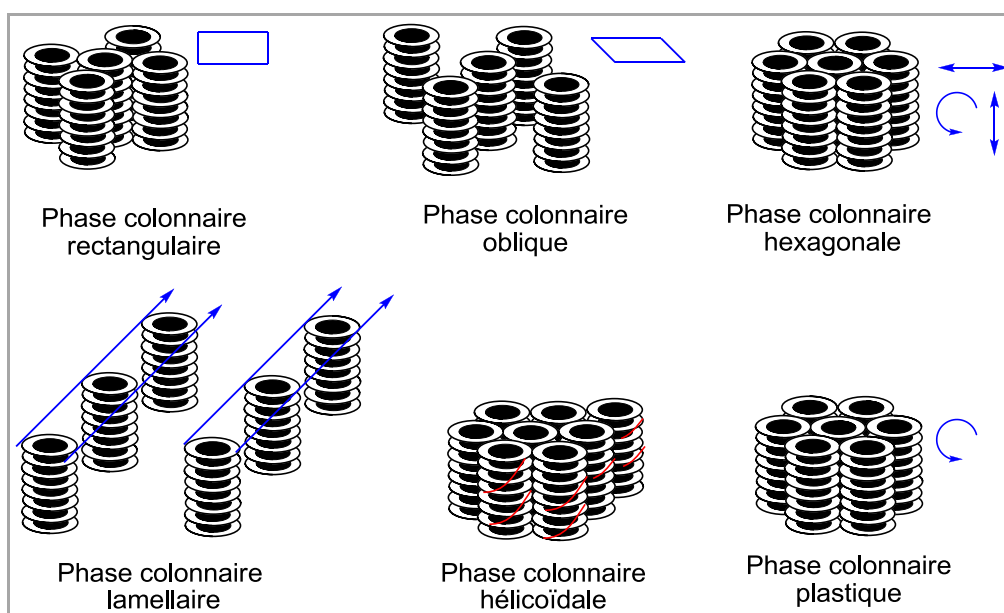


Figure 15. Représentation schématique des phases colonnaires : rectangulaire, oblique, hexagonale, plastique, hélicoïdale et lamellaire.

Dans la mésophase colonnaire rectangulaire (Col_r), les cœurs aromatiques s'empilent les uns sur les autres et sont entourés par les chaînes aliphatiques désordonnées. Les colonnes sont placées dans un réseau bidimensionnel rectangulaire. Dans la phase colonnaire oblique (Col_{ob}), les colonnes sont positionnées dans un réseau bidimensionnel oblique. La phase colonnaire hexagonale (Col_h) est caractérisée par un arrangement hexagonal des colonnes moléculaires. Certains désordres structuraux (disposition non parallèle des disques moléculaires, déplacements longitudinaux et latéraux des disques, rotation autour de l'axe de la colonne) peuvent se produire.

La phase colonnaire plastique (Col_p)^[88] se caractérise par un réseau hexagonal dans lequel les molécules discotiques formant les colonnes sont libres de tourner autour de l'axe de la colonne. La liberté de mouvement des disques dans la phase Col_p est limitée. Une mésophase hélicoïdale exceptionnelle a été mise en évidence avec le composé hexahexylthiotriphenylene.^[89] Dans cette phase, dite phase H, les colonnes hélicoïdales se développent et s'interdigitent en groupes de trois colonnes. Cette phase est illustrée dans la Figure 15. La Figure 15 présente enfin la phase discotique lamellaire (Col_l) où les colonnes s'empilent en couches. Cette dernière phase est trouvée dans les cas de métallomésogènes (par exemple : les complexes de nickel bisdithiolenes).^[90, 91]

Parmi toutes ces phases discotiques, les phases colonnaires hexagonales, plastiques et hélicoïdales sont les plus intéressantes pour des applications dans des dispositifs électroniques organiques, puisqu'elles favorisent le transport des charges électriques le long des colonnes. Dans la suite, nous nous intéressons à la structure moléculaire et au transport des charges dans ces systèmes.

1.3.2.2. Les structures chimiques du cristaux liquides discotiques

Les molécules discotiques sont généralement constituées de noyaux aromatiques plats et rigides entourés par des chaînes latérales flexibles (Figure 16).

Ces molécules ont souvent la symétrie de rotation de type C_2 , C_3 , C_4 ou C_6 avec trois ou plusieurs chaînes périphériques. Les chaînes flexibles sont reliées au noyau aromatique par l'intermédiaire d'un groupe connecteur tels que éther, ester, benzoate, alcyne. Quelques exemples de noyaux aromatiques pour les molécules discotiques sont représentés dans la Figure 16.

Du point de vue de la conception moléculaire, les stratégies pour imaginer des molécules cristaux liquides discotiques sont assez simples. Différents paramètres de conception moléculaire des mésophases discotiques tels que la taille du coeur conjugué ou du groupe connecteur, ainsi que différentes méthodologies synthétiques ont été largement décrits.^[69-71, 79-81, 86, 92, 93] La conception de nouvelles molécules discotiques à base de complexes neutres de nickel bisdithiolenes est la base de ce travail de thèse. Dans la suite, nous nous intéressons au transport des charges dans les molécules discotiques pour des applications ciblées en électronique organique.

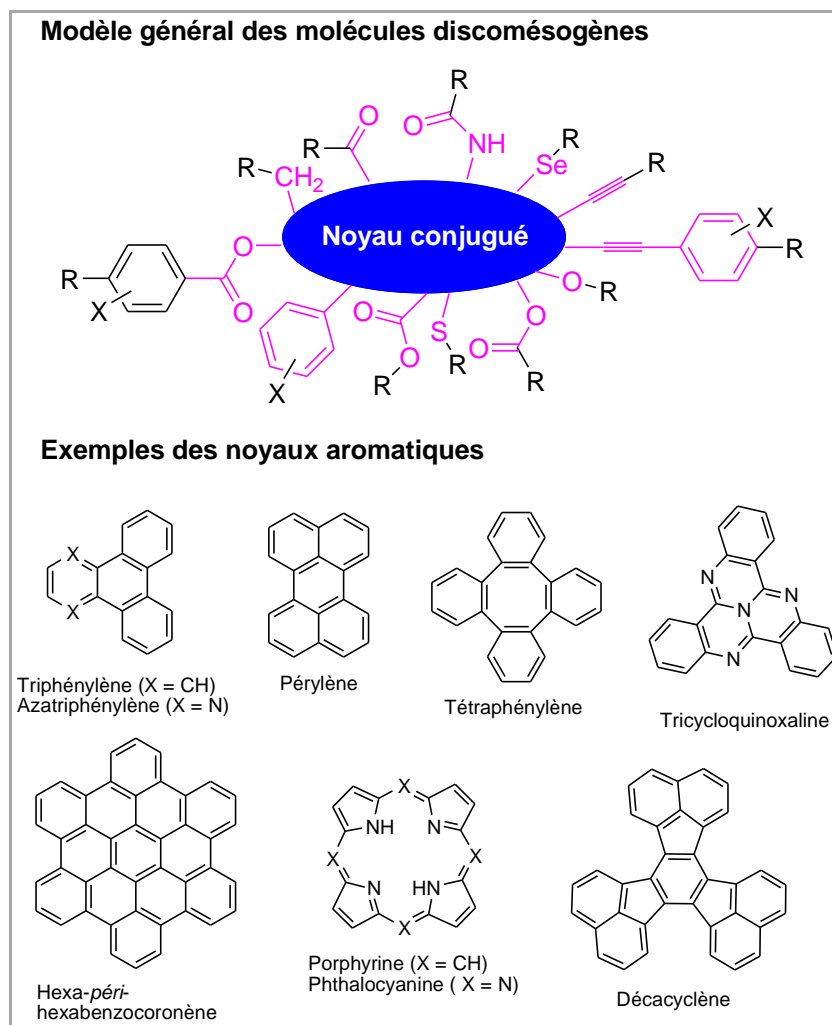


Figure 16. Un modèle général de structure pour les molécules mésogènes discotiques

1.3.2.3. Transport des charges dans les molécules cristallines liquides discotiques colonnaires

Au cours des deux dernières décennies, les matériaux semi-conducteurs organiques ont provoqué un grand intérêt pour des applications en électronique organique (transistors, photovoltaïque, diodes électroluminescentes, capteurs...). En comparaison avec les semiconducteurs inorganiques, les matériaux organiques offrent beaucoup d'avantages tels que la souplesse de l'ingénierie moléculaire par la synthèse organique et la mise en oeuvre facile par les techniques d'impression ou de dépôt à température ambiante. Ces propriétés rendent les matériaux organiques attractifs pour les nouvelles applications technologiques. Cependant, la mobilité des charges dans les matériaux semiconducteurs organiques est en général assez faible, de l'ordre de $10^{-4} \text{ cm}^2 \text{V}^{-1} \text{s}^{-1}$. Pour les échantillons bien alignés, ces valeurs peuvent atteindre de 1 à $5 \text{ cm}^2 \text{V}^{-1} \text{s}^{-1}$, valeurs comparables à celle du silicium amorphe.^[62]

La mobilité des charges n'est pas une propriété intrinsèque du matériau organique. Elle dépend surtout de l'organisation moléculaire dans le film mince. Dans ce contexte, les cristaux liquides discotiques colonnaires offrent des possibilités avantageuses. Les disques moléculaires s'empilent les uns sur les autres en formant des colonnes avec des distances inter-noyaux de l'ordre de 3,5 Å. Un recouvrement des orbitales π^* - π^* LUMOs devient possible, ce qui conduit à la formation d'une bande de conduction permettant de transporter les charges.^[69] De plus, dans ces matériaux, les colonnes entourées par des chaînes alkyles s'organisent dans un système hexagonal. Les chaînes alkyles jouent le rôle d'isolant des colonnes les unes par rapport aux autres. Il a été montré que la durée de vie des porteurs de charge dans les colonnes bien organisées de phtalocyanines et d'hexabenzocoronene augmente avec l'augmentation de la longueur des chaînes latérales alkyles ce qui confirme le rôle isolant des substituants périphériques.^[94] Les phases discotiques colonnaires vont donc se comporter comme des fils de conduction monodimensionnels. Autre point intéressant : lors de la présence d'impuretés, celles-ci sont rejetées à la périphérie des colonnes lors de leur formation et ne viennent pas entraver la mobilité des charges contrairement au cas des matériaux cristallins. La qualité de l'empilement dans la colonne détermine le recouvrement des systèmes π -conjugués de disques aromatiques, et constitue un critère important pour la mobilité des porteurs de charge dans les cristaux liquides.^[62] Une étape de traitement thermique est parfois utilisée pour améliorer la qualité de l'empilement moléculaire. Dans les systèmes parfaitement ordonnés, la rotation des disques est entravée. Cela conduit à une corrélation fixe entre l'orientation des disques selon l'axe de la colonne, par exemple dans les phases hélicoïdales, et à un recouvrement amélioré des orbitales π des disques individuels. En conséquence, la forte mobilité des porteurs de charge devient possible dans des phases colonnaires très ordonnées.

Plusieurs techniques permettent de mesurer la mobilité des charges dans des films semiconducteurs organiques.^[61, 95] La détermination absolue de la mobilité des charges est impossible et la comparaison directe des mobilités mesurées par différentes méthodes est difficile. La principale différence entre les méthodes de mesure de mobilité est la géométrie de l'échantillon analysé. L'épaisseur des films analysés et l'orientation de la direction de mobilité des charges mesurée varient selon la méthode employée.

- i. Les mesures dites « par temps de vol » (TOF) nécessitent de déposer la couche organique en film mince de quelques micromètres entre deux électrodes. Cette technique consiste à mesurer le temps mis par les charges photo-générées à une électrode pour parvenir à

l'autre électrode selon la direction transverse au substrat. Le signal enregistré, le courant en fonction du temps, est fin ou élargi selon que le matériau est ordonné ou non, et permet d'accéder aux valeurs de mobilités des électrons et des trous séparément.

- ii. Dans la même configuration, les mobilités peuvent également être mesurées à partir des caractéristiques de diodes dans lesquels électrons et trous sont injectés à faible tension. En absence de piège à charges et à faible champ électrique, la densité de courant J suit une évolution quadratique de la tension V , caractéristique d'un courant limité par une charge d'espace (SCLC), et est directement proportionnelle à la mobilité des charges.
- iii. Une autre technique consiste à mesurer la mobilité des charges dans un film organique déposé dans un dispositif ayant la configuration d'un transistor à effet de champ (FET). Là encore, le transport est affecté par les défauts structuraux au sein du matériau et aux interfaces. Ici, la mobilité des charges est mesurée dans le plan du substrat.
- iv. Enfin la technique dite « pulse-radiolysis time-resolved microwave conductivity » (PR-TRMC) donne une mesure intrinsèque des mobilités, sans prendre en compte les limitations dues aux impuretés ou défauts structuraux. L'échantillon est excité par une impulsion d'électrons très énergétiques (de l'ordre de MeV) pour créer une faible densité de porteurs de charges libres. La variation de conductivité mesurée au sein du matériau et à très faible échelle (de l'ordre de quelques molécules) permet d'accéder à la mobilité des charges sans pouvoir distinguer s'il s'agit de trous ou d'électrons.

Quelques exemples de molécules cristallines liquides colonnaires sont donnés dans la Figure 17. Leurs valeurs de mobilité des charges sont résumées dans la Tableau 1.

Tableau 1. Exemples de mobilités des charges des molécules cristallines liquides colonnaires

Composés	Mobilités des charges ($\text{cm}^2\text{V}^{-1}\text{s}^{-1}$)		Phases	Technique	Réfs
	Trous (μ_h)	Electrons (μ_e)			
TP1	0,1	8×10^{-2}	H	TOF	[96, 97]
	10^{-2}	$1,4 \times 10^{-3}$	Col _h		
TP2	$2,3 \times 10^{-2}$	$2,5 \times 10^{-2}$	Col _p	TOF	[98]
Pc	0,2	0,3	Col _r	TOF	[99, 100]
	0,1	0,2	Col _h		
HBC	1,13		Col _h	PR-TRMC	[101]
[Ni]		2,8	Col _h	SCLC	[72]
CDI1		3,1	Col _h	SCLC	[102]
CDI2		6,7	Col _h	SCLC	[102]

Une des familles de cristaux liquides colonnaires les plus populaires est celles des dérivés de triphénylène et deux exemples de cette famille sont présentés dans la Figure 17 (**TP1** & **TP2**). Une des premières mesures de mobilité des charges par la technique du temps de vol a été effectuée sur le composé 2,3,6,7,10,11-hexaethylthiotriphénylène (**TP1**). Les valeurs de mobilité des charges de 0,1 (trous) et 0,08 (électrons) $\text{cm}^2\text{V}^{-1}\text{s}^{-1}$ ont été mesurées pour sa phase cristalline liquide colonnaire hélicoïdale.^[96, 97] Dans la phase moins ordonnée (Col_h), ces deux valeurs expérimentales ont diminué significativement (Tableau 1). Les valeurs de mobilité des charges de 2,3,6,7,10,11-hexabutyloxy triphénylène (**TP2**) mesurées par la technique temps de vol pour sa phase colonnaire plastique est du même ordre de grandeur que les valeurs de **TP1** dans sa phase hexagonale (Tableau 1).^[98]

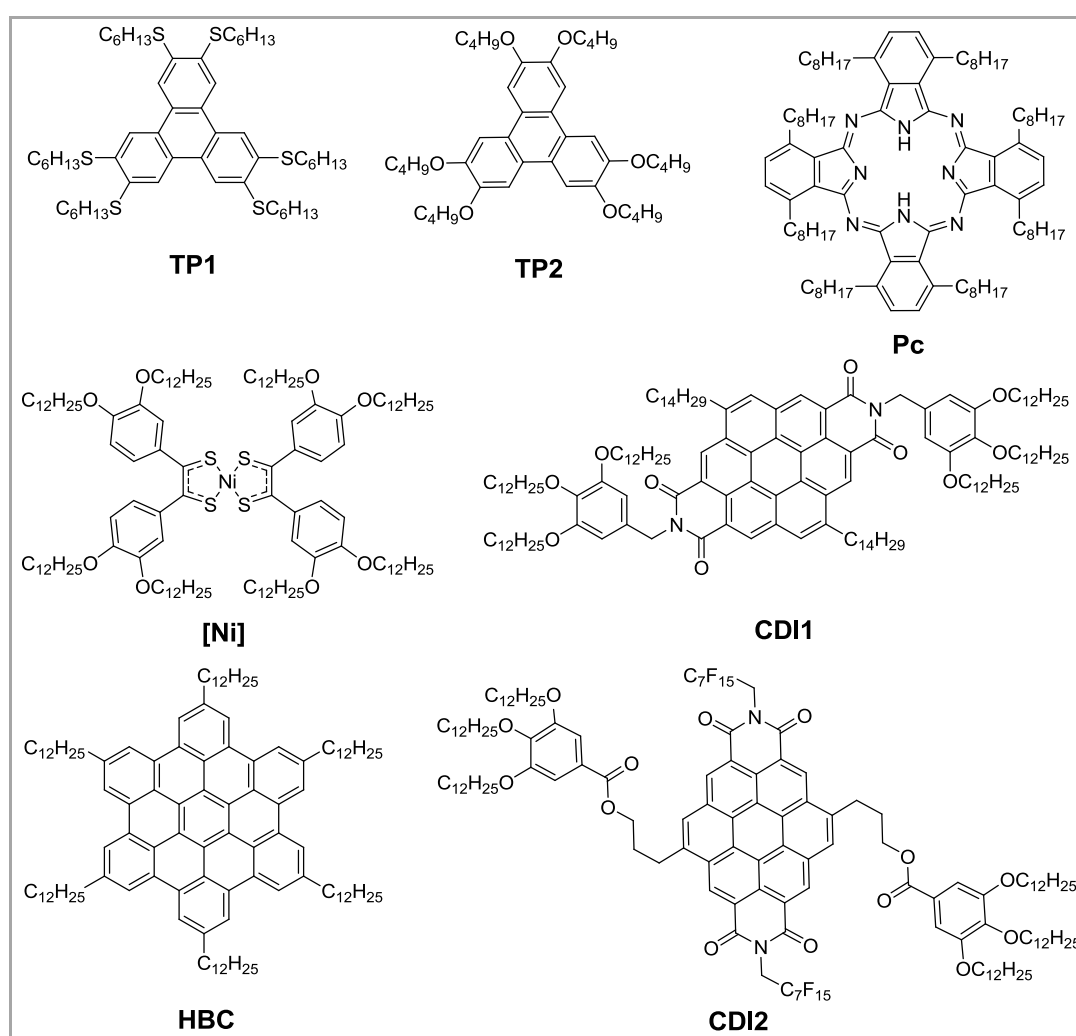


Figure 17. Exemples de cristaux liquides colonnaires

Le squelette phthalocyanine est souvent utilisé pour former des cristaux liquides colonnaires. Un exemple de cette famille, le 1,4,8,11,15,18,22,25-octaethylphthalocyanine (**Pc**, Figure 17), donne des bonnes valeurs de mobilités des charges mesurées pour ses phases cristallines liquides

colonnaires rectangulaires et hexagonales (Tableau 1). La valeur de mobilité des charges supérieure de $1 \text{ cm}^2\text{V}^{-1}\text{s}^{-1}$ a été mesurée pour un cristal liquide discotique hexagonal à base d'hydrocarbure aromatique polycyclique (**HBC**, Figure 17 et Tableau 1).^[101]

Il apparaît clairement que les composés cristallins liquides colonnaires possèdent des propriétés électroniques nécessaires pour leurs applications potentielles dans des dispositifs électroniques organiques. D'autre part, ces propriétés dépendent fortement de leurs structures supramoléculaires et de l'orientation macroscopique des colonnes en superstructures sur les surfaces des substrats. Bien que l'organisation supramoléculaire et l'alignement macroscopique puissent, en général, être contrôlés efficacement par des méthodes de traitement appropriées,^[103, 104] la fabrication de dispositifs électroniques réalistes à base des cristaux liquides discotiques reste un défi majeur.

Prenant en compte les avantages des matériaux cristallins liquides colonnaires par rapport aux matériaux organiques solides conventionnels, des exemples d'utilisation avec succès de ces matériaux dans des dispositifs photovoltaïques organiques sont décrits. Généralement, les rendements de conversion sont encore assez faibles ($< 1\%$).^[105-110] Les meilleurs rendements sont autour de 2% en utilisant une structure bicouche, soit d'un donneur cristallin liquide colonnaire et d'un accepteur solide organique,^[73] soit de deux cristaux liquides colonnaires.^[111] L'utilisation de cristal liquide colonnaire dans des cellules hybrides a donné également un rendement de conversion de 2% .^[112]

Ces quelques exemples des cellules solaires organiques utilisant des semiconducteurs cristallins liquides discotiques n'ont évidemment pas révélé tout leur potentiel. Dans la continuité, nous concentrons nos recherches pour concevoir et synthétiser des nouveaux semiconducteurs organiques cristallins liquides colonnaires performants en vue d'applications photovoltaïques organiques. Ces nouveaux matériaux moléculaires discotiques à base de complexes neutres de nickel bisdithiolènes, qui sont thermiquement stables à l'air et absorbent fortement dans le domaine du proche infrarouge, vont élargir le choix de matériaux accepteurs d'électrons. Dans la suite, nous présentons les propriétés et les caractéristiques de ces complexes de coordination.

1.4. Neutral nickel bisdithiolene complexes

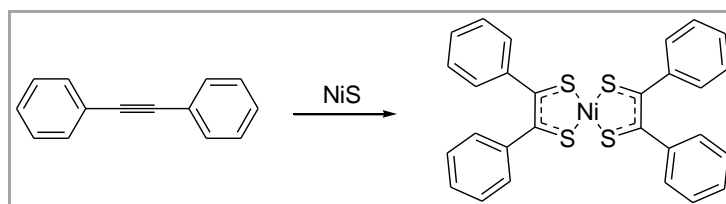
1.4.1. Introduction

Before the 1960s, the metal bisdithiolene complexes were mainly encountered in analysis of metal ions. The bisdithiolene complexes of d^8 transition metals (Ni, Pt, Pd) exhibit square-planar structures and various forms (from dianionic to cationic). Due to their remarkable coordination chemistry, mainly interests in structure, bonding and reactivity were developed until the end of the 1970s. Later on, new interests in these complexes appeared in the field of biology and more importantly in material science. The optical, magnetic, conductive, and superconductive properties evidenced in these complexes have placed them among the most important families of precursors to new generations of optoelectronic devices. There are various synthetic pathways leading to metal bisdithiolene complexes showing many structures aimed at numerous applications and these compounds are reported in many reviews by our group and others.^[7, 8, 113-126] In this section, the discussion is focused on the synthesis, properties and optoelectronic applications of disk-like d^8 metal bisdithiolene complexes: neutral nickel bis(1,2-diphenylethene-1,2-dithiolene) complexes, abbreviated as $[\text{Ni}(\text{dpedt})_2]$.

1.4.2. Synthesis of discotic nickel bisdithiolenes

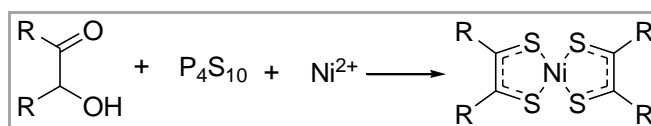
General synthetic strategies leading to bisdithiolene complexes have been well documented in several important reviews^[114, 121, 124, 125, 127] and references cited therein. In this section, we focus on the discussion on the synthesis of disk-like $[\text{Ni}(\text{dpedt})_2]$ derivatives.

Historically, the first neutral $[\text{Ni}(\text{dpedt})_2]$ was prepared in 1962 by Schrauzer and Mayweg.^[128] This coordination complex was obtained by heating nickel sulfide with diphenylacetylene in toluene in a closed tube. The reaction was conducted at 120°C: the toluene solution became dark green within 24 hours and upon cooling, a nearly black, crystalline complex of composition $\text{NiC}_{28}\text{H}_{20}\text{S}_4$ (Scheme 1) crystallized.^[128] However, these severe experiment conditions gave only low yields of complex formation.

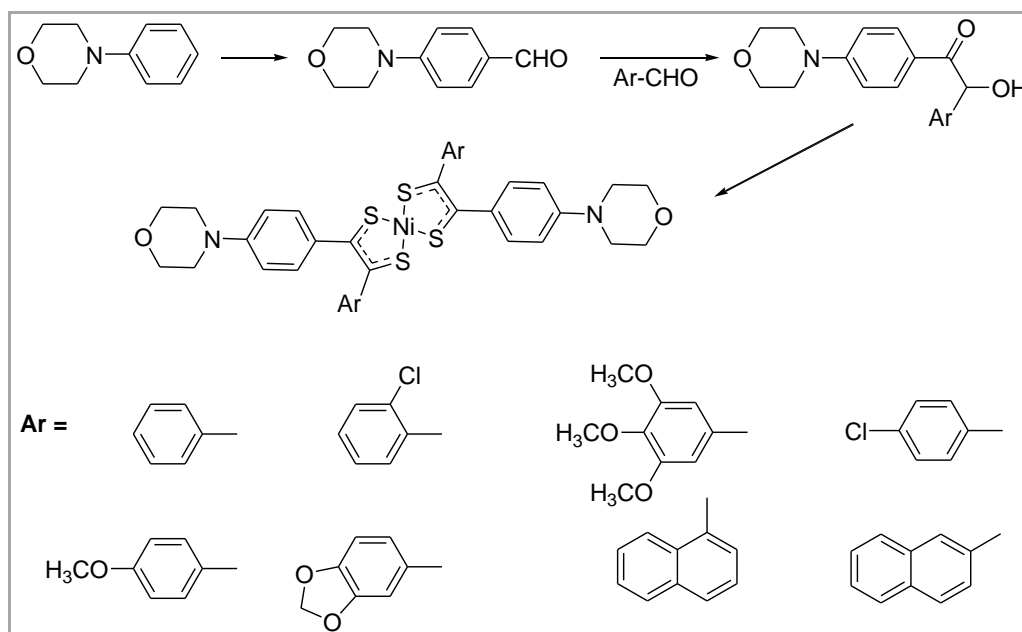


Scheme 1. The Schrauzer's first synthesis of [Ni(dppe)₂]

Later, these authors reported a new synthetic method using benzoin (Scheme 2).^[129-133] They successfully synthesized a large number of neutral metal complexes with diaryl and dialkyl “ α,β -dithioketones”. This method is still widely used nowadays in order to prepare (a)symmetric tetra(hetero)aryl-substituted nickel bis(1,2-dithiolene) complexes.^[134, 135] Scheme 3 illustrates the synthesis of several asymmetric tetraaryl-substituted nickel bisdithiolene complexes reported by Bie *et al.*^[134]



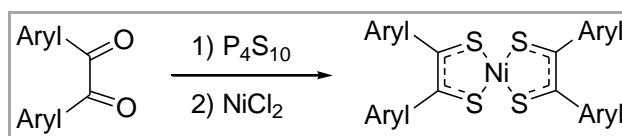
Scheme 2. The Schrauzer's benzoin method



Scheme 3. Synthesis of asymmetric tetraaryl-substituted nickel bisdithiolene complexes

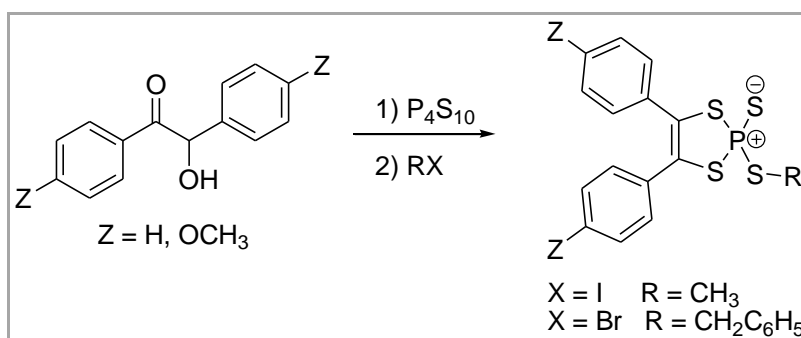
However, the Schrauzer's benzoin method is not appropriate for long-chain substituted complexes, because one cannot obtain long alkyl/alkoxy chain-substituted benzoin by the benzoin condensation, except for dimethyl-, dimethoxy- and tetramethoxy-benzoin. Ohta *et al.*^[91, 136-141] overcame this limitation and succeeded in obtaining several series of alkyl- and alkoxy-

substituted nickel bis(1,2-bisphenylethene-1,2-dithiolene) complexes by using the corresponding benzils as the precursors (Scheme 4).



Scheme 4. The Ohta's benzil method

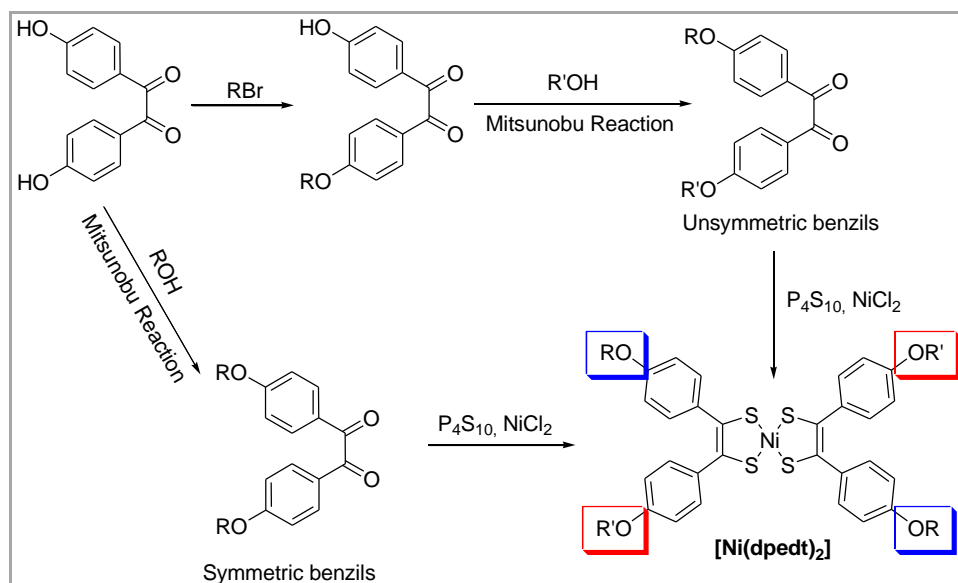
The thionating reaction of the α -diketone (Ohta's method) or α -hydroxyketone (Schrauzer's method) is performed by P_4S_{10} in boiling dioxane leading to thiophosphate ester intermediates.^[129] According to their synthetic pathways, this thiophosphate ester is not isolated but directly hydrolyzed in the reaction medium. The hydrolysis followed by adding nickel salt in air condition gives neutral products $[Ni(dpdt)_2]$ derivatives. Recently, Arumugam *et al.*^[142] demonstrated the preparation and isolation of stable thiophosphate ester consisting in the protected forms of 1,2-dithiolene ligands (Scheme 5).



Scheme 5. Preparations of thiophosphoryl dithiolene compounds

Recently, Im *et al.*^[143] have demonstrated the microwave assisted enhanced synthesis of $[Ni(dpdt)_2]$ derivatives. The yield of complex formation can be also improved by replacing the 1,4-dioxane in the conventional reaction conditions by 1,3-dimethyl-2-imidazolidinone (DMI).^[144] ^[145] As described in a patent,^[145] DMI has low toxicity, is chemically and thermally stable, has a high boiling point of 225°C and can be handled with ease. DMI has a strong dissolving power for both organic and inorganic compounds and is able to convert the reactants to a readily reactable form due to its high dielectric constant and solvation effect. Hence, DMI is efficient for ionic reactions such as the synthesis of $[Ni(dpdt)_2]$. In the DMI solvent method, the intermediate phosphorous compounds are obtained without formation of insoluble by-products, and the next reaction can be successively carried out without filtration. Consequently, this process is very advantageous for industrial process.

Based on Ohta's benzil method, we have recently developed^[9] new synthetic pathways leading to new long chain substituted $[\text{Ni}(\text{dpedt})_2]$ using the Mitsunobu's method.^[146, 147] Part of these syntheses is given in Scheme 6 and the full description of these syntheses can be found in synthesis section (2.2).



Scheme 6. New synthetic pathways developed in our group

The novelty in these syntheses is the use of the Mitsunobu reaction, which is very efficient in mild experimental conditions (ambient temperature) and offer an easy work-up reaction. This allows the conversion of primary and secondary alcohols to esters, phenyl ethers, thioethers and various other compounds with high yields.^[148, 149] Within the present work, we succeeded in synthesizing a large number of 4,4'-dialkoxy benzil derivatives in one step, particularly with branched alkyl chains that are often available as cheap primary or secondary alcohols (Scheme 6).

1.4.3. Properties and Optoelectronic applications

1.4.3.1. Structural properties

The crystal structure of the complex $[\text{Ni}(\text{dpedt})_2]$ has been clearly elucidated by Sartain and Truter.^[150] X-ray crystal structure analysis has been carried out on $[\text{Ni}(\text{dpedt})_2]$ at 115°K. In a monoclinic unit cell with the following parameters $a = 5.836 \text{ \AA}$, $b = 10.97 \text{ \AA}$, $c = 18.36 \text{ \AA}$, $\beta = 91.4^\circ$ organized in the space group $P2_1/n$, there are two molecules: the nickel atoms lie on the centers of symmetry and are coordinated to four sulfur atoms (Figure 18). The crystal structure

of $[\text{Ni}(\text{dpedt})_2]$ is given in Figure 18 and the structure projected on $[100]$ and $[010]$ plans are given in Figure 19 and Figure 20, respectively.

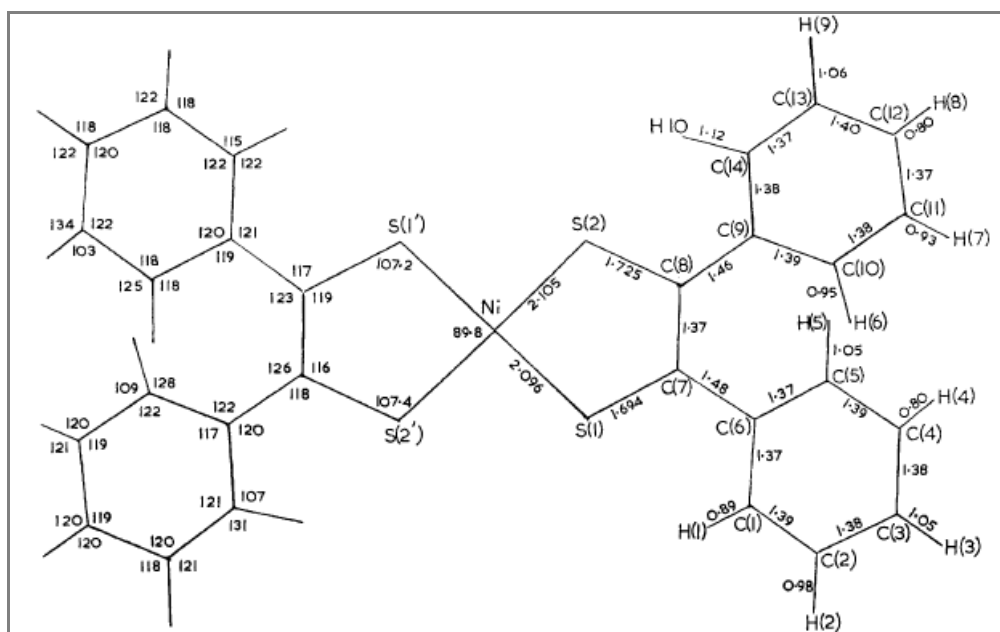


Figure 18. X-ray structure of $[\text{Ni}(\text{dpedt})_2]$ ^[150]

As can be observed in Figure 19 and Figure 20, the intermolecular distance between two neighbouring nickel is about 11 Å. This distance is quite large and there is no π -overlap between two neighbouring complexes.

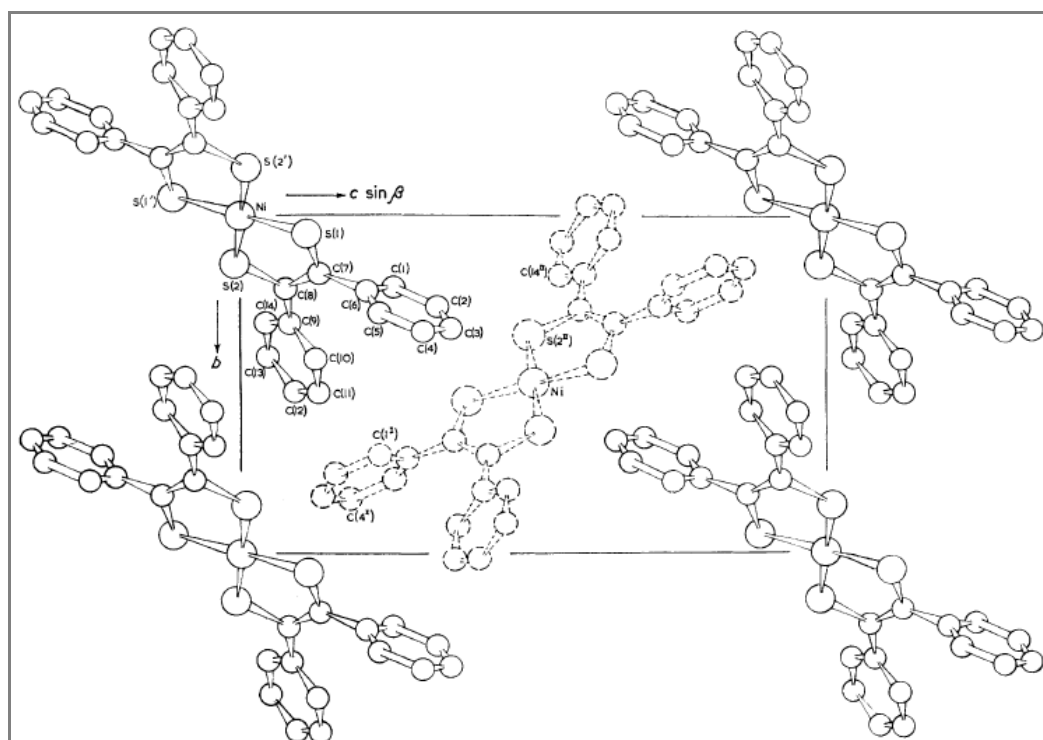


Figure 19. The $[\text{Ni}(\text{dpedt})_2]$ structure projected down $[100]$ ^[150]

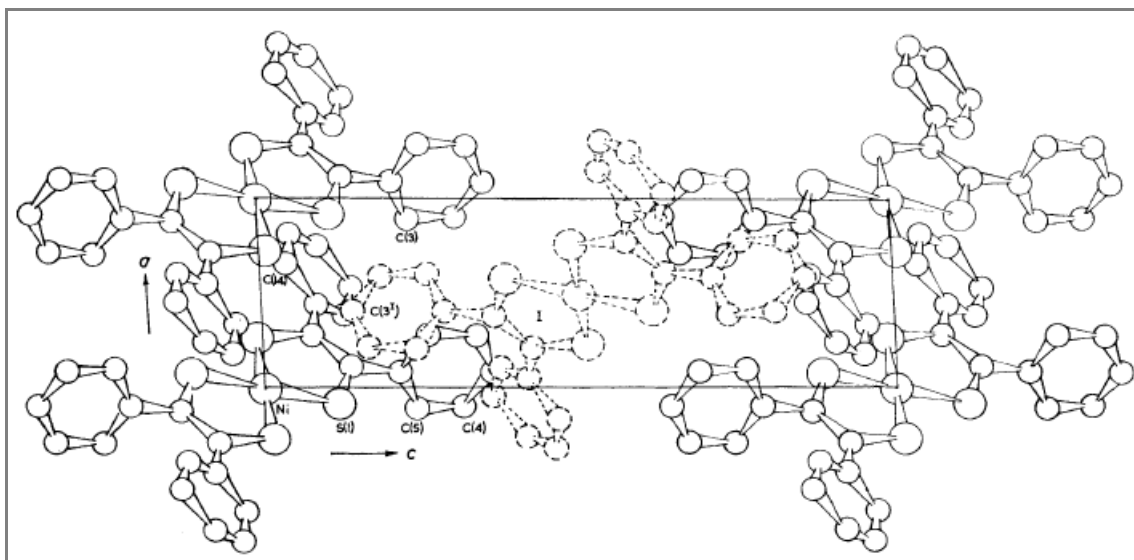


Figure 20. The $[\text{Ni}(\text{dpdt})_2]$ structure projected down $[010]$ ^[150]

Recently, Perochon *et al.*^[144] have established the X-ray crystal structures of several tetraalkoxy-substituted $[\text{Ni}(\text{dpdt})_2]$ and the structure of the tetrabutyloxy-substituted complex is presented in Figure 21. As described, the metal is in a square planar environment with a very limited tetrahedral distortion as the angles between the two NiS_2 planes do not exceed 5° (Figure 21).^[144]

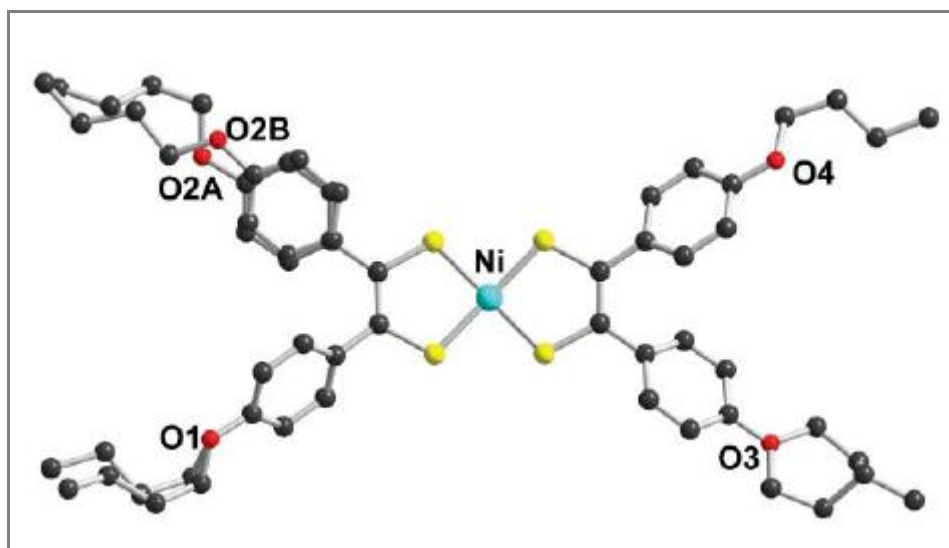


Figure 21. X-ray structure of tetrabutyloxy-substituted $[\text{Ni}(\text{dpdt})_2]$ ^[144]

The phenyl rings are not coplanar with the nickel bisdithiolene metallacycle but make dihedral angles from 29 to 51° (Figure 21).^[144] The strong distortions from planarity for the whole complexes is a consequence of free rotation of the phenyl rings out of the metallacycle planes. This structure is similar to those of tetramethoxy-substituted analogues reported by Arumugam *et al.*^[142]

1.4.3.2. Optical and electrochemical properties

The electronic properties of typical $[\text{Ni}(\text{dpedt})_2]$ derivatives are summarized below in two tables (Table 1 and Table 2) which display their absorption and electrochemical characteristics, respectively. When available, the given data have been chosen, in comparable solvents as much as possible.

The electronic absorption properties of typical neutral $[\text{Ni}(\text{dpedt})_2]$ complexes are given in Table 1. Their absorption in solution ranges from 700 to 1100 nm depending on the substituents nature. The influence of the electro donating/accepting group grafted onto the phenyl rings of dpedt ligands is observed. The more accepting the substituent is, the lower the maximum absorption wavelength is. The λ value exhibits a red-shift (around 0.13 eV) when the phenylalkyl or phenylalkoxy is replaced by a phenylamino (Table 1) substituent. The number of the grafted chains has also a slight influence.

The electrochemical data of several typical $[\text{Ni}(\text{dpedt})_2]$ complexes are given in Table 2. We observe a small influence of the nature of the grafted chain on the potential values. The introduction of alkyl or alkoxy chains on the phenyl rings of dpedt ligands decrease slightly the electron-accepting of the final complexes, which is expressed by the decreasing of first 1-electron reduction half wave potentials as in Table 2. This is due to the donor-effect of the alkyl and alkoxy-chains. The introduction of an electron-withdrawing group (Br) decreases the electron accepting property.

Based on the richness of their chemical reactivities and physical properties, nickel bis(1,2-dithiolene) complexes are found in many applications such as near infrared (NIR) photodetectors,^[151] optical switching devices,^[152, 153] organic dyes,^[135] non linear optics,^[154] and organic electronics.^[155-158]

Figure 22 illustrates the structures of some $[\text{Ni}(\text{dpedt})_2]$ derivatives used in organic field effect transistors (OFETs). The charge mobility properties issued from these experiments are gathered in Table 3. **BDT1** is an electron acceptor, and works as an n-channel OFET.^[158, 159] The experiments are carried out with bottom- (BC) or top-contact (TC) and under vacuum or in air. Generally, the electrons mobilities are at most in the order of $10^{-4} \text{ cm}^2\text{V}^{-1}\text{s}^{-1}$. Interestingly, the fluoro- and trifluoromethyl derivatives (**BDT4** and **BDT5**) show reasonably air-stable n-channel properties.^[159]

Table 1. Position of the maximum NIR absorption peak, corresponding extinction coefficient (ϵ) and solvent used for selected neutral nickel bis-dithiolene complexes.

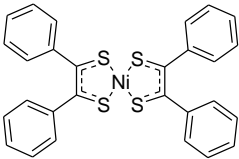
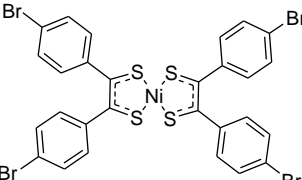
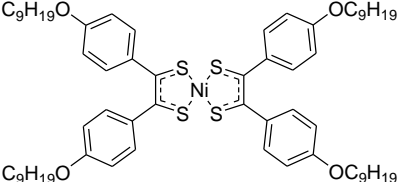
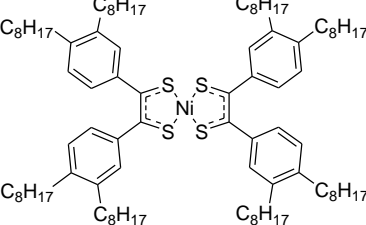
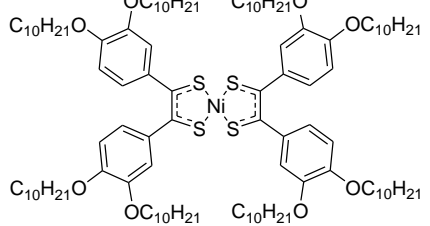
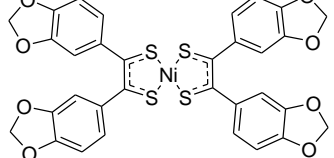
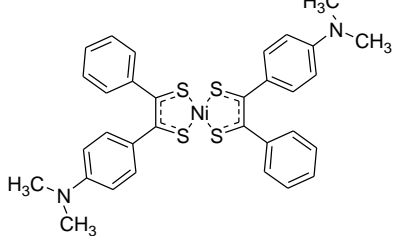
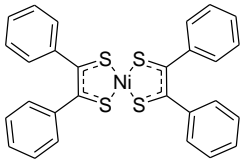
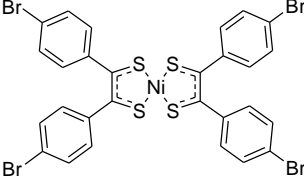
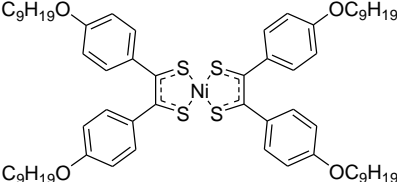
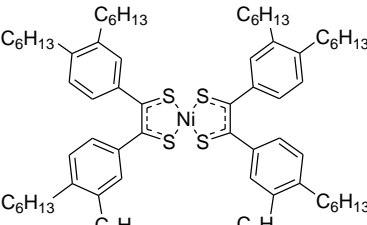
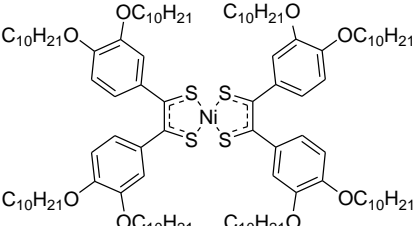
Complexes	λ_{\max} (nm)	ϵ (Lmol ⁻¹ cm ⁻¹)	Solvent	Refs
	866	30900	CHCl ₃	[160]
	866	29816	CHCl ₃	[160]
	925	25100	CHCl ₃	[161]
	898	33100	CHCl ₃	[162]
	959	36300	CHCl ₃	[162]
	934	32200	CH ₂ Cl ₂	[163]
	1006	2.5x10 ⁶	CH ₂ Cl ₂	[164]

Table 2. CV data *versus* saturated calomel electrode of several nickel bisdithiolene complexes

Complexes	$E_{1/2}^{\text{red}}$ (V/SCE)	Solvent	Refs
	0.03	CH ₂ Cl ₂	[91]
	0.09	CH ₂ Cl ₂	[165]
	-0.06	C ₂ H ₄ Cl ₂	[161]
	-0.04	C ₂ H ₄ Cl ₂	[162]
	-0.06	C ₂ H ₄ Cl ₂	[162]

The dimethylamino derivative **BDT6** has been demonstrated to have ambipolar OFET characteristics, where the hole and electron mobilities are of 2.5×10^{-4} and 2.0×10^{-5} $\text{cm}^2 \text{V}^{-1} \text{s}^{-1}$, respectively.^[166] **BDT6** is used for complementary OFET.^[157] Octadecyloxy-substituted **BDT7** has been used in top-contact OFET and the electron mobilities of the order of 1.3×10^{-3} $\text{cm}^2 \text{V}^{-1} \text{s}^{-1}$ have been found.^[72] Recently, optical and photovoltaic properties of **BDT1** in various states of aggregation (solution, vacuum-deposited film, polyvinylethylal polymers polymer composite) have been studied.^[167] The shift of the wavelength at the maximum absorption is explained by the formation of sandwich aggregates in deposited films, which are absent in the solution and polymer composites. The study of photovoltage spectra showed that both deposited and composite films are photosensitive in the range of 500-1000 nm.

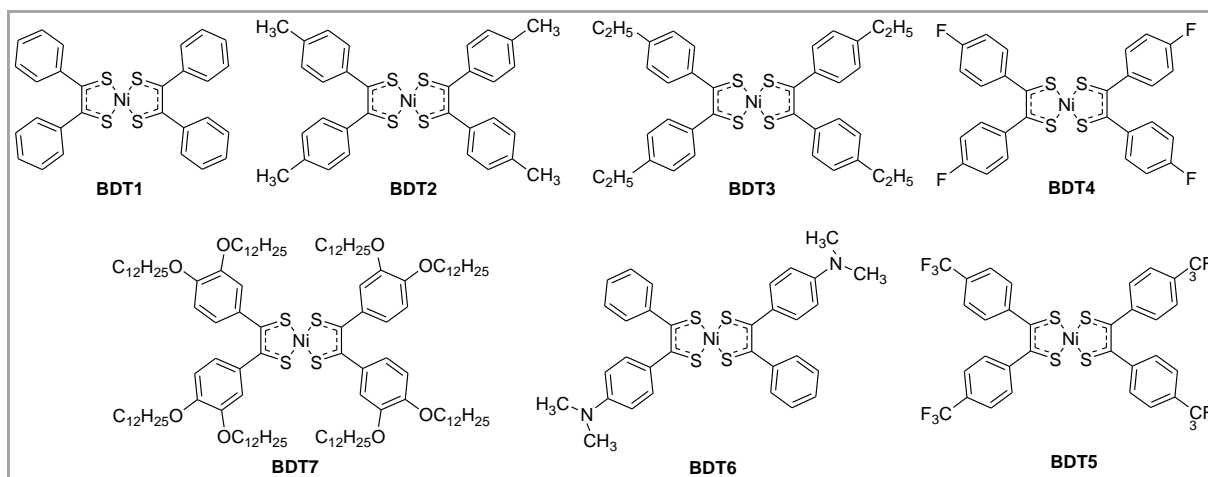


Figure 22. Examples of typical $[\text{Ni}(\text{dpedt})_2]$ used in OFET

Table 3. Charges mobilities of $[\text{Ni}(\text{dpedt})_2]$ determined from OFET

$[\text{Ni}(\text{dpedt})_2]$	Configuration	Condition	μ_e ($\text{cm}^2\text{V}^{-1}\text{s}^{-1}$)	μ_h ($\text{cm}^2\text{V}^{-1}\text{s}^{-1}$)	Ref
BDT1	bottom-contact	Vacuum	2.0×10^{-5}		[158, 159]
		Air	3.0×10^{-6}		[158, 159]
BDT2	"	Vacuum	1.3×10^{-4}		[159]
		Air	-		[159]
BDT3	"	Vacuum	6.0×10^{-5}		[159]
		Air	-		[159]
BDT4	"	Vacuum	5.0×10^{-5}		[159]
		Air	9.0×10^{-5}		[159]
BDT5	"	Vacuum	6.4×10^{-6}		[159]
		Air	6.6×10^{-6}		[159]
BDT6	"	Vacuum	2.0×10^{-5}	2.5×10^{-4}	[166]
BDT7	top-contact	Vacuum	1.3×10^{-3}		[72]

In conclusion, these results further indicate the promise of nickel bisdithiolene complexes for organic electronics applications, especially organic photovoltaic devices, while underscoring the importance of controlling solid-state packing in molecular electronic materials. In the next part, we will detail the design and synthesis of new discotic nickel bisdithiolene complexes.

2. Design and synthesis of new discotic nickel bisdithiolene complexes

2.1. Design of new discotic nickel bisdithiolene complexes

2.1.1. Bibliographical survey

Prior to this work, several groups have described columnar liquid crystalline compounds based on neutral nickel bis(1,2-dithiolene) complexes.^[91, 137-141, 168, 169] However, none of these compounds present columnar liquid crystalline properties at room temperature. Such property is mandatory in order to make their use easier as active materials for electronic devices. The lowest reported transition temperatures from crystalline states to columnar liquid crystalline phases, based on $[M(dpdt)_2]$ (Figure 23), are situated between 50°C and 60°C.^[91] These temperatures are still too high for targetted application. Our goal in the present work is to synthesize room temperature columnar liquid crystalline $[M(dpdt)_2]$ as near infrared absorbing molecular electron-acceptor materials for organic photovoltaic applications.

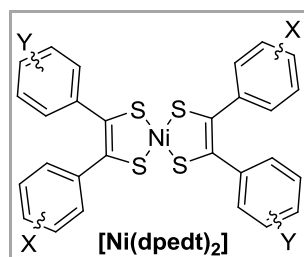


Figure 23. General structure of $[Ni(dpdt)_2]$ in the present work

Until now, all reported columnar liquid crystalline neutral metal bis(1,2-dithiolene) complexes are $[M(dpdt)_2]$ derivatives. Previously, Ohta *et al.*^[91, 136-140] have studied the influence of alkyl/alkoxy chain lengths on the mesomorphic properties of tetraalkyl-substituted, tetralkoxy-substituted and octaalkoxy-substituted $[Ni(dpdt)_2]$ (Figure 24).

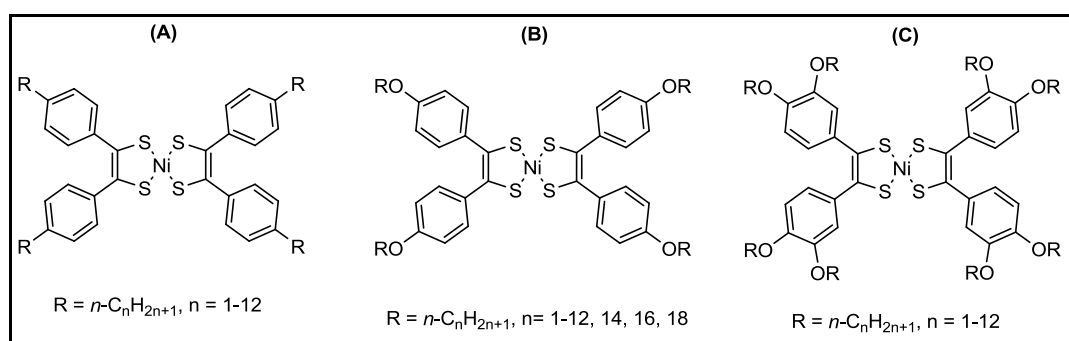


Figure 24. $[Ni(dpdt)_2]$ studied by Ohta *et al.*^[91, 136-140]

In these works, they have focused on the investigation of symmetric complexes substituted by linear alkyl/alkoxy chains.

Tetraalkyl-substituted nickel bisdithiolene complexes (Figure 24 A): None of these compounds has mesomorphic properties.^[91] In our work, this family is not investigated.

Tetraalkoxy-substituted nickel bisdithiolene complexes (Figure 24 B): Black needle-like crystals of nickel complexes with $n = 1-4$ directly melt into a green isotropic liquid (I.L.) with rapid decomposition at temperatures higher than 250°C. The $[\text{Ni}(\text{dpedt})_2]$ complexes with $n = 5-8$ do not show any mesophase but only crystal-crystal phase transitions. The tetranonyloxy-substituted compound ($n = 9$) shows a green mesophase between 110 and 190°C, and each of the complexes for $n \geq 10$ shows two differently colored mesophases.^[91] The nature of these two green and brown mesophases is cleared.

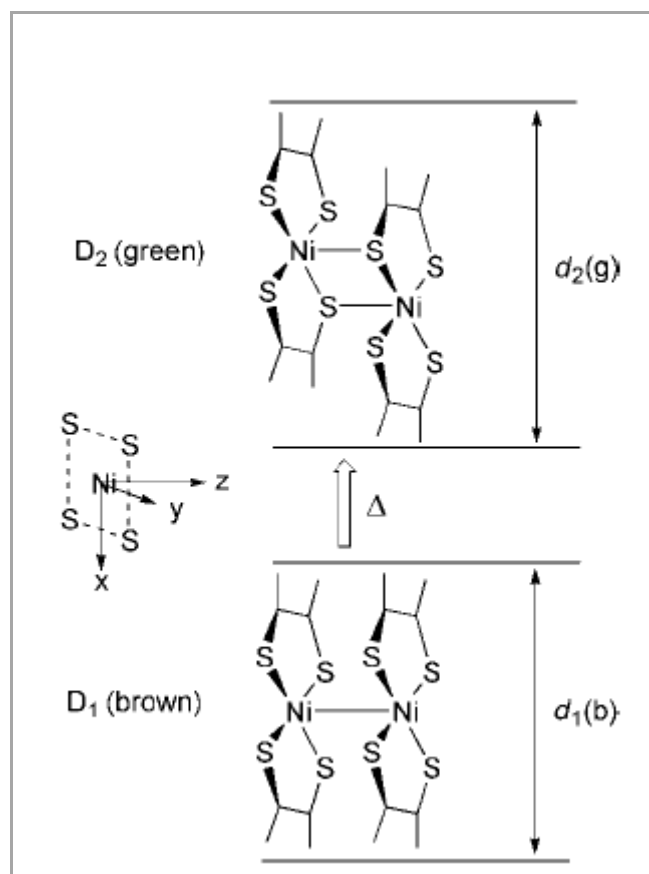


Figure 25. Nature of brown and green discotic mesophase proposed by Ohta *et al*^[91]

The tentative molecular models of these two lamellar discotic mesophases are proposed as shown in Figure 25. In the brown D_1 phase, two molecules form a dimer through a Ni–Ni bond. When D_1 is heated, the Ni–Ni bond is gradually broken and a new Ni–S bond between these two

molecules slowly forms because the Ni–Ni bond is at a higher energy level than a Ni–S bond, that is, the Ni–S bond is more stable than the Ni–Ni bond. Hence, two molecules slip over each other.^[91]

In Figure 26, phase transition temperatures of the virgin samples (i.e. the sample has not been thermally treated) and the non-virgin samples (i.e. the sample has already been thermally treated) are separately plotted against the carbon number (n) in the alkoxy-side-chain. As can be seen from this figure, each of the virgin samples with $n \geq 10$ gives both brown and green mesophases, whereas the non-virgin sample does not show the brown mesophase but only the green mesophase. The lowest transition temperatures of virgin and non-virgin samples are *ca.* 73°C and 56°C for $n = 12$.

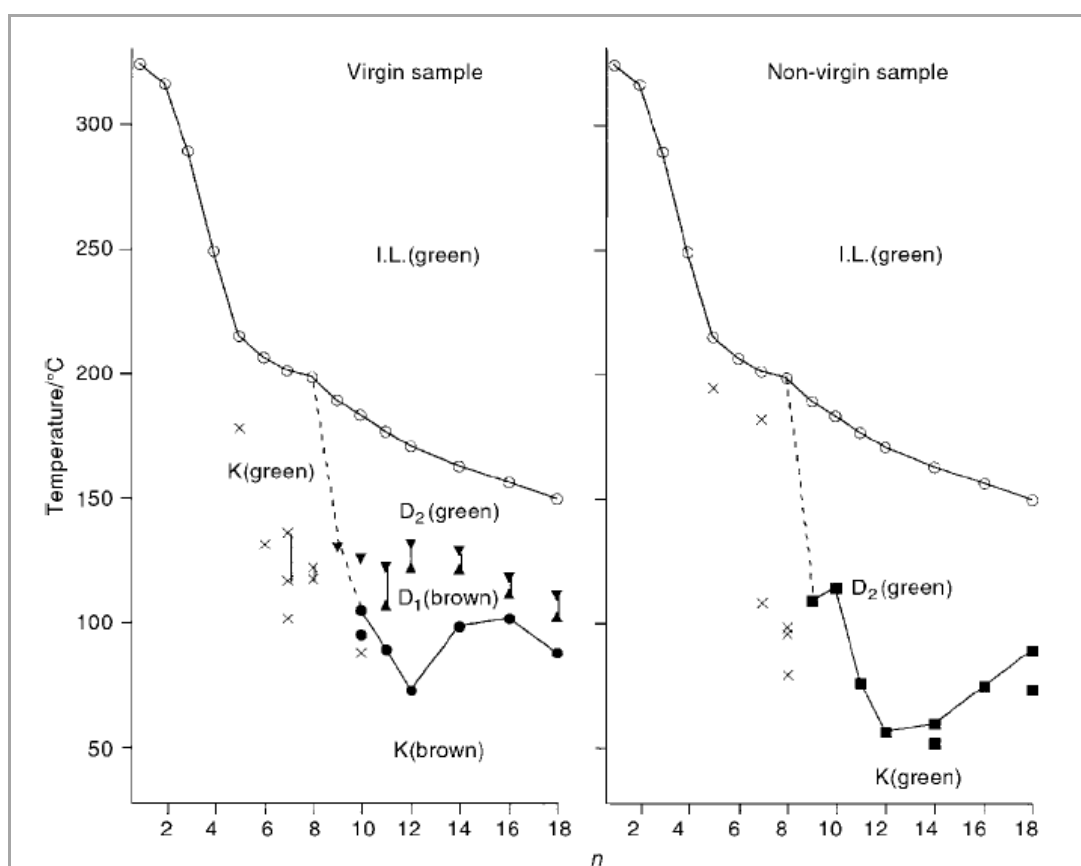


Figure 26. Phase transition temperature *versus* number of the carbon atoms in the alkoxy chain (n). Open circles: clearing points. Filled circles and squares: melting points of brown crystals and green crystals, respectively. Triangles: phase transitions from brown D_1 to green D_2 . Crosses: crystal–crystal phase transition.^[91] K: crystal, D: discotic mesophase, I.L.: isotropic liquid

Octaalkoxy-substituted nickel bisdithiolene complexes (Figure 24 C): It is found that for this family of nickel bisdithiolenes, the complexes with $n = 2-4$ have a monotropic discophase.^a With $n = 5-12$, the complexes have an enantiotropic discophase.^b The octamethoxy-substituted $[\text{Ni}(\text{dpedt})_2]$ does not exhibit a discophase and it decomposes at its melting point.^[140] All transition temperatures of the complexes are plotted against the number of carbon atoms (n) in the alkoxy chains in Figure 27. In Figure 27, “x” marks denote the unidentified phase transitions in the crystalline phases. As can be seen in this figure, the lowest transition temperature achieved is 66°C for the octaundecyloxy-substituted nickel complexes ($n = 11$).

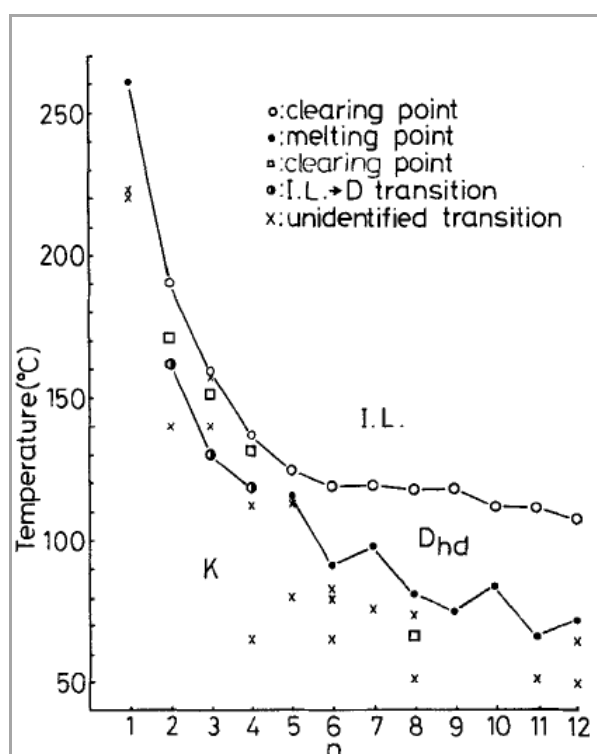


Figure 27. Phase transition temperatures *versus* the number of carbon atoms(n) in the alkoxy chains.^[140] K: crystal, D_{hd} : discotic mesophase, I.L.: isotropic liquid

Ohta *et al.* also investigated the influence of the central metal on the mesomorphism and π -acceptor properties of the octaalkoxy-substituted metal bis(1,2-dithiolene) complexes.^[140, 141] They focused their research on the symmetric $[\text{M}(\text{dpedt})_2]$ of d^8 transition metal (Ni, Pd, Pt).^[140, 141] The mesophases are established by microscopic observations, differential scanning calorimetry, and temperature dependent powder X-rays diffraction. The phase transition temperatures of the homologous Ni, Pd and Pt complexes are plotted against the number of carbon atoms (n) in the alkoxy chains in Figure 28, to investigate the influence of central

^aMonotropic liquid crystal: exhibits the liquid crystalline state only when the temperature changes in one direction

^bEnantiotropic liquid crystal: exhibits the liquid crystal state both on heating and cooling process

metal atom on the mesomorphism.

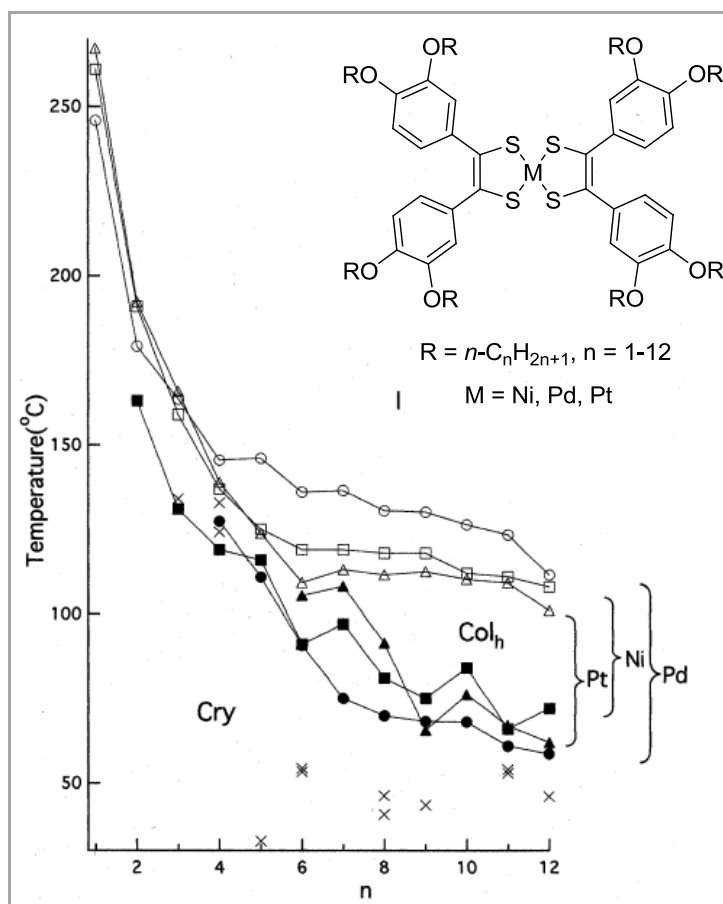


Figure 28. Phase transition temperatures vs. the number of carbon atoms (n) in the alkoxy chains of the metal complexes $[M(dpdt)_2]$ ($M = Ni, Pd, Pt$). Nomenclature: Cry = crystal; Col_h = hexagonal columnar mesophase; I = isotropic liquid; Ni, Pd, Pt designate the dithiolene complexes of Ni, Pd, Pt respectively.^[141] Circles, triangles and squares: melting points (filled) and clearing points (non-filled) of Pd, Pt and Ni complexes, respectively.

The nickel complexes show a Col_h mesophase for $n = 5$ to 12.^[138-140] On the other hand, the palladium and platinum complexes show a Col_h mesophase for $n = 4$ to 12 and $n = 6$ to 12, respectively.^[141] Thus, they give the Col_h mesophase for a shorter length of alkoxy chain in the order Pd, Ni, Pt (Figure 28). For $6 \leq n \leq 12$, the clearing points become higher in the order $Pt < Ni < Pd$. The intracolumnar stacking distances of these Ni, Pd and Pt complexes are observed at 3.64 ± 0.02 , 3.56 ± 0.03 , and 3.73 ± 0.02 Å, respectively. Thus, they give a longer stacking distance in the order $Pt > Ni > Pd$. Hence, the order of stacking distances is apparently related to the order of clearing points. Moreover, the Pt, Ni and Pd complexes show reduction potentials at -0.09 , -0.055 , and 0.00 V (*versus* SCE in CH_2Cl_2), respectively. They become better π -acceptors in the order $Pt < Ni < Pd$. They reveal from the electronic absorption spectra that the LUMO energy level of these metal complexes decreases in the

order Pt<Ni<Pd, and that the back donation of electrons from the central metal to the ligand occurs more in the same order Pt<Ni<Pd. This results in better π -acceptor properties in the order Pt<Ni<Pd for the octaalkoxy-substituted metal bisdithiolene complexes.

2.1.2. The design of new discotic nickel bisdithiolene complexes

In our work, we rely upon different approaches to obtain new neutral nickel bis(1,2-diphenyl-1,2-ethenedithiolene complexes ($[\text{Ni}(\text{dpedt})_2]$). All the modifications are performed on the phenyl ring of 1,2-diphenyl-1,2-ethenedithiolene (dpedt) ligands.^[8, 9] We focus on different factors concerning the dpedt ligands of tetraalkoxy-substituted and octaalkoxy-substituted complexes. These present approaches are aimed at understanding the molecular design requirements for reaching low temperature liquid crystalline phases in $[\text{Ni}(\text{dpedt})_2]$ derivatives. Furthermore, alkyl chains are expected to improve solubility of $[\text{Ni}(\text{dpedt})_2]$ derivatives which allows the fabrication of solution-processable devices.

2.1.2.1. Tetraalkoxy-substituted complexes

2.1.2.1.1. Influence of alkoxy chain lengths and configurations

Firstly, we study the influence of the alkoxy chain lengths and configurations, and of the symmetry on the physical properties of the targeted compounds. Therefore, both symmetric and asymmetric tetraalkoxy-substituted $[\text{Ni}(\text{dpedt})_2]$ are designed and investigated (Figure 29).

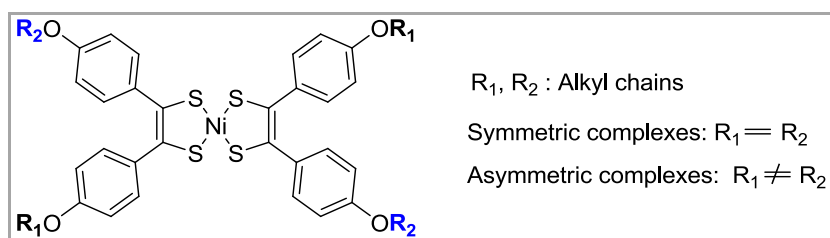


Figure 29. Symmetric and asymmetric tetraalkoxy-substituted $[\text{Ni}(\text{dpedt})_2]$

These complexes are substituted by either linear or branched alkyl chains. The linear alkyl chains vary from methyl to tetradecyl. The choice of branched chains is based on the results

from other columnar liquid crystalline systems. The 2-ethylhexyl chain is found in many columnar liquid crystalline polycyclic aromatic hydrocarbons.^[170-173] Other longer homologues of 2-ethylhexyl (such as 2-butyloctyl, 2-hexyldecyl ...) can be found in the columnar liquid crystalline metal-free octaalkoxycarbonyl phthalocyanines.^[174, 175] 3,7-dimethyloctyl chain is used in the synthesis of columnar liquid crystals based on tricycloquinazoline core.^[80] We also focus our interest on the effect of molecular symmetry on the formation of columnar liquid crystals. Asymmetric compounds, *by restricted definition in the present work*, are grafted by two different alkyl side chains, either linear or branched (Figure 29). For this purpose, we synthesized $[\text{Ni}(\text{dpedt})_2]$ substituted by two different kinds of alkoxy chains (linear or branched).^[8, 9] A recent study reported in the literature shows that the more symmetrical compound has a significantly higher melting temperature than its asymmetrical isomer and the phase transition temperatures show a strong dependence on molecular symmetry.^[176, 177] The introduction of bulky branched alkoxy chains could play an important role on the molecular packing, thus on the transition temperature.

2.1.2.1.2. Influence of connecting groups

Secondly, the role of connecting groups on the molecular design of columnar liquid crystalline molecules may be significant.

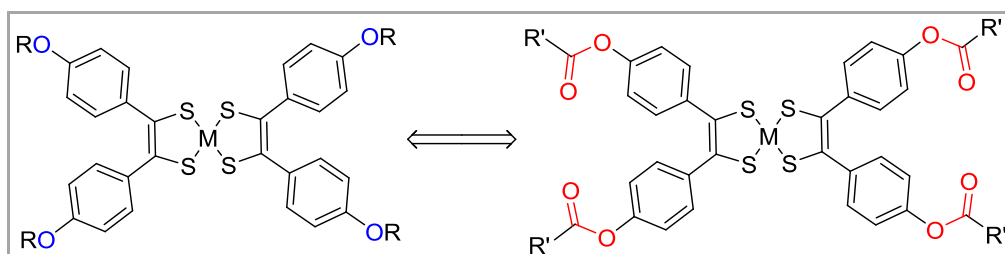


Figure 30. General structures and relationship of tetraalkoxy- and tetraalkanoate-substituted $[\text{Ni}(\text{dpedt})_2]$

To study its effect on tetraalkoxy-substituted nickel bisdithiolene complexes, we replace the ether linker group by the ester function which is more polarisable (Figure 30), whereas the side chain length remains unchanged.

2.1.2.1.3. Halogenation of [dpedt] ligand

Thirdly, we study the influence of the halogenations of the phenyl rings of dpedt ligand (Figure 31). Recently, Bao *et al.*^[178] have studied the influence of the chlorination of the π -conjugated

aromatic rigid core on the design and synthesis of electron acceptor organic semiconductors. They showed that adding chlorine atoms to aromatic conjugated cores is a general, effective route towards the design of n-type air-stable organic semiconductors. This is true for acenes, phthalocyanines, and perylene tetracarboxylic diimide (PDI)-based molecules. They also compared a series of fluoro- and chloro-functionalized acenes, phthalocyanines, and PDI-based molecules. The synthesized acenes showed high and balanced ambipolar transport in the top-contact OFET geometry. The electron-withdrawing halogen groups lowered the LUMO and the charge injection barrier for electrons, such that electron and hole transport occurred simultaneously. If the added chlorine atom does not distort the planarity of the conjugated core, they found that the chloro-functionalized molecules tend to have a slightly smaller HOMO-LUMO gap and a lower LUMO level than the fluoro-containing molecules, both from theoretical calculations and cyclic voltammetry measurements in solution. This is most likely due to the fact that chlorine atoms contain empty 3d orbitals that can accept π -electrons from the conjugated core, while fluorine atoms do not have energetically accessible empty orbitals for such delocalization.

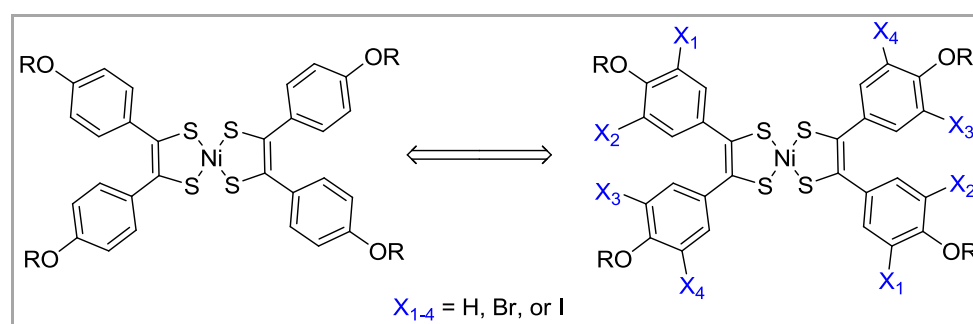


Figure 31. General structures and relationship of tetraalkoxy- and tetraalkoxy and halogenated-substituted $[\text{Ni}(\text{dpdt})_2]$

Inspired from the work of Bao *et al.*^[178], we decided to halogenate the phenyl rings of dpdt ligand with bromine or iodine atoms. As in the case of chlorine atom, both bromine and iodine atoms contain empty d orbitals that could accept π -electrons from the phenyl moieties of dpdt ligand. This could favour the electron acceptor properties of targeted compounds. On the other hand, the dimensions of bromine and iodine atoms larger than that of hydrogen could have an impact on the molecular packing, thus on the mesomorphic properties.

2.1.2.2. Octaalkoxy-substituted complexes and related compounds

2.1.2.2.1. Influence of alkoxy chain lengths and configurations

As in the case of tetraalkoxy-substituted complexes, we also focus our research on the influence of branched alkyl chains. 2-ethylhexyl (branched octyl chain) and 3,7-dimethyloctyl (branched decyl chain) are selected for the study. Firstly, these two chains are found in numerous columnar liquid crystalline compounds.^[80, 170-173, 179] Secondly, the nickel complexes bearing linear octyl or decyl chains show columnar liquid crystalline properties at relatively high temperature.^[138-140] By replacing these chains by bulky branched homologues, molecular packing should be affected; the transition temperature should be reduced.

2.1.2.2.2. Influence of the side chains position

The molecular structures of “traditional” octaalkoxy-substituted $[\text{Ni}(\text{dpedt})_2]$, studied by Ohta *et al.*,^[140] are shown in Figure 32.

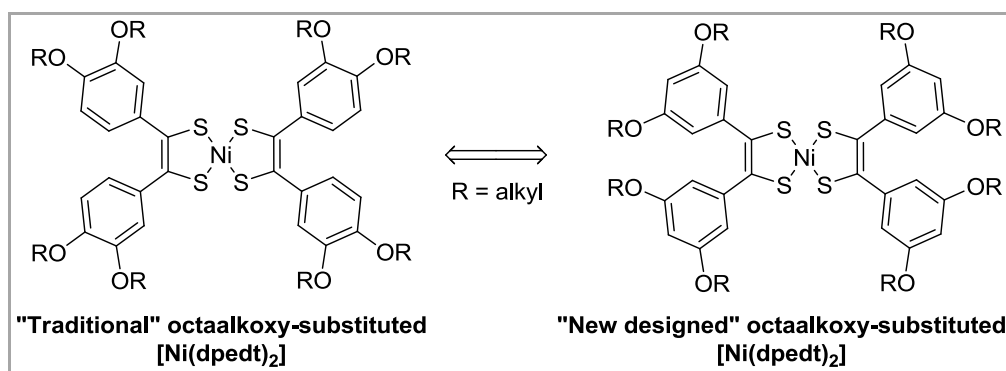


Figure 32. General structures and relationship of tetraalkoxy- and octaalkoxy-substituted $[\text{Ni}(\text{dpedit})_2]$

The relative position of two alkoxy chains on the phenyl rings of dpedit ligand is “-1,2”. What is the influence on the columnar liquid crystalline property of $[\text{Ni}(\text{dpedit})_2]$ if the two chains are in position “-1,3” as presented in “new designed” octaalkoxy-substituted $[\text{Ni}(\text{dpedit})_2]$ in Figure 32? We will synthesize a new $[\text{Ni}(\text{dpedit})_2]$ in order to investigate its properties in comparison with its traditional isomer.

2.1.2.2.3. Extension of the aromatic rigid core of [Ni(dpdt)₂]

It is well known that the two phenyl rings of dpdt ligand are not in the plane of the nickel bisdithiolene core.^[150] The connection of these two phenyl rings results in new benzenoid nickel complexes based on phenanthrene-9,10-dithiolate ligand (Figure 33). The first examples of this kind of compound are reported by Mueller-Westerhoff *et al.*^[180] The extension of the aromatic rigid core of nickel complexes should favour the intermolecular π -stacking, thus favour the formation of columnar liquid crystalline phase.

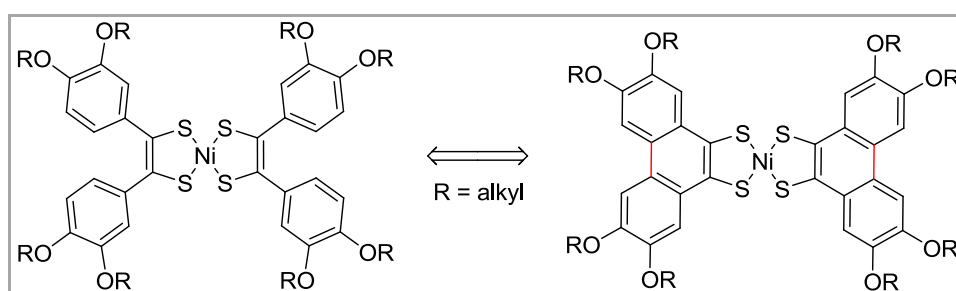


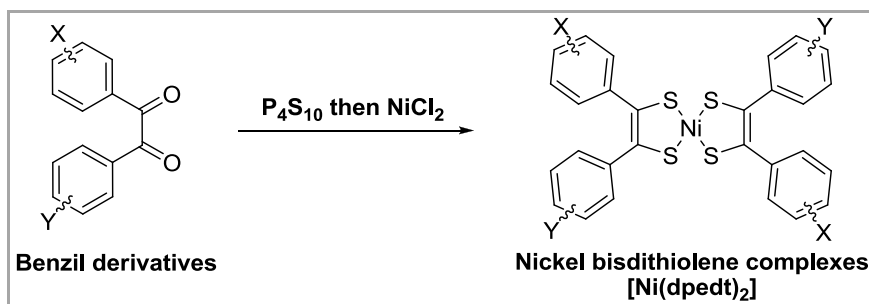
Figure 33. Benzenoid nickel complexes based on phenanthrene-9,10-dithiolate ligand

Following the above described approaches, thirty-one nickel complexes, including twenty seven new compounds, are designed and synthesized. Four of them (**BT22**, **BT65**, **BT113**, and **BT163**) have been previously reported and they are re-synthesized and used as model compounds. The synthesis and characterization of all intermediates and final targeted products are presented and discussed in the following paragraph.

2.2. Synthesis of new nickel bisdithiolene complexes

2.2.1. Synthesis of precursors of dithiolene ligands

As discussed in the previous paragraph (1.4.2), 1,2-dithiolene ligands and neutral nickel bis(1,2-dithiolene) complexes can be synthesized from different precursors such as α -hydroxy ketone, α -halogenated ketone, α -diketone... In the present work, all neutral nickel complexes were achieved via α -diketone precursor. More specifically, benzil derivatives are used.

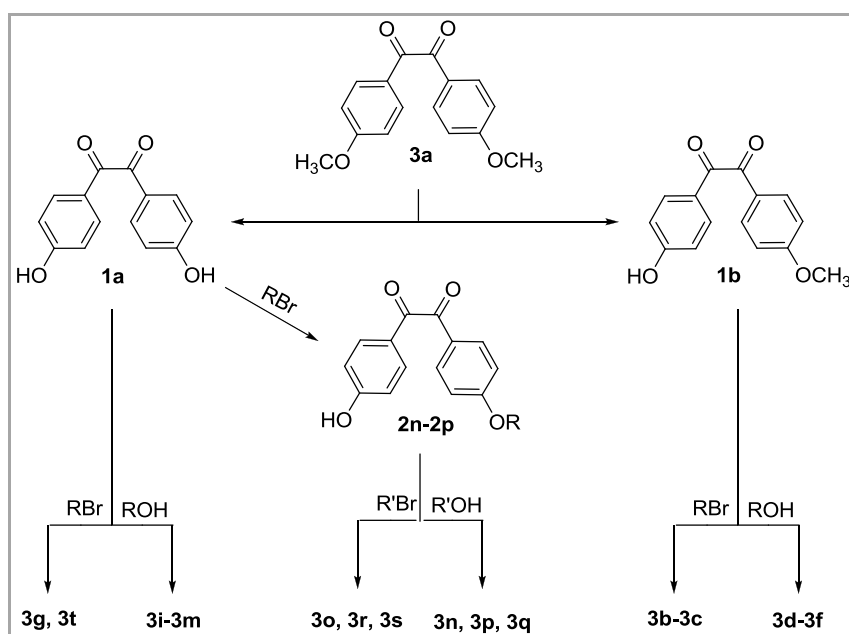


Scheme 7. General synthesis of nickel bisdithiolene complexes

2.2.1.1. Synthesis of precursors of tetraalkoxy-substituted complexes

2.2.1.1.1. Synthesis of 4,4'- dialkoxy-substituted benzils

The general synthetic pathways are gathered in Scheme 8.



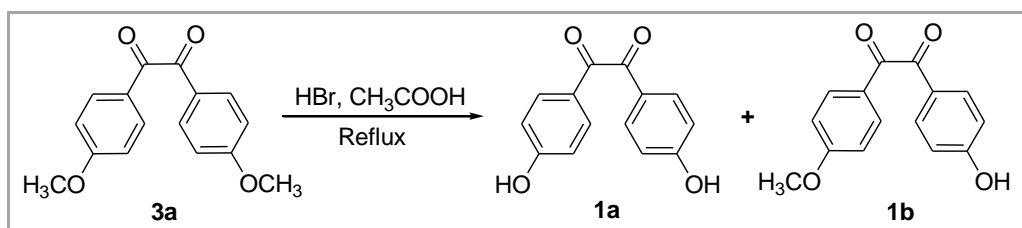
Scheme 8. General synthesis of 4,4'-dialkoxy-substituted benzil derivatives

A series of 4,4'-dialkoxy-substituted benzil derivatives are synthesized, with different combinations of linear or racemic branched, long or short alkyl chains.

2.2.1.1.2. Synthesis of common starting materials 1a & 1b

In order to obtain the long alkoxy chain-substituted benzil derivatives **3b-3t**, *p*-anisole **3a** is

chosen as the commercial starting material. The synthetic pathways started from the synthesis of **1a** and **1b**, two common intermediate materials (Scheme 9).



Scheme 9. Synthesis of **1a** and **1b**; Reagents and conditions: HBr 48%/glacial CH₃COOH (1/1 v/v), reflux 17-50h

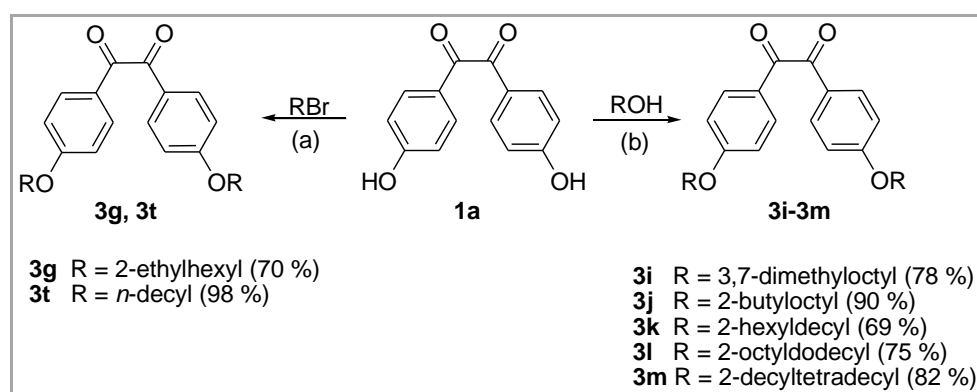
By removing one methyl-group of **3a** in hydrobromic acid we obtain the phenol derivative **1b**. We are then able to graft another linear or branched alkyl chain to get asymmetric benzils **3b-3f**. If both methoxy groups are removed, two free phenol functions are available for chemical modification (**1a**). The introduction of two-fold alkyl chain yields to symmetric benzils **3g-3m** & **3t**. It is also possible to graft two different alkyl chains on **1a** by successive substitutions. The corresponding monoalkoxy-substituted intermediates **2n-2p** (detailed later in Scheme 11) are systematically purified before any second alkylation. The 4,4'-dihydroxybenzil **1a** is prepared in large quantity from **3a**. The demethylation reaction is performed with high yield by a boiling mixture of concentrated hydrobromide acid and glacial acetic acid according to the literature.^[181] In these conditions of reaction, the conversion of 4,4'-dimethoxybenzil to α -diketone **1a** strongly depends on the reaction duration. Depending on experimental conditions, we obtain either a mixture of **1a** and **1b** or only **1a** (see experimental part for further details). In the present work the synthesis of **1b** is not optimized. Both **1a** and **1b** are engaged in the next steps for preparing long chain substituted benzils: the precursors of 1,2-dithiolene ligands.

2.2.1.1.3. Synthesis of symmetric 4,4'-dialkoxybenzils (**3g-3m**, **3t**)

The symmetric 4,4'-dialkoxybenzils **3g-3m** and **3t** are synthesized by grafting alkyl chains on the phenol function of **1a** as depicted in the Scheme 10.

Two different methods are used, depending on the commercial availability of alkyl chains as halogenated alkanes or alcoholic compounds. In the first case, the classical nucleophilic substitution reaction gives **3g** and **3t** in high yields (Scheme 10) by heating the mixture of **1a** and large excess of 2-ethylhexyl bromide (for **3g**) or decyl bromide (for **3t**) and a Lewis base (K₂CO₃)

in dimethylformamide (DMF). In the later case, the Mitsunobu method^[182, 183] is applicable leading to **3i-3m**. The Mitsunobu reaction is a versatile and widely used method for the dehydrative coupling of an “alcohol” with an “acid” by using a combination of an oxidizing azo reagent, most commonly diethyl azodicarboxylate (DEAD), and a reducing phosphine reagent, usually triphenylphosphine (PPh₃), under mild reaction conditions.^[148] Carboxylic acids, phenols, diols, activated carbon acids, imides, and the like can all serve as the “acid” reaction component. Thus, this reaction can be used to prepare esters, aryl ethers, cyclic ethers, carbon-carbon and carbon-nitrogen bonds, and so on. Besides the desired product, a hydrazide such as diethyl hydrazinedicarboxylate (DEAD-H₂) from DEAD and a phosphine oxide such as triphenylphosphine oxide (POPh₃) from PPh₃ are also formed as by-products. More detailed discussions about the origin, mechanism, advance and applications of the Mitsunobu and related reactions have been recently reviewed.^[148, 149]



Scheme 10. Synthesis of symmetrical benzils **3i-3m**, **3g** and **3t**; Reagents and conditions: (a) RBr (2.4 equiv.), K₂CO₃ (3.0 equiv.), DMF, 90°C; (b) Mitsunobu reaction: ROH (2.4 equiv.), DEAD (2.4 equiv.), PPh₃ (2.4 equiv.), THF, 0°C then 1h at r.t.

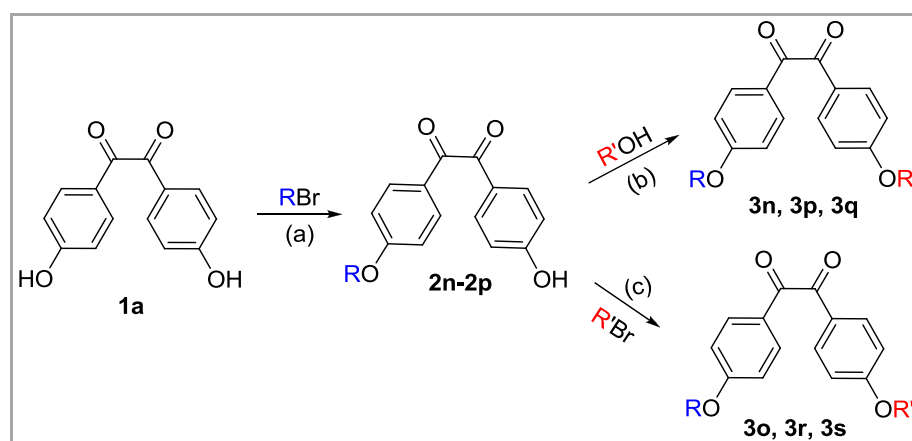
By application of classical nucleophilic substitution and Mitsunobu reaction, we are able to graft a large choice of alkyl chains in one step, particularly branched ones that are often available as cheap primary or secondary alcohols.

2.2.1.1.4. Synthesis of asymmetric 4,4'-dialkoxybenzils (**3b-3f**, **3n-3s**)

The asymmetric precursors 4,4'-dialkoxybenzil **3n-3s**, which contain two different alkyl chains (different from methyl), are synthesized from **1a** (Scheme 11).

For this, the two chains are successively introduced. The reaction of **1a** with a little less than one equivalent of alkyl bromide in short reaction time forms monoalkoxy-substituted benzil

derivatives **2n-2p** with acceptable yields (41%-57%) without any optimization. The symmetric benzils **3** are also isolated as co-product (*e.g.* 4,4-dodecyloxybenzil **3h** is isolated in the synthesis of **2p** in 30 % yield). The quantitative conversion of **1a** to **2o-2p** could be realized by using a large excess of **1a** as described elsewhere for similar reaction.^[184] The introduction of the second alkyl chain is performed either by nucleophilic substitution or the Mitsunobu reaction as described above in resulting **3n-3s** (Table 4).



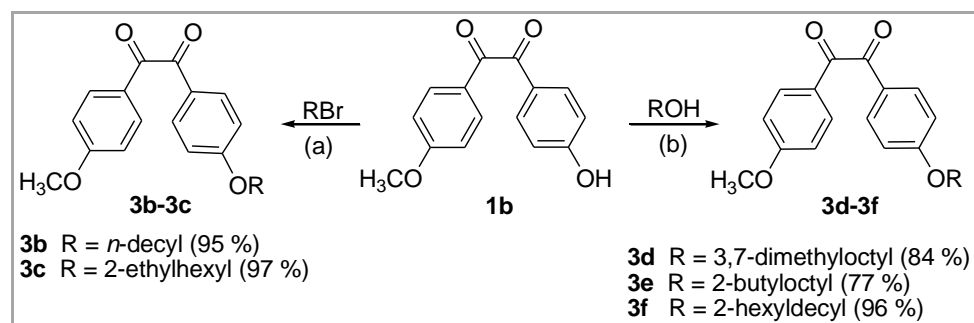
Scheme 11. Synthesis of asymmetrical benzils 3n-3s; Reagents & conditions: (a) RBr (0.9 equiv.), K₂CO₃ (0.9 equiv.), DMF, 90°C, 1h; (b) R'OH (1.2 equiv.), DEAD (1.2 equiv.), PPh₃ (1.2 equiv.), THF, 0°C then 1h at R.T.; (c) R'Br (1.2 equiv.), K₂CO₃ (1.5 equiv.), DMF, 90°C

Table 4. The list of monoalkoxy-substituted benzils (2n-2p) and asymmetric 4,4'-dialkoxybenzils (3n-3s). **3h** was isolated from the synthesis of **2p**; all branched alkyl chains are racemic mixtures and yields in %

R	R'	2 (yield)	3 (yield)
2-ethylhexyl	H	2n (41)	-
<i>n</i> -decyl	H	2o (57)	-
<i>n</i> -dodecyl	H	2p (46)	-
<i>n</i> -dodecyl	<i>n</i> -dodecyl	-	3h
2-ethylhexyl	<i>n</i> -decyl	-	3n (69)
<i>n</i> -decyl	3,7-dimethyloctyl	-	3o (91)
<i>n</i> -dodecyl	<i>n</i> -tetradecyl	-	3p (99)
<i>n</i> -dodecyl	<i>n</i> -undecyl	-	3q (80)
<i>n</i> -dodecyl	2-butyloctyl	-	3r (100)
<i>n</i> -dodecyl	3,7-dimethyloctyl	-	3s (95)

The asymmetric 4,4'-dialkoxy-substituted benzils containing one methyl chain and another linear or branched alkyl one **3b-3f** are synthesized from **1b** in similar conditions as discussed

above (Scheme 12).

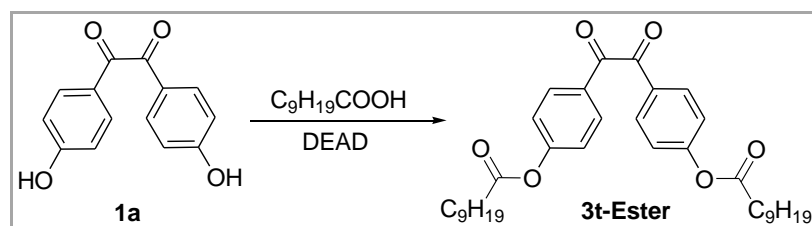


Scheme 12. Synthesis of asymmetrical benzils 3b-3f; Reagents and conditions: (a) RBr (1.2 equiv.), K₂CO₃ (1.5 equiv.), DMF, 90°C; (b) ROH (1.2 equiv.), DEAD (1.2 equiv.), PPh₃ (1.2 equiv.), THF, 0°C then 1h at r.t.

In comparison with other methods using alkyne intermediate of synthesis of asymmetrical long alkoxy-substituted benzils,^[185] our method presents some advantages. It uses common intermediates such as **1a** and **1b** and allow synthesizing many asymmetric benzil derivatives without major difficulty. Moreover, the alkyl chains are introduced in the last steps starting from either halogenated alkane or alcohols that allow numerous alkyl chain combinations.

2.2.1.1.5. Synthesis of 4,4'-dialkanoate-substituted benzils

In order to study the influence of the connecting group on the mesomorphic and physical properties of nickel complexes, the ether function is replaced by ester function. As discussed and illustrated above, the Mitsunobu reaction is a very powerful tool for the synthesis of aromatic ethers directly from phenol derivatives and alcoholic compounds. In this case, phenol derivatives play the role of weak acid. But interestingly, in the Mitsunobu reaction, the phenol derivatives play an ambivalent role. When the alcoholic compound is replaced by *n*-decanoic acid, dihydroxy benzil **1a** reacts as an alcohol (Scheme 13). The corresponding ester **3t-Ester** is obtained in good yield (93 %) without any optimization.

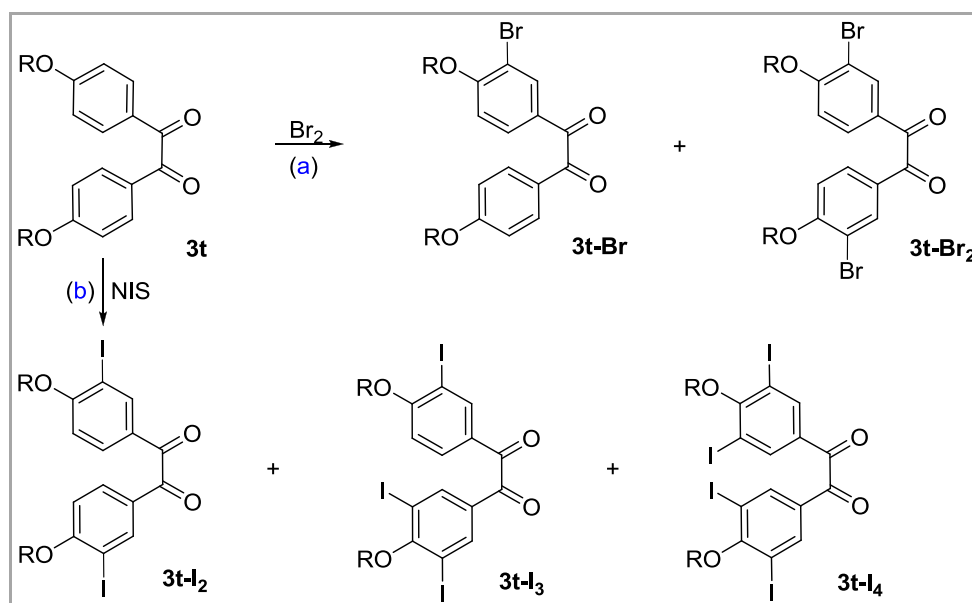


Scheme 13. Synthesis of ester 3t-Ester by the Mitsunobu reaction; Reagents and conditions: DEAD (2.4 equiv.), PPh₃ (2.4 equiv.), Decanoic acid (2.4 equiv.), THF, 0°C then 1h at R.T.

2.2.1.1.6. Synthesis of halogenated benzils

The halogenations of 4,4'-didecyloxy benzil (**3t**) resulting in halogenated benzil derivatives **3t-Br**, **3t-Br₂**, **3t-I₂**, **3t-I₃** and **3t-I₄** is depicted in Scheme 14. These syntheses are adapted from literature.^[186, 187]

All halogenated compounds are synthesized from 4,4'-didecyloxy benzil **3t**. The treatment of **3t** with excess of bromine in CH₂Cl₂ only gives 3-bromo-4,4'-didecyloxy benzil **3t-Br** in low yield (12 % after 12 h at room temperature). The introduction of one molar equivalence of FeCl₃ gives a mixture of **3t-Br** and dibromo-substituted benzil **3t-Br₂** with mass ratio *ca.* 1/2 after reacting overnight at room temperature. Finally, **3t-Br₂** is achieved in good yield (94%) by reflux overnight **3t** with Br₂ and FeCl₃ in an equivolometric mixture of CH₂Cl₂ and CH₃CN (Scheme 14). The synthesis of di/tris/tetraiodo-substituted benzils **3t-I₂**, **3t-I₃** and **3t-I₄** is performed by reflux of **3t** with N-iodosuccinimide (NIS) in trifluoroacetic acid as solvent. Depending on the NIS molar equivalence (2.0, 3.0, or 5.0), **3t-I₂**, **3t-I₃** or **3t-I₄** are respectively isolated as major product in acceptable yields (88%, 43%, and 59 % respectively). In the synthesis of **3t-I₂**, careful purification of crude product gives a small quantity of **3t-I₃**. When the quantity of NIS is increased up to five equivalents, **3t-I₄** is obtained as the main product and a small quantity of **3t-I₃** is isolated. The use of three equivalents of NIS gives a mixture of three compounds **3t-I₂**, **3t-I₃** and **3t-I₄** with **3t-I₃** as the major product.

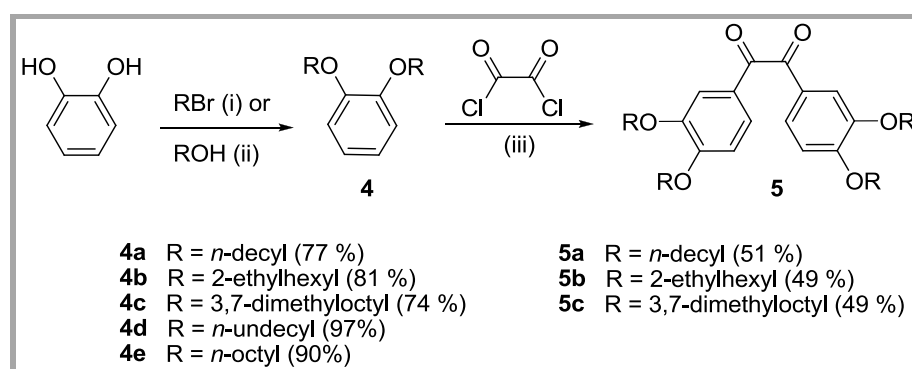


Scheme 14. Synthesis of halogenated benzils **3t-Br**, **3t-Br₂**, **3t-I₂**, **3t-I₃** and **3t-I₄**; Reagents and conditions: (a) Br₂ (5.0 equiv.), FeCl₃ (2.0 equiv.), CH₂Cl₂, CH₃CN, Reflux overnight (b) NIS, CF₃COOH, reflux 3.5 h

2.2.1.2. Synthesis of precursors of octaalkoxy-substituted discotic nickel bisdithiolene complexes

2.2.1.2.1. Synthesis of 3,3',4,4'-tetraalkoxy-substituted benzils

The octaalkoxy-substituted benzil derivatives **5** are achieved by a double Friedel-Crafts reaction^[188-193] with oxalyl chloride as the acylation agent. This powerful reaction creates the 1,2-diketone function in only one step (Scheme 15).

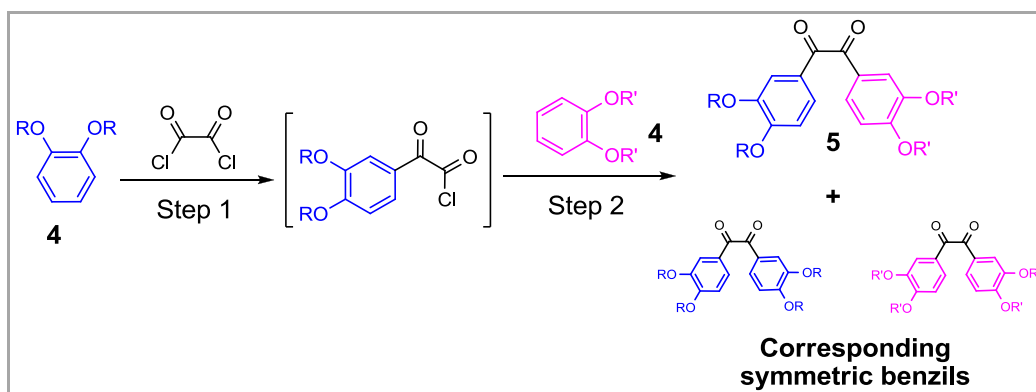


Scheme 15. Synthesis of 3,3',4,4'-tetraalkoxy-substituted benzils. Reagents and conditions:

- (i) RBr (2.4 equiv.), K₂CO₃ (3.0 equiv.), DMF, 90°C;
- (ii) ROH (2.4 equiv.), DEAD (2.4 equiv.), PPh₃ (2.4 equiv.), THF, 0°C then 1h at R.T.;
- (iii) Oxalyl chloride (0.6 equiv.), AlCl₃ (0.5 equiv.), 1,2-dichloroethane, 0°C then overnight at r.t.

The synthesis of benzils **5** starts by the preparation of 1,2-dialkoxybenzene **4** from pyrocatechol, a commercially available product. The desired linear and branched alkyl chains are grafted on the phenol functions by either the classical nucleophilic substitution (**4a-4b**, **4d-4e**) or the Mitsunobu method^[182, 183] (**4c**) depending on the commercial availability of the alkyl chains. The next step involves a double Friedel-Crafts acylation-type reaction using oxalyl chloride as the acylation agent and aluminum chloride as the promoter. In 1994, Mohr *et al.* developed this method for the synthesis of a series of tetraalkyl and alkoxy-substituted benzils with moderate yields.^[194] Based on this work, we were successful in preparing three 3,3',4,4'-tetraalkoxy-substituted benzils **5a-5c** in acceptable yields (Scheme 15). Although Mohr *et al.*^[194] reported that the use of two molar equivalents of AlCl₃ for one equivalent of oxalyl chloride is necessary for this reaction; we evidenced that only one equivalent is sufficient.

We then tried to perform the *in-situ* coupling of the intermediate complex acyl chloride with additional 1,2-dialkoxybenzene to prepare the asymmetrical 1,2-diketones following a one pot procedure as presented in Scheme 16 (see experimental section for more detail).



Scheme 16. Attempt of synthesis of asymmetrical benzils

However, mixtures of inseparable benzil derivatives were obtained. These mixtures are given in Table 5. From thin layer chromatography analysis, only one spot was observed under UV light exposure. This is due to very similar molecular weights and polarities of the products.

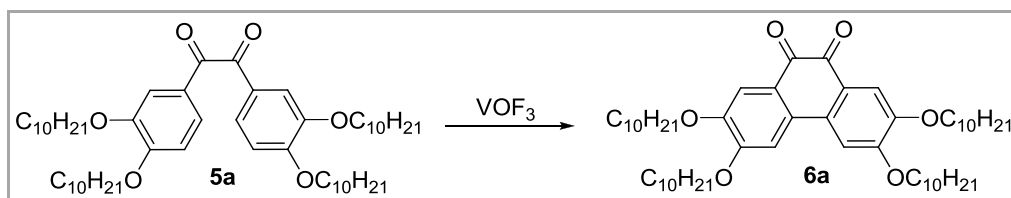
Table 5. Three mixtures of tetraalkoxy-substituted benzils

Mixtures	R	R'
M1	<i>n</i> -decyl	3,7-dimethyloctyl
M2	<i>n</i> -undecyl	3,7-dimethyloctyl
M3	<i>n</i> -undecyl	<i>n</i> -octyl

These mixtures were then analyzed by high-performance liquid chromatography. The results showed the presence of three benzils in each mixture with mass proportion *ca.* 1/2/1. These mixtures were neither further purified and nor characterized but transformed directly into mixtures nickel bisdithiolene complexes.

2.2.1.2.2. Synthesis of 2,3,6,7-tetraalkoxy-substituted phenanthrene-9,10-dione

The synthesis of 2,3,6,7-tetradecyloxy-substituted phenanthrene-9,10-dione is presented in Scheme 17.

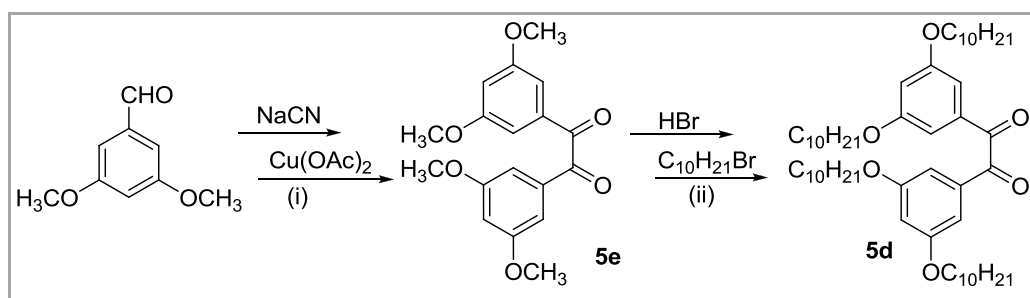


Scheme 17. Synthesis of tetradecyloxy-substituted phenanthrene-9,10-dione. Reagents and conditions: VOF_3 (3.3 equiv.), $\text{BF}_3 \cdot \text{OEt}_2$ (2.1 equiv.), CH_2Cl_2 , 30 minutes at r.t.

The intramolecular oxidative coupling with vanadium(V) oxyfluoride/boron trifluoride diethyl etherate of white solid **5a** results in the corresponding phenanthrene-9,10-dione derivative **6a**, recovered after chromatography, as a deep red solid in good yield (71%).^[194, 195]

2.2.1.2.3. Synthesis of 3,3',5,5'-tetraalkoxy-substituted benzils

The synthesis of 3,3',5,5'-tetradecyloxy-substituted benzils is depicted in Scheme 18.



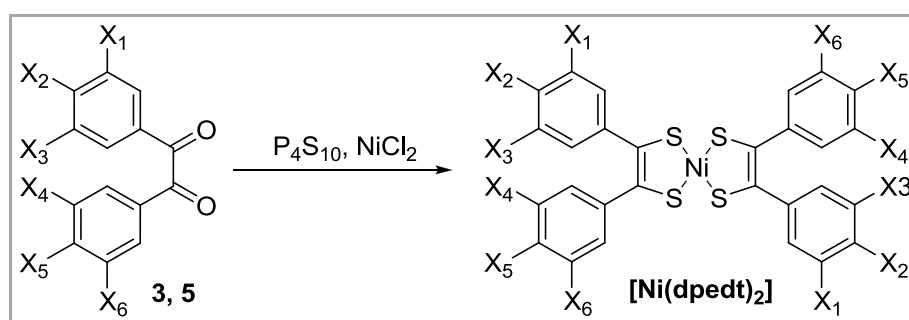
Scheme 18. Synthesis of 3,3',5,5'-tetraalkoxy-substituted benzil **5g**. Reagents and conditions: (i) 1) NaCN (0.4 equiv.), $\text{H}_2\text{O}/\text{EtOH}$ (1/2 v/v), reflux 36h 2) $\text{Cu}(\text{OAc})_2$ (0.01 equiv.), NH_4NO_3 (1.25 equiv.), $\text{AcOH}/\text{H}_2\text{O}$ (4/1 v/v), reflux 2h (ii) 1) HBr/AcOH (1/1 v/v), reflux 5h 2) Excess $\text{C}_{10}\text{H}_{21}\text{Br}$, K_2CO_3 , DMF, 18h at 90°C

This synthesis is performed following a route modified from Wenz^[196] and Ohta^[139] works. The benzoin condensation of 3,5-dimethoxybenzaldehyde catalyzed by sodium cyanide gives the corresponding benzoin. This later is not purified but is directly used in the next step. The cupric acetate catalytic oxidation of benzoin to benzil^[197] provides the 3,3',5,5'-tetramethoxy benzil **5e** in moderate yield after two steps (22 %). The benzil derivative **5e** is then demethylated by a mixture of bromic acid and acetic acid as described above, giving the 3,3',5,5'-tetrahydroxy benzil intermediate as a yellow solid. This later is then heated without any purification with a large excess of decyl bromide and potassium carbonate, providing the 3,3',5,5'-tetradecyloxy benzil **5d**. A yellow solid **5d** is obtained in 53 % yield after 2 steps of demethylation and alkylation from **5e**.

Globally, the desired benzil **5d** is achieved in 12 % yield from the commercially available 3,5-dimethoxybenzaldehyde.

2.2.2. Synthesis of nickel bisdithiolene complexes

As depicted in Scheme 19, the final neutral nickel complexes are achieved from the benzil precursors **3** and **5**. The transformation of these benzil derivatives into nickel bis(1,2-dithiolene) complexes is well known as a “one-pot” procedure.^[129, 198] The thionating reaction of the α -diketone **3** and **5** is performed by P_4S_{10} in boiling dioxane leading to thiophosphate ester intermediates.^[129] Recently, Arumugam *et al.*^[142] have demonstrated the preparation and isolation of stable thiophosphate ester consisting in the protected forms of 1,2-dithiolene ligands. According to our synthesis pathway, this thiophosphate ester is not isolated but directly hydrolyzed in the reaction medium. The hydrolysis followed by adding nickel salt in air conditions gives neutral $[Ni(dpdt)_2]$ derivatives after purification by repeated processes of precipitation and column chromatography. Almost nickel complexes are obtained in quite good yields (18-73%).



Scheme 19. Synthesis of neutral nickel bisdithiolene complexes. Reagents and conditions: P_4S_{10} (2.2 equiv.), Dioxane, Reflux 5h then adding $NiCl_2 \cdot 6H_2O$ (0.55 equiv.), H_2O , reflux 2h in air

By convention, all $[Ni(dpdt)_2]$ derivatives in the present work are presented as *trans* configuration as their exact configurations are not elucidated. These complexes are identified by usual analytical methods such as ¹H and ¹³C nuclear magnetic resonance, mass spectroscopy, electronic absorption spectroscopy and elemental analyses. All attempts to form suitable crystals for single crystal x-ray diffraction analysis failed.

2.2.2.1. Tetraalkoxy-substituted discotic nickel bisdithiolene complexes

Starting from twenty 4,4'-dialkoxy-substituted benzils **3a-3t**, twenty corresponding $[\text{Ni}(\text{dpedt})_2]$ derivatives, including seventeen new complexes, are synthesized and identified. The yields vary from 18 % for **BT65** to 73 % for **BT81**. These complexes are then divided into four groups depending on the alkyl chain lengths and configurations. The first group (Figure 34) is composed of three symmetric complexes which contain only linear alkyl chains. All of these three members of **Group 1** have been previously described in the literature.^[91] These complexes served as models for comparison and discussion of new compounds.

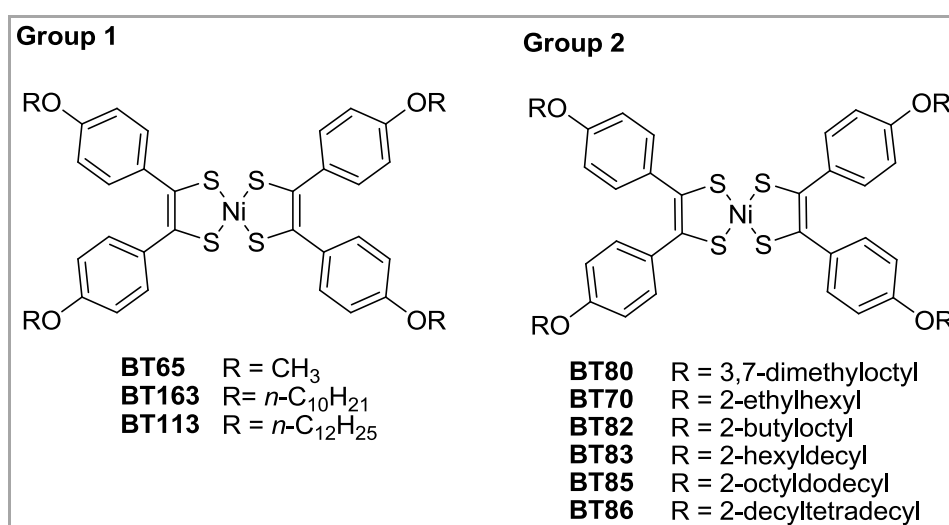


Figure 34. Structure of symmetric tetraalkoxy-substituted $[\text{Ni}(\text{dpedt})_2]$ in Groups 1 & 2

The second group is shown in Figure 34. It is composed of six other symmetric complexes substituted by long and branched alkyl chains which contains from 8 (2-ethylhexyl) to 24 (2-decyltetradecyl) carbons. None of these complexes in this group has ever been reported in the literature.

Both **Group 3** and **Group 4** contain asymmetric compounds as shown in Figure 35. The eleven new complexes are divided into two groups: the first one substituted by two methyl chains and two other long linear or branched one while the second one contains two kinds of long alkyl chains, different from methyl. ¹H NMR spectra of benzil derivatives and corresponding nickel complexes are similar. Two typical spectra are gathered in Figure 36: ¹H NMR spectra of 4-decyloxy-4'-methoxybenzil **3b** (Figure 36b) and the corresponding nickel dithiolene complex **BT71** (Figure 36a).

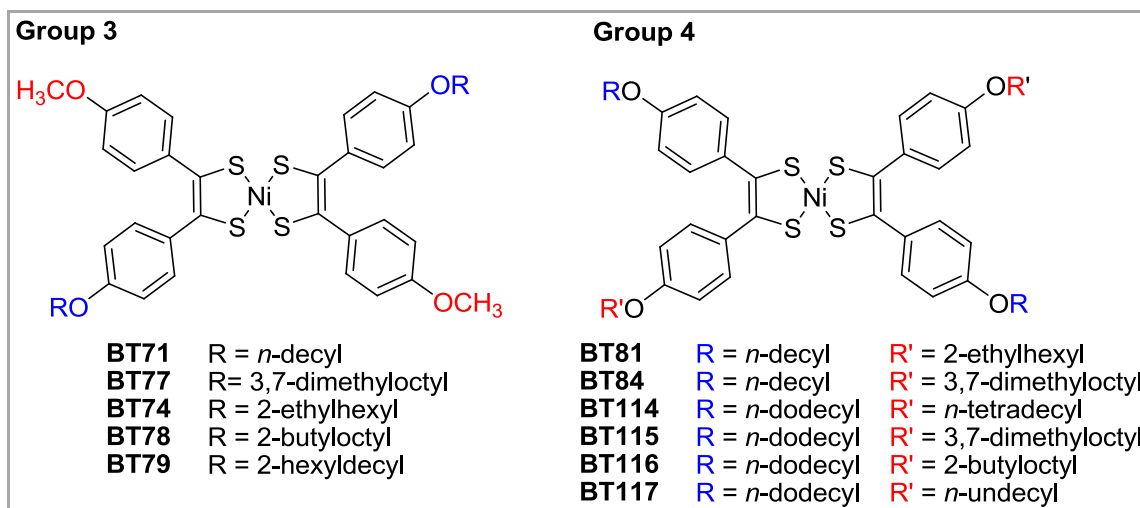


Figure 35. Structure of asymmetric tetraalkoxy-substituted [Ni(dpedt)₂] in Groups 3 & 4

As observed, the peaks corresponding to protons H_c (triplet) and H_d (singlet) are well distinguished, both in the case of benzil and dithiolene complex. In the aromatic region, the protons in the metal complex are shifted to higher fields. The metal bis(1,2-dithiolene) core is less electroattractive than the corresponding 1,2-diketonic group.

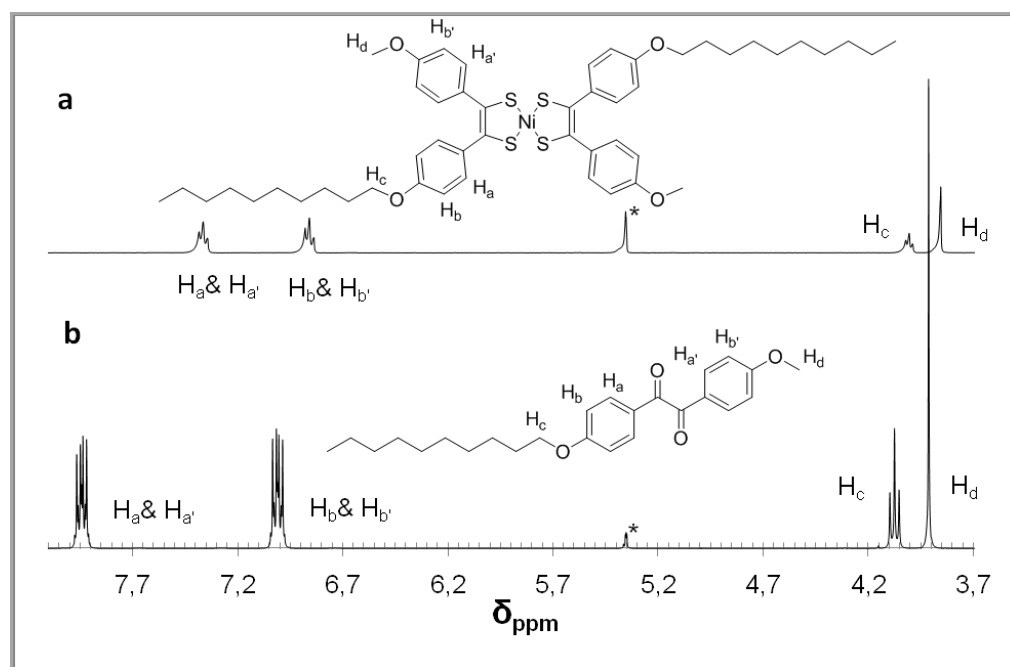


Figure 36. Partial ¹H NMR spectra of (a) complex BT71 and (b) 3b; the picks of CD₂Cl₂ solvent are stared.

In summary, twenty tetraalkoxy-substituted nickel bisdithiolene complexes have been synthesized and classed into four groups as a function of alkyl chain lengths and configurations. Three complexes in Group 1 were synthesized as models for the studies of other complexes. All the seventeen other ones have never been reported previously.

2.2.2.2. Halogen-substituted discotic nickel bisdithiolene complexes

Five halogenated benzils **3t-Br**, **3t-Br₂**, **3t-I₂**, **3t-I₃**, and **3t-I₄** are converted into nickel complexes in quite good yields (30-81%). All of them are obtained as black solids. Figure 37 shows the structures of these compounds (Group 5).

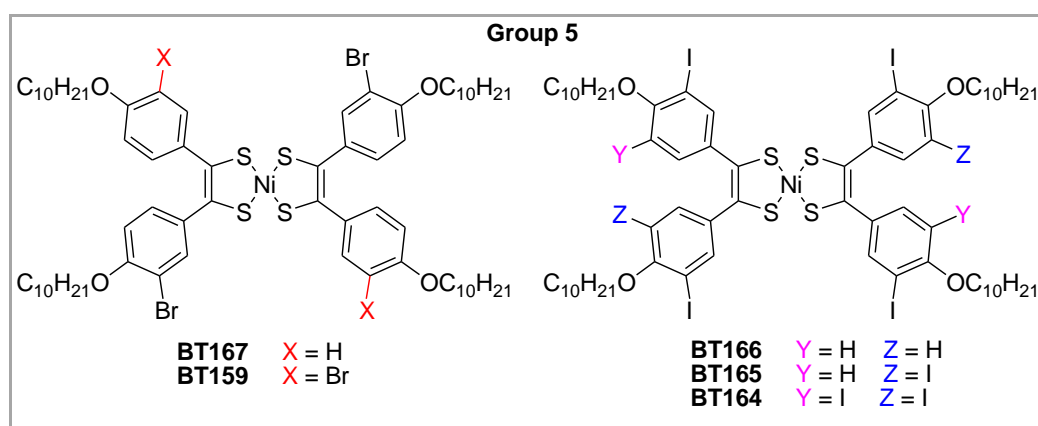


Figure 37. Structure of halogenated-substituted [Ni(dpdt)₂] in Group 5

2.2.2.3. Tetraalkanoate-substituted discotic nickel bisdithiolene complexes

This is the first time that tetraalkanoate-substituted [Ni(dpdt)₂] derivatives has been reported. The thionating reaction of the α -diketone **3t-Ester** by P₄S₁₀ followed by addition of NiCl₂ gives the desired nickel complexes in low yield. The complete treatment of the reaction mixture gives a black mixture of products. Repeated column chromatography purification gives two green compounds in small quantities. The structures of these complexes, named **BT153F1** and **BT153F2**, were elucidated by NMR and mass spectroscopy. As illustrated in Figure 38, one oxygen atom of the ester function of **BT153F2** is replaced by sulfur atom resulting in the **BT153F1**.

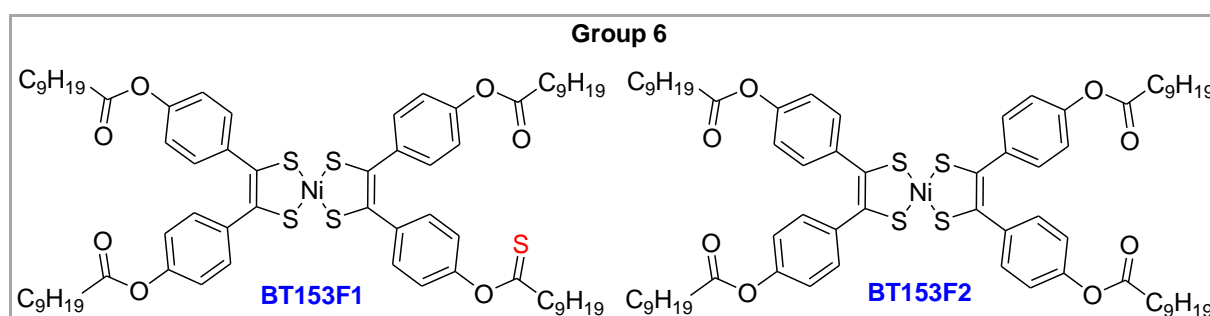


Figure 38. Structure of tetraalkanoyl-substituted [Ni(dpdt)₂]

Figure 39 presents partial ^1H NMR spectra of the precursor **3t-Ester** and of two corresponding complexes **BT153F1** and **BT153F2**. The spectrum of **BT153F2** is very similar to that of **3t-Ester**. Triplet and quintet signals are observed for two CH_2 groups in the α - and β -positions of the decanoate chains.

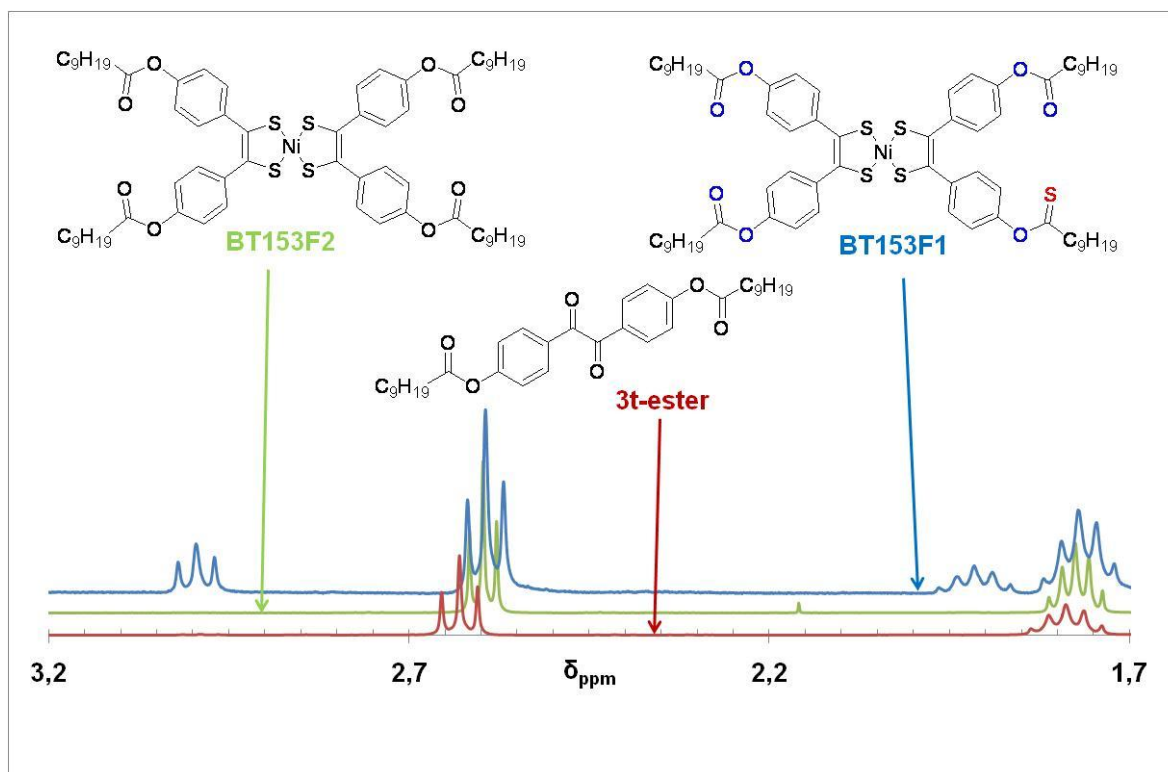


Figure 39. Partial ^1H NMR spectra of **3t-Ester**, **BT153F1** and **BT153F2**

The spectrum of **BT153F1** is somewhat more complicated. It clearly shows the dedoublement of the two signals of two CH_2 groups in the α - and β -positions of the decanoyl chains. Two triplet signals with integration proportion *ca.* 3/1, corresponding to 3 groups $-\text{CH}_2\text{C}(=\text{O})\text{O}-$ and 1 group $-\text{CH}_2\text{C}(=\text{X})\text{O}-$, respectively, and two quintet signals also with integration proportion *ca.* 3/1, corresponding to 3 groups $-\text{CH}_2\text{CH}_2\text{C}(=\text{O})\text{O}-$ and 1 group $-\text{CH}_2\text{CH}_2\text{C}(=\text{X})\text{O}-$, respectively, are observed. This suggests that one oxygen atom is replaced by sulfur atom ($\text{X}=\text{S}$). This is confirmed by the results of high resolution mass analysis and elemental analysis.

2.2.2.4. Octaalkoxy-substituted discotic nickel bisdithiolene complexes

The treatment of the four benzil derivatives **5a-5d** with P_4S_{10} and then NiCl_2 gives the four corresponding nickel bisdithiolene complexes as depicted in Figure 40. The complex **BT22** of

Group 7 was previously reported by Ohta *et al.*^[138-140] **BT22** is used as a model for studies of other complexes of this group.

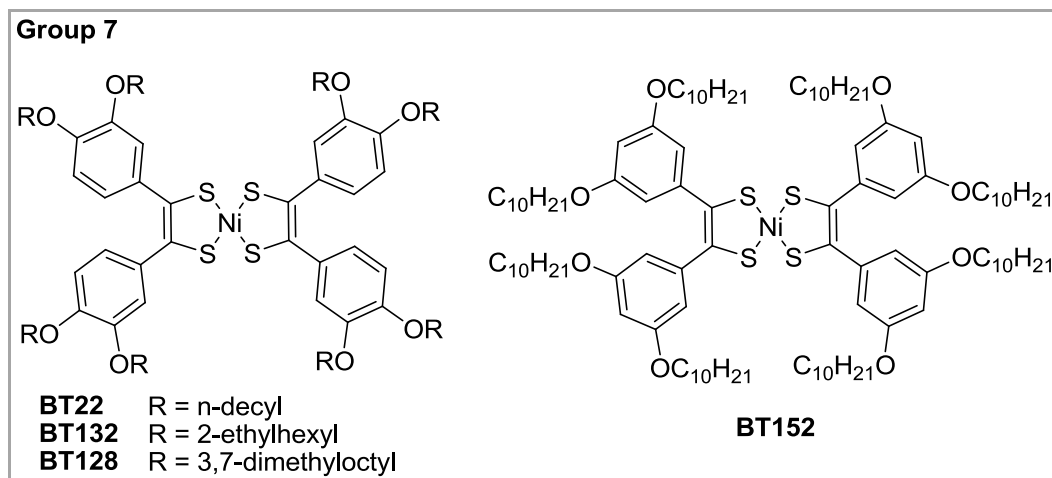
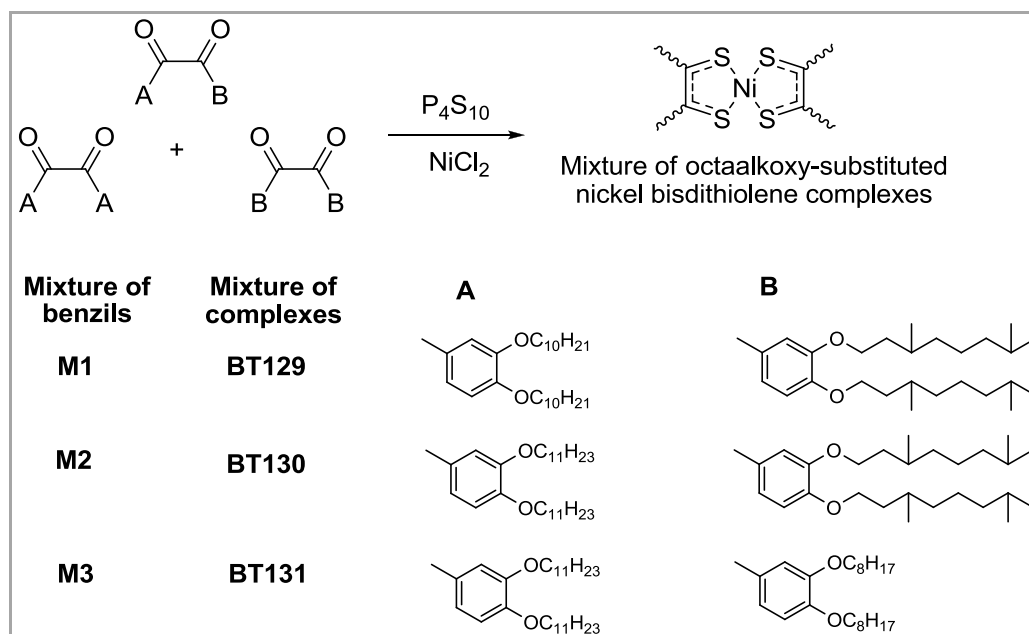


Figure 40. Structure of octaalkoxy-substituted [Ni(dpdt)₂]

Mixtures of octaalkoxy-substituted nickel bisdithiolene complexes

Three mixtures of tetraalkoxy-substituted benzils **M1**, **M2** and **M3** (Table 5) are transformed into three black mixtures of octaalkoxy-substituted nickel bisdithiolene complexes, called **BT129**, **BT130** and **BT131**, respectively (Scheme 20).



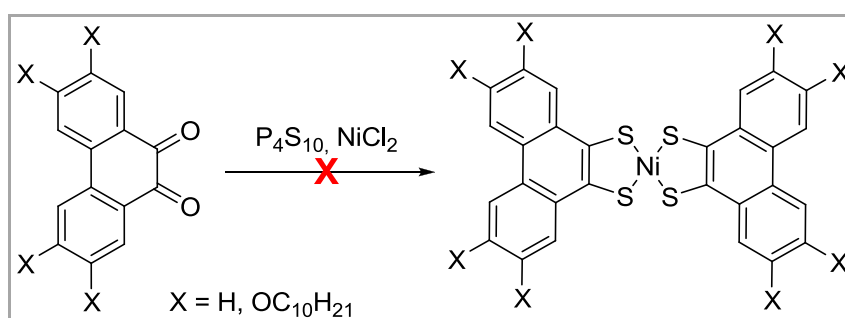
Scheme 20. Synthesis of mixtures of octaalkoxy-substituted nickel complexes

Theoretically, each of the three mixtures can be composed of up to 8 nickel complexes (cis/trans configuration is ignored). Byproducts and impurities are then eliminated by repeated precipitation

process from CH_2Cl_2 solution and repeated column chromatography using mixtures of hexane and CH_2Cl_2 as eluents. However, it is not possible to separate the nickel complex component of these mixtures. The typical mass spectra of benzil **5b** (Figure 83) and mixture of benzils **M3** (Figure 84) together with their corresponding nickel complex **BT132** (Figure 86) and mixture of complexes **BT131** (Figure 85) are given in experimental section. The thermal and physical properties of the three mixtures are then studied and will be discussed in a following section.

Nickel complexes based on phenanthrene-9,10-dithione ligand

All attempts to synthesize nickel complexes based on phenanthrene-9,10-dithione ligands with different reaction conditions failed (Scheme 21).



Scheme 21. Attempts to synthesize of nickel complexes based on phenanthrene-9,10-dithione ligands.

The reflux of 2,3,6,7-tetradecyloxy-substituted phenanthrene-9,10-dione **6a** or 9,10-phenanthrene-9,10-dione (commercial product) with P_4S_{10} using 1,4-dioxane or *o*-Xylene as solvent followed by adding of NiCl_2 does not give any trace of the desired products. In this case, it seems that P_4S_{10} is not powerful enough to perform the thionating reaction of phenanthrene-9,10-diones derivatives leading to dithiolene ligands. Due to the difficulty of the synthesis, the nickel complexes based on phenanthrene-9,10-dithione ligands are not further studied in the present work.

In conclusion, different synthetic pathways for nickel bisdithiolene complexes preparation were developed. Thirty-one compounds were designed, synthesized and characterized by usual structural analysis methods.

3. Physical properties and electronic applications

3.1. Physical properties of new neutral [Ni(dpedit)₂] derivatives

In order to envisage their use as active materials in organic electronics devices, physical properties of [Ni(dpedit)₂] derivatives have to be characterized. In this part of the thesis, the electrochemical, optical and thermal properties of all [Ni(dpedit)₂] derivatives will be provided and discussed.

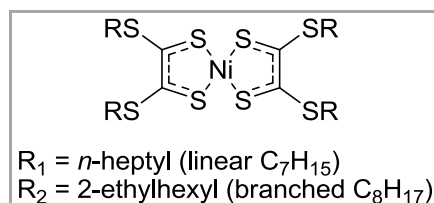


Figure 41. Structures of two nickel bisdithiolene complexes previously studied^[199]

Prior to the present work, we have reported^[199] on the electrochemical properties and electronic structures of two neutral long chain substituted nickel bisdithiolene complexes (Figure 41) owing to the non cyclic SR family^[8] and selected for their potential application in solar cells. Electrochemical and optical properties of these compounds have been fully examined in solution as well as in condensed state by different methods and techniques and the results are in very good consistency. That makes nickel bisdithiolene complexes becoming very attractive for organic photovoltaic applications.^[199] In this work, we now concentrate our investigations on the electrochemical and optical properties of [Ni(dpedit)₂] derivatives in solution. These measurements will allow determining the principal parameters such as electron affinity, ionization potential, optical and electrochemical bandgap. The influence of the different kinds of side chains (their length, configuration, etc) on these characteristics will be studied.

3.1.1. Electrochemical properties

The electrochemical properties of these long chain substituted [Ni(dpedit)₂] complexes are fully investigated by cyclic (CV) and square wave (SWV) voltammetries. The experiments are performed in dichloromethane solution with standard saturated calomel (SCE) reference electrode, using both platinum metal (Pt) and glassy carbon (GC) working electrodes. In some case on platinum metal electrode, we record irreversible redox processes and the results

are somewhat less exploitable than those issued from using glassy carbon one. However, they remain in very good accordance. In the following paragraph, the full results obtained with a typical nickel bis-dithiolene complex, the tetra(2-ethylhexyloxy)-substituted $[\text{Ni}(\text{dpedt})_2]$ **BT70** (Figure 42), are detailed and discussed. For all other complexes, only the results obtained from cyclic voltammetry are discussed. All measurements were carried out at room temperature. Error on the mesuarement is 5 mV. The chemical structure of **BT70** is showed in (Figure 42). Its cyclic voltammogram recorded in dichloromethane solution using $(\text{Bu}_4\text{N})\text{PF}_6$ electrolyte with glassy carbon working electrode between -1.3 and +1.4 V versus saturated calomel reference electrode is shown in Figure 42. The measurement starts from the potential drop of the solution which is located around 0.2 V/SCE.

As observed from Figure 42, three reversible redox processes are observed. The nature of these monoelectronic electrochemical reactions is described in Scheme 22, assuming that they have the same nature as those of the two other neutral nickel bisdithiolene complexes recently studied.^[199]

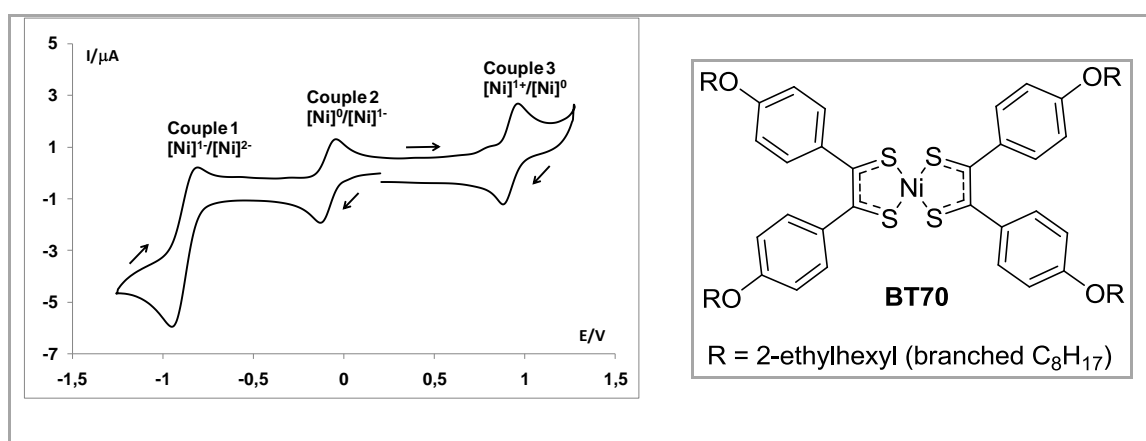
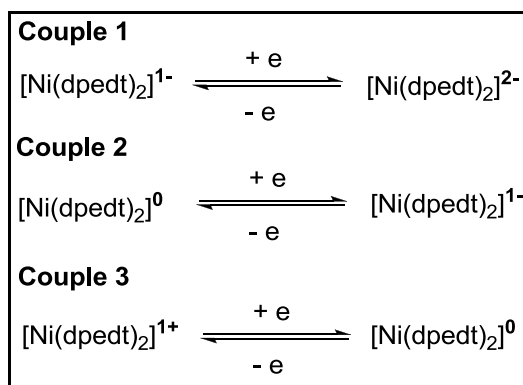


Figure 42 Cyclic voltammogram of BT70, solvent: CH_2Cl_2 , electrolyte: $(\text{Bu}_4\text{N})\text{PF}_6$ (0.1 mol.L⁻¹), working electrode: glassy carbon, reference electrode: standard SCE at rt (scan rate 0.1 V/s).



Scheme 22. Electrochemical reactions of nickel bisdithiolene complexes

In reduction, two successive waves near -0.1 and -0.8 V/SCE correspond to the first and the second 1-electron reduction (respectively, Couple 2 and Couple 1^[199] in Scheme 22 and Figure 42). In oxidation, the first 1-electron oxidation is observed near 1.0 V (Couple 3^[199] in Scheme 22 and Figure 42). Electrochemical bandgap, determined from the half wave potentials of Couple 3 and Couple 2 in cyclic voltammetry measurement, is around 1.01 V. Table 6 summarizes the full electrochemical data corresponding to Couple 2 and Couple 3 of **BT70**.

Table 6. Half wave potentials (V/SCE) of BT70 obtained by SWV and CV in CH₂Cl₂ solution with (Bu₄N)[PF₆] (0.1 mol L⁻¹) electrolyte on Pt and GC electrodes. ΔE (V) = $E_{1/2}^3 - E_{1/2}^2$

Pt electrode					
CV			SWV		
$E_{1/2}^2$	$E_{1/2}^3$	ΔE_{CV}	$E_{1/2}^2$	$E_{1/2}^3$	ΔE_{SWV}
-0.10	0.93	1.02	-0.11	0.99	1.10
GC electrode					
CV			SWV		
$E_{1/2}^2$	$E_{1/2}^3$	E_{CV}	$E_{1/2}^2$	$E_{1/2}^3$	ΔE_{SWV}
-0.09	0.92	1.01	-0.10	0.94	1.05

Obviously from Table 6, electrochemical properties of **BT70** do not depend on the nature of working electrode, platinum metal or glassy carbon. The results are also reproducible whether using cyclic voltammetry or square wave voltammetry. We thus decided to pursue the electrochemical studies by using only glassy carbon working electrode.

3.1.1.1. Tetraalkoxy-substituted [Ni(dpedit)₂]

The structure of the other tetraalkoxy-substituted [Ni(dpedit)₂] derivatives are given in the synthesis section (2.2.2.1). Table 7 summarizes the electrochemical data of all complexes, obtained by cyclic voltammetry and square wave voltammetry using glassy carbon working electrode and standard saturated calomel electrode as reference.

Similar results are obtained whatever the tetraalkoxy-substituted [Ni(dpedit)₂] derivatives. All the redox processes are reversible. The redox potentials and the electrochemical bandgaps, calculated according to the equation: ΔE (V) = $E_{1/2}^3 - E_{1/2}^2$, of tetraalkoxy-substituted [Ni(dpedit)₂] derivatives are detailed in Table 7.

Table 7. Half wave redox potentials (V/SCE) for tetraalkoxy-substituted [Ni(dpdt)₂] derivatives obtained by CV and SWV in (Bu₄N)[PF₆] (0.1 mol L⁻¹) solution in CH₂Cl₂, ΔE(V) = E_{1/2}³ - E_{1/2}²

Complexes	Group	CV			SWV		
		E _{1/2} ²	E _{1/2} ³	ΔE _{CV} ^a	E _{1/2} ²	E _{1/2} ³	ΔE _{SWV} ^a
BT65	G1	-0.08	0.93	1.01	-0.09	0.93	1.02
BT163		-0.09	0.91	1.00	-0.11	0.94	1.04
BT113		-0.10	0.91	1.01	-0.11	0.93	1.04
BT70	G2	-0.09	0.92	1.01	-0.10	0.94	1.05
BT80		-0.10	0.91	1.00	-0.11	0.95	1.04
BT82		-0.11	0.92	1.03	-0.11	0.95	1.06
BT83		-0.09	0.91	1.00	-0.11	0.94	1.05
BT85		-0.04	1.00	1.04	-0.06	1.03	1.09
BT86		-0.11	0.92	1.03	-0.11	0.97	1.08
BT71	G3	-0.09	0.91	1.01	-0.10	0.92	1.02
BT74		-0.10	0.93	1.02	-0.10	0.94	1.04
BT77		-0.10	0.92	1.01	-0.11	0.93	1.04
BT78		-0.11	0.90	1.01	-0.12	0.92	1.03
BT79		-0.09	0.91	1.00	-0.10	0.93	1.04
BT81	G4	-0.09	0.90	0.99	-0.09	0.92	1.01
BT84		-0.03	0.98	1.01	-0.09	1.00	1.09
BT114		-0.11	0.91	1.02	-0.12	0.93	1.05
BT115		-0.11	0.89	1.00	-0.12	0.95	1.06
BT116		-0.12	0.91	1.02	-0.13	0.93	1.05
BT117		-0.11	0.92	1.03	-0.12	0.93	1.05

Generally, the value of the half wave potential of the first 1-electron reduction of all tetraalkoxy-substituted [Ni(dpdt)₂] is slightly less positive than that of the [Ni(dpdt)₂] core complex, (E_{1/2}^{red} = 0.03 V/SCE in CH₂Cl₂^[91] or E_{1/2}^{red} = 0.02 V/Ag/AgCl in benzonitrile^[159]). This difference is attributed to the mesomeric electron donating effect of the alkoxy substituents which weakens the electron accepting ability of nickel bisdithiolene complexes.

3.1.1.1.1. Influence of alkoxy chain lengths

Ohta *et al.* have studied the influence of the linear alkyl chain length on the electrochemical properties of tetraalkyl-substituted and tetraalkoxy-substituted [Ni(dpdt)₂]^[91]. They claim that the reduction potentials of these complexes are nearly constant irrespective of the alkyl

or alkoxy chain length.^[91] In this work, we are interested in the influence of both linear and branched alkyl chain lengths on the redox properties.

Group 1: each of three members of this group is substituted by four linear alkoxy chains. The redox electrochemical properties of **BT65** (four methoxy), **BT163** (four *n*-decyloxy), and **BT113** (four *n*-dodecyloxy) are given in Table 7. By comparing the measured potentials, the complexes have nearly the same redox properties. In cyclic voltammetry measurements, for example, the half wave potential of the first 1-electron reduction changes slightly from 0.08 V (chain: methoxy) to 0.09 V (chain: *n*-decyloxy) and 0.10 V (chain: *n*-dodecyloxy). The absence of major variation shows the independence of redox properties on the linear chain length. This finding is in accordance with reported data for these compounds.^[91, 144]

Group 2: prior to our work, none of the six members of Group 2 (**BT80**, **BT70**, **BT82**, **BT83**, **BT85** and **BT86**) has ever been described. Each compound is substituted by four branched alkoxy chains. Their electrochemical properties are summarized in Table 7. It appears that the half wave potential of the first 1-reduction of these complexes is nearly unchanged, except for **BT85** for which small increases of values of both redox potentials are observed while the electrochemical bandgap remains unchanged in comparison with the other complexes of the subseries. It is noteworthy that the alkyl chain length varies from 2-ethylhexyl (8 carbons) in **BT70** to 2-decyltetradecyl (24 carbons) in **BT86**. However, no important reduction potential change is observed. This means that, similarly to Group 1 complexes, the length of alkyl chains has no important impact on electrochemical properties of Group 2 complexes.

Group 3: the five members of Group 3 (**BT71**, **BT77**, **BT74**, **BT78** and **BT79**) are also new compounds. Each of them contains two methoxy and two other long, linear or branched, alkoxy chains. Their structures are given in the synthesis section and the electrochemical properties are summarized in Table 7. As can be observed, the reduction potentials vary insignificantly. The redox properties of these compounds seem to be independent on the alkyl chain length as for Groups 1 and 2 complexes.

3.1.1.1.2. Influence of alkoxy chain configurations

BT80 (Group 2) and **BT163** (Group 1) differentiate from each other by the configuration of decyl chains: linear in **BT163** and branched in **BT80**. From the data in Table 7, one can

observe that they have the same electrochemical properties, either redox properties or bandgaps, measured both from cyclic and square wave voltammetries. This observation suggests that the electrochemical properties of such tetraalkoxy-substituted $[\text{Ni}(\text{dpedt})_2]$ do not depend on the configuration of alkyl chains. This assumption can be corroborated by further comparisons of **BT82** *versus* **BT113** (same dodecyloxy chains), **BT71** *versus* **BT77** (same decyloxy chains). These couples are substituted by the same alkoxy chains but with different configurations. Thus, one can conclude that the alkoxy chain lengths and configurations do not have any impact on the electrochemical properties of tetraalkoxy-substituted $[\text{Ni}(\text{dpedt})_2]$.

3.1.1.1.3. Influences of symmetry, asymmetry and *cis/trans* mixtures

As discussed in the synthesis section, neither the absolute configurations (*cis/trans*) of asymmetric complexes (Groups 3 and 4) nor the composition of these *cis/trans* mixtures are elucidated. Each member of Group 3 is substituted by two methoxy chains and two other long linear or branched alkoxy chains. In Group 4, the $[\text{Ni}(\text{dpedt})_2]$ core is grafted by two kinds of long alkoxy chains, and different from methoxy. One can consider complexes in Group 4 as intermediate between Group 1 (substituted only by linear chains) and Group 2 (substituted only by branched chains) complexes. These complexes are so-called “asymmetric” due to the difference in alkoxy chain lengths and configurations. Table 7 summarizes the electrochemical data of the members of Group 4 (**BT81**, **BT84**, **BT114**, **BT115**, **BT116**, and **BT117**). The electrochemical properties of these compounds are nearly similar, except for **BT84**. For this compound, as in the case of **BT85**, one observes small increase of values of both redox potentials but the electrochemical bandgap remains unchanged in comparison with the others. All these comments are linked with the non-influence of the symmetry/asymmetry nor the *cis/trans* factors on the electrochemical properties of these tetraalkoxy-substituted $[\text{Ni}(\text{dpedt})_2]$.

In conclusion, the electrochemical properties of tetraalkoxy-substituted $[\text{Ni}(\text{dpedt})_2]$ are independent of the alkyl chain length and configuration. They are also independent of the symmetry or configuration of complexes. The experimental values are in good agreement with those reported in the literature.^[91] For all complexes and whatever the measurement method, electrochemical bandgaps are of about 1.05 ± 0.04 V. The values of the first 1-electron reduction, -0.03 to -0.12 V *versus* SCE in CH_2Cl_2 , observed for these complexes are less positive than that of the $[\text{Ni}(\text{dpedt})_2]$ core complex ($E_{\text{red}}^{1/2} = 0.03$ V/SCE in CH_2Cl_2).^[91]

This difference is attributed to the mesomeric electron donating effect of the alkoxy substituent, which increases the electron density on these complexes. As a consequence, the electron-attracting properties of these compounds are slightly decreased.

3.1.1.1.4. Influence of connecting-group on the tetra long chain substituted series

In the previous paragraph, the influence of the length and configuration of the side chains has been mentioned and discussed through twenty complexes, including seventeen new compounds. Ohta *et al.* have demonstrated that the replacement of alkoxy substituents by the alkyl ones causes moderate variation on the electrochemical properties of the tetra long chain substituted $[\text{Ni}(\text{dpedt})_2]$.^[91] This is due to the difference of the nature of the connecting group: -O- in the case of alkoxy substituents and -CH₂- in the case of alkyl substituents. For the purpose of the study of connecting group influence, **BT153F1** and **BT153F2** complexes have been synthesized. The synthesis of these two compounds is fully discussed in the synthesis section. **BT153F2** differentiates from **BT163** by the nature of the connecting group (-O- is replaced by -OC(=O)-, which is more electron withdrawing whereas the chain length remains unchanged (10 carbons in the side chain backbones in both compounds, the carbon atoms of ester functions included). **BT153F1**, in which one oxygen atom of one ester function has been sulfonated, is isolated as an accidental byproduct during the synthesis of **BT153F2**. Table 8 sums up the electrochemical properties of these compounds with those of **BT163** as reference.

Table 8. Electrochemical properties (V/SCE) of **BT153F1** and **BT153F2** versus **BT163**,

$$\Delta E = E_{1/2^3} - E_{1/2^2}$$

Complexes	CV			SWV		
	$E_{1/2^2}$	$E_{1/2^3}$	ΔE_{CV}	$E_{1/2^2}$	$E_{1/2^3}$	ΔE_{SWV}
BT163	-0.09	0.91	1.00	-0.11	0.94	1.04
BT153F1	0.04	1.18	1.14	0.03	1.21	1.18
BT153F2	0.05	1.17	1.13	0.03	1.21	1.18

The replacement of *n*-decyloxy substituent by *n*-decanoate slightly increases the values of both **BT153F2** reduction and oxidation potentials in comparison with those of **BT163** (Table 8). This is attributed to the electron attracting effect of the decanoate chain which decreases

the electron density on the complexes. As a consequence, the $E_{1/2}^2$ value of **BT153F2** increases to 0.05 V in cyclic voltammetry and 0.03 V in square wave voltammetry. The decanoate chains slightly broaden (130 mV) the electrochemical bandgap of the corresponding compound in comparison to **BT163**. The experimental values of **BT153F1** are nearly identical to those of **BT153F2**. The replacement of one oxygen atom in **BT153F2** by a sulfur atom has a negligible influence on the electrochemical properties of the complex. In conclusion, the electrochemical properties of tetra long chain substituted $[\text{Ni}(\text{dpedt})_2]$ depend slightly on the nature of the connecting group.

3.1.1.1.5. Influence of the dpedt ligand's halogenations

As discussed in the materials design, the introduction of halogen atoms such as bromine and iodine on the phenyl rings of dpedt ligands is expected to have important influence on the physical properties of long chain substituted $[\text{Ni}(\text{dpedt})_2]$. The substitution of hydrogen atoms by more electron attractive ones and disposing empty d orbitals such as bromine and iodine atoms should modify the electronic properties of targeted complexes. The structures of complexes based on halogenated dpedt ligands are provided in the synthesis section.

The redox properties of these compounds are summed up in Table 9. The number of halogen atoms in each compound is given in the second column from the left of Table 9. All electrochemical reactions are monoelectronic and reversible. The measured results of cyclic voltammetry and square wave voltammetry are in good accordance. The redox potentials and electrochemical bandgaps issued from cyclic voltammetry studies are schematically presented in Figure 43 and Figure 44, respectively to **BT163** as reference.

Table 9. Electrochemical data of complexes based on halogenated ligands (**Group 5**) versus **BT163**,

$$\Delta E \text{ (V)} = E_{1/2}^3 - E_{1/2}^2$$

Complexes	N° X	CV			SWV		
		$E_{1/2}^2$	$E_{1/2}^3$	ΔE_{CV}	$E_{1/2}^2$	$E_{1/2}^3$	ΔE_{SWV}
BT163	0	-0.09	0.91	1.00	-0.11	0.94	1.04
BT167	2 Br	-0.04	0.97	1.01	-0.05	0.98	1.03
BT159	4 Br	0.01	1.04	1.03	0.01	1.07	1.06
BT166	4 I	0.01	1.02	1.01	0.00	1.06	1.06
BT165	6 I	0.09	1.17	1.08	0.07	1.19	1.12
BT164	8 I	0.18	1.32	1.14	0.17	1.36	1.19

As mentioned in Table 9, Figure 43 and Figure 44, the halogenations of dpedt ligands by bromine and iodine atoms increase the values of both redox processes and electrochemical bandgap, visually as a linear function of the total number of halogen atoms.

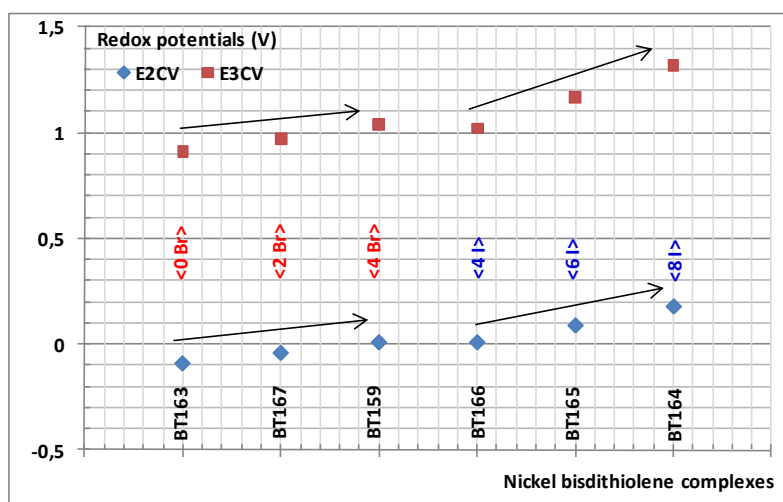


Figure 43. Schematic presentation of redox properties issued from CV of complexes based on halogenated ligands vs BT163

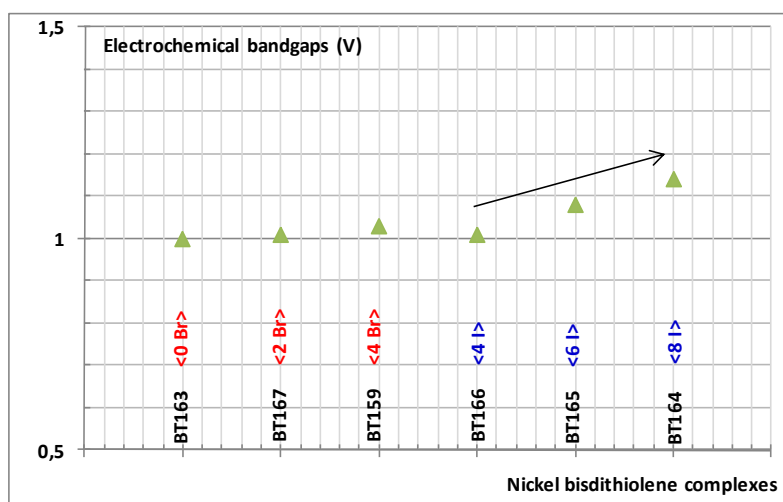


Figure 44. Schematic presentation of energy bandgap issued from CV of complexes based on halogenated ligands vs BT163

The replacement of two hydrogen atoms by two bromine atoms results in **BT167**. The electron acceptor property of this compound increases very slightly in comparison with the parent complex **BT163**. The electrochemical bandgap also changes slightly. If two more hydrogen atoms are replaced (**BT159**), the electron affinity and ionization potentials of the complex, expressed by the $E_{1/2}^2$ and $E_{1/2}^3$ values, show more significant variation (100 mV in comparison with **BT163**), whereas the corresponding electrochemical bandgaps slightly changes. The tendency to increase of redox potentials and electrochemical bandgaps are

demonstrated by black arrows in Figure 43 and Figure 44. The replacement of four hydrogen atoms by four iodine atoms gives **BT166**. The properties of this compound are provided in Table 9 and are nearly identical to those of **BT159**. This is due to the small difference of electron affinity between the two elements. When the number of iodine atoms in the complex increases, one clearly observes the linear increasing of both redox properties and bandgap energies as a function of the iodine atoms number as demonstrated by black arrows in Figure 43 and Figure 44. The more iodine atom is abundant, the stronger the electron accepting property of tetra long chain substituted $[\text{Ni}(\text{dpedt})_2]$ is. The adding of iodine atoms on the phenyl ring modifies the electrochemical properties of $[\text{Ni}(\text{dpedt})_2]$ derivatives.

Generally, we show that adding halogen atoms to dpedt ligand is a general, effective route, towards the modulation of the redox properties of tetra long chain substituted $[\text{Ni}(\text{dpedt})_2]$ without major change of their electrochemical bandgaps. This interesting finding opens the way to modulate the energy levels of $[\text{Ni}(\text{dpedt})_2]$ derivatives based semiconducting materials for organic electronic applications.

3.1.1.2. Octaalkoxy-substituted $[\text{Ni}(\text{dpedt})_2]$

The full presentation of chemical structures of octaalkoxy-substituted $[\text{Ni}(\text{dpedt})_2]$ can be found in the synthesis section. The electrochemical data of these $[\text{Ni}(\text{dpedt})_2]$ derivatives are gathered in Table 10.

Table 10. Electrochemical data of octaalkoxy-substituted $[\text{Ni}(\text{dpedt})_2]$. ΔE (V) = $E_{1/2}^3 - E_{1/2}^2$

Complexes	CV			SWV		
	$E_{1/2}^2$	$E_{1/2}^3$	ΔE_{CV}	$E_{1/2}^2$	$E_{1/2}^3$	ΔE_{SWV}
BT22	-0.10	-	-	-0.11	0.92	1.03
BT152	-0.01	-	-	-0.03	1.28	1.31
BT128	-0.10	-	-	-0.11	0.96	1.07
BT132	-0.12	-	-	-0.13	0.93	1.06

The results issued from cyclic and square wave voltammetry experiments are in good consistency with data reported elsewhere.^[139, 140] The first 1-electron oxidation processes of these compounds are irreversible both with platinum metal or glassy carbon working electrodes, except for **BT152**. Due to the irreversibility of the first 1-electron oxidation

process, the cyclic voltammetry electrochemical bandgap of these compounds is undeterminable. Analyzing and comparing the electrochemical data of octaalkoxy-substituted [Ni(dpdt)₂] **BT22**, **BT128** and **BT132** summed up in Table 10, it can be deduced that their electrochemical properties depend neither on the alkyl chain length nor on their configuration.

BT152 differentiates from its **BT22** analogue by the position of *n*-decyloxy chains on the peripheral phenyl rings of dpdt ligand (Figure 45).

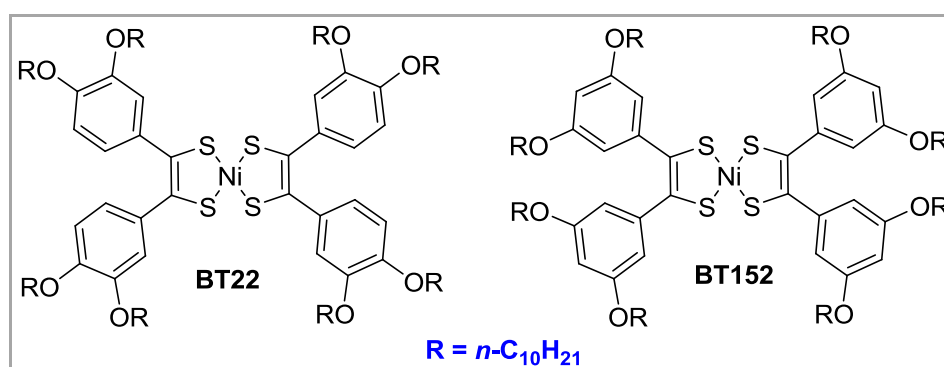


Figure 45. Chemical structures of **BT22** and **BT152**

It is observed from Table 10 a significant variation of electrochemical properties of **BT152** to those of **BT22**. The first 1-electron reduction potentials are -0.10 V (cyclic voltammetry) and -0.11 V (square wave voltammetry) for **BT22**. Meanwhile those values are -0.01 V (cyclic voltammetry) and -0.03 V (square wave voltammetry) for **BT152**. This means that the electron affinity of **BT152** is stronger than that of **BT22**. The ionization potential of **BT152** is also higher than that of **BT22**. The electrochemical bandgaps of **BT152** raises to 1.31 V (square wave voltammetry). It is well known that for [Ni(dpdt)₂] derivatives (or their heteroaromatic analogues), there is a large steric constraint on the ligand and two phenyl (or heteroaromatic) pendent groups are out-of-plane twist as approved by X-ray crystal structures.^[144, 150, 165, 200, 201] This has an important impact on the electrochemical properties of nickel bisdithiolene complexes. For systems where this steric constraint is reduced, or removed altogether, better electronic communication between the dithiolene core and the (hetero)aromatic pendent groups of the ligands is achieved by the free rotation of the pendent groups. In this case, when the position of substituents on the phenyl peripheric moieties is changed from “3,4” in “traditional” octaalkoxy-substituted [Ni(dpdt)₂] (**BT22**, **BT128**, **BT132**) to “3,5” in “new designed” octaalkoxy-substituted [Ni(dpdt)₂] (**BT152**, Figure 45), the two phenyl rings of dpdt ligand should be much more twisted due to highly steric constraint. As a consequence, the electronic communication between the phenyl rings

and the bisdithiolene complex core should be reduced compared to “traditionnal” octaalkoxy-substituted complexes. The bad electronic communication between phenyl rings and bisdithiolene core is responsible for better electron accepting property found in **BT152**. Another reason is the absence of electron-donating group in *para* position. This very interesting result is further confirmed by optical measurement which is discussed in the next section.

In conclusion, the results of electrochemical measurements show that the size as well as the configuration of alkoxy chains, the number of substituent grafted on dpedt ligands, and the symmetry of complexes do not influence significantly electrochemical properties in the alkoxy-substituted $[\text{Ni}(\text{dpedt})_2]$ series. This is a very interesting result because the mesomorphic properties of the complexes depend on the alkoxy chain length and configuration in contrast to redox potentials. Therefore, we can act on the nature of the peripheral chains to obtain the mesomorphic properties without changing the electrochemical properties, *i.e.* molecular energy levels. Partial claim concerning this series of $[\text{Ni}(\text{dpedt})_2]$ are also reported by Ohta *et al.*^[91, 140] Meanwhile, the halogenations of dpedt ligand and the change of connecting groups have moderate influence on the electrochemical properties of target compounds. This opens the way to design and synthesize new $[\text{Ni}(\text{dpedt})_2]$ based semiconducting materials for organic electronic applications.

3.1.1.3. Energy level engineering

To a first approximation, the reduction potential can be related to the electron affinity and thus to the LUMO energy level according to the following equation: $\text{EA} (E_{\text{LUMO}}) = -(E_{1/2}^2 + 4.8)$.^[202-205] A similar relationship can be used for the oxidation potential, the ionization potential, and HOMO energies: $\text{IP} (E_{\text{HOMO}}) = -(E_{1/2}^3 + 4.8)$.

3.1.1.3.1. Tetraalkoxy-substituted $[\text{Ni}(\text{dpedt})_2]$

The HOMO and LUMO energy levels and energy bandgaps ($E_{\text{g}}^{\text{el}}(\text{eV}) = E_{\text{LUMO}} - E_{\text{HOMO}}$) of the tetraalkoxy-substituted $[\text{Ni}(\text{dpedt})_2]$ are determined (Table 11) from the values of cyclic voltammetry redox potentials given in Table 7.

As can be observed, the LUMO and HOMO levels of tetraalkoxy-substituted $[\text{Ni}(\text{dpedt})_2]$ are of about -4.7 and -5.7 eV, respectively. The energy bandgap is about 1.0 eV. This result indicates

that the side chain has no influence on the HOMO-LUMO energy levels although it could play a crucial role in the molecular packing.

Table 11. LUMO and HOMO energy levels of tetraalkoxy-substituted [Ni(dpdt)₂]

Complexes	E _{LUMO}	E _{HOMO}	E _g ^{el}	Complexes	E _{LUMO}	E _{HOMO}	E _g ^{el}
	eV	eV	eV		eV	eV	eV
BT65	-4.7	-5.7	1.0	BT74	-4.7	-5.7	1.0
BT163	-4.7	-5.7	1.0	BT77	-4.7	-5.7	1.0
BT113	-4.7	-5.7	1.0	BT78	-4.7	-5.7	1.0
BT70	-4.7	-5.7	1.0	BT79	-4.7	-5.7	1.0
BT80	-4.7	-5.7	1.0	BT81	-4.7	-5.7	1.0
BT82	-4.7	-5.7	1.0	BT84	-4.8	-5.8	1.0
BT83	-4.7	-5.7	1.0	BT114	-4.7	-5.7	1.0
BT85	-4.8	-5.8	1.0	BT115	-4.7	-5.7	1.0
BT86	-4.7	-5.7	1.0	BT116	-4.7	-5.7	1.0
BT71	-4.7	-5.7	1.0	BT117	-4.7	-5.7	1.0

The high electron affinities (-4.7 eV) and ionization potentials (-5.7 eV) of these compounds are in the same order as that of fullerene derivatives.^[66, 206-208] That makes these compounds very attractive for photovoltaic applications. In the past decade, many works have been devoted to organic solar cells based on the bulkheterojunction concept because of their ease of processing, mechanical flexibility, and potential low cost. The most popular blends are a mixture of poly (3-hexylthiophene) (P3HT) and (1-[3-(methoxycarbonyl)propyl]-1-phenyl-[6,6]C₆₀) (PCBM). The best yields of bulkheterojunction solar devices employing this P3HT:PCBM combination is now about 5%.^[209] Nowadays, many works focus on the improvement of organic solar cells by lowering the material bandgap.^[65, 207, 210] In this context, the use of nickel bisdithiolene complexes is a good alternative to that of PCBM as acceptor by shifting the material absorption to the red or even to the near infrared part of the spectrum.

3.1.1.3.2. Halogenated [Ni(dpdt)₂]

The HOMO and LUMO energy levels derived from cyclic voltammetry measurements are given in Table 12 for halogenated complexes. When comparing these results to those of the parent complex **BT163**, the introduction of halogen atoms on the peripheral phenyl rings of dpdt ligands lowers slightly both HOMO and LUMO levels.

Table 12. LUMO and HOMO energy levels and bandgaps of halogenated [Ni(dpdt)₂]

Complexes	E _{LUMO}	E _{HOMO}	E _g ^{el}
	eV	eV	eV
BT163	-4.7	-5.7	1.0
BT167	-4.8	-5.8	1.0
BT159	-4.8	-5.8	1.0
BT166	-4.8	-5.8	1.0
BT165	-4.9	-6.0	1.1
BT164	-5.0	-6.1	1.1

The more abundant the halogen atoms are, the lower the energy levels are. However, as already discussed previously, the more abundant the halogen atoms are, the larger the bandgaps are (Figure 44).

3.1.1.3.3. Tetradecanoate-substituted [Ni(dpdt)₂]

The energy levels of **BT153F1** and **BT153F2** are given together with those of their parent complex **BT163** in Table 13.

Obviously, the nature of connecting group has a significant effect on the energy levels and bandgaps of targeted complex. As can be observed from Table 8 and Table 13, both HOMO and LUMO levels are lowered and the bandgap of the new materials are enlarged when the *n*-decyloxy chain in **BT163** is replaced by *n*-decanoate in **BT153F1** and **BT153F2**. The energy levels of **BT153F2** and its byproduct **BT153F1** are identical.

Table 13. LUMO and HOMO energy levels and bandgaps of tetradecanoate-substituted [Ni(dpdt)₂]

Complexes	E _{LUMO}	E _{HOMO}	E _g ^{el}
	eV	eV	eV
BT163	-4.7	-5.7	1.0
BT153F1	-4.8	-6.0	1.2
BT153F2	-4.8	-6.0	1.2

3.1.1.3.4. Octaalkoxy-substituted [Ni(dpdt)₂]

Table 14 gathers the energy levels derived from electrochemical study of all the octaalkoxy-substituted [Ni(dpdt)₂]. The values for the tetradecyloxy-substituted [Ni(dpdt)₂] **BT163** are also given as external references. The LUMO energy levels of “traditional” octaalkoxylated complexes

(**BT22**, **BT128**, and **BT132**) are around -4.7 eV (Table 14). These values are nearly identical to that of reference **BT163**, whereas the HOMO levels of these compounds are undeterminable due to the irreversibility of the oxidation process in cyclic voltammetry experiments.

Table 14. LUMO and HOMO energy levels of octaalkoxy-substituted [Ni(dpdt)₂]

Complexes	E_{LUMO}	E_{HOMO}	E_{g}^{el}
	eV	eV	eV
BT163	-4.7	-5.7	1.0
BT22	-4.7	-	-
BT128	-4.7	-	-
BT132	-4.7	-	-
BT152	-4.8	-	-

As already discussed in the previous section, significant change is observed in the case of **BT152** in comparison with its isomer **BT22**. The difference in chemical structures of these two compounds is illustrated in Figure 45. The “new-designed” octadecyloxy-substituted [Ni(dpdt)₂] **BT152** is found to have slightly lower LUMO energy level and a larger bandgap.

Generally, all the synthesized [Ni(dpdt)₂] derivatives have their LUMO energy levels around 4.7-5.0 eV. The HOMO levels are somewhat about 5.7-6.1 eV, depending on the substitutions on the dpdt ligands. The air stability of [Ni(dpdt)₂] is well described in the literature. The stability of [Ni(dpdt)₂] based materials in organic electronic devices have been demonstrated.^[159] Recently, systematic studies of the origin of the stability of electron transporting organic semiconducting materials have been reported.^[156, 211] Series of organic molecules with different electrochemical characteristics have been investigated. The results indicate that molecules with LUMO energies higher than approximately 4 eV are far less sensitive to atmospheric air than molecules characterized by a lower LUMO. The LUMO energies of our synthesized molecules lie about 4.7-5.0 eV, thus in the air stable zone as reported by Anthopoulos *et al.*^[156]

3.1.2. Optical properties

All the synthesized complexes are characterized by UV-VIS-NIR absorption spectroscopy in the CH₂Cl₂ solution with concentrations in the order of 10⁻⁵ molL⁻¹. The experimental values of λ_{max} , λ_{onset} , ϵ , and optical bandgap are summarized in following tables. All complexes show a maximum absorption peak in the near-infrared spectral region, which can be attributed to a π - π^* transition of nickel bisdithiolene core.

3.1.2.1. Tetraalkoxy-substituted complexes

Table 15 resumes optical data of tetraalkoxy-substituted nickel complexes. The typical spectra of two compounds **BT70** and **BT82**, recorded from CH₂Cl₂ solution and spin-coated thin films on ITO-coated glass substrate from CHCl₃ solution are in Figure 46.

Table 15. Electronic absorption data of tetraalkoxy-substituted [Ni(dpdt)₂], ^aE_g^{opt} = hc/λ_{onset}

Complexes	λ _{max}	λ _{onset}	ε	E _g ^{opt}	E _g ^{opt}
	nm	nm		Lcm ⁻¹ mol ⁻¹	solution
BT65	924	1060	47000	1.17	
BT163	932	1062	39000	1.17	
BT113	934	1062	49000	1.17	
BT80	933	1065	50000	1.16	
BT70	934	1079	47000	1.15	1.18
BT82	935	1066	43000	1.16	1.21
BT83	936	1069	54000	1.16	
BT85	935	1069	51000	1.16	
BT86	935	1073	54000	1.16	
BT71	929	1062	51000	1.17	
BT77	928	1061	44000	1.17	
BT74	931	1065	37000	1.16	
BT78	931	1059	52000	1.17	
BT79	929	1059	51000	1.17	
BT81	934	1066	48000	1.16	
BT84	933	1069	51000	1.16	
BT114	933	1067	48000	1.16	
BT115	933	1066	51000	1.16	
BT116	934	1071	51000	1.16	
BT117	933	1065	52000	1.16	

As observed from Table 15, for all the tetraalkoxy-substituted [Ni(dpdt)₂], the values of λ_{max} and λ_{onset} change very slightly around 925-930 nm and 1065-1070 nm, respectively. The optical bandgap of these compounds, determined from the value of λ_{onset} by the equation: E_g = hc/λ_{onset} according to the Tauc plots,^[204] varies from 1.15 eV to 1.17 eV. From all these results, it can be concluded that the nature of the alkoxy chains does not influence the optical properties of the tetraalkoxy-substituted [Ni(dpdt)₂]. These optical data in solution are perfectly coherent with electrochemical data in solution.

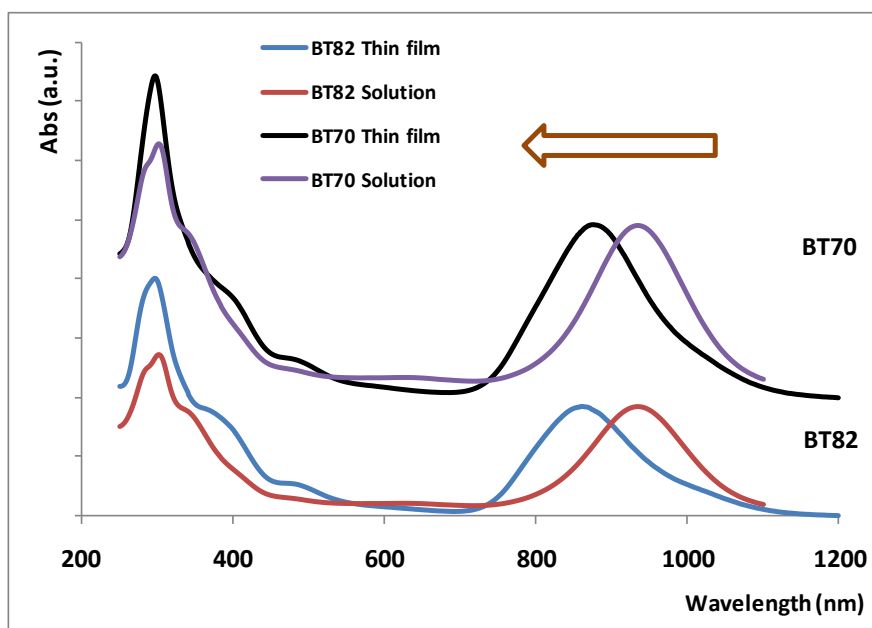


Figure 46. Absorption spectra of **BT70** and **BT82** in solution and spin-coated film

The electronic absorption spectra of both **BT70** and **BT82** as thin films, exhibits hypsochromic shifts (Figure 46). Both absorption curves show a maximum beyond 800 nm: $\lambda_{\text{max}} = 877$ and 861 nm for **BT70** and **BT82**, respectively. The optical bandgaps of these two compounds, measured on thin film, and derived from the Tauc plots^[204] are equal to 1.18 and 1.21 eV for **BT70** and **BT82**, respectively. These values are in good accordance with reported data in Table 15.

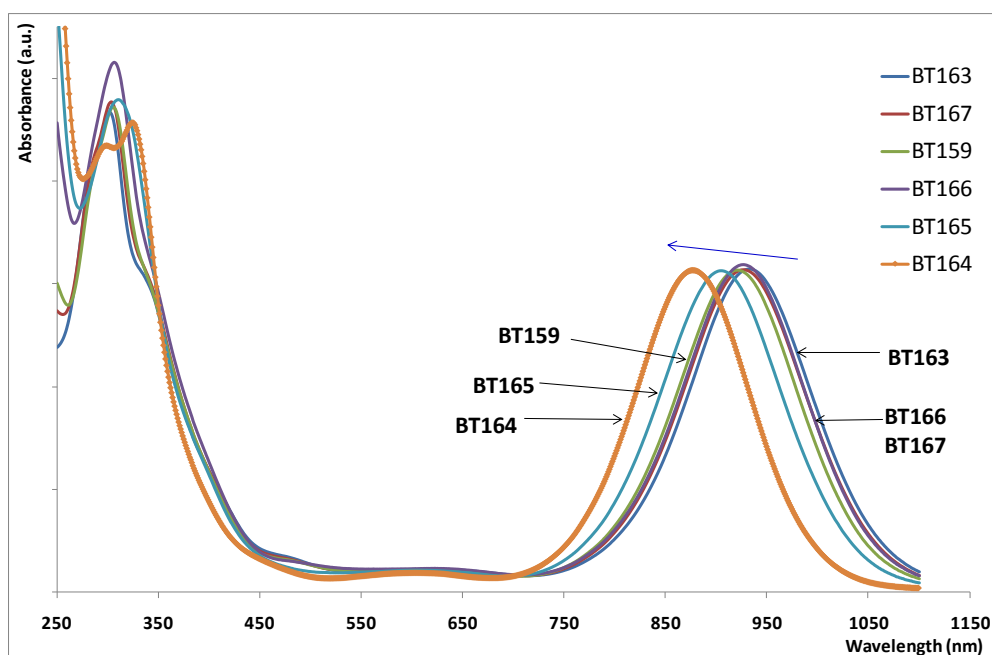
Prior to this study, we have reported the electronic absorption spectroscopy of two neutral nickel bisdithiolene complexes.^[199] For these compounds the thin films have given broader spectra than those of solution. However, neither hypsochromic nor bathochromic shift has been recognized. In the present work, the absorption spectra of discotic **BT70** and **BT82** spin-coated thin films shows hypsochromic shift compared with the solution indicating that nickel bisdithiolene complexes exist predominantly as aggregates in the films.^[167]

3.1.2.2. Halogenated complexes

Table 16 resumes optical data of halogenated complexes. The spectra of **BT166**, **BT167** and **BT159** are nearly identical to that of **BT163**). However, **BT165** (containing 6 I) and **BT164** (containing 8 I) show more important hypsochromic shift. The optical bandgaps vary from 1.16 to 1.23 eV (Table 16). These values are in good accordance with electrochemical data cited in Table 9.

Table 16. Optical data of halogenated complexes with **BT163** as reference

Complexes	λ_{\max} nm	λ_{onset} nm	ϵ L cm ⁻¹ mol ⁻¹	E_g^{opt} eV
BT163	932	1062	39000	1.17
BT167	927	1059	39000	1.17
BT159	920	1051	33000	1.18
BT166	927	1065	31000	1.16
BT165	900	1039	50000	1.19
BT164	877	1005	43000	1.23

**Figure 47.** Absorption spectra of **BT163** and halogenated complexes in CH_2Cl_2 solution

3.1.2.3. Tetradecanoate-substituted complexes

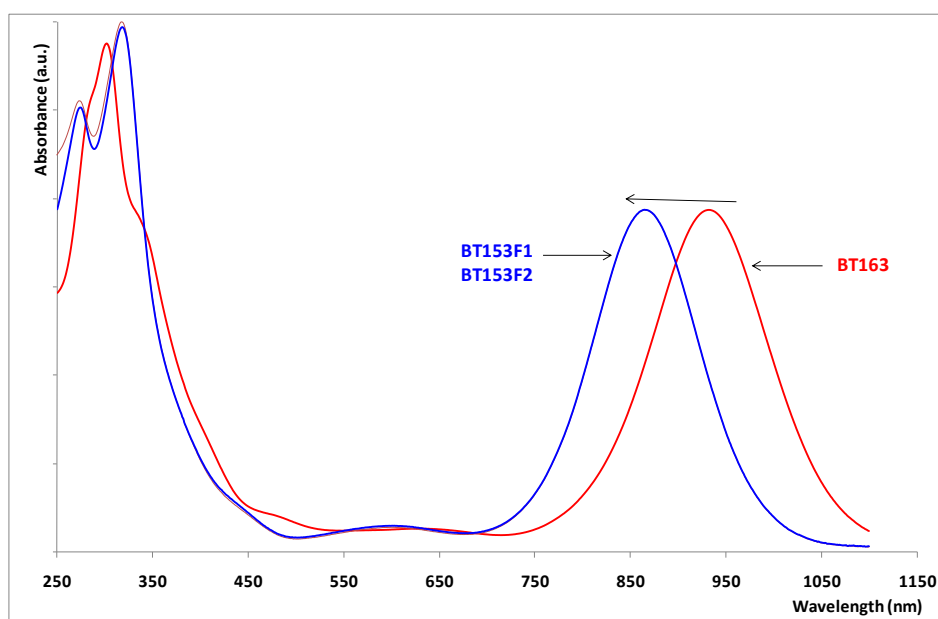
Table 17 presents the optical data of two compounds **BT153F1** and **BT153F2** and a reference, **BT163**.

The electronic absorption spectra of these compounds are gathered in Figure 48. **BT153F1** and **BT153F2** have identical absorption spectra due to a very little difference between the two compounds. These compounds show hypsochromic shift compared to **BT163**.

As can be observed from Table 17, the values of λ_{\max} are 865 nm for **BT153F1** and **BT153F2** while the corresponding value of **BT163** is 932 nm. From the onset of absorption spectra in Figure 48, optical bandgaps of **BT153F1** and **BT153F2** are determined (1.26 eV). The difference in energy is in the same range as that already noticed after electrochemical measurements.

Table 17. Optical data of **BT153F1**, **BT153F2**, and **BT163**

[Ni(dppe)₂]	λ_{\max}	λ_{onset}	ϵ	E_g^a
	nm	nm	L cm ⁻¹ mol ⁻¹	eV
BT163	932	1062	39000	1.17
BT153F1	865	987	36000	1.26
BT153F2	865	987	34000	1.26

**Figure 48.** Absorption spectra of **BT163** vs **BT153F1** and **BT153F2** in CH₂Cl₂ solution

3.1.2.4. Octaalkoxy-substituted complexes

All octaalkoxy-substituted complexes are also characterized by UV-VIS-NIR spectroscopy in solution. Table 18 summarizes optical properties of these compounds.

Table 18. Optical data of octaalkoxy-substituted complexes and **BT163**

Complexes	λ_{\max}	λ_{onset}	ϵ	E_g^{opt}
	nm	nm	L cm ⁻¹ mol ⁻¹	eV
BT163	932	1062	39000	1.17
BT22	961	1103	50000	1.12
BT128	965	1104	48000	1.12
BT132	971	1106	45000	1.12
BT152	870	994	41000	1.25

All the three “traditional” complexes (**BT22**, **BT128** and **BT132**) have the same electronic absorption behavior (Table 18). Only typical spectrum of **BT22** is presented in Figure 49

together with other ones. In comparison with tetraalkoxy-substituted complexes, octaalkoxy-substituted compounds show very slight red-shift (Figure 49).

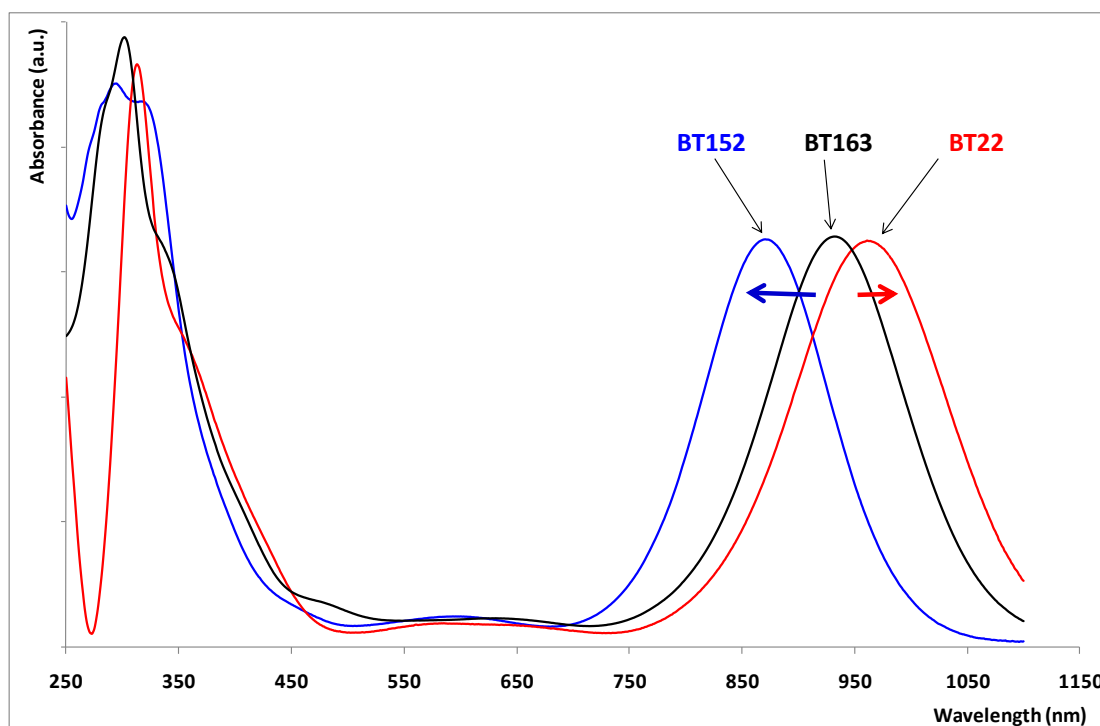


Figure 49. Absorption spectra of **BT163** vs **BT22** and **BT152** in CH_2Cl_2 solution

By comparison of the values of λ_{max} , λ_{onset} and optical bandgaps of **BT22**, **BT132** and **BT128** with those of **BT163**, **BT70** and **BT80** respectively, the increase the number of peripheral substituents of $[\text{Ni}(\text{dpedt})_2]$ results in small bathochromic shift (about 30 nm). The optical bandgaps of these compounds change slightly (about 0.05 eV). However, the results obtained with **BT22** and **BT152** from Table 18 show that the change of the position of two *n*-decyloxy chains on the phenyl rings of the dpedt ligand from “3,4” (in **BT22**) to “3,5” (in **BT152**) induces an hypsochromic shift by about 100 nm. In addition, its optical bandgap moderately changed from 1.12 eV (**BT22**) to 1.25 eV. This could be attributed to the loss of conjugation between peripheric phenyls and nickel bisdithiolene core due to a twist of the phenyl rings out of the plane of the core induced by steric effect of *n*-decyloxy chains in the position “3,5”. Another reason is the absence of electron-donating group in *para* position.

Generally, the optical properties of $[\text{Ni}(\text{dpedt})_2]$ derivatives can be modulated by different factors as discussed for each group of complexes above. From all these results, one can conclude that playing on the number and the position of alkoxy chain on the peripheric phenyl rings can modulate optical properties of targeted complexes. Additionally, the high values of molecular

absorption coefficient ϵ ranging from 30000 to 55000 $\text{Lcm}^{-1}\text{mol}^{-1}$ demonstrate that all synthesized $[\text{Ni}(\text{dpedt})_2]$ are efficient NIR absorbent materials.

3.1.3. Comparison of electrochemical and optical data

The optical and electrochemical data of all the new synthesized nickel bisdithiolene complexes are well discussed in 3.1.1 and 3.1.2. Generally, these two data are in very good accordance. The values of optical bandgap are slightly higher than those of electrochemical bandgap. This difference, in the order of several hundreds of meV, is attributed to the binding energy of excitons.^[212-215]

3.1.4. Thermal stability

A highly thermal stability of targeted compounds is required to envisage their use as active materials in organic electronic devices (e.g. OPV, OFET). Thermogravimetric analysis (TGA) studies show that neutral nickel bis(1,2-dithiolene) complexes are thermally stable until the temperature around 300 °C under nitrogen atmosphere.

The typical thermogravimetric analysis curves of tetraalkoxy-substituted $[\text{Ni}(\text{dpedt})_2]$ **BT70** and octaalkoxy-substituted $[\text{Ni}(\text{dpedt})_2]$ **BT22** are illustrated in

Figure 50. At higher temperatures, the major weight loss observed is due to the decomposition of products. This thermal behavior is in good accordance with data reported in the literature for long chain-substituted $[\text{Ni}(\text{dpedt})_2]$ derivatives.^[216]

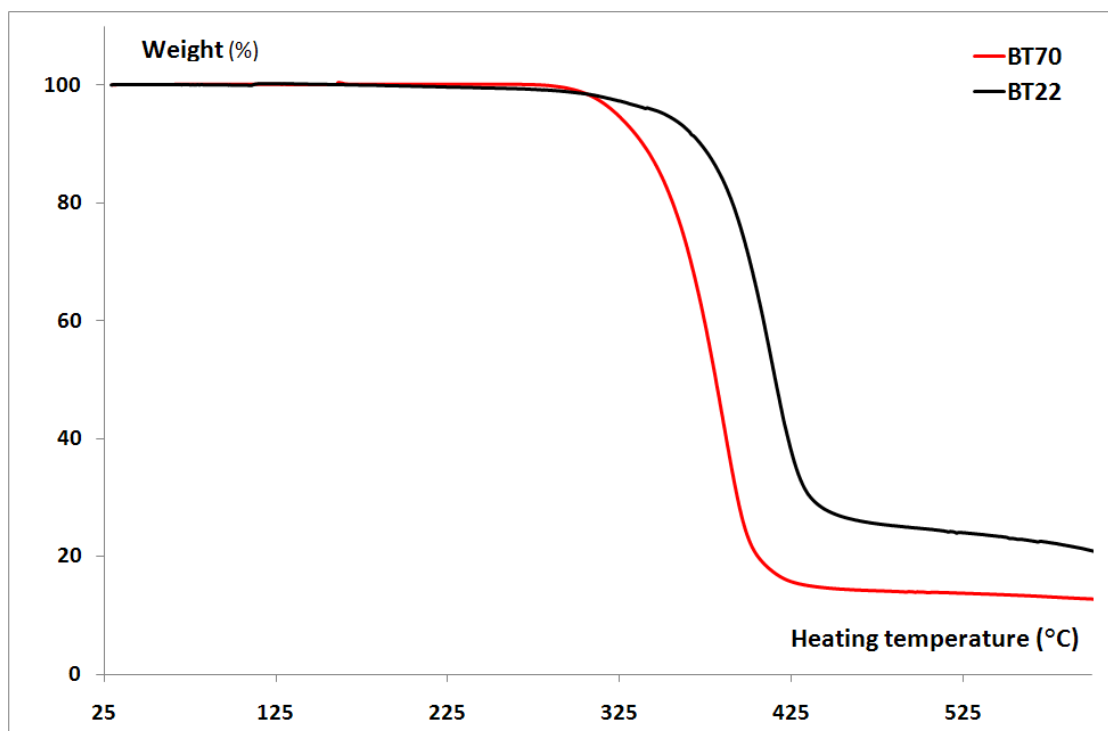


Figure 50. Thermal analysis traces of two $[\text{Ni}(\text{dpdt})_2]$: BT70 and BT22

3.1.5. Liquid crystalline properties

In the present work, preliminary investigations of phase transition behaviors of long chain substituted $[\text{Ni}(\text{dpdt})_2]$ are performed by combination of differential scanning calorimetry (DSC) and polarized optical microscopy (POM).

3.1.5.1. Tetraalkoxy-substituted $[\text{Ni}(\text{dpdt})_2]$ (Groups 1-4)

The existence of mesomorphic properties of tetraalkoxy-substituted $[\text{Ni}(\text{dpdt})_2]$ is ambiguous. In 1983, Veber *et al.* reported for the first time that tetraalkoxy-substituted $[\text{Ni}(\text{dpdt})_2]$, the nickel bis[1,2-bis(4-*n*-dodecyloxyphenyl)ethene-1,2-dithiolene], showed a mesophase.^[168] In 1986, Ohta *et al.* also synthesized two homologous complexes with two chains (*n*-nonyloxy and *n*-undecyloxy), using a different synthetic route and reported that these complexes exhibit a discotic mesophase.^[136, 137] However, in 1987, based on the results of X-Ray diffraction study, Veber *et al.* denied the existence of mesomorphism in these tetraalkoxy-substituted complexes and they claimed that the phase was not mesomorphic but crystalline.^[217] Ohta *et al.* were not satisfied with this report. They re-synthesized and fully re-studied two series of nickel bis[1,2-bis(4-*n*-alkylphenyl)ethene-1,2-dithiolene] complexes (alkyl = methyl to *n*-dodecyl), and nickel bis[1,2-

bis(4-*n*-alkoxyphenyl)ethene-1,2-dithiolene] complexes (alkoxy = methoxy to *n*-octadecyloxy).^[91] Their mesomorphism, thermochromism, supramolecular structures and π -acceptor property have been investigated by using differential scanning calorimetry, polarized optical microscopy, temperature-dependent X-ray diffraction technique, electronic spectroscopy and cyclic voltammetry. They have found that none of the tetraalkyl-substituted [Ni(dpdt)₂] has a mesophase whereas tetraalkoxy-substituted, with alkoxy chain length from *n*-decyloxy to larger exhibited two differently colored discotic lamellar mesophases. They attributed the thermochromism of the complexes (changing from brown to green on heating) to a slow transformation from the Ni–Ni bonded dimers to the Ni–S bonded dimers.^[91] In 2004, Chou *et al.*^[216] resynthesized the tetra-*n*-undecyloxy-substituted [Ni(dpdt)₂] for micropacked gas chromatography application and they also reported the same mesomorphic properties for this compound, in good accordance with data reported previously by Ohta *et al.*^[91] However in a recent report, Perochon *et al.* have denied the existence of mesomorphic properties of tetra-*n*-dodecyloxy-substituted [Ni(dpdt)₂] (compound **BT113** in our present work).^[144] *Does the mesomorphic property of tetraalkoxy-substituted [Ni(dpdt)₂] exist?* This question is still open although nearly three decades passed since the first paper was published.

In this present work, we are also interested in the investigation of these compounds as photoactive materials for organic photovoltaic devices. Twenty-seven tetraalkoxy-substituted complexes have been synthesized and studied. According to the literature, the black powder **BT65** directly melt into a green isotropic liquid with rapid decomposition.^[91] In the next part, the thermal property of **BT65** will not be studied. **BT163** and **BT113** have been also reported elsewhere.^[91, 144] They will serve as references for new tetraalkoxy-substituted analogues.

The phase transitions of all synthesized tetraalkoxy-substituted [Ni(dpdt)₂] are firstly studied by differential scanning calorimetry measurements and polarized optical microscopy observations.^c All pristine samples are heated from room temperature until they melt into isotropic liquid and subsequently cooled down. The heating-cooling cycles are generally repeated twice with a scan rate of 10K/min, unless specific indication. Unfortunately, except for **BT113**, **BT114**, **BT117** and **BT163**, DSC traces of all other tetraalkoxy-substituted complexes suggest that they do not have liquid crystalline properties. Polarized optical observations confirm this result. In the following paragraph, the phase transitions of these compounds will not be discussed. Meanwhile, the phase

^c Polarized optical microscopy observations have been carried out at CRPP Bordeaux

transition behaviors of **BT113**, **BT114**, **BT117** and **BT163** are much more complex and more interesting. We focus our investigations only on these four compounds.

The differential scanning calorimetry curve of **BT163** is presented in Figure 51. All phase transitions and heats in the range of temperature from 50°C to 200°C are listed in Table 19. As can be observed, **BT163** possesses multi phase transitions both on heating and cooling. On the first heating process of pristine sample from room temperature to around 200°C, the first endothermic transitions are recorded around 90°C ($\Sigma\Delta H = 50.92$ kJ/mol). By further heating, a small transition at 139°C (1.31 kJ/mol) is recorded. The highest endothermic transition occurs at 178°C ($\Delta H = 46.2$ kJ/mol). The later is thought to be the melting point of the compound. Upon cooling down, multi phase transitions are recorded. The earliest exothermic phase transition occurs about 170°C (39 kJ/mol). By further cooling, we observe two more exothermic transitions at 157°C (-0.84 kJ/mol) and at 120°C before the apparition of the transition at 85°C (-18.42 kJ/mol).

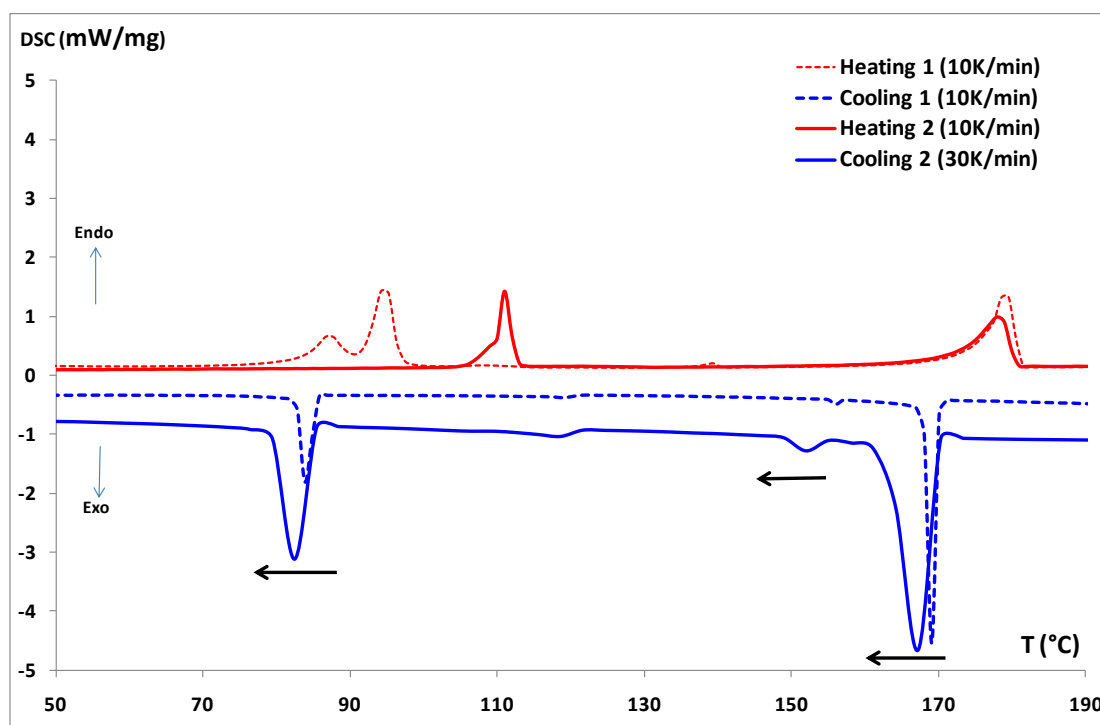


Figure 51. DSC trace of BT163

On second cycle, the first endothermic transition is recorded at 111°C (+21.42 kJ/mol) and the later at 178°C (+39.66 kJ/mol). On second cooling at a higher scan rate of 30 K/min, all three exothermic transitions of the first cooling cycle are reproduced (Figure 51 and Table 19). As observed from Figure 51, all these transitions show slightly cooling rate dependence. This observation suggests that the highest transition around 170°C is likely to be an isotropic liquid – liquid crystal transition. It is important to remember that the **BT163** is already reported as the

compound “**C₁₀O-Ni**”, which shows mesomorphic properties, in the work of Ohta *et al.*^[91] Our differential scanning calorimetry studies of **BT163** is in perfect agreement with data reported for **C₁₀O-Ni**.^[91] Nevertheless, further study by X-ray diffraction technique is needed for understanding the nature of these phase transition.

Table 19. Phase transitions of BT163

Heating-Cooling cycle	Scan rate (K/min)	T (°C)	ΔH (kJ/mol)
Heating 1	10	88	+50.92
		94	
		139	+1.31
		178	+46.20
Cooling 1	10	170	-39.00
		157	-0.84
		120	
		85	-18.42
Heating 2	10	111	+21.42
		178	+39.66
Cooling 2	30	167	-34.96
		151	-0.82
		118	-0.80
		82	-17.76

Another complex is also already reported is **BT113**, which is named **C₁₂O-Ni** in the work of Ohta *et al.*^[91] and **Ni-OC₁₂** in the work of Fourmigue *et al.*^[144] According to Ohta *et al.*,^[91] **C₁₂O-Ni** possesses mesomorphic properties. However, Fourmigue *et al.*^[144] denied the existence of mesomorphic properties of **Ni-OC₁₂** based on cross-polarisers POM observation. Our DSC analysis of **BT113** is shown in Figure 52. Likely in the case of **BT163**, our DSC observation is in quite good accordance with data reported for the compound **C₁₂O-Ni**.^[91]

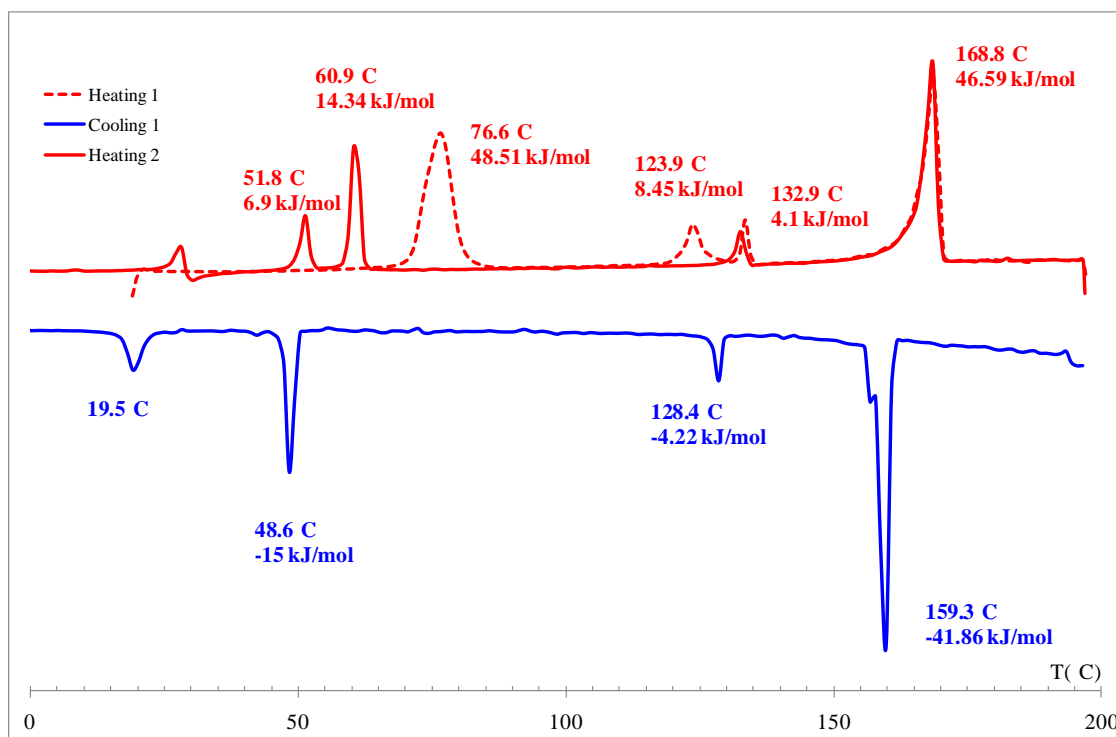


Figure 52. DSC curve of **BT113**, scan rate 10K/min

As can be observed, **BT113** possesses multi phase transitions both on heating and cooling. On the first heating process of pristine sample from room temperature to around 200°C, the first endothermic transition is recorded around 76°C ($\Delta H = 48.51$ kJ/mol), and two small successive transitions are observed around 120°C ($\Delta H = 8.45$ kJ/mol) - 130°C ($\Delta H = 3.71$ kJ/mol). The highest transition is recorded at 170°C ($\Delta H = 46.59$ kJ/mol). The later is thought to be the melting point of the compound. Upon cooling down and, on second heating, multi phase transitions are recorded. It is difficult to interpret the phase transition on optical microscopy. Upon heating, the pristine brown powder changes color from brown to green. The isotropic phase appears when the sample is heated up to 175 °C.

Figure 53 shows polarized optical microscopy images of **BT113** recorded at temperatures corresponding to different phases as observed from differential scanning calorimetry analysis. It seems there is no liquid crystal phase but probably a succession of crystal-crystal phase transitions. In fact, we note every time a slight change in texture that could correspond to changes in crystal symmetry, but no crystal-liquid crystal transition. The observation during the cooling cycle leads to the same conclusion. Nevertheless, further study by X-ray diffraction technique is needed in order to understand the nature of these phase transitions.

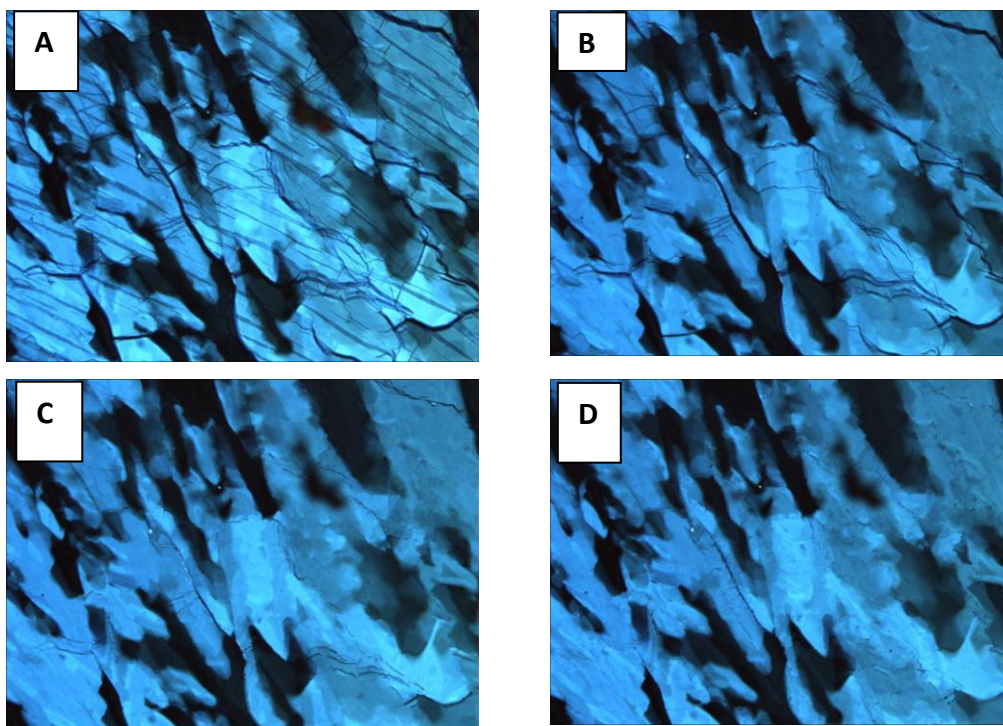


Figure 53. POM images of BT113 photographed at r.t. (A), 85°C (B), 130°C (C) and 140°C (D)

Unlike **BT113** or **BT163**, **BT114** and **BT117** are new compounds. The DSC analysis results of these two complexes are shown in Figure 54 (**BT114**) and in Figure 55 (**BT117**).

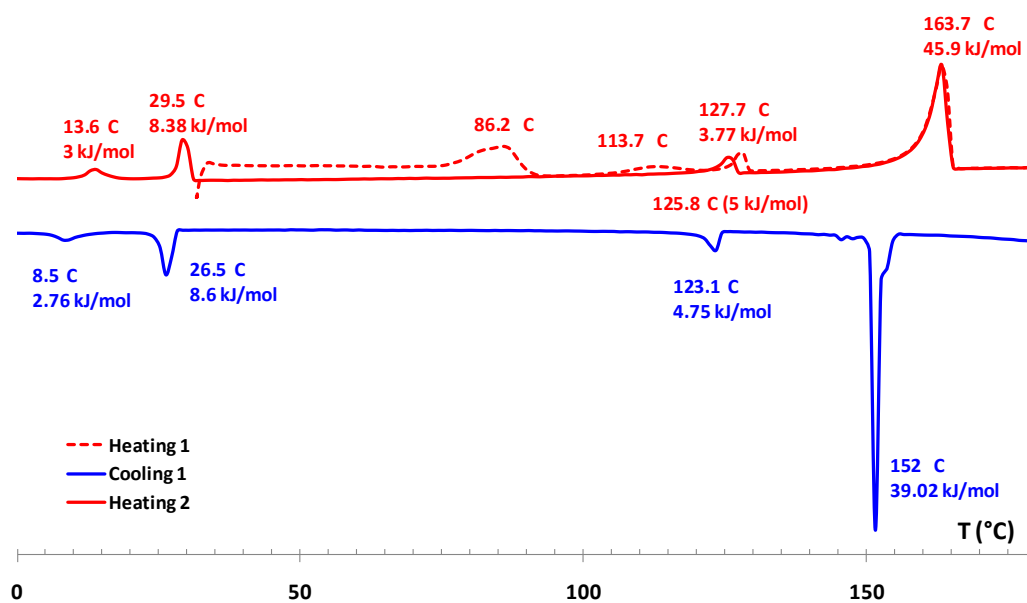


Figure 54. DSC curve of **BT114**, scan rate 10K/min

The thermal behaviors of these two compounds are very similar to those of **BT113** and **BT163**. POM observation reveals that both **BT114** and **BT117** exhibit a crystalline phase below the isotropic phase, characterized by angular growth and prominent areas (see pictures in Figure 56).

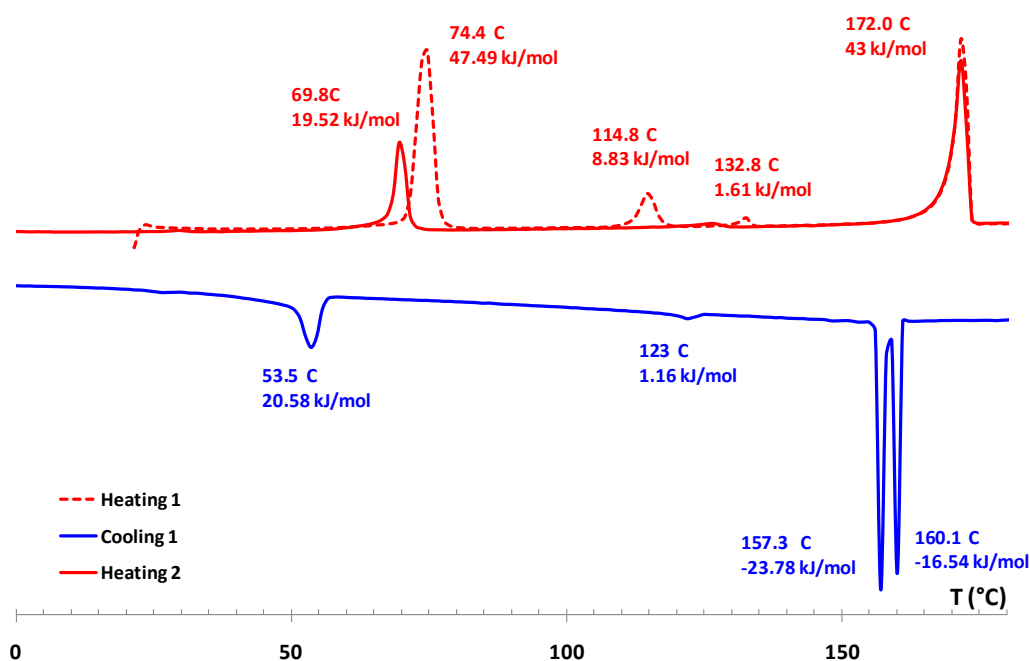


Figure 55. DSC curve of **BT117**, scan rate 10K/min

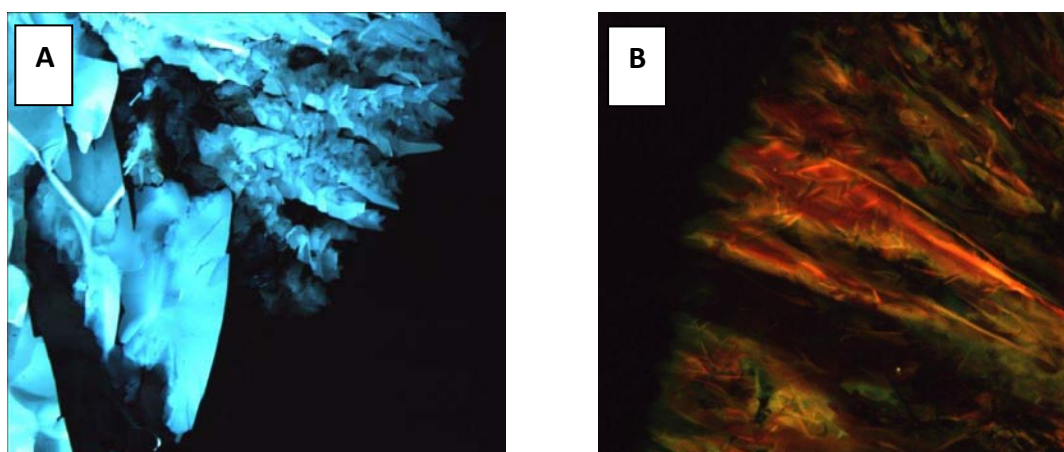


Figure 56. POM images of **BT114** (A) and **BT117** (B)

In conclusion, from investigation by differential scanning calorimetry and polarized optical microscopy, it appears that all tetraalkoxy-substituted complexes do not possess mesomorphic properties. However, further characterization techniques such as temperature variant X-ray diffraction should be carried out in order to clearly identify the nature of all phase transitions in these compounds.

3.1.5.2. Halogenated complexes (Group 5)

The design of new complexes based on halogenated dpedt ligands are well mentioned in paragraph 2.1.2.1.3. Surprisingly, the introduction of halogen atoms, either bromine or iodine, dramatically influences the thermal responses of the new compounds giving simpler thermal behaviors than that of parent compound **BT163**. The thermal behavior of **BT167** (2 Br), which shows a crystal – isotropic liquid phase transition, is given Figure 57.

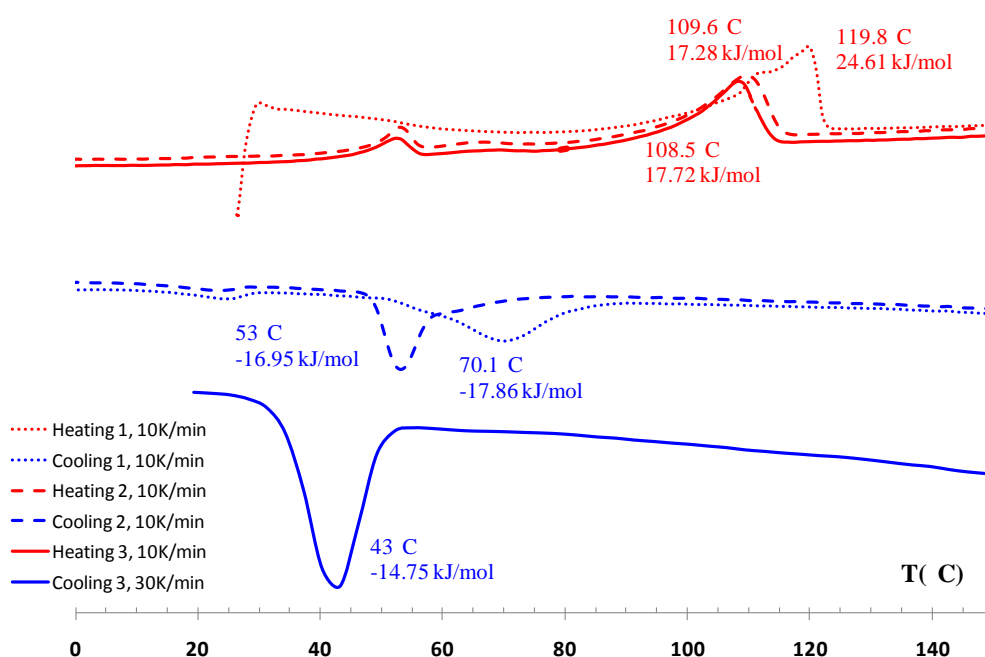


Figure 57. DSC curve of **BT167**, scan rate 10K/min and 30K/min

Unfortunately, differential scanning calorimetry and polarized light microscopy analyses confirm that none of these new designed complexes have liquid crystalline properties. **BT159** (4 Br) and **BT166** (4 I) melt into isotropic liquid at 127° and 119°C, respectively. Upon cooling down, no phase transition is recorded and the samples are in amorphous state. By differential scanning calorimetry analysis, **BT165** (6I) and **BT164** (8 I) show no phase transition below 200°C and polarized light microscopy observations reveal that these compounds melt into isotropic liquid around 250°C.

3.1.5.3. Tetradecanoate-substituted complexes (Group 6)

As discussed in the synthesis section, **BT153F1** and **BT153F2** are obtained as green powders after purification.

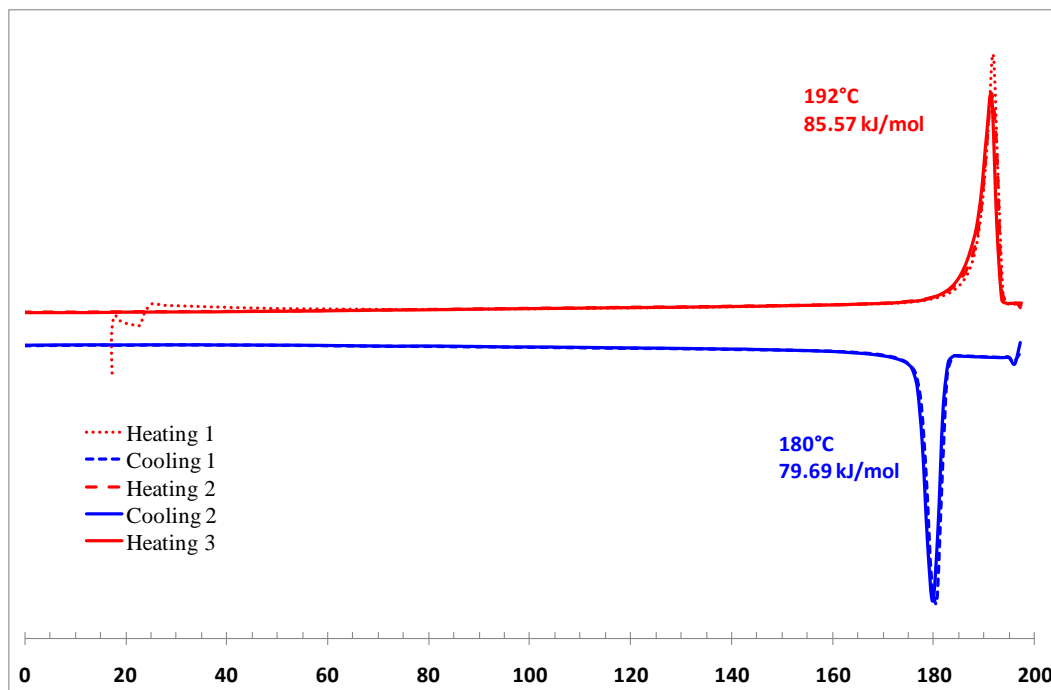


Figure 58. DSC curve of **BT153F2**, scan rate 10K/min

The differential scanning calorimetry curves of **BT153F2** and **BT153F1** are nearly identical. As can be observed from Figure 58, differential scanning calorimetry response of **BT153F2** is very simple as only one phase transition occurs, both upon heating and cooling. These phase transitions are really reproducible with a very low supercooling. They actually look well like as corresponding to a liquid crystal–crystal phase transition.

Figure 59 shows a picture of the growth of **BT153F2** taken under a polarizing microscope. One can notice the major growth of needle like structures which are very prominent. It is certainly a crystal growth. There is also a fractal dendritic growth that may correspond to another form of crystal growth.

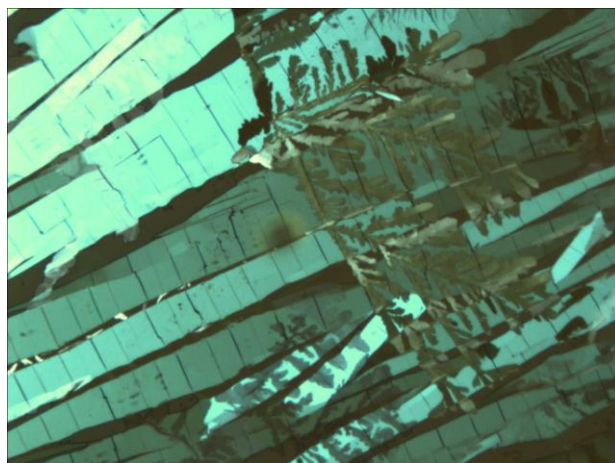


Figure 59. POM image of BT153F2 recorded after annealing at 87°C

3.1.5.4. Octaalkoxy-substituted [Ni(dpdt)₂] (Group 7)

Prior to our work, the nickel complex **BT22** has been reported as a discotic liquid crystal by Ohta *et al.*^[138-140] In the present work, this compound is re-synthesized and re-studied as a reference for other new designed analogues. The differential scanning calorimetry analysis of **BT22** is presented in Figure 60.

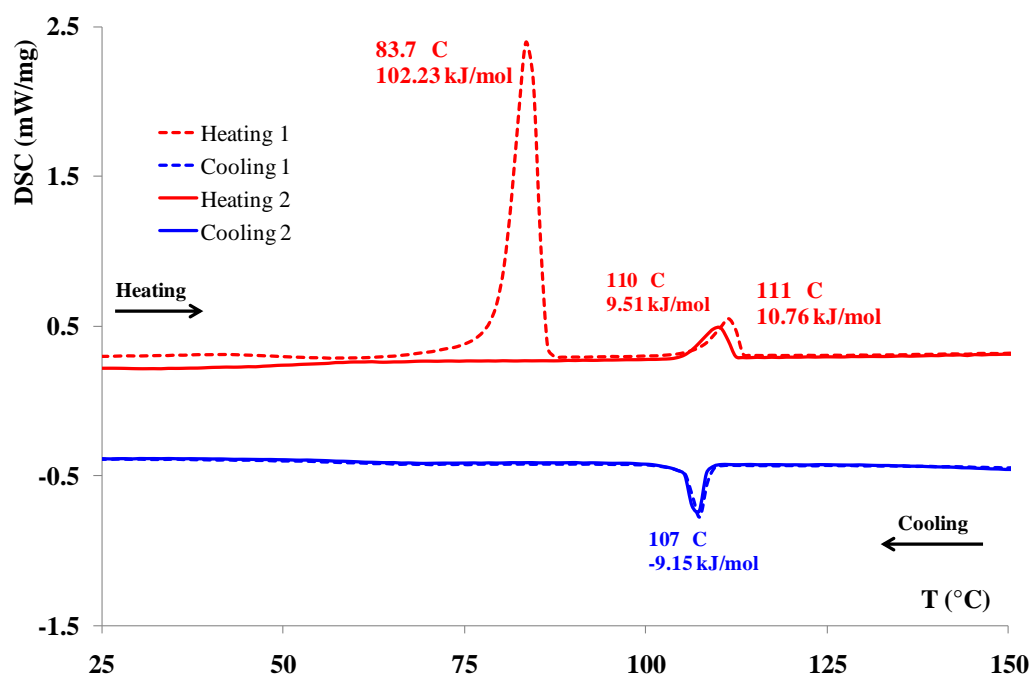


Figure 60. DSC curve of **BT22**, scan rate 10K/min

When the pristine black green powder **BT22** is heated from room temperature at a heating rate 10K/min, two endothermic phase transitions with different enthalpy, appear. The first one is

recorded at *ca.* 84°C ($\Delta H = 102.23$ kJ/mol) and the second one appears at 111°C ($\Delta H = 10.76$ kJ/mol). On cooling down **BT22** from isotropic liquid state to -100°C, only one exothermic transition appears at 107°C ($\Delta H = 9.15$ kJ/mol). In the second heating, the endothermic peak at 84°C do not appear anymore and only the endothermic one at 110°C ($\Delta H = 9.51$ kJ/mol) is recorded. We also recognized the important difference of the two ΔH values (57 kJ/mol *versus ca.* 5-6 kJ/mol) of the first transition at *ca.* 84°C and the second one at *ca.* 110°C, respectively. On the other hand, it is important to note that the supercooling of the transition at 110°C is very small. This kind of DSC behavior is typical of a liquid crystal compound: the first transition (84°C) is the transformation of crystalline state into liquid crystalline state and the higher transition corresponds to the melting of the liquid crystalline state into isotropic liquid. The energy needed for the first transition is normally much bigger than that for the second one. **BT22** melts into isotropic liquid at 110°C and on cooling down, it recrystallizes into a liquid crystalline phase which is stable down to -100°C.

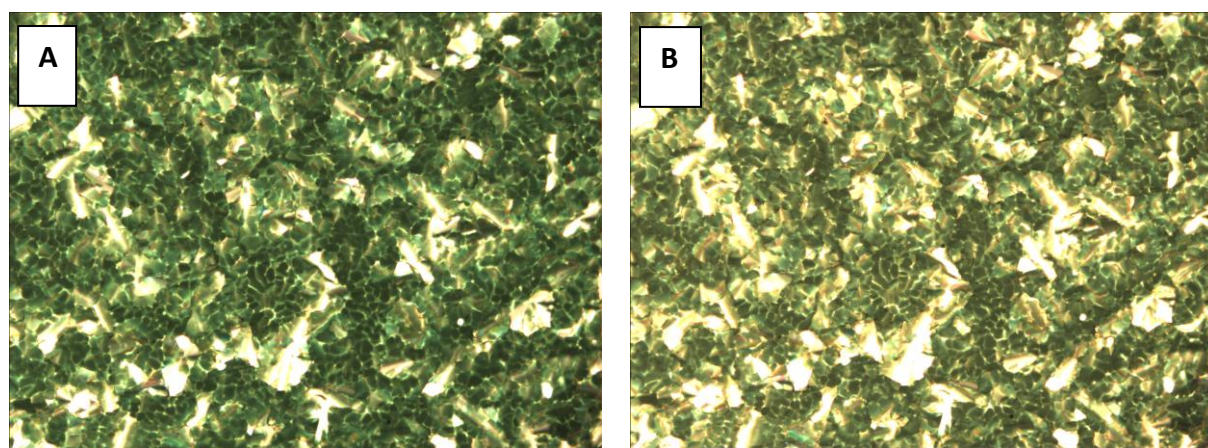


Figure 61. POM images of **BT22** at 65°C (A) and r.t. (B) on cooling down from isotropic liquid, 1K/min

The nature of the liquid crystalline phase is then further studied by the polarized optical microscopy. The pristine **BT22** is heated into isotropic liquid and subsequently cooled down at 1°C/min. Pretty dendritic growth, which is typical of a columnar liquid crystal phase, is observed. Figure 61 shows two pictures of **BT22** taken at 65°C and at room temperature after cooling down from isotropic liquid. In interference contrast mode observation of free droplet of **BT22** (Figure 62), the formation of germs with 6 petals can be observed: this confirms the hexagonal symmetry of the compound. Unfortunately, this hexagonal columnar liquid crystal phase is only preserved at room temperature for about 18 h. It completely recrystallizes after a couple of days. This result is in good accordance with data reported in literature.^[138-140]

All other octaalkoxy-substituted nickel bisdithiolene complexes have never been described prior to our present work. Considerable change in the thermal behaviors of new complexes is observed, depending on the nature and configuration of the side alkoxy chains. The replacement of *n*-decyl by 3,7-dimethyloctyl, a branched decyl chain, results in **BT128**. The differential scanning calorimetry behavior of **BT128** is completely different from that of **BT22**. The results of differential scanning calorimetry and polarized light microscopy studies clear up that, upon heating from room temperature, the pristine black pasty powder of **BT128** directly melts into isotropic liquid at *ca.* 50°C. Upon cooling down, the recrystallization peak was recorded at *ca.* 25°C and no mesophase was detected. When comparing the melting temperature of parent compound **BT22** and new compound **BT128**, it is revealed that the use of bulky 3,7-dimethyloctyl chain influences dramatically the molecular packing and decreases dramatically the melting point.

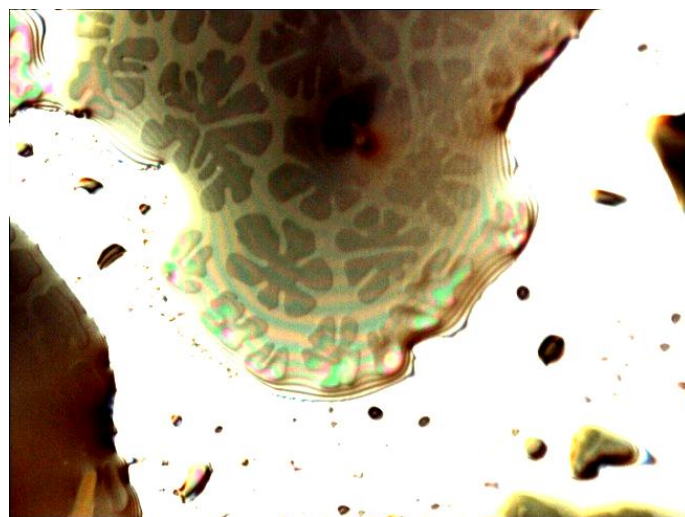


Figure 62. POM image of free droplet of BT22

When the linear decyl chain is replaced by 2-ethylhexyl, usually used to form “organic-pure” stable discotic liquid crystals,^[170-173, 179] **BT132** is obtained and shows much more surprising results. The pristine black pasty powder of **BT132** directly melts into isotropic liquid (around 60°C) upon heating from room temperature. Upon cooling down, no phase transition is observed and the compound stays in the glassy state. No mesophase is detected for **BT132**. In the “organic-pure” stable discotic liquid crystals,^[170-173, 179] the bulky steric effect of the 2-ethylhexyl chain plays a very important role and helps decreasing the intermolecular interactions. Consequently, the transition temperature of solid state into discotic liquid crystal phase should decrease. Therefore, the introduction of branched alkyl chain should be a favorable factor for forming room temperature stable discotic liquid crystals. Within our [Ni(dpdt)₂] derivatives, the introduction of that kind of bulky groups completely destroys the mesomorphic properties. This

could be due to the fact that two alkoxy chains on a same phenyl ring of dpedt ligand are too close. The ramification of the principal alkyl backbone at the positions “2” or “3” give them less freedom of rotation. As a consequence, the intermolecular π -stacking effect could be dramatically reduced. Another consequence is the important difference of melting point between **BT22** (*ca.* 110°C) and **BT128** (*ca.* 50°C) and **BT132** (*ca.* 60°C) although they have nearly the same molecular weights.

Let's approach the problem from another point of view. We study the influence of two substituent positions on the same phenyl ring of dpedt ligand. The **BT152** differentiates from **BT22** only by the position of two *n*-decyloxy groups in the same phenyl. In **BT152**, the two aliphatic chains are far enough that we hope they could freely rotate and auto-organize to optimize the intermolecular organization. The differential scanning calorimetry curve (heating-cooling rate: 10K/min) of **BT152** is illustrated in Figure 63 and phase transitions are resumed in Table 20.

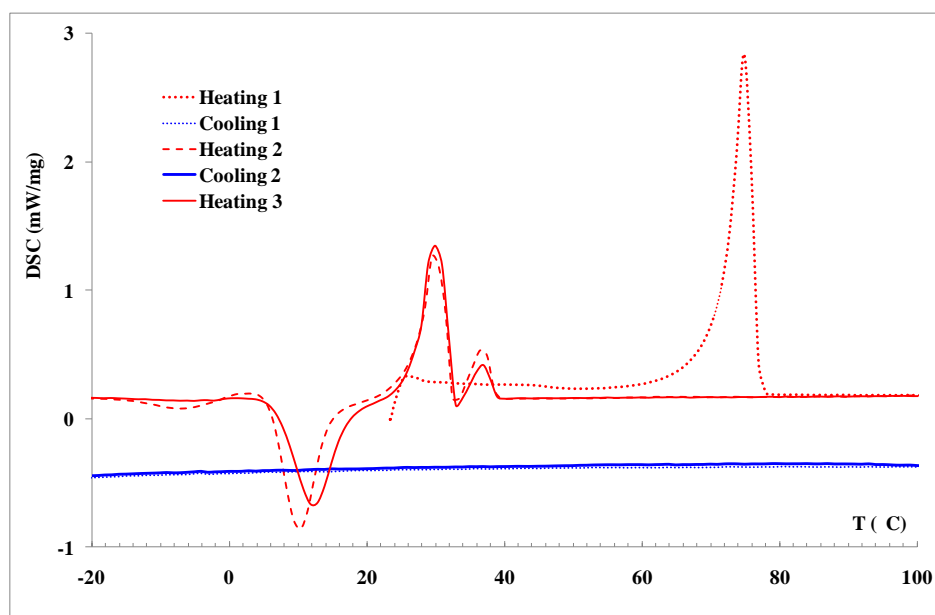


Figure 63. DSC trace of BT152. Scan rate: 10K/min

When the pristine black powder of **BT152** is heated from ambient temperature, an endothermic peak is recorded at 75°C. The enthalpy value of this transition (Table 20) suggests that it should be a melting point into isotropic liquid. Upon cooling down, this compound presents a high supercooling effect. No transition is recorded until -60°C, both during the first and second cooling cycles. On second and third heating cycles, numerous phase transitions, both endo- and exo-thermic, are recorded (Table 20).

These exothermic transitions on heating are thought to be recrystallization peaks. **BT152** is then studied by polarized optical microscopy and the results confirm the comments from thermal analysis. When the virgin **BT152** is heated to temperature higher than 75°C, it becomes isotropic liquid and it does not recrystallize on cooling down until ambient temperature. This observation was well coherent with thermal analysis.

Table 20. Phase transition and T/ΔH of **BT152**

Heating-Cooling cycle	T (°C)	ΔH (kJ/mol)
Heating 1	75.0	64.88
Heating 2	-7.5	-6.22
	10.0	-38.42
	29.3	27.29
Heating 3	36.7	7.84
	12.1	-37.74
	29.3	31.38
	36.9	5.60

By comparing the thermal behaviors of **BT128**, **BT132** and **BT152** with that of the reference (**BT22**), one can conclude that: the mesomorphic properties of octaalkoxy-substituted [Ni(dpdt)₂] are very sensitive to the chemical structures of the compounds. The replacement of linear alkyl chains by ramified ones destroys brutally the mesophase. The modification of peripheral substituent position of dpdt ligand decreases the melting point but doesn't preserve the mesophase properties.

3.1.6. Octalkoxy-substituted [Ni(dpdt)₂] mixtures

The thermal and physical properties of the three nickel bisdithiolene complex mixtures **BT129**, **BT130** and **BT131** are investigated by different methods and they give very similar results.

The typical absorption spectrum of **BT131** recorded in CH₂Cl₂ solution is presented in Figure 64. The mixture **BT131** gives an absorption profile similar to the other single octa-substituted nickel complexes (**BT22**, **BT128**, **BT132**), with a maximum absorption peak (961 nm) in the near infrared spectral domain. All optical data of the three mixtures are summarized in Table 21 with the values of λ_{max} around 960 nm. The molar extinction coefficients of these mixtures are undeterminable due unknown compositions. The values of optical bandgaps are identical to that of the other single octa-substituted nickel complexes (**BT22**, **BT128**, **BT132**) (Table 18).

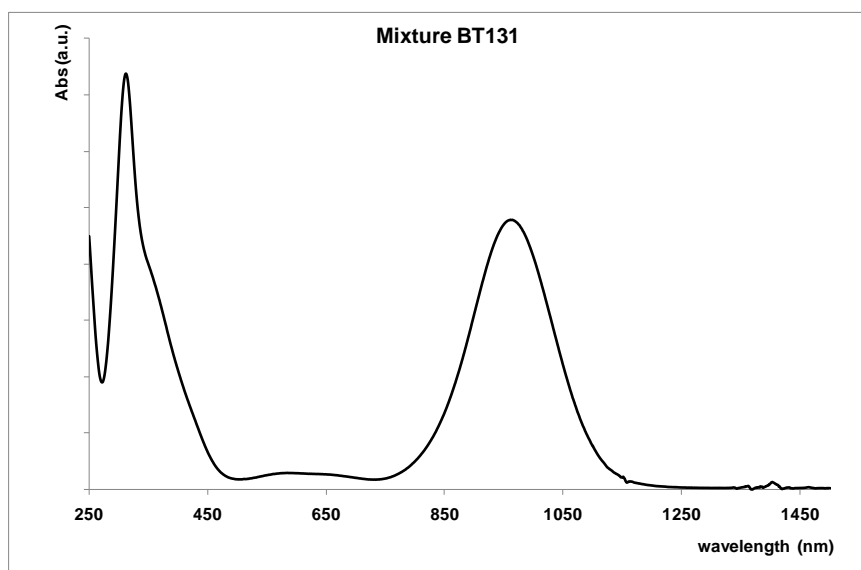


Figure 64. UV-VIS-NIR absorption spectroscopy of **BT131** in CH_2Cl_2 solution

Table 21. Optical data of BT129, BT130 and BT131

Mixtures	λ_{max} (nm)	$E_{\text{g}}^{\text{opt}}$ (eV)
BT129	964	1.13
BT130	961	1.13
BT131	961	1.13

The electrochemical behaviors of these mixtures are revealed using cyclic and square wave voltammetries. $(\text{Bu}_4\text{N})[\text{PF}_6]$ (0.1 mol L^{-1} in CH_2Cl_2) is used as electrolyte with glassy carbon working electrode and saturated calomel reference electrode. Typical cyclic voltammogram of **BT131** is presented in Figure 65 and all electrochemical data are summarized in Table 22.

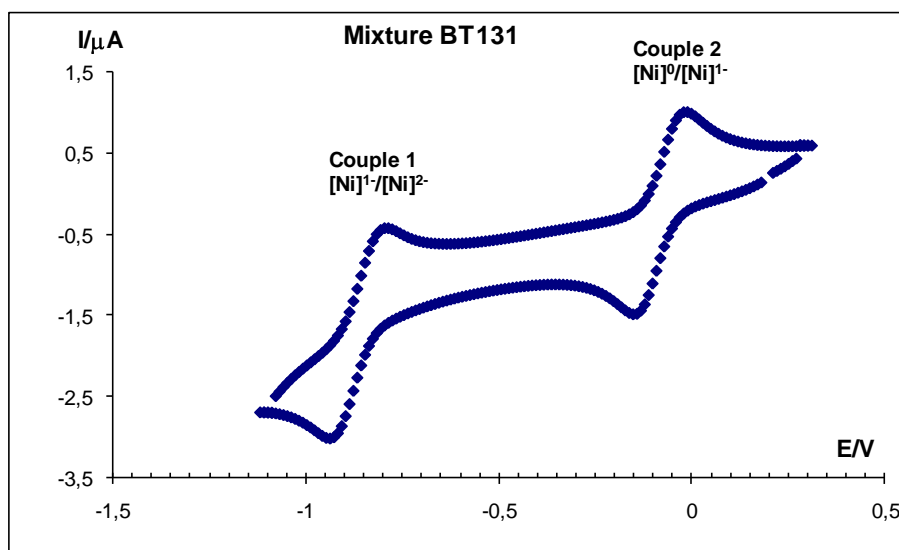


Figure 65. Cyclic voltammogram of mixture **BT131**

The first monoelectronic oxidation of **BT131** is irreversible, in contrast to its first and second monoelectronic reductions, which are shown in Figure 65. As can be seen in Table 22, the measured data by cyclic and square wave voltammetries of these mixtures are in very good agreement. Especially, these values are close to those of pure complexes reported by Ohta *et al.*^[140]

Table 22. Electrochemical data of **BT129**, **BT130** and **BT131**

Complexes	CV		SQW	
	$E_{1/2}^2$ (V)	$E_{1/2}^2$ (V)	$E_{1/2}^3$ (V)	$\Delta E_{1/2}$ (V)
BT129	-0.09	-0.10	0.96	1.07
BT130	-0.09	-0.09	0.95	1.05
BT131	-0.08	-0.08	0.95	1.03

From obtained optical and electrochemical data, it can be concluded that the three mixtures have the same physical properties as the pure complexes. This means that **BT129**, **BT130** and **BT131** are “**chemically mixtures**” but “**electronically pure**”.

The thermal analysis of these mixtures gives similar differential scanning calorimetry responses and the first analysis of these phase transitions suggests that **BT129**, **BT130**, and **BT131** probably possess liquid crystal phases. The most promising thermal behavior is that of **BT131** (Figure 66) and will be further investigated. The two other compounds (**BT129** and **BT130**) will not be further studied in the present work.

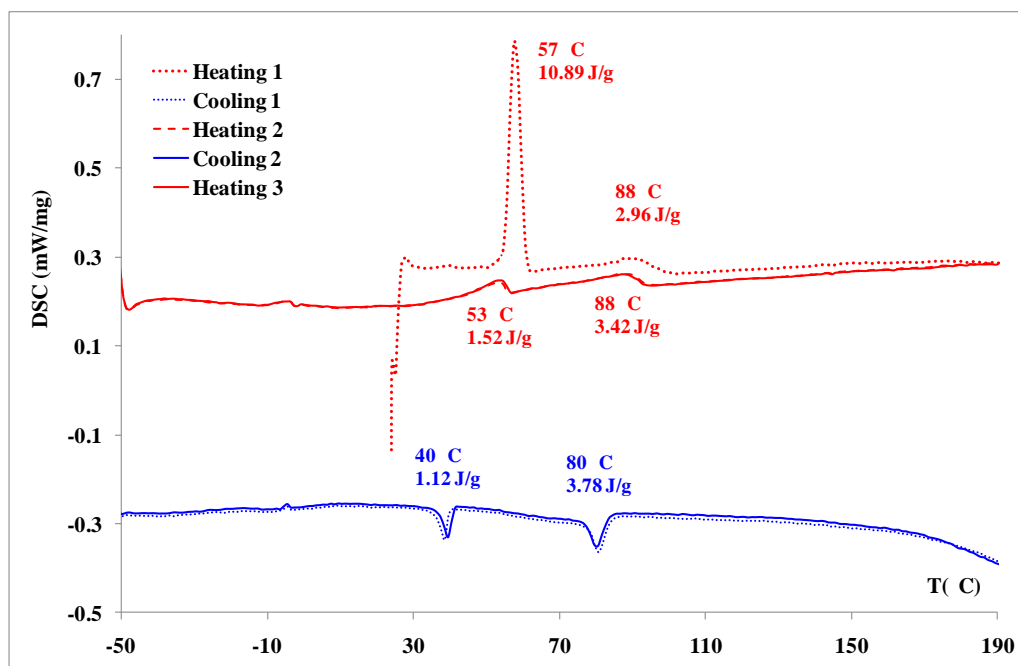
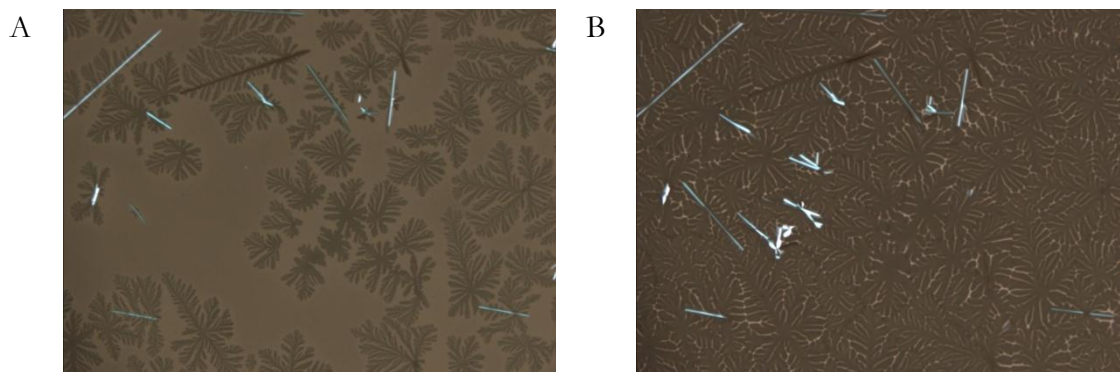


Figure 66. DSC trace of **BT131**, scan rate 10K/min

Figure 66 evidences two possible liquid crystal phases in **BT131**, one of them being metastable at room temperature. Further polarized optical microscopy studies support this claim and several typical optical images of **BT131** at different temperatures are given in Figure 67. **BT131** does show, as expected, a hexagonal columnar liquid crystal phase at relative high temperature, as shown in Figure 67 A. This photo obtained after annealing at 84°C shows the growth of dense branching sprouts without birefringence, typically for columnar hexagonal mesophase homeotropic orientation with some structural orientation defect (the birefringence lines). This optically isotropic texture covers the entire sample at room temperature after a slow cooling process (Figure 67 B). The liquid crystal is in a metastable state (see Figure 66 in which the transition occurs at about 40°C) and finally crystallized (or "liquid-crystallized") the next day (Figure 67 C and D) to a new phase. The nature of this new phase is ambiguous and it is difficult to conclude whether it is liquid crystalline or crystalline.



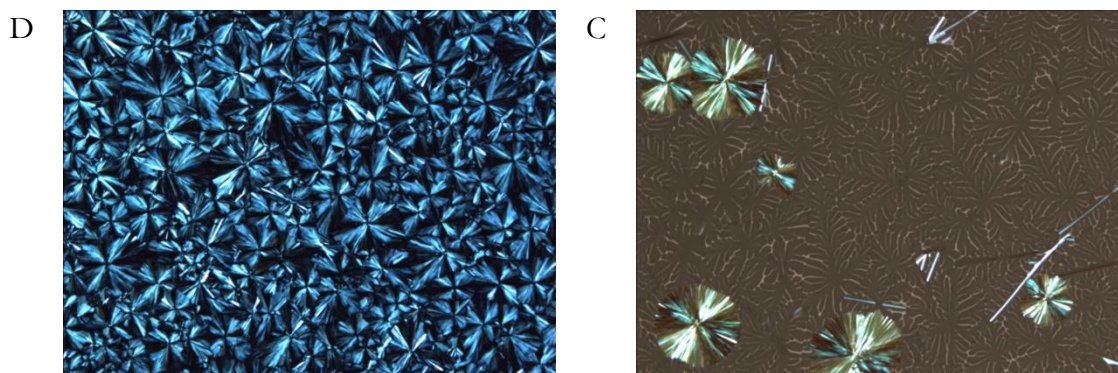


Figure 67. Optical images of **BT131** recorded at 84°C (A), 28°C (B), 1 day after annealing at r.t. (C) and optical texture after 1 day annealing at r.t. (D)

The differential scanning calorimetry analysis of **BT131** suggests that the second liquid crystal phase (below 40 °C) is metastable. Further thermal analysis shows that: on heating the pristine **BT131** up to 150°C and then cooling slowly down to ambient temperature in two days, the fusion peak at 57°C, which is attributed as the melting of crystalline phase into liquid crystal phase, reappears on the second heating cycle. This means that the liquid crystal is metastable at ambient temperature and slowly recrystallizes.

The powder X-ray diffractogram and pattern of **BT131** is presented in Figure 68.^d The diffractogram shows the Bragg reflections as the typical signature of a hexagonal packing of columns.^[69] The X-ray diffraction pattern shows clearly the 6-fold symmetries, the typical signature of the face-on (homeotropic) alignment of the hexagonal columnar mesophases.

In conclusion, the hexagonal columnar liquid crystal phase of **BT131** is well studied by different methods including differential scanning calorimetry, polarized light microscopy and X-ray diffraction. The mesophase is metastable at ambient temperature. The electrochemical and optical studies show that **BT131** behaves like a pure nickel complex.

^dCarried out at CRPP Bordeaux

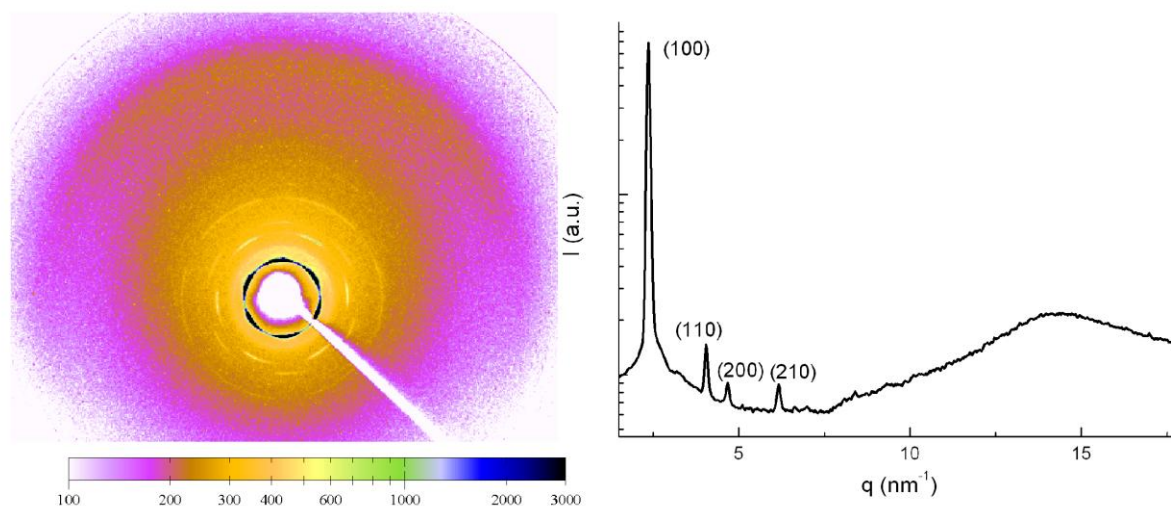


Figure 68. Powder X-ray diffractogram and pattern of **BT131**

This interesting finding opens new ways to form room temperature columnar liquid crystals based on nickel bisdithiolene complexes. As the design and the synthesis of pure nickel bisdithiolene discotic liquid crystals are delicate, the formulation of different nickel complexes seems to be very a promising direction.

3.2. Preliminary applications of discotic nickel bisdithiolene complexes in electronic devices

3.2.1. Zone-Casting studies

The work described in this part was performed during a 1-month research stay with Prof. Jacek Ulanski at the Department of Molecular Physics, Technical University of Lodz (Lodz, Poland) on July 2009.

3.2.1.1. Zone-Casting technique

The zone casting technique^[218-221] consists in casting a suitable organic semiconducting material solution, continuously supplied by a nozzle, onto a moving non pre-oriented substrate as presented in Figure 69.

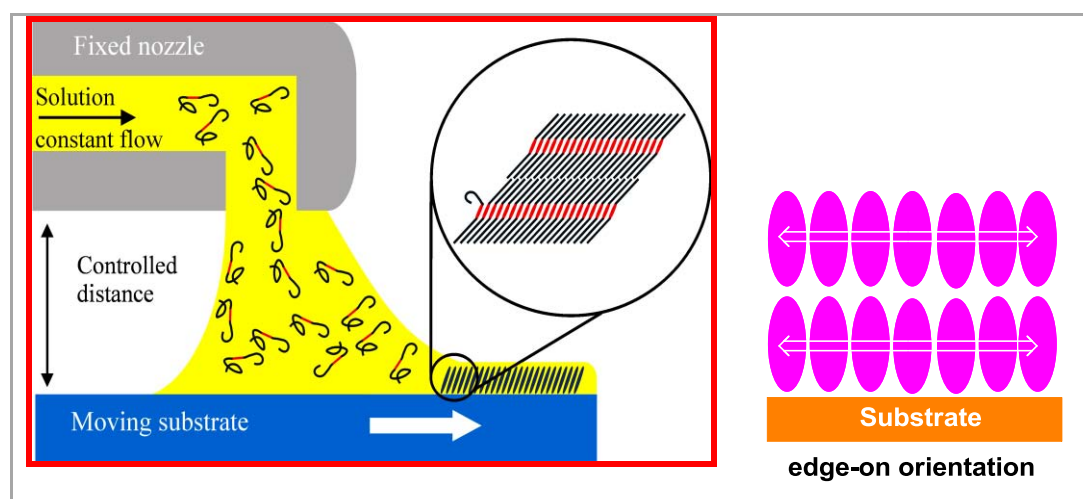


Figure 69. Zone-casting working principle and discotic molecules' edge-on orientation, white arrows indicate privileged charge carriers transport pathway

Both substrate and nozzle are independently thermally controlled. The solution supply rate, substrate's velocity, initial solute concentration, solvent evaporation rate, meniscus' height, and crystallization rate must be chosen properly to obtain stationary conditions. The last two parameters can be controlled by a choice of the solvent and casting temperature. The zone-casting is used to obtain anisotropic layers of many different low-molecular-weight and macromolecular materials. The first application of the zone-casting was a successful preparation of anisotropic oriented networks, micro- or nanowires of the molecular metal tetrathiotetracene-tetracyanoquinodimethane, embedded in a polymer matrix.^[218-222] Recently, this method was

extended to prepare oriented anisotropic thin layers (edge-on orientation, Figure 69) of small-molecule organic semiconductors, including discotic molecules such as hexabenzocoronene^[223, 224] or phthalocyanine^[225] derivatives for organic field effect transistors.^[223-233] These interesting reported results encouraged us to apply the zone-casting technique to our transition metal coordination complexes based semiconducting molecules. For the first studies, the discotic liquid crystalline octadecyloxy-substituted nickel bisdiphenylethanedithiolene complex (**BT22**) was chosen. **BT22** is a wellknown compound with columnar liquid crystalline phase between 83 and 110°C. Another hand, **BT22** has never been used in organic electronic applications.

3.2.1.2. Zone-casting apparatus

The zone-casting apparatus setup is presented in Figure 70 and consists of two main parts: the control and the mechanical unit.

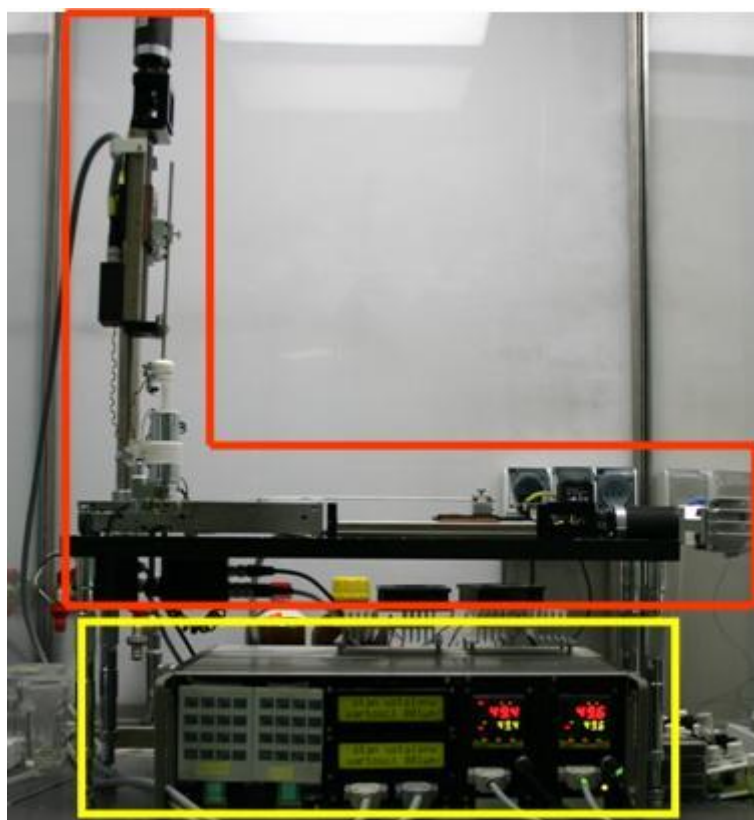


Figure 70. Image of zone-casting apparatus, mechanical part is show in red rectangle; electronic part is shown in yellow rectangle.

The control unit is responsible for controlling the temperature and shifting the speed of executing parts. The mechanical part is responsible for the linear shift of the substrate, the solution supply and temperature maintaining. Two separated setups exist which are responsible

for the solution dosing and the substrate shifting. The substrate shifting is realised by dragging of the glass support on which the substrate is placed, mechanically connected to the linear stage. The solution flow is realized by pressing the piston in the syringe by the plastic piston connected to the linear stage. A flat nozzle is built in such a way that exchangeable cylinders with width 1.5 and 3 cm can be used. The distance between the nozzle and the substrate can be changed with the use of micrometer screws with an accuracy of 10 μm .

3.2.1.3. Preliminary results

The optimization process can be divided into two stages: solvent selection and casting condition optimization. The choice of solvent is based on the results from the drop-casting: in fact, the meniscus movement at the droplet edges during the solvent evaporation in drop-casting is very similar to the process in the meniscus formed between the nozzle and the moving substrate in the zone-casting. In order to choose the most suitable solvent for each material, a solution series of **BT22** was prepared with different solvents and were then casted on a heated glass substrate at different temperatures. The chosen solvent is the one which gave the most promising results from drop casting with small microcrystalline-like domains. The next step is the optimization of the casting process. This consists of changing several parameters as solute concentration (C), solution supply rate (V_{sol}), substrate shifting speed (V_{sub}), solution (T_{sol}) and substrate (T_{sub}) temperatures, meniscus height (h). The above described steps are schematically illustrated in **Figure 71**.

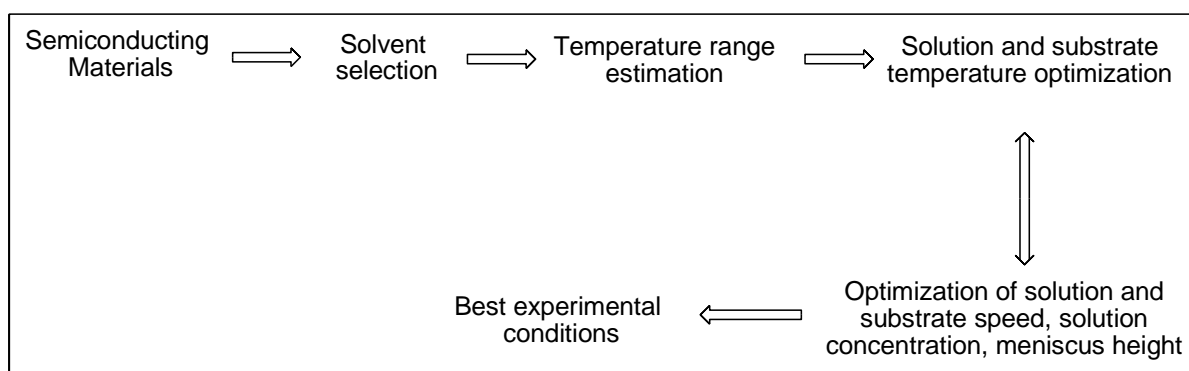


Figure 71. Zone-casting optimization process

Five solvents (chloroform, dichloroethane, toluene, dichlorobenzene and cyclohexanone) were tested and optimized in about a hundred experiments and toluene gave the most promising results. Two pictures of a **BT22** zone-casted layer obtained from a toluene solution on glass substrate are shown in Figure 72. These pictures were taken at the same position and the

polarization plane is parallel (Figure 72, left) and diagonal (Figure 72, right) to the zone-casting direction.

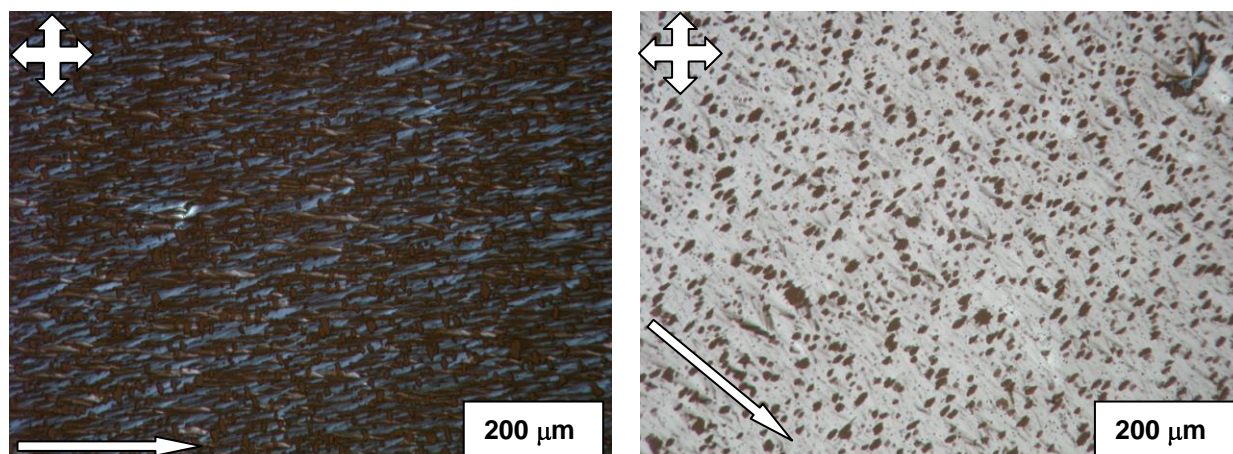


Figure 72. POM images of BT22 zone-casted layer, white arrow: casting direction, crossed white arrows: crossed polarizer and analyser, left (0°) and right (45°) respect to polarizer. Condition: see Table 23

As can be observed from the two pictures, the zone-casted layer responded differently when the angle between polarization light plane and zone-casting direction changes. It means that the layer has some anisotropic properties under polarized light. The most suitable zone-casting conditions for glass substrate are resumed in Table 23.

Table 23. Most suitable zone-casting conditions

Solvent	C (mg/ml)	$T_{\text{sol}}(^{\circ}\text{C})$	$T_{\text{sub}}(^{\circ}\text{C})$	$V_{\text{sol}}(\mu\text{m}/\text{S})$	$V_{\text{sub}}(\mu\text{m}/\text{S})$	h(mm)
Toluene	2.5-3.5	87	85	10	25	≈ 1.0

As observed by polarized light microscopy images, the thin film prepared by zone-casting technique was highly continuous and anisotropic. In order to perform more thorough studies and also field effect transistor applications of **BT22** zone-casted layers, the substrate was changed from non-treated glass into non pre-treated and non pre-oriented silicon wafer coated by a thin layer of silicon dioxide.

The most suitable casting conditions applied for glass substrate were not appropriate for silicon wafer substrate and other experiments were performed in order to find new good conditions. The difference between experimental conditions on glass and silicon substrates may be due to the differences between the surface profiles of the two substrates. Finally, we succeeded in making some oriented continuous layer and one of the most beautiful pictures is shown in Figure 73.

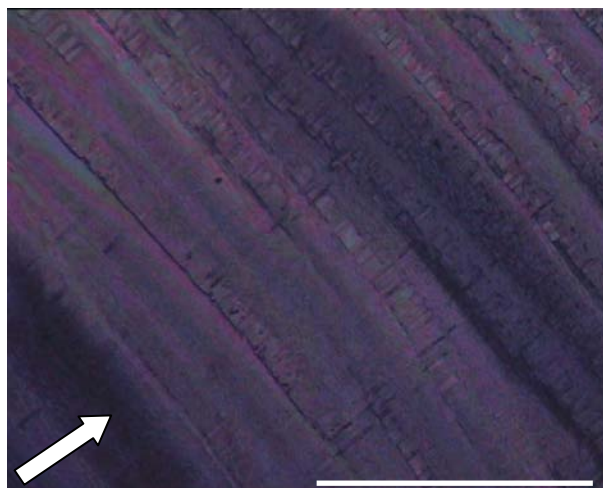


Figure 73. Optical microscopy image in reflection mode of the BT22 zone-casted layer on silicon wafer substrate from toluene solution. Scale bar denotes 1 mm and white arrow denotes casting direction.

Experimental conditions: see Table 24

In this picture, an area of *ca.* 2x2 mm² of continuous zone-casted film is shown. The stepwise surface profile is observed with the “ribbons” perpendicular to the casting direction. The most suitable zone-casting conditions on a silicon wafer substrate are summed up in Table 24.

Table 24. The most suitable zone-casting conditions for silicon wafer substrate

Solvent	C (mg.mL ⁻¹)	T_{sol} (°C)	T_{sub} (°C)	V_{sol} (μm.s ⁻¹)	V_{sub} (μm.S ⁻¹)	h (mm)
Toluene	2.5-3.5	87	83/85	15	20/25	0.3-0.5

The morphology and anisotropy of zone-casted films were then studied by polarized Raman and atomic force spectroscopy. We could also use polarized UV-VIS-NIR absorption spectroscopy, thin film X-rays diffraction for studying the molecular orientation of zone-casted films.

As discussed above, polarized light microscopy and reflection optical microscopy observations give the first ideas about the homogeneity and the anisotropy of the zone-casted films. The atomic force microscopy reveals the layer surface profile at nanoscale.

Atomic force microscopy

The morphology of one of the zone-casted layer is shown in Figure 74. The morphology of an area of 100x120 μm² is presented in Figure 74 A and a smaller area is zoomed in Figure 74 B.

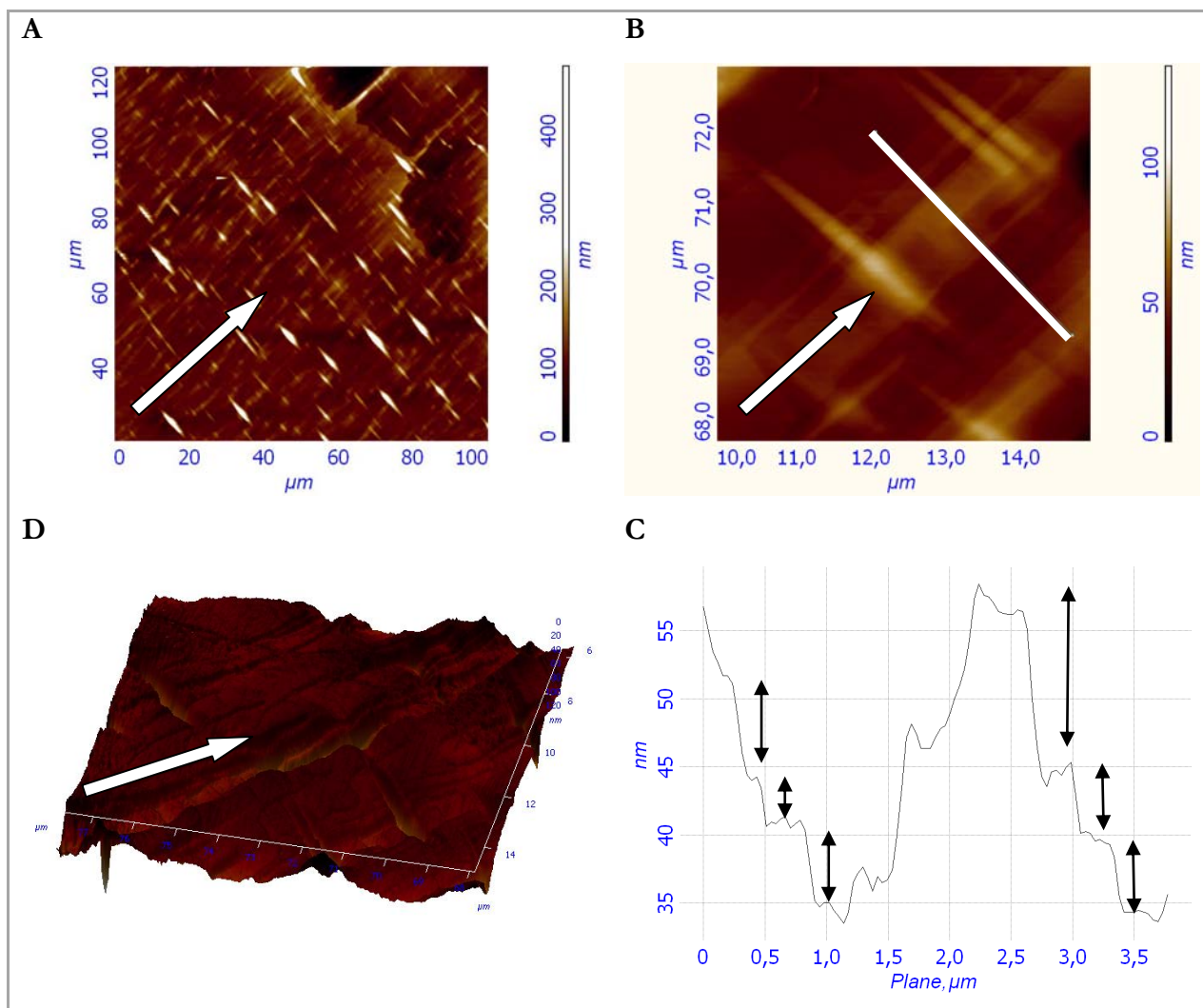


Figure 74. AFM images and surface profile of **BT22** zone-casted layer from toluene solution on silicon wafer substrate. Experimental conditions: see Table 24, white arrows indicate the casting directions

The surface of the film is cracked in both directions: perpendicular and parallel to the casting direction. Surface profile analysis is carried out along the white line in Figure 74 B and the result is presented in Figure 74 C in which regular steps of *ca.* 5 nm and 10 nm are observed. Assuming that the diameter of $[\text{Ni}(\text{dpedt})_2]$ core is *ca.* 1 nm, the steps observed in Figure 74 C should correspond to 5-molecule layer (in case of five-nanometer steps) and 10-molecule layer (in case of ten-nanometer steps). Of course, the nickel complex molecules could be either perpendicular or tilted to the substrate surface.

Polarized Raman spectroscopy

Polarized Raman spectra were recorded on a zone-casted layer of **BT22** on silicon wafer substrate obtained from the experimental conditions of Table 24. Figure 75 shows the 3D Raman

intensity piloted against the angle between the zone-casting direction and the polarization plane of the exciting laser light which vary from 0° to 180° .

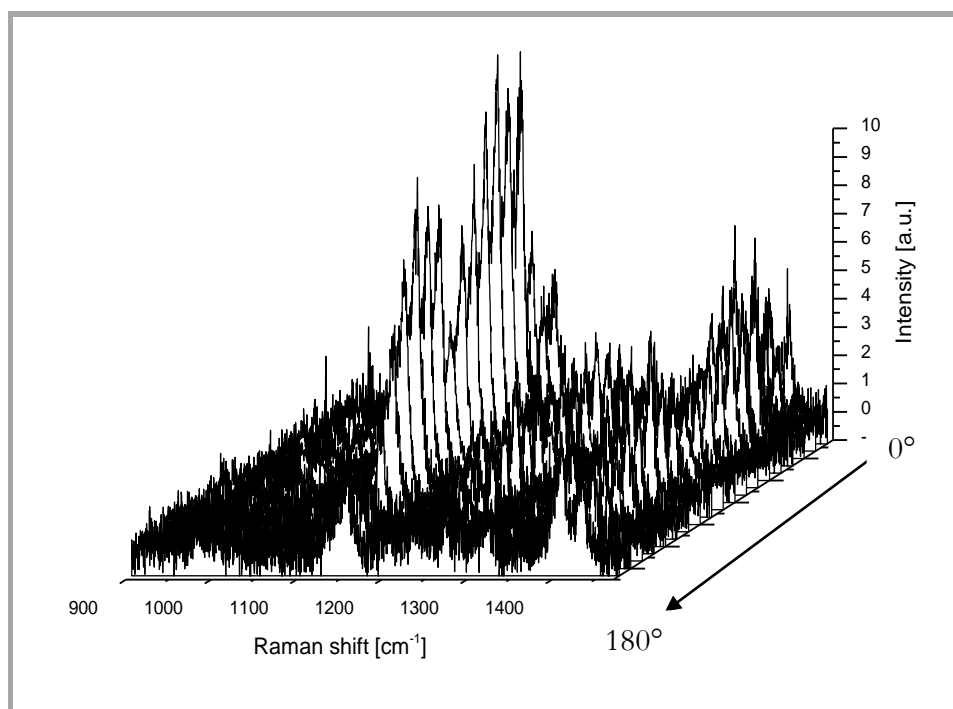


Figure 75. 3D polarized Raman spectra of a zone-casted layer. Zone-casting condition: see Table 24

2D Raman pick intensity piloted against the angle between the zone-casting direction and the polarization plane of exciting laser light with the normalization of pick 1319 cm^{-1} to intensity 1 is given in Figure 76.

As observed on Figure 75 and Figure 76, six main bands (1152 , 1229 , 1268 , 1319 , 1402 , and 1425 cm^{-1}) were observed and one pick at 1319 cm^{-1} , which is attributed to nickel bisdithiolenes core's C=C double bond vibration mode,^[234] is not polarized and is normalized to intensity equal 1. Obviously from Figure 76, all five polarized bands have two maxima and they reach the maximum intensities when the angles between the polarization of exciting laser light and the zone-casting direction are about 50 and 120° . This behavior of the layer under polarized Raman studies suggests that the layer is anisotropic and may contain two kinds of molecular orientations. The discotic nickel complex should be arranged in a “herringbone” structure fashion, which is very commonly observed in zone-casted layer of small disklike organic semiconductors such as hexa-*peri*-benzocoronene derivatives.^[235]

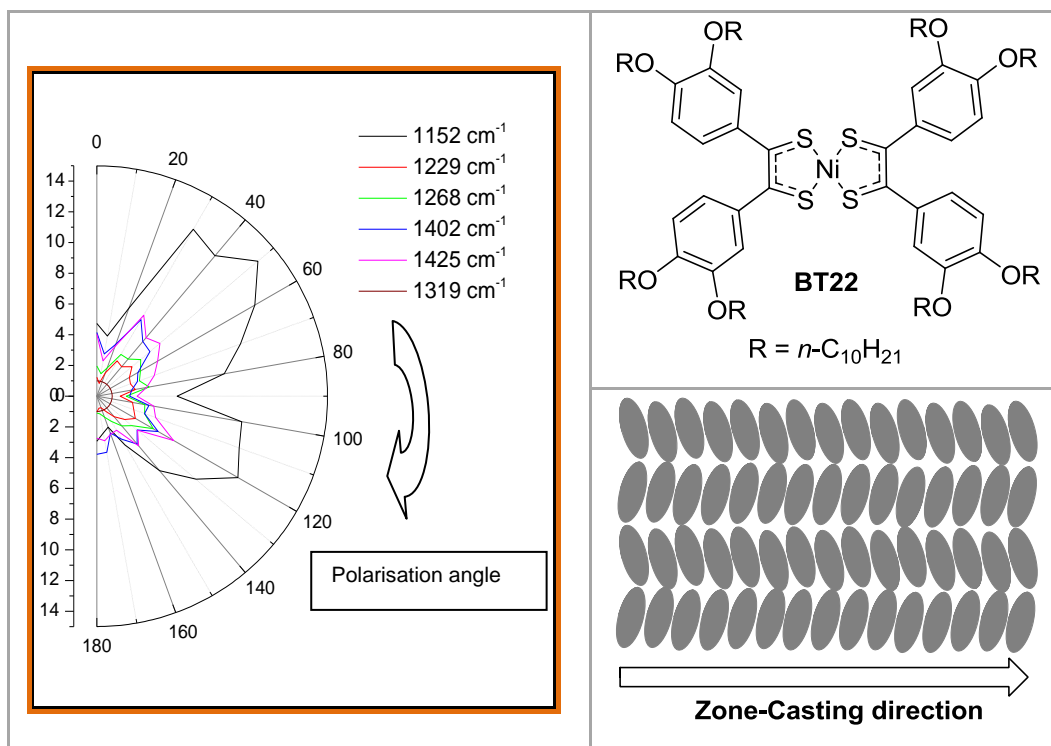


Figure 76. 2D polarized Raman spectra (left) of a BT22 zone-casted layer. Zone-casting condition: see Table 24. Structure of discotic BT22 (top right) and herring-bone molecular orientation (bottom right).

Field effect transistor measurements of zone-casted films

A dozen of golden electrode top-contact field effect transistors (Figure 77) were prepared and characterized both as *p*-type and *n*-type materials. However, no field effect was observed in any tested devices.

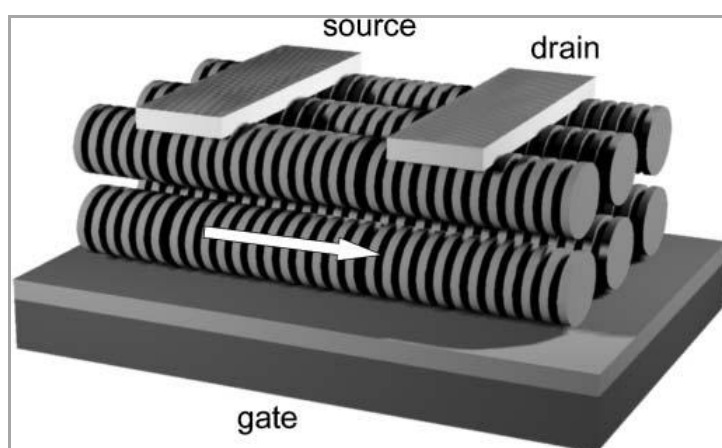


Figure 77. Schematic illustration of a top-contact field effect transistor based on edge-on arranged discotic molecules and uniaxially aligned columns connecting the source-drain contacts. The arrow indicate the direction of the charge carrier transport within the first monolayers.^[70]

The reasons for no field effect may be due to oxygen and/or moisture in the atmosphere, in which both zone-casted films and field effect transistors measurement were performed. Other reasons may be due to the discontinuity at the interface of the layers and the top-electrodes or the discontinuity of the zone-casted films as observed by atomic force microscopy experiments.

It has been demonstrated with hexa-*peri*-benzocoronene derivatives that herring bone orientation can be thermally switched into higher anisotropy edge-on orientation through a change in the intramolecular tilt angle as schematically presented in Figure 78.^[226,236]

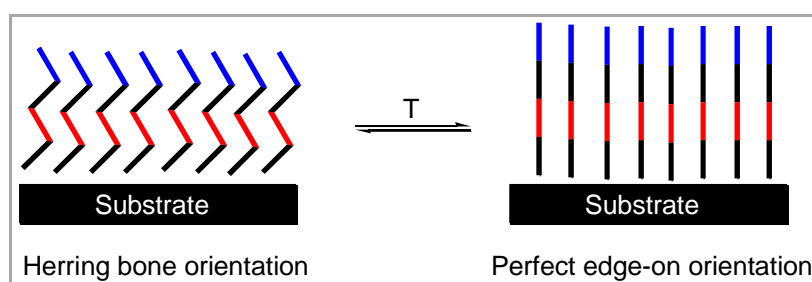


Figure 78

Inspired from this idea, we tried to perform variant temperature field effect transistor measurements but unfortunately, we did not succeed in improving the film quality.

In conclusion, the zone-casting technique was used to perform preliminary study on a columnar liquid crystalline nickel bisdithiolene complex: the **BT22**. The first results demonstrate that the zone-casting is applicable to this kind of semiconducting material. The orientation and continuity of zone-casted layers were confirmed by polarized light microscopy, reflection optical microscopy, atomic force measurements and polarized Raman spectroscopy. Although the first attempts of top-contact field effect transistor measurement were not yet successful, the zone-casting technique seems to be very interesting for preparing highly oriented thin films of discotic nickel bisdithiolene complexes. More work should be now devoted to the optimization of the zone-casting conditions. The anisotropy of zone-casted thin films should be also investigated by additional techniques such as polarized UV-VIS-NIR absorption spectroscopy and thin film X-ray diffraction.

3.2.2. Organic field-effect transistor application

The work described in this part was performed during a 2-week research stay with Prof. Kazuhito Hashimoto at the Department of Applied Chemistry, The University of Tokyo, (Tokyo, Japan) on March 2010.

The ambipolar charge transport in nickel bisdithiolene complex based organic field effect transistors has been well discussed.^[157, 166] In the present work, top contact field effect transistors with channel length of *ca.* 100 μm using discotic nickel bisdithiolenes complexes as charge transporting materials are prepared and characterized. The first studies concerned two new compounds, **BT70** and **BT82**, which are grated by four branched alkoxy chains and do not possess liquid crystalline property. Aluminum ($E_{\text{F(Al)}} = 4.3 \text{ eV}$) and gold ($E_{\text{F(Au)}} = 4.8 \text{ eV}$)^[166] are used as electrodes for electron and hole injection, respectively. All preparation process, from spin-coating thin film deposition to electrode evaporation was carried out in a closed system under dry nitrogen atmosphere and electrical measurements were carried out under vacuum. Example of n-channel transistor response based on **BT70** is given in Figure 79.

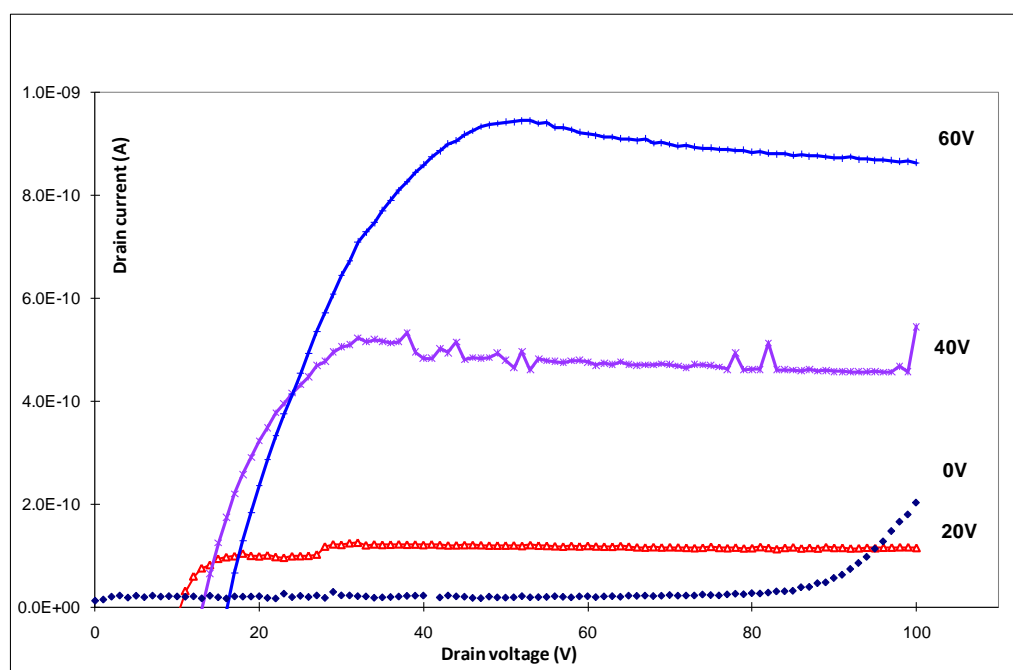


Figure 79. n-channel transistor response based on BT70

From the transistor measurements, the values of both electron and hole mobilities were determined to be in the order of 10^{-6} - $10^{-5} \text{ cm}^2\text{V}^{-1}\text{s}^{-1}$ for the two molecules **BT70** and **BT82**. These values are of course very inferior to those reported in the literature for $[\text{Ni}(\text{dpedt})_2]$ derivatives (in the order of $10^{-4} \text{ cm}^2\text{V}^{-1}\text{s}^{-1}$).^[156-159, 166, 237] It is noteworthy that these values are obtained without any

device optimization and the transistor channel length is *ca.* 100 μm (typically, in small molecule organic field effect transistor, the channel length is about 10 μm). These results demonstrate the capacity of long chain substituted $[\text{Ni}(\text{dpedt})_2]$ derivatives to act as charge transporting materials in electronic devices.

In conclusion, we have preliminarily demonstrated the use of tetraalkoxy-substituted $[\text{Ni}(\text{dpedt})_2]$ as charge transporting materials in electronic devices. Although, more work is needed to optimize all experiments, the preliminary results are very optimistic.

4. General conclusion and perspectives

4.1. General conclusion

The present work is part of a research project funded by the ANR dedicated to the design of a new type of organic photovoltaic cells, based on the use of liquid crystals as active materials. The goal was to design a new device architecture, bilayer or multilayer, composed of two columnar liquid crystalline molecular materials. This thesis describes the design, synthesis and characterizations of new electron acceptor materials combining several properties: thermal stability, stability in air, capability of self-organizing into columnar liquid crystals, strong absorption in the near infrared spectral domain. In this context, the neutral nickel bisdithiolene complexes were anticipated as promising candidates as demonstrated all through this manuscript.

4.1.1. Synthesis of new complexes

One of the main objectives of the present work is the design and the synthesis of columnar liquid crystalline compounds acting as electron-accepting material in bilayer organic photovoltaic devices. For this purpose, several series of long chain substituted discotic nickel bisdithiolene complexes based on dpedt (1,2-diphenyl-1,2-ethylenedithiolene) ligands have been designed and synthesized (Figure 80). In order to explore the impact of the substituents introduced on the phenyl rings on the molecular organization in the material, we examined the number of grafted alkyl chains on the complex core, the chemical nature of the connections of these chains with the phenyl ring, the chains structures and the presence of bulky halogen atoms on the phenyl rings. Thirty-one complexes have been achieved by different new synthetic pathways developed within this work. All discotic nickel bisdithiolene complexes were synthesized from benzil precursors by one pot procedure. Part of these syntheses has been published in a recent paper.^[9]

❖ **Dialkoxybenzils and related compounds:** Starting from commercially available 4,4'-dimethoxybenzil, the two common intermediates 4,4'-dihydroxybenzil and 4-hydroxy-4'-methoxybenzil were synthesized. Two different methods were used to graft alkyl chains on the phenol functions of these two products. By application of classical nucleophilic substitution, we obtained a limited panel of compounds. By using the Mitsunobu reaction, we were then able to graft a larger choice of alkyl chains in one step, particularly branched ones that are often available as cheap primary or secondary alcohols. Numerous 4,4'-dialkoxybenzils, both symmetric or asymmetric, were synthesized. The ester derivatives of 4,4'-dihydroxybenzil could be also easily synthesized by Mitsunobu reaction. The halogenated benzils could be

efficiently synthesized by treatment of 4,4'-dialkoxybenzil by either bromine or N-Iodosuccinimide.

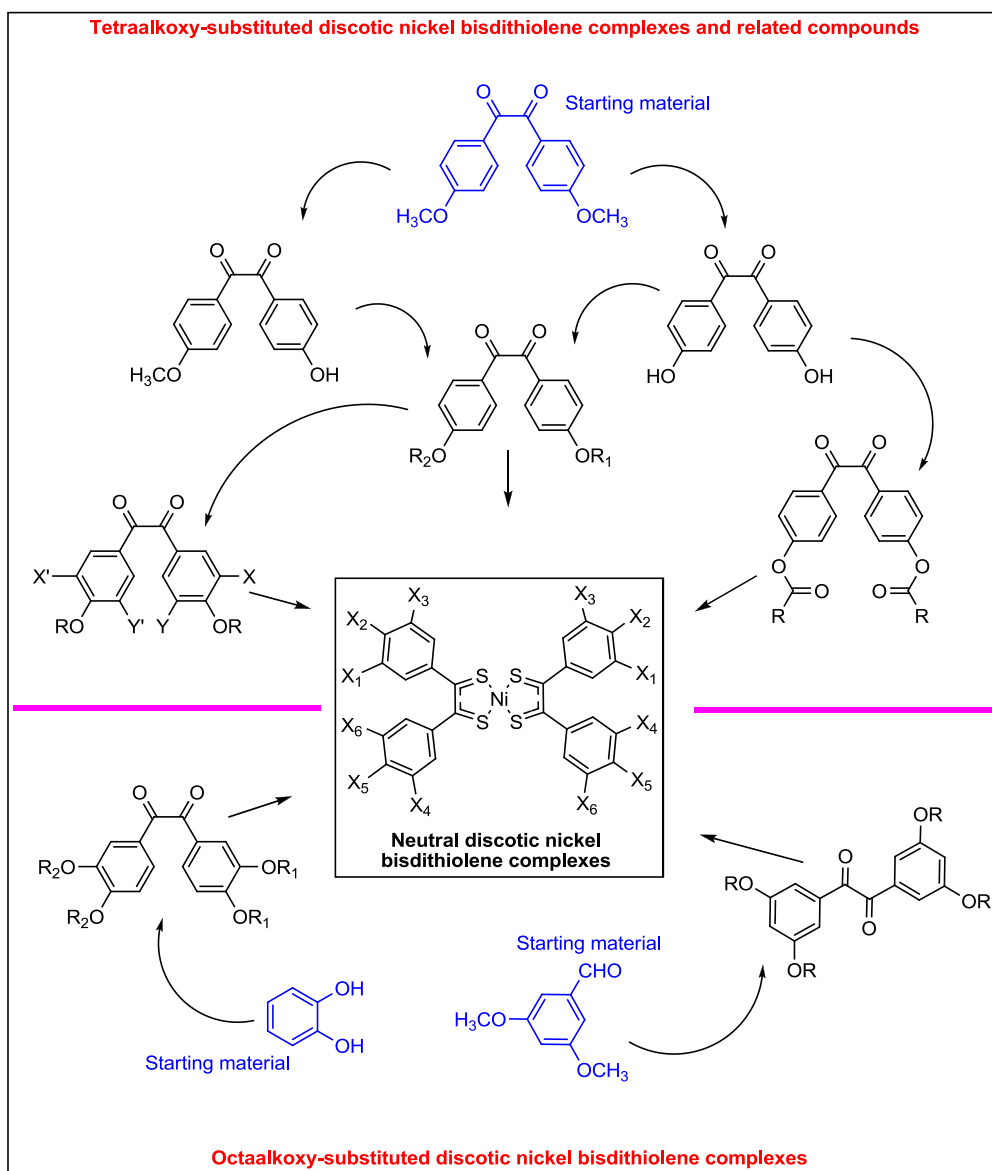


Figure 80. Different synthetic pathways developed in this work

- ❖ **Tetraalkoxybenzils:** starting from 1,2-benzenediol or 3,5-dimethoxybenzaldehyde, several tetraalkoxybenzils were synthesized. The treatment of 1,2-benzenediol with halogenated alkanes or primary alcohol led to 1,2-dialkoxybenzenes. In this work, we propose to use the double Friedel-Crafts acylation reaction between the 1,2-dialkoxybenzenes and oxalylchloride to obtain 3,3',4,4'-tetraalkoxybenzils. In this way, we are able to synthesize a large panel of precursors of nickel dithiolene complexes. The benzoin condensation of 3,5-dimethoxybenzaldehyde followed by the cupric acetate catalytic oxidation of benzoin

derivative gave 3,3',5,5'-tetramethoxybenzil. The later benzil was demethylated and then realkylated to provide new 3,3',5,5'-tetraalkoxybenzil.

In conclusion, we propose here new ways of synthesis for obtaining a large choice of tetraalkoxy-substituted and octaalkoxy-substituted discotic nickel bisdithiolene complexes and related compounds.

4.1.2. Characterization of the synthesized complexes

The physicochemical behaviors of isolated complexes were characterized by using different techniques: differential scanning calorimetry and thermo-gravimetric analysis, polarized optical microscopy, cyclic and square wave voltammetries, absorption spectroscopy and powder X-ray diffraction. The obtained results show that nickel bisdithiolene complexes are all very stable in air and can be heated up to 300°C under nitrogen atmosphere.

Our results seem to demonstrate that eight chains are at least necessary to reach liquid crystalline structures. We also examined the impact of the structure of these chains. Surprisingly, it seems that only linear chains lead to liquid crystals, whereas in numerous other cases reported in the literature, branched ones are liquid crystal promoters. In some case, a mixture of different linear grafted chain seems to be a favorable factor. Moreover, we investigated the impact of the linker, ether or ester. Owing to our results, neither the ester connections, nor the introduction of bulky atoms (halogens) on the phenyl rings provide any noticeable improvement on the molecular packing.

Some of our compounds show hexagonal columnar liquid crystalline phases at relatively high temperature (about 85°C) but these phases are metastable at room temperature in the condensed state and in non-constrained conditions. It is noteworthy that, without any specific substrate surface treatment, this well homeotropic alignment of discophases is maintained at room temperature for *ca.* 24h before the recrystallization occurs. We may anticipate that in optimized conditions of surface treatment and when embedded in a solar cell structure, this molecular arrangement could be frozen for longer times.

The electronic absorption spectroscopy studies show that all the synthesized nickel complexes absorb strongly between 700 nm to 1200 nm with molar extinction coefficients as high as *ca.* 40000 Lcm⁻¹mol⁻¹. The optical bangaps are of *ca.* 1.1 eV. The electrochemical studies reveal that

these complexes have high electron affinities. The electrochemical bandgaps are of *ca.* 1.0 V, a very similar value to that measured by electronic absorption. The HOMO and LUMO energy levels are determined from electrochemical data. The values of the HOMO and LUMO energies are of *ca.* -5.7 eV and of *ca.* -4.7 eV, respectively. In particular, it appears that the optical and electrochemical properties of discotic nickel bisdithiolene complexes can be only moderately tuned as a function of the functional groups grafted on the dithiolene ligands.

4.1.3. Device application

During the one-month stay at the Technical University of Lodz (Lodz, Poland), in the laboratory of Prof. Ulanski, one octaalkoxy-substituted nickel complex (**BT22**) was studied by Zone-Casting, a solution processing technique for obtaining highly oriented organic thin films for transistors applications. Preliminary results showed that well organized thin films could be obtained but more investigations are required before obtaining satisfactory results.

During a two-week stay at The University of Tokyo (Tokyo, Japan), in the laboratory of Prof. Hashimoto, two other tetraalkoxy-substituted nickel bisdithiolene complexes (**BT70** and **BT82**) were tested as components in organic transistors configurations. The first measurements show that these compounds have ambipolar charge transport properties. The obtained values are still very modest but encouraging us to optimize experimental conditions.

4.2. Perspectives

In order to use nickel bisdithiolene complexes as electron acceptor photoactive materials in organic photovoltaic devices and due to their quite low energy levels of both LUMO (-4.7 eV) and HOMO (-5.7 eV), a suitable electron donor material should be chosen. Some structures and HOMO and LUMO energy levels of potential donors^[65] are given in Figure 81 and Figure 82.

Besides the classical P3HT (**D1**), we could envisage to associate our compounds with carbazolenes based polymers (**D7** and **D8**) and with some fluorene based polymers (such as **D5**) for which the LUMO energy levels are in the best accordance with that of [Ni(dpdt)₂].

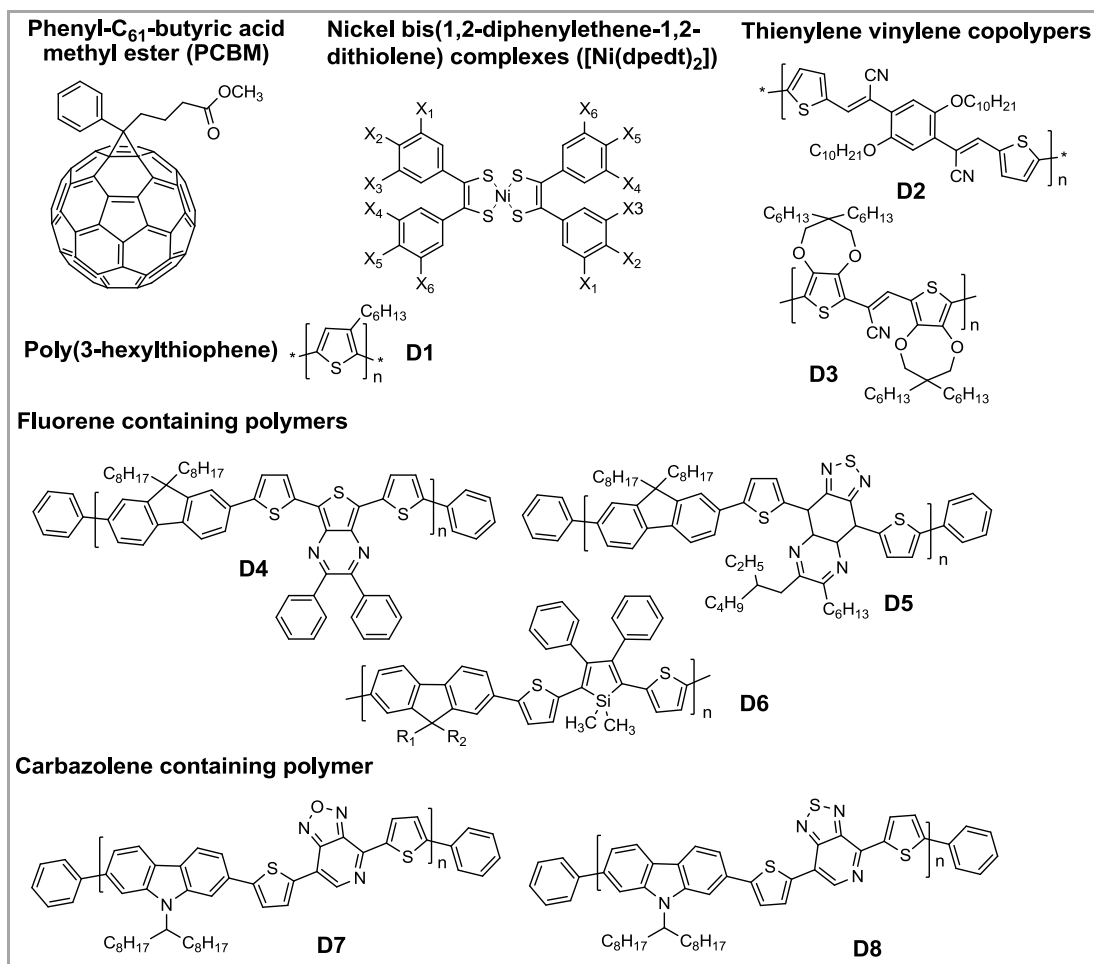


Figure 81. Structure of PCBM, nickel complexes and several potential donor materials

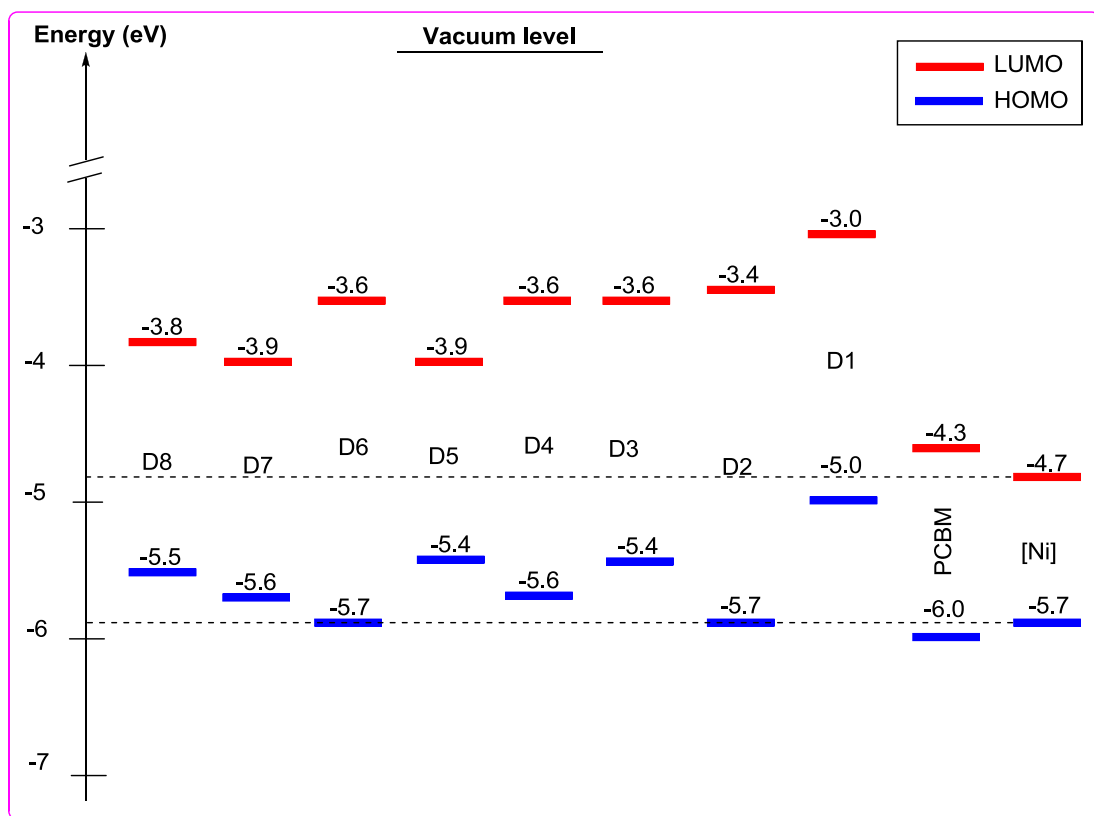


Figure 82. LUMO-HOMO levels of materials given in Figure 81

As demonstrated in the present work, the effect of the alkoxy side chain length, the connecting group and the halogenations of the ligands are not efficient enough to lead to the desired stable room temperature hexagonal columnar liquid crystals. This structure is reached only around 85°C and may be maintained at room temperature only for *ca.* one day. A stable liquid crystalline state may be obtained with these compounds only after surface treatments. A chemical way could also be envisaged with future synthesis work focused on the introduction of hydrogen bonds between the molecules. Functional groups able to induce hydrogen bonds (as imide, acide, and alcoholic) could be introduced directly on the phenyl ring in order to promote intracolumnar interactions between pairs of neighbouring complexes. They could also be introduced on the side chains in order to promote intercolumnar interactions between neighbouring columns. Example of hydrogen bonds assisted stable room temperature columnar liquid crystals can be found with the hexamide derivative of triphenylene which exhibits an intracolumnar inter-disc distance as short as 3.18 Å.^[238]

Another strategy that can be adopted is the grafting of the nickel bisdithiolene core on one big discotic template well known as discotic liquid crystal, such as hexa-*peri*-hexabenzocoronene or phthalocyanine derivative. Other examples of stable room temperature columnar liquid crystals can be found at.^[62, 69-71, 80, 81, 93]

Recently, Thiebaut, Bock and Grelet at Centre de Recherches Paul Pascal in Bordeaux, our partners within the CPA-FALLOIR project, have succeeded, for the first time, in the preparation of a face-on oriented bilayer of two discotic columnar liquid crystals for organic donor-acceptor heterojunction.^[239] By applying this technique to one of their electron donor stable room temperature discotic liquid crystals and one of our electron acceptors showing liquid crystalline properties, even metastable at room temperature, interesting results may be obtained. Due to the electrical difference between the two compounds (the one electron rich and the other electron deficient), the hexagonal columnar liquid crystal packing of the nickel bisdithiolene complexes could be “frozen” during a sufficient time at ambient temperature for electronic characterization.

The collaboration with the researchers of the Prof. Hashimoto’s group at The University of Tokyo could help further characterization of nickel bisdithiolene complexes. The HOMO levels of these molecules can be determined there by ultraviolet photoelectron spectroscopy technique. Furthermore, this laboratory has the expertise of the organic synthesis of donor materials to be

associated with fullerene derivatives. Through further collaborative work, we aim at testing nickel bisdithiolene compounds in their prototypes.

The collaboration with the theoretical chemists of the Laboratoire de Chimie et Physique Quantiques at The University of Toulouse could help further understanding of experimental results or predicting properties of new designed nickel bisdithiolene complexes.^[234]

5. Experimental section and References

5.1. Experimental section

5.1.1. General remarks

All used chemicals and solvents were purchased from chemical companies and used as received, unless otherwise mentioned. All reactions were performed under ambient atmosphere and under air exposition unless special indication.

^1H and ^{13}C NMR experiments were recorded in the listed deuterated solvents (internal standard) on 4 Bruker Spectrometers (ARX 250, DPX 300, Avance 300 and Avance 400). Multiplicity of NMR signal was denoted as br (broad), m (massif), s (singlet), d (doublet), t (triplet), quart (quartet), quint (quint), sext (sextet), sept (septet), dd (double doublet), dt (double triplet).

Purification of products was performed by column chromatography on silica gel from Merck with a grain size of 0.04-0.063 mm (flash silica gel, Geduran Si 60) with analytically pure solvents. For analytical thin layer chromatography (TLC), silica gel coated substrates "60 F254" from Merck were used and compounds were detected by fluorescence quenching at 254 nm, self-fluorescence at 365 nm.

Melting points were determined by DSC thermograms, which were obtained on a DSC 204 NETZSCH system using 2-5 mg samples in 30 μl sample pans and a scan rate of 10°C min⁻¹. ΔH is calculated in kJ.mol⁻¹.

Mass analyses were performed at the Service de Spectrométrie de Masse de la Structure Fédérative Toulousaine en Chimie Moléculaire.

Elemental analyses (C, H, S, Ni) were carried out at the Service Central d'Analyse du CNRS in Lyon.

Voltammetric measurements were carried out with a potentiostat Autolab PGSTAT100 controlled by GPES 4.09 software. Experiments were performed at room temperature in a homemade airtight three-electrode cell connected to a vacuum/argon line. The reference electrode consisted in a saturated calomel electrode (SCE) separated from the solution by a bridge compartment. The counter electrode was a platinum wire of ca 1cm² apparent surface. The working electrode was a Pt microdisk (0.5mm diameter) or a glassy carbon (1mm diameter). The supporting electrolyte (nBu₄N)[PF₆] (Fluka, 99% electrochemical grade) was used as received

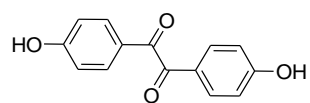
and simply degassed under argon. CH_2Cl_2 was freshly distilled over CaH_2 prior to use. The solutions used during the electrochemical studies were typically $10^{-3} \text{ mol.L}^{-1}$ in complex compound and 0.1 mol.L^{-1} in supporting electrolyte. Before each measurement, the solutions were degassed by bubbling Ar and the working electrode was polished with a polishing machine (Presi P230).

UV-VIS-NIR absorption spectra were recorded on two spectrometers Perkin Elmer Lambda 35 and Perkin Elmer GX 2000, using DCM as solvent. The solutions used during the electronic absorption studies were typically about $10^{-5} \text{ mol.L}^{-1}$ in complex.

Zone-casting layer preparation was realized in dust-free air atmosphere clean room and the humidity was not controlled. Samples on glass were prepared with use of microscopic glass side with dimensions *ca.* 2.6 x 7.6 cm purchased from Comex (Wroclaw, Poland). The glasses were cleaned in warm (*ca.* 40°C) ultrasonic bath with chloroform for about 10 minutes and then dried under nitrogen stream. Zone-casting layers for use in organic field effect transistors were prepared on the substrates which were highly doped silicon wafers (resistivity in the range 0.001-0.004 Ohm.cm^{-1} , orientation $\langle 100 \rangle$, thickness 285-315 μm , Cemat Silicon, Poland) with thin ($1500 \pm 150 \text{ \AA}$) thermal silicon dioxide. Solvents used for substrate cleaning and materials solution preparation were “pure per analysis” grade. Solutions for thin films preparation were stirred about 10 minutes at room temperature (chloroform, dichloroethane) or at *ca.* 70°C (toluene, dichlorobenzene and cyclohexanone). Oriented thin layers of investigated material were obtained using the zone-casting apparatus built at the Technical University of Lodz as described above. In this work 2-cm and 3-cm width nozzles were used. Field effect transistors with top contact source and drain electrodes were prepared by metal evaporation through the shadow mask with wires with different diameter, creating channels 80 μm in length and 2 mm in width. Metal electrodes were evaporated in Bottom Contact Configuration Edwards vacuum evaporator from tungsten sources placed about 15 cm from the sample. The process conditions were as follow: starting pressure *ca.* 2×10^{-6} mbar, rate of evaporation *ca.* $0.03 \div 0.1$ nm per second. Thickness of the evaporated electrodes was in the range 90-125 nm.

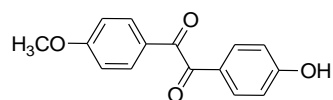
5.1.2. Material Synthesis

4,4'-dihydroxybenzil (**1a**)



4,4'-Dimethoxybenzil (26 g, 96.2 mmol) was heated to reflux for 50h in a mixture of aqueous HBr (48%) and glacial acetic acid (550 mL, 50/50). The reaction mixture was cooled by a bath of ice-water and the yellow precipitate was collected by filtration. The filtrate was then extracted several times with ethyl acetate. The organic phases and the yellow precipitate were combined, washed several times with water, dried with MgSO₄ and the solvent was removed under reduced pressure. The residue was purified by column chromatography (CH₂Cl₂/Acetone: 85/15) giving **1a** as pure yellowish solid (22.45 g, 96%). δ_{H} (250 MHz, CD₃OD) 7.82 (4 H, d, J = 9.0 Hz, aromatic H), 6.91 (4 H, d, J = 9.0 Hz, aromatic H), 4.92 (2 H, br s, phenol H). δ_{C} (75 MHz, CD₃OD) 194.26, 164.09, 132.17, 124.89, 115.51. **HRMS**(CI-CH₄): found 243.0669, [M+H]⁺ requires 243.0657

4-hydroxy-4'-methoxybenzil (**1b**)

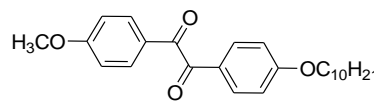


As described for the synthesis of **1a** but the reflux time was decreased to 17h. Complete workup gave a mixture of three products: 4,4'-dimethoxybenzil (18% of starting material), **1a** (yellowish solid, 33 %) and **1b** (yellow solid, 28%). δ_{H} (250 MHz, (CD₃)₂CO) 9.58 (1 H, s, phenol H), 7.93 (2 H, d, J = 9.0 Hz, aromatic H), 7.87 (2 H, d, J = 9.0 Hz, aromatic H), 7.13 (2 H, d, J = 9.0 Hz, aromatic H), 7.03 (2 H, d, J = 9.0 Hz, aromatic H), 3.94 (3 H, s, -OCH₃). δ_{C} (62.5 MHz, (CD₃)₂CO) 193.46, 165.04, 163.51, 132.30, 131.94, 126.29, 125.45, 115.95, 114.47, 55.31. **HRMS**(CI-CH₄): found 257.0826, [M+H]⁺ requires 257.0814

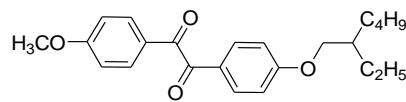
General procedure for the synthesis of benzils **3b**, **3c**, **3n**, **3p**, **3q**

A mixture of **1b** (for **3b-3c**) or **2n-2p** (for **3n**, **3o**, **3p**, **3q**) (3.9 mmol), alkyl bromide (5.9 mmol), and powdered potassium carbonate (1.1 g, 7.8 mmol) was stirred in DMF (25 mL) at 90°C. The reaction was monitored by TLC (Hexane/CH₂Cl₂ 50/50). Upon cooling to room temperature, the reaction was quenched by adding water and the resulting mixture was extracted by CH₂Cl₂. The organic phases were combined, rinsed several time by water, dried over anhydrous magnesium sulfate and concentrated under reduced pressure resulting in the crude product which was purified by silica gel column chromatography (Hexane/CH₂Cl₂ 50/50).

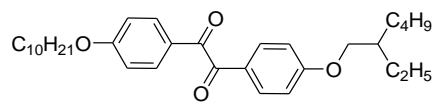
4-decyloxy-4'-methoxybenzil (3b)

 Yellowish solid (1.47 g, 95%). δ_{H} (300 MHz, CD_2Cl_2) 7.95 (4 H, m, aromatic H), 7.02 (4 H, m, aromatic H), 4.08 (2 H, t, $J = 6.6$ Hz, $-\text{OCH}_2-$), 3.92 (3H, s, $-\text{OCH}_3$), 1.84 (2 H, m, $-\text{OCH}_2\text{CH}_2-$), 1.49-1.32 (14 H, m), 0.92 (3 H, t, $J = 6.6$ Hz, $-\text{CH}_2\text{CH}_3$). δ_{C} (75 MHz, CD_2Cl_2) 193.58, 193.51, 164.94, 164.61, 132.18, 126.25, 125.95, 114.69, 114.25, 68.60, 55.68, 31.89, 29.53, 29.30, 28.99, 25.88, 22.67, 13.86

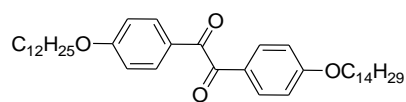
4-methoxy-4'-(2-ethylhexyloxy)benzil (3c)

 Yellowish oil (1.4 g, 97%). δ_{H} (300 MHz, CD_2Cl_2) 7.96 (4 H, m, aromatic H), 7.03 (4 H, m, aromatic H), 3.98 (2 H, d, $J = 5.7$ Hz, $-\text{OCH}_2-$), 3.92 (3 H, s, $-\text{OCH}_3$), 1.79 (1 H, m, $-\text{CH}_2\text{CH}-$), 1.53-1.35 (8 H, m), 0.97 (6 H, t, $J = 7.5$ Hz, $-\text{CH}_3$). δ_{C} (75 MHz, CD_2Cl_2) 193.60, 193.52, 164.94, 164.84, 132.17, 132.10, 126.26, 125.92, 114.72, 114.28, 70.99, 55.68, 39.24, 30.37, 28.99, 23.75, 23.00, 13.81, 10.82

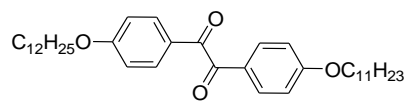
4-decyloxy-4'-(2-ethylhexyloxy)benzil (3n)

 Yellow oil (0.54 g, 69%). δ_{H} (250 MHz, CD_2Cl_2) 7.96 (4 H, dd, $J = 1.75-7.0$ Hz, aromatic H), 7.02 (4 H, m, aromatic H), 4.09 (2 H, t, $J = 6.5$ Hz, $-\text{OCH}_2\text{CH}_2-$), 4.00 (2 H, d, $J = 5.75$ Hz, $-\text{OCH}_2\text{CH}-$), 1.87-1.77 (3 H, m), 1.51-1.33 (22 H, m), 1.00-0.90 (9 H, m, $-\text{CH}_3$). δ_{C} (62.5 MHz, CD_2Cl_2) 193.60, 164.82, 164.60, 132.17, 126.01, 125.97, 114.70, 71.01, 68.61, 39.27, 31.91, 30.40, 29.55, 29.32, 29.02, 25.90, 23.77, 23.02, 22.69, 13.88, 13.82, 10.84

4-dodecyloxy-4'-tetradecyloxybenzil (3p)

 Yellow solid (1.17 g, 99%). δ_{H} (250 MHz, CD_2Cl_2) 7.96 (4 H, m, aromatic H), 7.03 (4 H, m, aromatic H), 4.11 (4 H, t, $J = 6.5$ Hz, $-\text{OCH}_2-$), 1.87-1.32 (44 H, m, $-\text{CH}_2-$), 0.95 (6 H, t, $J = 6.3$ Hz, $-\text{CH}_3$). δ_{C} (62.5 MHz, CD_2Cl_2) 193.57, 164.59, 161.06, 132.17, 126.00, 114.68, 68.60, 64.01, 31.92, 29.64, 29.57, 29.54, 29.50, 29.34, 29.31, 29.19, 29.00, 28.53, 25.88, 25.80, 22.68, 13.87

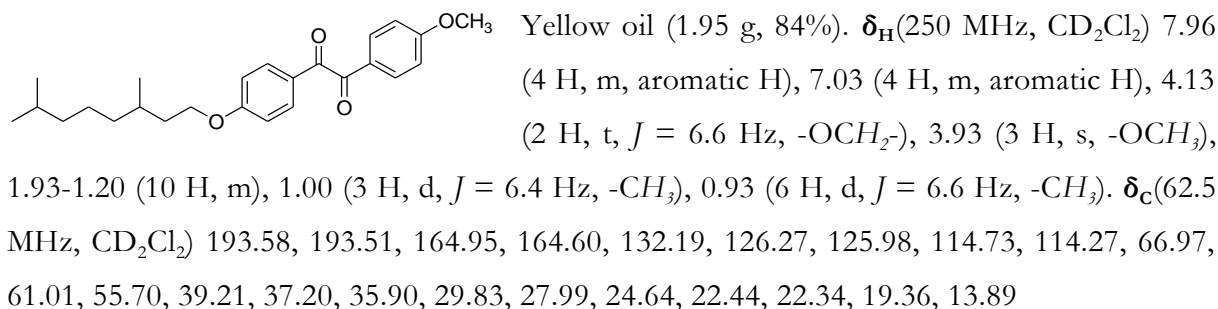
4-dodecyloxy-4'-undecyloxybenzil (3q)

 Yellowish solid (1.1 g, 80%). δ_{H} (300 MHz, CD_2Cl_2) 7.96 (4 H, dt, $J = 9.6 - 2.7$ Hz, aromatic H), 7.03 (4 H, dt, $J = 9.6 - 2.7$ Hz, aromatic H), 4.08 (4 H, t, $J = 6.6$ Hz, $-\text{OCH}_2-$), 1.84 (4 H, m, $-\text{OCH}_2\text{CH}_2-$), 1.51-1.31 (34 H, m), 0.92 (6 H, t, $J = 6.3$ Hz, $-\text{CH}_3$). δ_{C} (75 MHz, CD_2Cl_2) 193.57, 164.59, 132.17, 125.99, 114.69, 68.60, 66.75, 31.93, 29.59, 29.55, 29.33, 29.01, 25.90, 22.70, 13.89. **HRMS**(CI- CH_4): found 565.4244, $[\text{M}+\text{H}]^+$ requires 565.4257

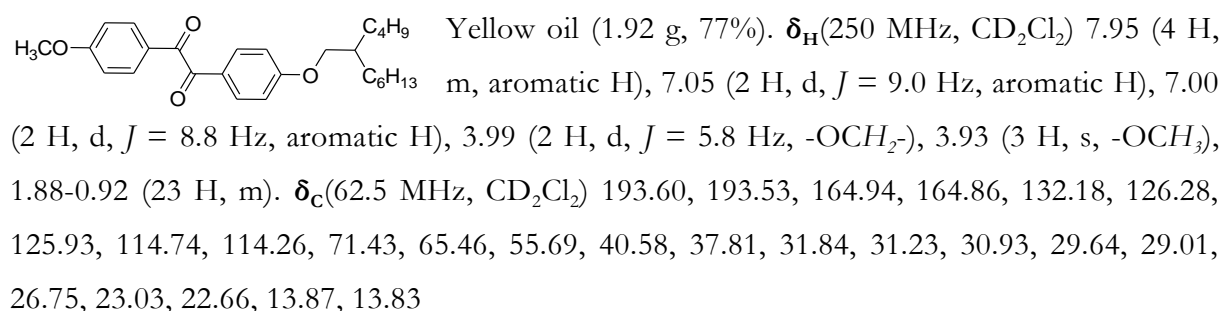
General procedure for the synthesis of benzils 3d, 3e, 3f, 3o, 3r, 3s

A THF (50 mL) solution of 4-hydroxy-4'-methoxy benzil (1.5 g, 5.85 mmol), PPh₃ (1.85 g, 7.02 mmol), and alcohol (7.02 mmol) were cooled to 0°C. To the solution was added diethyl azodicarboxylate in toluene solution (3.2 mL, 7.02 mmol, 40% w/v), the mixture was kept at that temperature for 1h and then was allowed to warm to room temperature and stirred for 1 h. The reaction mixture was then evaporated. After addition of 300 mL of hexane, the mixture was filtered. The filtrate was evaporated, and the residue was purified by silica gel column chromatography (Hexane/CH₂Cl₂ 50/50)

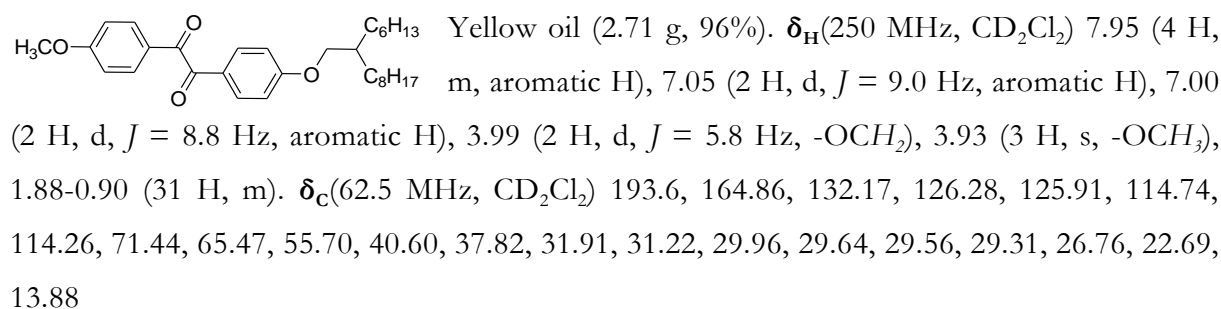
4-(3,7-dimethyloctyloxy)-4'-methoxybenzil (3d)



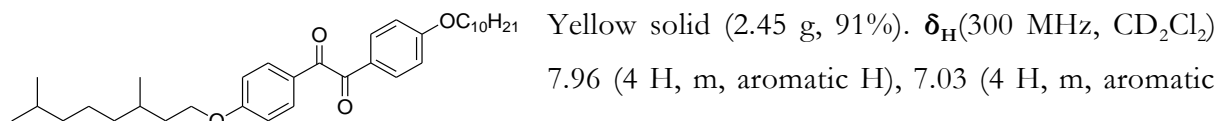
4-(2-butyloctyloxy)-4'-methoxybenzil (3e)



4-(2-hexyldecyloxy)-4'-methoxybenzil (3f)

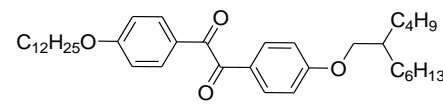


4-decyloxy-4'-(3,7-dimethyloctyloxy)benzil (3o)



H), 4.15-4.06 (4 H, m, $-\text{OCH}_2$), 1.86-1.19 (26 H, m), 1.00-0.90 (12 H, m, $-\text{CH}_3$). δ_{C} (75 MHz, CD_2Cl_2) 193.56, 164.58, 164.56, 132.17, 126.00, 114.69, 68.59, 66.95, 39.19, 37.18, 35.88, 31.89, 29.80, 29.54, 29.31, 29.00, 27.97, 25.89, 24.62, 22.68, 22.43, 22.33, 19.35, 13.88

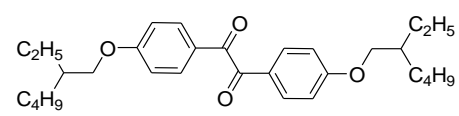
4-dodecyloxy-4'-(2-butyloctyloxy)benzil (3r)

 Yellow solid (1.97 g, 100 %). δ_{H} (300 MHz, CD_2Cl_2) 7.96 (4 H, dt, $J = 9.6 - 2.7$ Hz, aromatic H), 7.03 (4 H, dt, $J = 9.6 - 2.7$ Hz, aromatic H), 4.09 (2 H, t, $J = 6.6$ Hz, $-\text{OCH}_2\text{CH}_2-$), 3.98 (2 H, d, $J = 6.6$ Hz, $-\text{OCH}_2\text{CH}$), 1.86 (4 H, m), 1.51-1.31 (33 H, m), 0.94 (9 H, m, $-\text{CH}_3$). δ_{C} (75 MHz, CD_2Cl_2) 193.59, 164.83, 164.59, 132.17, 126.01, 125.95, 114.72, 114.69, 71.41, 68.60, 37.80, 31.93, 31.84, 31.23, 30.92, 29.64, 29.59, 29.55, 29.36, 29.33, 29.01, 26.75, 25.90, 23.03, 22.70, 22.67, 13.87, 13.83. **HRMS**(CI- CH_4): found 579.4433, $[\text{M}+\text{H}]^+$ requires 579.4413

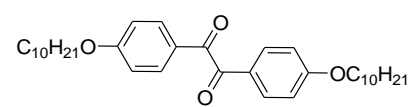
General procedure for the synthesis of benzils 3g, 3t

A mixture of 4,4'-dihydroxybenzil **1a** (3.26 g, 13.5 mmol), alkyl bromide (40.5 mmol), and powdered potassium carbonate (54 mmol) was stirred in DMF (80 mL) at 100 °C and the reaction was monitored by TLC. Upon cooling to room temperature, the reaction was quenched by adding water and the resulting mixture was extracted by CH_2Cl_2 . The organic phases were combined, rinsed several time by water, dried over anhydrous magnesium sulfate and concentrated under reduced pressure resulting in a crude product which was purified by silica gel column chromatography (Hexane/ CH_2Cl_2 50/50).

4,4'-di(2-ethylhexyloxy)benzil (3g)

 Yellowish oil (4.32 g, 70%). δ_{H} (250 MHz, CD_2Cl_2) 7.94 (4 H, d, $J = 9.0$ Hz, aromatic H), 7.02 (4 H, d, $J = 9.0$ Hz, aromatic H), 3.99 (4 H, d, $J = 5.8$ Hz, OCH_2CH), 1.83-1.78 (2 H, m, OCH_2CH), 1.52-1.24 (16 H, m, $-\text{CH}_2-$), 1.01-0.93 (12 H, m, $-\text{CH}_3$). δ_{C} (75 MHz, CD_2Cl_2) 193.61, 164.81, 132.15, 125.97, 114.71, 70.98, 39.25, 30.37, 29.00, 23.75, 23.00, 13.81, 10.82

4,4'-di(decyloxy)benzil (3t)

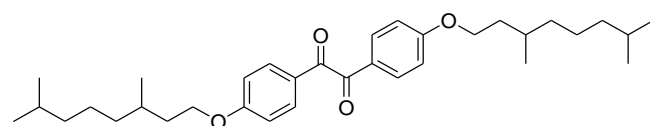
 Yellowish solid (6.35 g, 98 %). δ_{H} (300 MHz, CD_2Cl_2) 7.94 (4 H, dt, $J = 2.7-9.0$ Hz, aromatic H), 7.01 (4 H, dt, $J = 2.7-9.0$ Hz, aromatic H), 4.08 (4 H, t, $J = 6.3$ Hz, $-\text{OCH}_2-$), 1.84 (4 H, quint, $J = 6.6$ Hz, $-\text{OCH}_2\text{CH}_2-$), 1.52-1.32 (28 H, m), 0.92 (6 H, t, $J = 6.3$ Hz, $-\text{CH}_3$). δ_{C} (75 MHz, CD_2Cl_2) 193.55, 164.58, 132.17,

126.00, 114.68, 68.58, 31.90, 29.54, 29.31, 29.00, 25.89, 22.68, 13.88. **MS**(CI-NH₃): found 523.4 ([M]⁺), 540.4 ([M+NH₄]⁺)

General procedure for the synthesis of benzils 3i-3m

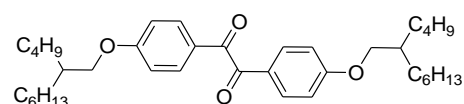
A THF (50 mL) solution of 4,4'-dihydroxy benzil (1.5 g, 6.2 mmol), PPh₃ (3.9 g, 14.9 mmol), and alcohol (14.9 mmol) was cooled to 0 °C. To the solution was added diethyl azodicarboxylate in toluene solution (6.8 mL, 14.9 mmol, 40% w/v), the mixture was kept at that temperature for 1h and then was allowed to warm to room temperature and stirred for 1 h. The reaction mixture was then evaporated. After addition of 300 ml of hexane, the mixture was filtered. The filtrate was evaporated, and the residue was purified by silica gel column chromatography (Hexane/CH₂Cl₂ 50/50)

4,4'-di(3,7-dimethyloctyloxy)benzil (3i)



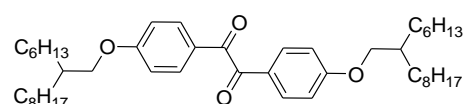
Yellow oil (2.52 g, 78%). δ_{H} (300 MHz, CD₂Cl₂) 8.13 (4 H, d, $J = 9.0$ Hz, aromatic H), 7.20 (4 H, d, $J = 9.0$ Hz, aromatic H), 4.31 (4 H, m, -OCH₂-), 2.09-1.37 (20 H, m), 1.17 (6 H, d, $J = 6.6$ Hz, -CH₃), 1.10 (12 H, d, $J = 6.6$ Hz, -CH₃). δ_{C} (75 MHz, CD₂Cl₂) 193.75, 164.75, 132.36, 126.18, 114.89, 67.15, 39.39, 37.37, 36.07, 31.78, 30.00, 28.17, 24.82, 22.62, 22.52, 19.54, 14.07

4,4'-di(2-butyloctyloxy)benzil (3j)



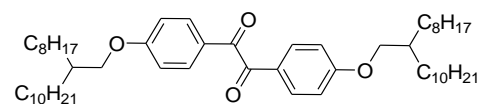
Yellow oil (4.3 g, 90%). δ_{H} (250 MHz, CD₂Cl₂) 7.96 (4 H, dd, $J = 1.8$ -8.8 Hz, aromatic H), 7.03 (4 H, d, $J = 8.8$ Hz, aromatic H), 3.99 (4 H, d, $J = 5.8$ Hz, -OCH₂-), 1.88-1.83 (2 H, m, -OCH₂CH-), 1.47-1.34 (32 H, m, -CH₂-), 0.95-0.91 (12 H, m, -CH₃). δ_{C} (62.5 MHz, CD₂Cl₂) 193.62, 164.83, 132.16, 125.98, 114.73, 71.42, 37.81, 31.84, 31.24, 30.94, 29.65, 29.01, 26.76, 23.03, 22.67, 13.87, 13.84

4,4'-di(2-hexyldecyloxy)benzil (3k)

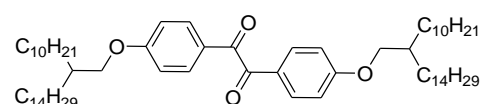


Yellow oil (3.94 g, 69%). δ_{H} (250 MHz, CD₂Cl₂) 7.96 (4 H, d, $J = 9.0$ Hz, aromatic H), 7.04 (4 H, d, $J = 9.0$ Hz, aromatic H), 3.99 (4 H, d, $J = 5.5$ Hz, -OCH₂-), 1.88-1.81 (2 H, m, -OCH₂CH-), 1.46-1.21 (48 H, m, -CH₂-), 0.95-0.90 (12 H, m, -CH₃). δ_{C} (62.5 MHz, CD₂Cl₂) 193.61, 164.83, 132.16, 125.98, 114.73, 71.44, 37.83, 31.91, 31.85, 31.61, 31.24, 29.97, 29.65, 29.57, 29.32, 26.77, 22.69, 13.88

4,4'-di(2-octyldodecyloxy)benzil (3l)

 Yellow oil (5 g, 75%). δ_{H} (250 MHz, CD_2Cl_2) 7.96 (4 H, d, $J = 8.8$ Hz, aromatic H), 7.03 (4 H, d, $J = 8.8$ Hz, aromatic H), 3.99 (4 H, d, $J = 5.6$ Hz, $-\text{OCH}_2-$), 1.87-1.83 (2 H, m, $-\text{OCH}_2\text{CH}-$), 1.46-1.31 (64 H, m, $-\text{CH}_2-$), 0.95-0.90 (12 H, t, $J = 5.9$ Hz, $-\text{CH}_3$). δ_{C} (62.5 MHz, CD_2Cl_2) 193.60, 164.82, 132.14, 125.96, 114.72, 71.42, 37.80, 31.91, 31.20, 29.95, 29.63, 29.58, 29.55, 29.34, 29.30, 26.75, 22.68, 13.87

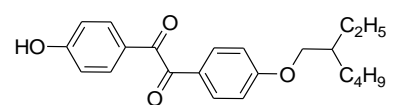
4,4'-di(2-decyltetradecyloxy)benzil (3m)

 Yellow oil (6.21g, 82%). δ_{H} (250 MHz, CD_2Cl_2) 7.96 (4 H, d, $J = 8.8$ Hz, aromatic H), 7.04 (4 H, d, $J = 8.8$ Hz, aromatic H), 3.99 (4 H, d, $J = 5.6$ Hz, $-\text{OCH}_2-$), 1.88-1.31 (82 H, m), 1.03-0.90 (12 H, m, $-\text{CH}_3$). δ_{C} (62.5 MHz, CD_2Cl_2) 193.60, 164.82, 132.14, 125.97, 114.72, 71.43, 37.80, 31.92, 31.20, 29.95, 29.64, 29.59, 29.35, 26.76, 22.69, 13.87

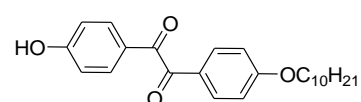
General procedure for the synthesis of 4-alkoxy-4'-hydroxybenzil 2n-2p and 3h

To a mixture of 4,4'-dihydroxybenzil (**3**) (1.0 g, 4.13 mmol), powdered potassium carbonate (3.72 mmol) in DMF (40 mL) at 100 °C was added dropwise and slowly (in about 1 h) a solution of alkyl bromide (3.72 mmol) in DMF (40 mL). After 1h, the reaction was quenched by adding water and the resulting mixture was extracted by ethyl acetate. The organic phases were combined, rinsed several time by water, dried over anhydrous magnesium sulfate and concentrated under reduced pressure resulting the crude product which was purified by silica gel column chromatography (Hexane/ $\text{CH}_3\text{COOC}_2\text{H}_5$ 75/25).

4-(2-ethylhexyloxy)-4'-hydroxybenzil (2n)

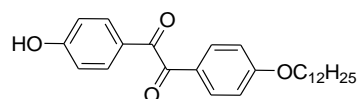
 Yellow oil (0.54 g, 41%). δ_{H} (300 MHz, CD_2Cl_2) 7.91 (4 H, m, aromatic H), 7.00 (4 H, m, aromatic H), 6.74 (1 H, br s, phenol H), 3.98 (2 H, d, $J = 5.7$ Hz, $-\text{OCH}_2-$), 1.79 (1 H, m, $-\text{OCH}_2\text{CH}-$), 1.50-1.28 (8H, m, $-\text{CH}_2-$), 0.99-0.91 (6 H, m, $-\text{CH}_3$). δ_{C} (75 MHz, CD_2Cl_2) 193.79, 193.69, 164.98, 162.00, 132.56, 132.27, 126.16, 125.80, 115.89, 114.78, 71.04, 60.55, 39.25, 30.38, 29.00, 23.76, 23.01, 20.85, 13.96, 13.82, 10.83

4-decyloxy-4'-hydroxybenzil (2o)

 Yellow solid (4.06 g, 57%). δ_{H} (300 MHz, CD_2Cl_2) 7.96-7.88 (4 H, m, aromatic H), 7.03-6.93 (4 H, m, aromatic H), 6.01 (1 H, H, m, aromatic H)

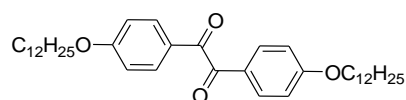
br s, phenol H), 4.1 (2 H, t, $J = 6.3$ Hz, $-\text{OCH}_2-$), 1.88-1.79 (2 H, m, $-\text{OCH}_2\text{CH}_2-$), 1.51-1.31 (14 H, m, $-\text{CH}_2-$), 0.94 (3 H, t, $J = 6.3$ Hz, $-\text{CH}_3$). δ_{C} (62.5 MHz, CD_2Cl_2) 193.72, 193.64, 164.75, 161.86, 132.56, 132.28, 126.25, 125.86, 115.88, 114.76, 68.66, 31.91, 29.55, 29.32, 29.01, 25.90, 22.69, 13.98, 13.88

4-dodecyloxy-4'-hydroxybenzil (2p)



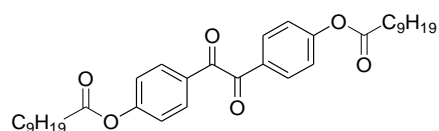
Yellow solid (3.47g, 46%). δ_{H} (250 MHz, CD_2Cl_2) 8.04 (1 H, br s, phenol H), 7.96 (4 H, m, aromatic H), 7.09 (4 H, m, aromatic H), 4.11 (2 H, t, $J = 6.5$ Hz, $-\text{OCH}_2-$), 1.87-1.31 (20 H, m), 0.95 (3 H, t, $J = 6.2$ Hz, $-\text{CH}_3$). **HRMS**($\text{CI}-\text{CH}_4$): found 411.2546, $[\text{M}+\text{H}]^+$ requires 411.2535

4,4'-didodecyloxybenzil (3h)



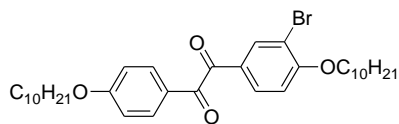
Yellowish solid Isolated from the synthesis of **2p** (3.59 g, 30%). δ_{H} (250 MHz, CD_2Cl_2) 7.96 (4 H, m, aromatic H), 7.03 (4 H, m, aromatic H), 4.11 (4 H, t, $J = 6.5$ Hz, $-\text{OCH}_2-$), 1.87-1.32 (40 H, m, $-\text{CH}_2-$), 0.95 (6 H, t, $J = 6.3$ Hz, $-\text{CH}_3$). δ_{C} (62.5 MHz, CD_2Cl_2) 193.57, 164.59, 132.17, 126.00, 114.68, 68.60, 45.33, 31.93, 29.64, 29.59, 29.56, 29.36, 29.33, 29.02, 25.90, 22.70, 13.89. **HRMS**($\text{CI}-\text{CH}_4$): found 579.4441, $[\text{M}+\text{H}]^+$ requires 579.4413

4,4'-di(decanoate)benzil (3t-Ester)



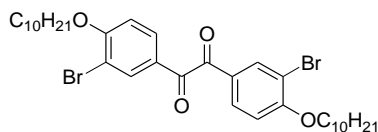
A THF (50 mL) solution of 4,4'-dihydroxyl benzil (2 g, 8.26 mmol), PPh_3 (5.2 g, 19.82 mmol), and decanoic acid (3.4 g, 19.82 mmol) was cooled to 0 °C. To the solution was added diethyl azodicarboxylate in toluene solution (9 mL, 19.82 mmol, 40% w/v), the mixture was kept at that temperature for 1h and then was allowed to warm to room temperature and stirred for 1 h. The reaction mixture was then evaporated. After addition of 500 ml of hexane, the mixture was filtered. The filtrate was evaporated, and the residue was purified by silica gel column chromatography (Hexane/ CH_2Cl_2 25/75) to give a pure yellow solid (4.25 g, 93 %). δ_{H} (300 MHz, CD_2Cl_2) 8.06 (4 H, dt, $J = 2.4-9.3$ Hz, aromatic H), 7.31 (4 H, dt, $J = 2.4-9.3$ Hz, aromatic H), 2.63 (4 H, t, $J = 7.5$ Hz, $-\text{OC}(=\text{O})\text{CH}_2-$), 1.79 (4 H, m, $-\text{OC}(=\text{O})\text{CH}_2\text{CH}_2-$), 1.49-1.30 (24 H, m), 0.94 (6 H, t, $J = 6.6$ Hz, $-\text{CH}_3$). δ_{C} (75 MHz, CD_2Cl_2) 192.91, 171.42, 156.09, 131.51, 130.29, 122.44, 34.27, 31.88, 29.42, 29.26, 29.25, 29.03, 24.75, 22.68, 13.89; **MS**($\text{CI}-\text{NH}_3$): found 568.3 ($[\text{M}+\text{NH}_4]^+$)

3-bromo-4,4'-di(decyloxy)benzil 3t-Br



A suspension of FeCl_3 (0.28 g, 1.72 mmol) and 4,4'-didecyloxybenzil (**3t**, 0.9 g, 1.72 mmol) in CH_2Cl_2 (30 mL) was cooled to 0°C . To the suspension was added Br_2 (0.2 mL) and the mixture was warmed to r.t. overnight. The reaction was quenched by a 10 % aqueous solution of $\text{Na}_2\text{S}_2\text{O}_3$ (50 mL) and then extracted by CH_2Cl_2 . The organic phases were combined, rinsed several time by water, dried over anhydrous magnesium sulfate and concentrated under reduced pressure resulting in a crude product which was purified by silica gel column chromatography (Hexane/ CH_2Cl_2 40/60 then 60/40) to provide a yellowish solid (0.51 g, 49 %). δ_{H} (250 MHz, CD_2Cl_2) 8.22 (1 H, d, $J = 2.1$ Hz, aromatic H), 7.94 (3 H, m, aromatic H), 7.90 (3 H, dt, $J = 2.8$ -9.8 Hz, aromatic H), 4.16 (2 H, t, $J = 6.3$ Hz, $-\text{OCH}_2-$), 4.09 (2 H, t, $J = 6.5$ Hz, $-\text{OCH}_2-$), 1.87 (4 H, m, $-\text{OCH}_2\text{CH}_2-$), 1.55-1.44 (28 H, m), 0.93 (6 H, $-\text{CH}_3$). δ_{C} (62.5 MHz, CD_2Cl_2) 192.70, 192.39, 164.77, 160.61, 134.68, 132.27, 131.45, 126.91, 125.71, 114.75, 112.64, 112.30, 69.78, 68.64, 31.89, 29.51, 29.30, 29.22, 28.98, 28.80, 25.87, 25.83, 22.67, 13.86. **MS**(CI- NH_3): found 601.3 ($[\text{MBr}^{79}+\text{H}]^+$), 603.3 ($[\text{MBr}^{81}+\text{H}]^+$), 618.3 ($[\text{MBr}^{79}+\text{NH}_4]^+$) and 620.3 ($[\text{MBr}^{81}+\text{NH}_4]^+$)

3,3'-dibromo-4,4'-di(decyloxy)benzil 3t-Br₂



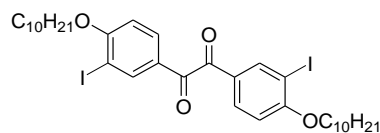
To a solution of 4,4'-didecyloxybenzil (**3t**, 1.5 g, 2.87 mmol) in a mixture of CH_2Cl_2 (25 mL) and acetonitrile (25 mL), Br_2 (0.73 mL, 14.35 mmol) and FeCl_3 (0.93 g, 5.74 mmol) were added. The mixture was reflux overnight (*ca.* 16h). The reaction was quenched by a 10 % aqueous solution of $\text{Na}_2\text{S}_2\text{O}_3$ (200 mL) and then extracted by CH_2Cl_2 . The organic phases were combined, rinsed several time by water, dried over anhydrous magnesium sulfate and concentrated under reduced pressure resulting in a crude product which was purified by silica gel column chromatography (Hexane/ CH_2Cl_2 50/50) to provide a yellowish solid (1.83 g, 94 %). δ_{H} (300 MHz, CDCl_3) 8.22 (2 H, d, $J = 2.1$ Hz, aromatic H), 7.90 (2 H, dd, $J = 2.1$ -8.4 Hz, aromatic H), 6.96 (2 H, d, $J = 8.4$ Hz, aromatic H), 4.13 (4 H, t, $J = 6.6$ Hz, $-\text{OCH}_2-$), 1.88 (4 H, m, $-\text{OCH}_2\text{CH}_2-$), 1.57-1.29 (28 H, m), 0.89 (6 H, t, $J = 6.6$ Hz, $-\text{CH}_3$). δ_{C} (75 MHz, CDCl_3) 191.46, 160.74, 135.02, 131.55, 126.67, 113.00, 112.16, 69.69, 31.89, 29.51, 29.30, 29.23, 28.79, 25.86, 22.68, 14.11; **MS**(CI- NH_3): found 696.3 ($[\text{MBr}^{79}\text{Br}^{79}+\text{NH}_4]^+$), 698.3($[\text{MBr}^{79}\text{Br}^{81}+\text{NH}_4]^+$), 700.3 ($[\text{MBr}^{81}\text{Br}^{81}+\text{NH}_4]^+$)

General procedure for the synthesis of 3t-I₂, 3t-I₃ and 3t-I₄

To a round bottom flask 4,4'-didecyloxybenzil (**3t**, 1.54 g, 2.95 mmol), TFA (35 mL), and NIS (2.0; 3.0; or 5.0 molar equivalences for **3t-I₂**, **3t-I₃** and **3t-I₄**, respectively) were added. After

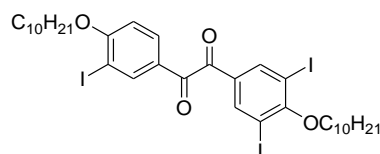
stirring for 5 min at r.t., the reaction mixture was heated to reflux for 3.5 h. The mixture was cooled to r.t. overnight and was poured into ice water (300 mL), then CH₂Cl₂ (200 mL) was added. The organic layers were separated and the aqueous phase was extracted with CH₂Cl₂. The combined organic phase was washed with 10 % aqueous solution of Na₂S₂O₃ and dried over MgSO₄. Removal of solvent in vacuo followed by silica gel column chromatography (Hexane/CH₂Cl₂) provides desired products.

3,3'-diiodo-4,4'-di(decyloxy)benzil 3t-I₂



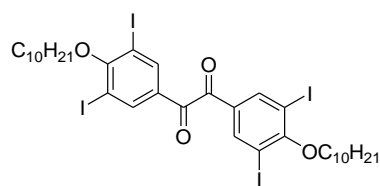
Yellowish solid (2.24 g, 88 %); δ_{H} (300 MHz, CDCl₃) 8.41 (2 H, d, $J = 2.1$ Hz, aromatic H), 7.90 (2 H, dd, $J = 2.1$ -8.4 Hz, aromatic H), 6.83 (2 H, d, $J = 8.7$ Hz, aromatic H), 4.10 (4 H, t, $J = 6.3$ Hz, -OCH₂-), 1.86 (4 H, m, -OCH₂CH₂-), 1.55-1.27 (28 H, m), 0.88 (6 H, t, $J = 6.6$ Hz, -CH₃). δ_{C} (75 MHz, CDCl₃) 191.31, 162.74, 141.26, 132.56, 127.36, 111.08, 87.09, 69.81, 31.91, 29.52, 29.31, 29.22, 28.81, 25.96, 22.69, 14.13; **MS**(CI-NH₃): found 775.2 ([M+H]⁺), 792.2 ([M+NH₄]⁺)

3,3',4-triiodo-4,4'-di(decyloxy)benzil 3t-I₃



White solid (1.14 g, 43 %). δ_{H} (300 MHz, CDCl₃) 8.40 (1 H, d, $J = 2.1$ Hz, aromatic H), 8.34 (2 H, s, aromatic H), 7.91 (1 H, dd, $J = 2.1$ -8.7 Hz, aromatic H), 6.84 (1 H, d, $J = 8.7$ Hz, aromatic H), 4.11 (2 H, t, $J = 6.3$ Hz, -OCH₂-), 4.03 (2 H, t, $J = 6.6$ Hz, -OCH₂-), 1.50 (4 H, m, -OCH₂CH₂-), 1.58-1.28 (28 H, m), 0.88 (6 H, m, -CH₃). δ_{C} (75 MHz, CDCl₃) 190.10, 189.94, 163.44, 163.06, 141.54, 141.40, 132.69, 131.89, 126.86, 111.16, 91.54, 87.21, 73.99, 69.88, 31.90, 30.94, 30.04, 29.59, 29.52, 29.46, 29.34, 29.31, 29.22, 28.80, 25.95, 25.88, 22.69, 14.13; **MS**(CI-NH₃): found 901.1 ([M+H]⁺), 918.1 ([M+NH₄]⁺)

3,3',4,4'-tetraiodo-4,4'-di(decyloxy)benzil 3t-I₄

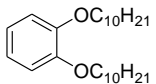


Yellowish solid (2.12 g, 59 %); δ_{H} (300 MHz, CDCl₃) 8.34 (4 H, s, aromatic H), 4.04 (4 H, t, $J = 6.6$ Hz, -OCH₂-), 1.94 (4 H, m, -OCH₂CH₂-), 1.60-1.28 (28 H, m), 0.88 (6 H, t, $J = 6.3$ Hz, -CH₃). δ_{C} (62.5 MHz, CDCl₃) 188.81, 163.81, 141.66, 131.39, 91.65, 74.08, 31.91, 30.05, 29.59, 29.47, 29.34, 25.89, 22.71, 14.14. **HRMS**(CI-CH₄): found 1026.9668 and 1054.9985, [M+H]⁺ and [M+C₂H₅]⁺ require 1026.9653 and 1054.9966

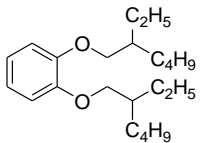
General procedure for the synthesis of dialkyloxy 4a-4c

A mixture of benzenediol (1.0 eq.), alkyl bromide (2.4 eq.) and powdered potassium carbonate (3.0 eq.) was stirred in DMF at 90 °C. The reaction was monitored by TLC (hexane/ethyl acetate: 95/5 v/v). Upon cooling to room temperature, the reaction was quenched by adding water and the resulting mixture was extracted with dichloromethane. The organic phases were combined, rinsed several times with water, dried over anhydrous magnesium sulfate and concentrated under reduced pressure. The crude products were then purified by column chromatography (hexane/ethyl acetate).

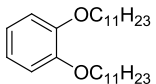
1,2-didecyloxybenzene (4a)

 White solid (3.6 g, yield 77%). δ_{H} (300 MHz, CD_2Cl_2) 6.91 (4 H, s, aromatic H), 4.00 (4 H, t, $J = 6.6$ Hz, $-\text{OCH}_2-$), 1.86-1.32 (32 H, m, $-\text{CH}_2-$), 0.92 (6 H, t, $J = 6.9$ Hz, $-\text{CH}_3$). δ_{C} (75 MHz, CDCl_3) 149.29, 121.02, 114.15, 69.29, 31.95, 29.68, 29.63, 29.48, 29.39, 26.10, 22.72, 14.13. **GC-MS**: found 390 ($[\text{M}]^+$)

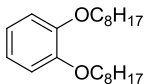
1,2-di(2-ethylhexyloxy)benzene (4b)

 Colorless liquid (7.35 g, yield 81%). δ_{H} (250 MHz, CD_2Cl_2) 6.93 (4 H, m, aromatic H), 3.92 (4 H, d, $J = 5.8$ Hz, $-\text{OCH}_2-$), 1.84-1.73 (2 H, m, $-\text{OCH}_2\text{CH}-$), 1.62-1.39 (16 H, m, $-\text{CH}_2-$), 1.00 (12 H, t, $J = 7.5$ Hz, $-\text{CH}_3$). δ_{C} (62.5 MHz, CD_2Cl_2) 149.68, 120.77, 113.89, 71.58, 39.70, 30.59, 29.14, 23.91, 23.10, 13.86, 10.95. **HRMS**(CI- NH_3): found 335.2948, $[\text{M}+\text{H}]^+$ requires 335.2950

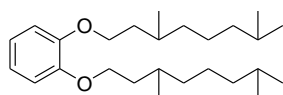
1,2-diundecyloxybenzene (4d)

 White solid (45.9 g, yield 97%). δ_{H} (250 MHz, CD_2Cl_2) 6.93 (4 H, m, aromatic H), 4.02 (4 H, t, $J = 6.6$ Hz, $-\text{OCH}_2-$), 1.81 (4 H, m, $-\text{OCH}_2\text{CH}_2-$), 1.55-1.35 (32 H, m, $-\text{CH}_2-$), 0.95 (6 H, t, $J = 6.2$ Hz, $-\text{CH}_3$). δ_{C} (62.5 MHz, CD_2Cl_2) 149.35, 120.92, 114.12, 69.23, 31.96, 29.68, 29.48, 29.47, 29.40, 26.10, 22.72, 13.90. **MS**(CI- NH_3): found 436.3 ($[\text{M}+\text{NH}_4]^+$)

1,2-dioctyloxybenzene (4e)

 Colorless oil (13.47 g, yield 90%). δ_{H} (300 MHz, CD_2Cl_2) 6.94 (4 H, m, aromatic H), 4.03 (4 H, t, $J = 6.6$ Hz, $-\text{OCH}_2-$), 1.90 (4 H, m, $-\text{OCH}_2\text{CH}_2-$), 1.60-1.38 (20 H, m, $-\text{CH}_2-$), 1.00-0.95 (6 H, m, $-\text{CH}_3$). δ_{C} (75 MHz, CD_2Cl_2) 149.36, 120.94, 114.11, 69.22, 31.91, 29.49, 29.47, 29.36, 26.13, 22.73, 13.92. **HRMS**(CI- CH_4): found 335.2948, $[\text{M}+\text{H}]^+$ requires 335.2950

Synthesis of 1,2-di(3,7-dimethyloctyloxy)benzene (4c)

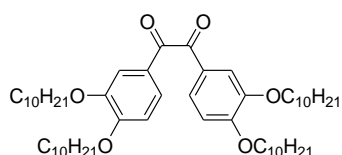


A THF (50 mL) solution of pyrochatecol (1.5 g, 6.2 mmol), PPh_3 (3.9 g, 14.9 mmol), and alcohol (14.9 mmol) was cooled to 0 °C. To the solution was added diethyl azodicarboxylate in toluene solution (6.8 mL, 14.9 mmol, 40% w/v), the mixture was kept at that temperature for 1h and then was allowed to warm to room temperature and stirred for 1 h. The reaction mixture was then evaporated. After addition of 300 ml of hexane, the mixture was filtered. The filtrate was evaporated, and the residue was purified by silica gel column chromatography (eluent: Hex/DCM 1/1 v/v) to provide a colorless oil (3.95 g, yield 74%). δ_{H} (250 MHz, CDCl_3) 6.93 (4 H, m, aromatic H); 4.08 (4 H, m, $-\text{OCH}_2-$); 1.95-1.14 (20 H, m); 1.00-0.91 (18 H, m, $-\text{CH}_3$). δ_{C} (62.5 MHz, CD_2Cl_2) 149.43, 133.89, 133.58, 128.74, 128.58, 128.47, 120.98, 114.11, 67.56, 39.37, 37.47, 36.49, 30.01, 28.09, 24.82, 22.59, 22.50, 19.57. **HRMS**(CI- CH_4): found 391.3584, $[\text{M}+\text{H}]^+$ requires 391.3576

General procedure for the synthesis of tetraalkoxy-substituted benzils (5a-5c)

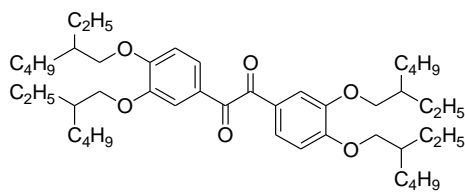
Solvents and glassware used in this synthesis were dried thoroughly prior to use. In a 100 mL side arm round-bottom flask under argon containing a solution of dialkyloxybenzene (7.68 mmol) in 30 ml of 1,2-dichloroethane, oxalyl chloride (400 μL , 4.61 mmol) was added by a microsyringe at 0°C. The reaction mixture was hold at 0°C for 10 minutes and then aluminum chloride (0.51 g, 3.84 mmol) was added. After 30 minutes at 0°C, the mixture was warmed gently to room temperature overnight. The reaction mixture was then poured into a 1M HCl solution. The organic layer was separated, and the aqueous layer was extracted twice with CH_2Cl_2 . The combined organic extracts were dried over MgSO_4 and concentrated. The residue was chromatographed (hexane/ CH_2Cl_2) to give 5 as pure product.

3,3',4,4'-tetrakis(decyloxy)benzil (5a)



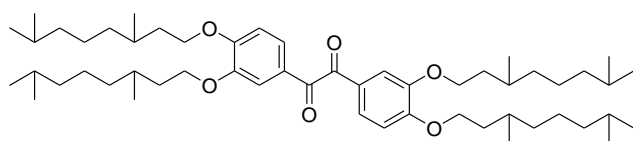
White solid (0.55 g, yield 51%). δ_{H} (250 MHz, CD_2Cl_2) 7.58 (2 H, d, $J = 1.75$ Hz, aromatic H), 7.47 (2 H, dd, $J = 2.0-8.5$ Hz, aromatic H), 6.94 (2 H, d, $J = 8.25$ Hz, aromatic H), 4.10 (8 H, m, $-\text{OCH}_2-$), 1.86 (8 H, m, $-\text{OCH}_2\text{CH}_2-$), 1.52-1.33 (56 H, m), 0.93 (12 H, t, $J = 4.75$ Hz, $-\text{CH}_3$). δ_{C} (62.5 MHz, CD_2Cl_2) 193.81, 155.00, 149.32, 126.22, 126.13, 112.31, 111.61, 69.26, 69.14, 31.94, 29.65, 29.60, 29.41, 29.36, 29.10, 28.95, 26.01, 25.94, 22.71, 14.14. **MS**(CI- NH_3): found 835.6 ($[\text{M}]^+$), 836.7 ($[\text{M}+\text{H}]^+$)

3,3',4,4'-tetrakis(2-ethylhexyloxy)benzil (5b)



Yellowish oil (1.69 g, yield 49%). δ_{H} (300 MHz, CD_2Cl_2) 7.58 (2 H, d, $J = 2.1$ Hz, aromatic H), 7.45 (2 H, dd, $J = 2.1$ -8.4 Hz, aromatic H), 6.93 (2 H, d, $J = 8.4$ Hz, aromatic H), 3.99 (8 H, d, $J = 5.4$ Hz, $-\text{OCH}_2\text{CH}-$), 1.80 (4 H, m, $-\text{OCH}_2\text{CH}-$), 1.58-1.35 (32 H, m), 1.00-0.91 (24 H, m, $-\text{CH}_3$). δ_{C} (75 MHz, CD_2Cl_2) 193.95, 155.40, 149.70, 126.02, 125.83, 111.77, 111.37, 71.46, 71.37, 39.52, 39.40, 30.57, 30.49, 29.08, 29.03, 23.93, 23.92, 23.87, 23.85, 23.05, 23.02, 13.83, 13.81, 10.96, 10.91. **HRMS**(CI- CH_4): found 723.5578, $[\text{MH}]^+$ requires 723.5564

3,3',4,4'-tetrakis(3,7-dimethyloctyloxy)benzil (5c)

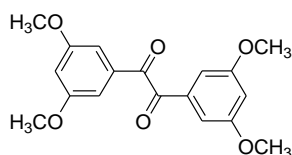


Yellowish oil (1.58 g, yield 49%). δ_{H} (300 MHz, CD_2Cl_2) 7.59 (2 H, d, $J = 2.1$ Hz, aromatic H), 7.47-7.42 (2 H, m, aromatic H), 6.94 (2 H, m, aromatic H), 4.16 (8 H, m, $-\text{OCH}_2-$), 1.94-0.89 (76 H, m). δ_{C} (75 MHz, CD_2Cl_2) 193.83, 155.06, 152.75, 149.36, 148.67, 130.67, 126.12, 125.89, 124.44, 114.49, 112.11, 111.56, 111.46, 67.60, 39.24, 39.21, 37.33, 37.28, 36.25, 36.10, 35.90, 29.96, 28.02, 24.74, 22.48, 22.38, 19.47, 19.41. **HRMS**(CI- NH_3): found 835.6859, $[\text{M}+\text{H}]^+$ requires 835.6816

General procedure for the synthesis of mixtures of tetraalkoxy-substituted benzils (**M1**, **M2**, **M3**)

Solvents and glassware used in this synthesis were dried thoroughly prior to use. In a 100 mL side arm round-bottom flask under argon containing a solution of dialkoxybenzene (3.84 mmole) in 20 ml of 1,2-dichloroethane, oxalyl chloride (400 μL , 4.61 mmol) was added by a microsyringe at 0°C . The reaction mixture was hold at 0°C for 10 minutes and then aluminum chloride (0.51 g, 3.84 mmole) was added. After 30 minutes at 0°C , the solution of another dialkoxybenzene (3.84 mmole) in 20 ml of 1,2-dichloroethane was added dropwise over a period of 30 minutes. The mixture was then warmed gently to room temperature overnight. The reaction mixture was then poured into a 1M HCl solution. The organic layer was separated, and the aqueous layer was extracted twice with CH_2Cl_2 . The combined organic extracts were dried over MgSO_4 and concentrated. The residue was chromatographed using a mixture of hexane and CH_2Cl_2 to give mixture **M1**, **M2** and **M3**. (**M1**: 1.77 g, yellow solid; **M2**: 1.71 g, yellow solid; **M3**: 4.65 g, yellow solid)

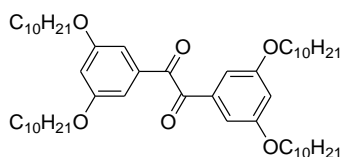
Synthesis of 3,3',5,5'-tetramethoxybenzil (5e)



Sodium cyanide (1.0 g, 22.4 mmol) was dissolved in 10 mL of water. To this solution, 3,5-dimethoxybenzaldehyde (9.3 g, 56.0 mmol) and 20 ml of ethanol were added. The mixture was refluxed with stirring for 36 h.

The mixture was extracted with CH_2Cl_2 , and the organic layer was washed with water, and then dried over MgSO_4 . The dichloromethane was evaporated to give a yellowish brown viscous liquid ($m = 7.8$ g). Purification was not carried out but directly used in the next step: the mixture of crude 3,3',5,5'-tetramethoxybenzoin (7.8 g), copper (II) acetate (0.1 g, 0.24 mmol), NH_4NO_3 (2.5 g, 29.35 mmol) in acetic acid (20 mL) and water (5 mL) was heated to reflux. After 2h of reflux, water was introduced and the yellow precipitate was collected by filtration. The filtrate was then extracted several times with CH_2Cl_2 . The organic phases and the yellow precipitate were combined, washed several times with water, dried with MgSO_4 and the solvent was removed under reduced pressure. The residue was purified by recrystallization from ethyl acetate to provide a yellow solid (2.0 g, yield 22 %). δ_{H} (250 MHz, CD_2Cl_2) 7.09 (4 H, d, $J = 2.3$ Hz, aromatic H), 6.79 (2 H, t, $J = 2.3$ Hz, aromatic H), 3.86 (12 H, s, $-\text{OCH}_3$).

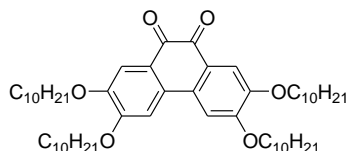
Synthesis of 3,3',5,5'-tetradecyloxybenzil (5d)



3,3',5,5'-tetramethoxybenzil (1.05 g) was heated to reflux for 5 h in a mixture of aqueous HBr (48%) and glacial acetic acid (100 mL, 50/50). The reaction mixture was cooled by a bath of ice-water and

extracted several times by diethylether. The organic phases were combined and the solvent was removed under reduced pressure. The residue was analysed by TLC using a mixture of acetone and CH_2Cl_2 (50/50): only one product was observed. The residue was not purified but directly used in the next step: to this residue, decyl bromide (4 mL), K_2CO_3 (5.5 g) and DMF (40 mL) were added and the mixture was heated to reflux for 18 h. The reaction mixture was cooled by a bath of ice-water and extracted several times by CH_2Cl_2 . The organic phases were combined, rinsed several times by water, dried over MgSO_4 and the solvent was removed under reduced pressure. The crude product was purified by column chromatography (silica gel: hexane/dichloromethane 50/50) to provide a yellow solid (1.41 g, yield 53 %). δ_{H} (300 MHz, CD_2Cl_2) 7.04(4 H, d, $J = 2.1$ Hz, aromatic H), 6.76 (2 H, t, $J = 2.1$ Hz, aromatic H), 4.00 (8 H, t, $J = 6.6$ Hz, $-\text{OCH}_2-$), 1.79 (8 H, quint, $J = 6.6$ Hz, $-\text{OCH}_2\text{CH}_2-$), 1.49-1.32 (56 H, m), 0.92(12 H, t, $J = 6.3$ Hz, $-\text{CH}_3$). δ_{C} (75 MHz, CD_2Cl_2) 194.48, 160.71, 134.60, 107.95, 107.68, 104.46, 68.52, 68.34, 31.90, 29.55, 29.34, 29.31, 29.23, 29.18, 29.10, 25.94, 22.68, 13.87. **MS**(CI- NH_3): found 835.7 ($[\text{M}+\text{H}]^+$), 853.7 ($[\text{M}+\text{NH}_4]^+$).

Synthesis of 2,3,6,7-Tetrakis(decyloxy)phenanthrene-9,10-dione (6a)

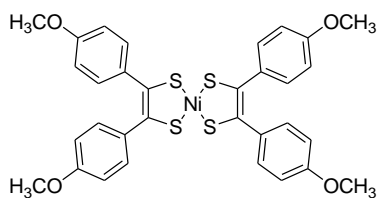


To a stirred solution of 0.6 mmol of alkoxy-substituted benzil 5a and 160 μL (1.25 mmol) of boron trifluoride etherate in 15 mL of anhydrous dichloromethane under argon was added 245 mg (1.98 mmol) of vanadium(V) oxyfluoride. The reaction mixture was stirred for 30 min at ambient temperature and poured into citric acid (10%, 50 mL), and the organic layer was separated. The aqueous layer was extracted twice with 50 mL of dichloromethane and the combined organic layers were washed with water, dried (MgSO_4), and reduced *in vacuo*. The resulting dark residue was subjected to column chromatography (silica gel/dichloromethane) to provide a pure deep red solid (yield 71%). δ_{H} (300 MHz, CD_2Cl_2) 7.56 (2 H, s, aromatic H), 7.22 (2 H, s, aromatic H), 4.24 (4 H, t, $J = 7.8$ Hz, $-\text{OCH}_2-$), 4.12 (4 H, t, $J = 7.8$ Hz, $-\text{OCH}_2-$), 1.95-1.84 (8 H, m), 1.57-1.33 (56 H, m), 0.95-0.90 (12 H, m). δ_{C} (75 MHz, CD_2Cl_2) 179.09, 155.65, 149.54, 131.08, 124.50, 112.73, 107.27, 69.53, 69.18, 31.91, 29.61, 29.56, 29.36, 29.34, 29.15, 29.08, 25.98, 22.68, 13.86. **HRMS**($\text{Cl}-\text{CH}_4$): found 833.6660, $[\text{M}+\text{H}]^+$ requires 833.6659

General procedure for the synthesis of nickel bis(1,2-dithiolene) complexes

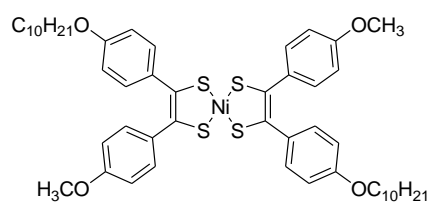
A mixture of dialkoxybenzil (4.91 mmol) and P_4S_{10} (4.8 g, 10.80 mmol) in 25 mL of dioxane was heated to reflux at 130 $^\circ\text{C}$ for 5 h. When the initial yellow suspension became a clear dark brown solution, the hot mixture was filtered to remove an insoluble pale yellow solid. To the filtrate was added a solution of $\text{NiCl}_2 \cdot 6\text{H}_2\text{O}$ (0.64 g, 2.70 mmol) in 5 mL of water, and the mixture was heated to reflux for 2h. The mixture was then cooled to room temperature and a small quantity of water was added. The black crystalline precipitate appeared and was collected by filtration. The crude product was purified by repeated precipitation from solution in CH_2Cl_2 by ethanol (3 times) and the final purification was performed by column chromatography (Hexane/ CH_2Cl_2).

Compound BT65: nickel bis[1,2-di(4-methoxyphenyl)ethene-1,2-dithiolene] complex



Black powder (0.87g, 18%). **Elemental Analysis:** found C, 57.88; H, 4.19; Ni, 8.71; S, 19.58. $\text{C}_{32}\text{H}_{28}\text{NiO}_4\text{S}_4$ requires C, 57.93; H, 4.25; Ni, 8.85; S, 19.33 %. δ_{H} (300 MHz, CD_2Cl_2) 7.39 (8 H, d, $J = 7.5$ Hz, aromatic H), 6.88 (8 H, d, $J = 7.5$ Hz, aromatic H), 3.86 (12 H, s, $-\text{OCH}_3$). δ_{C} (75 MHz, CD_2Cl_2) 180.77, 160.48, 134.28, 130.34, 113.81, 55.37. **HRMS**($\text{Cl}-\text{CH}_4$): found 663.0297, $[\text{M}+\text{H}]^+$ requires 663.0302.

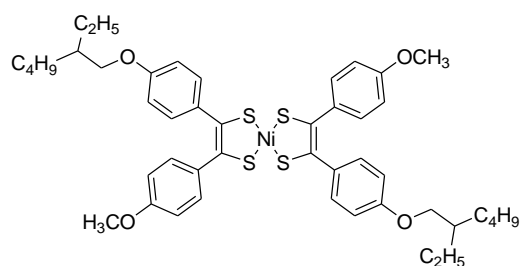
Compound BT71: nickel bis[1-(4-decyloxyphenyl)-2-(4-methoxyphenyl)ethene-1,2-dithiolene] complex



Black powder (0.86 g, 51%, mp 147.3 °C). **Elemental Analysis:** found C, 65.60; H, 7.10; Ni, 6.25; S, 14.10. $C_{50}H_{64}NiO_4S_4$ requires C, 65.56; H, 7.04; Ni, 6.41; S, 14.00 %.

δ_H (400 MHz, CD_2Cl_2) 7.37 (8 H, m, aromatic H), 6.86 (8 H, m, aromatic H), 4.03 (4 H, t, $J = 6.4$ Hz, $-OCH_2CH_2-$), 3.86 (6 H, s, $-OCH_3$), 1.85-1.80 (4 H, m, $-OCH_2CH_2-$), 1.56-1.33 (28 H, m, $-CH_2-$), 0.94 (6 H, t, $J = 6.8$ Hz, $-CH_3$). δ_C (75 MHz, CD_2Cl_2) 183.52, 180.93, 160.47, 160.12, 134.08, 130.35, 114.30, 113.81, 68.22, 55.36, 31.89, 29.56, 29.55, 29.37, 29.31, 29.19, 25.98, 22.67, 13.86. **HRMS**(CI- CH_4): found 915.3100, $[M+H]^+$ requires 915.3119.

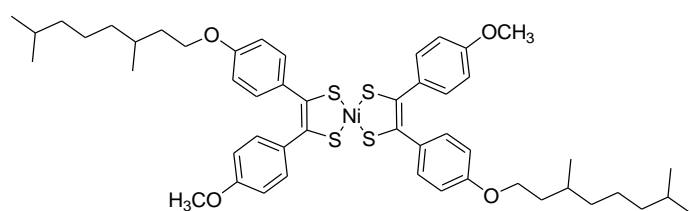
Compound BT74: nickel bis[1-(4-(2-ethylhexyloxy)phenyl)-2-(4-methoxyphenyl)ethene-1,2-dithiolene] complex



Brown powder (0.64 g, 45%, mp 199.1°C). **Elemental Analysis:** found C, 64.11; H, 6.44; Ni, 6.61; S, 15.20. $C_{46}H_{56}NiO_4S_4$ requires C, 64.25; H, 6.56; Ni, 6.83; S, 14.92 %.

δ_H (400 MHz, CD_2Cl_2) 7.39 (8 H, m, aromatic H), 6.88 (8 H, m, aromatic H), 3.92 (4 H, d, $J = 5.6$ Hz, $-OCH_2CH-$), 3.86 (6 H, s, $-OCH_3$), 1.79-1.71 (2 H, m, $-OCH_2CH-$), 1.57-1.39 (16 H, m, $-CH_2-$), 1.00 (12 H, t, $J = 7.6$ Hz, $-CH_3$). δ_C (100 MHz, CD_2Cl_2) 180.75, 180.50, 160.43, 160.32, 134.37, 134.03, 130.35, 130.33, 114.33, 113.80, 70.66, 55.34, 39.39, 30.47, 29.07, 23.83, 23.05, 13.85, 10.88. **HRMS**(CI- CH_4): found 859.2512, $[M+H]^+$ requires 859.2493.

Compound BT77: nickel bis[1-(4-(3,7-dimethyloctyloxy)phenyl)-2-(4-methoxyphenyl)ethene-1,2-dithiolene] complex

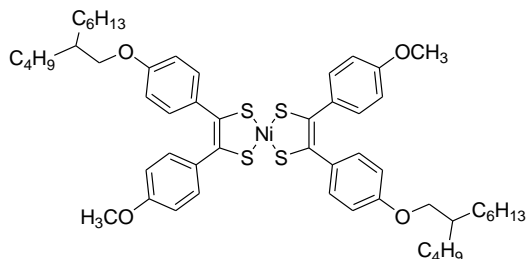


Black powder (1.08 g, 53%, mp 170.3 °C). **Elemental Analysis:** found C, 65.64; H, 6.91; Ni, 6.32; S, 14.63. $C_{50}H_{64}NiO_4S_4$ requires C, 65.56; H, 7.04; Ni, 6.41; S, 14.00 %.

δ_H (300 MHz, CD_2Cl_2) 7.38 (8 H, m, aromatic H), 6.87 (8 H, m, aromatic H), 4.07 (4 H, m, $-OCH_2CH_2-$), 3.85 (6 H, s, $-OCH_3$), 1.88-1.20 (20 H, m), 1.00 (6 H, d, $J = 6.3$ Hz, $-CH_3$), 0.93 (12 H, d, $J = 6.6$ Hz, $-CH_3$). δ_C (75 MHz, CD_2Cl_2) 180.72, 180.53, 160.43, 160.07, 134.34, 134.07, 130.35, 114.30, 113.80, 66.55, 55.34, 39.23, 37.25, 36.11, 29.87, 27.98,

24.65, 22.45, 22.35, 19.41. HRMS(CI-CH₄): found 915.3079 and 943.3484, [M+H]⁺ requires 915.3119 and [M+C₂H₅]⁺ requires 943.3432

Compound BT78: nickel bis[1-(4-(2-butyloctyloxy)phenyl)-2-(4-methoxyphenyl)ethene-1,2-dithiolene] complex

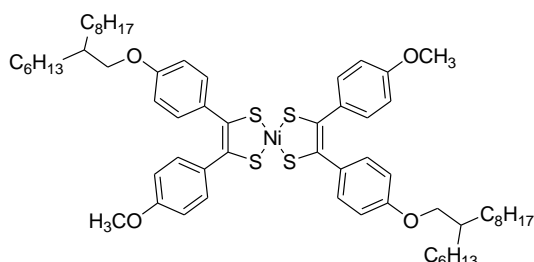


Black powder (1.06 g, 49%, mp 154.8 °C).

Elemental Analysis: found C, 66.93; H, 7.36; Ni, 5.86; S, 13.02. C₅₄H₇₂NiO₄S₄ requires C, 66.72; H, 7.47; Ni, 6.04; S, 13.19 %. δ_{H} (300 MHz, CD₂Cl₂) 7.40 (8 H, m, aromatic H), 6.89 (8 H, m, aromatic H),

3.91 (4 H, d, $J = 5.7$ Hz, -OCH₂CH-), 3.86 (6 H, s, -OCH₃), 1.84 (2 H, m, -OCH₂CH-), 1.57-1.32 (32 H, m), 0.97-0.90 (12 H, m, -CH₃). δ_{C} (75 MHz, CD₂Cl₂) 180.93, 180.68, 160.45, 160.34, 134.40, 134.06, 130.32, 130.30, 114.34, 113.80, 71.07, 55.34, 37.90, 31.85, 31.30, 30.99, 29.66, 29.04, 26.78, 23.04, 22.66, 13.86, 13.84. HRMS(CI-CH₄): found 971.3742, [M+H]⁺ requires 971.3745.

Compound BT79: nickel bis[1-(4-(2-hexyldecyloxy)phenyl)-2-(4-methoxyphenyl)ethene-1,2-dithiolene] complex

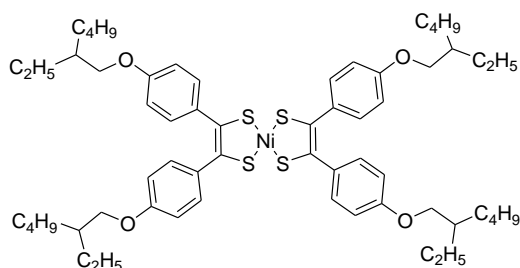


Black powder (1.47 g, 50%, mp 147.4°C).

Elemental Analysis: found C, 68.43; H, 8.18; Ni, 5.17; S, 12.08. C₆₂H₈₈NiO₄S₄ requires C, 68.68; H, 8.18; Ni, 5.41; S, 11.83. δ_{H} (400 MHz, CD₂Cl₂) 7.39 (8 H, m, aromatic H), 6.87 (8 H, m, aromatic H),

3.90 (4 H, d, $J = 5.2$ Hz, -OCH₂CH-), 3.86 (6 H, s, -OCH₃), 1.84 (2 H, m, -OCH₂CH-), 1.50-1.35 (48 H, m), 0.94 (12 H, m, -CH₃). δ_{C} (100 MHz, CD₂Cl₂) 180.66, 180.40, 160.42, 160.31, 134.40, 134.04, 130.38, 130.35, 114.34, 113.80, 71.10, 55.33, 37.96, 31.93, 31.88, 31.33, 30.03, 29.70, 29.61, 29.35, 26.84, 26.82, 22.70, 13.91. HRMS(CI-CH₄): found 1083.5101, [M+H]⁺ requires 1083.4997.

Compound BT70: nickel bis[1,2-di(4-(2-ethylhexyloxy)phenyl)ethene-1,2-dithiolene] complex

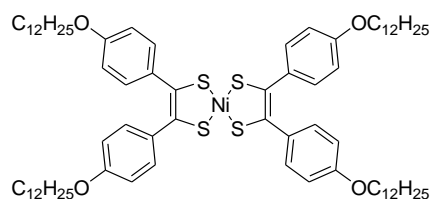


Brown powder (2 g, 47%, mp 163.7 °C). **Elemental**

Analysis: found C, 68.55; H, 8.07; Ni, 5.42; S, 12.10. C₆₀H₈₄NiO₄S₄ requires C, 68.23; H, 8.02; Ni, 5.56; S, 12.14. δ_{H} (400 MHz, CD₂Cl₂) 7.38 (8 H, d, $J = 8.4$ Hz,

aromatic H), 6.88 (8 H, d, $J = 8.4$ Hz, aromatic H), 3.92 (8 H, d, $J = 5.6$ Hz, $-\text{OCH}_2\text{CH}-$), 1.80 (4 H, m, $-\text{OCH}_2\text{CH}-$), 1.57-1.37 (32 H, m, $-\text{CH}_2-$), 0.99-0.95 (24 H, m, $-\text{CH}_3$). δ_{C} (100 MHz, CD_2Cl_2) 180.78, 160.34, 134.07, 130.33, 114.33, 70.67, 39.38, 30.46, 29.06, 23.82, 23.04, 13.83, 10.87. HRMS($\text{CI}-\text{CH}_4$): found 1055.4709, $[\text{M}+\text{H}]^+$ requires 1055.4684.

Compound BT113: nickel bis[1,2-di(4-dodecyloxyphenyl)ethene-1,2-dithiolene] complex



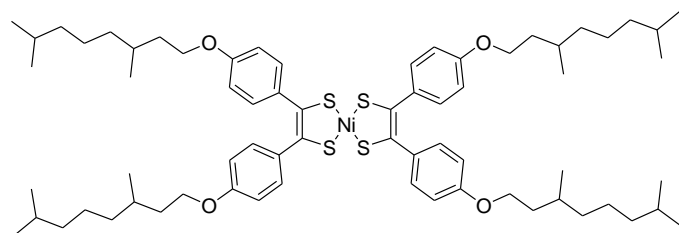
Brown powder (1.6 g, 48%, mp 168.8 °C). **Elemental**

Analysis: found C, 71.62; H, 9.08; Ni, 4.46; S, 9.32.

$\text{C}_{76}\text{H}_{116}\text{NiO}_4\text{S}_4$ requires C, 71.28; H, 9.13; Ni, 4.58; S, 10.01

%. δ_{H} (300 MHz, CD_2Cl_2) 7.37 (8 H, dd, $J = 2.0$ -9.0 Hz, aromatic H), 6.86 (8 H, dd, $J = 2.0$ -9.0 Hz, aromatic H), 4.00 (8 H, t, $J = 6.6$ Hz, $-\text{OCH}_2\text{CH}_2-$), 1.86-1.77 (8 H, m, $-\text{OCH}_2\text{CH}_2-$), 1.51-1.42 (72 H, m), 0.92 (12 H, t, $J = 6.3$ Hz, $-\text{CH}_3$). δ_{C} (75 MHz, CD_2Cl_2) 180.73, 160.09, 134.11, 130.33, 114.29, 68.21, 31.94, 29.65, 29.61, 29.40, 29.36, 29.30, 29.21, 26.01, 22.71, 13.89. HRMS($\text{CI}-\text{CH}_4$): found 1279.7148, $[\text{M}+\text{H}]^+$ requires 1279.7188.

Compound BT80: nickel bis[1,2-di(4-(3,7-dimethyloctyloxy)phenyl)ethene-1,2-dithiolene] complex



Black powder (1.44 g, 59%, mp 129.9

°C). **Elemental Analysis:** found C,

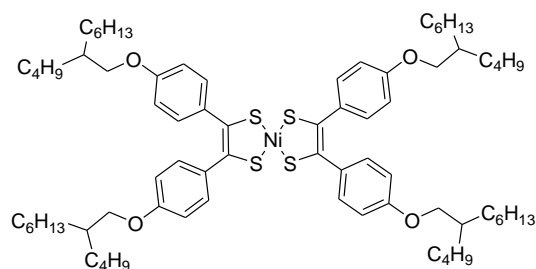
69.85; H, 8.74; Ni, 4.78; S, 11.25.

$\text{C}_{68}\text{H}_{100}\text{NiO}_4\text{S}_4$ requires C, 69.90; H,

8.63; Ni, 5.02; S, 10.98 %. δ_{H} (400 MHz,

CD_2Cl_2) 7.37 (8 H, d, $J = 8.4$ Hz, aromatic H), 6.86 (8 H, d, $J = 8.4$ Hz, aromatic H), 4.07 (8 H, m, $-\text{OCH}_2\text{CH}_2-$), 1.90-1.84 (8 H, m, $-\text{OCH}_2\text{CH}_2-$), 1.73-1.21 (32 H, m), 1.01 (12 H, d, $J = 6.4$ Hz, $-\text{CH}_3$), 0.94 (24 H, d, $J = 6.4$ Hz, $-\text{CH}_3$). δ_{C} (100 MHz, CD_2Cl_2) 180.58, 160.05, 134.14, 130.35, 114.30, 66.55, 39.24, 37.27, 36.14, 29.88, 28.00, 24.66, 22.47, 22.37, 19.43. HRMS($\text{CI}-\text{CH}_4$): found 1167.5953, $[\text{M}+\text{H}]^+$ requires 1167.5936.

Compound BT82: nickel bis[1,2-di(4-(2-butyloctyloxy)phenyl)ethene-1,2-dithiolene] complex



Black powder (2.36 g, 51%, mp 103.2°C).

Elemental Analysis: found C, 71.57; H, 9.14; Ni,

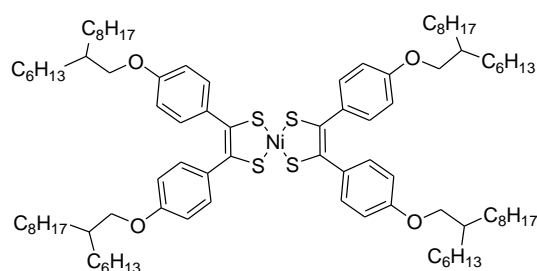
4.32; S, 10.06. $\text{C}_{76}\text{H}_{116}\text{NiO}_4\text{S}_4$ requires C, 71.28; H,

9.13; Ni, 4.58; S, 10.01 %. δ_{H} (300 MHz, CD_2Cl_2)

7.39 (8 H, m, aromatic H), 6.88 (8 H, m, aromatic

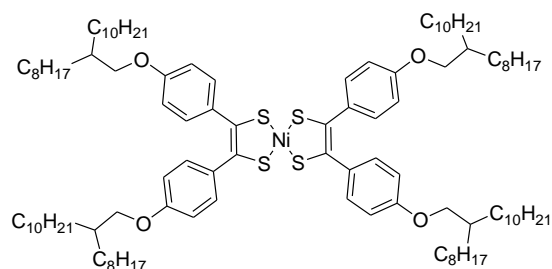
H), 3.91 (8 H, d, $J = 5.7$ Hz, $-\text{OCH}_2\text{CH}-$), 1.85-1.79 (4 H, m, $-\text{OCH}_2\text{CH}-$), 1.54-1.34 (64 H, m, $-\text{CH}_2-$), 0.97-0.91 (24 H, m, $-\text{CH}_3$), δ_{C} (75 MHz, CD_2Cl_2) 180.71, 160.32, 134.07, 130.29, 114.33, 71.05, 37.91, 31.85, 31.30, 31.00, 29.67, 29.05, 26.78, 23.05, 22.67, 13.87, 13.85. HRMS(CI- CH_4): found 1279.7188, $[\text{M}+\text{H}]^+$ requires 1279.7188.

Compound BT83: nickel bis[1,2-di(4-(2-hexyldecyloxy)phenyl)ethene-1,2-dithiolene] complex



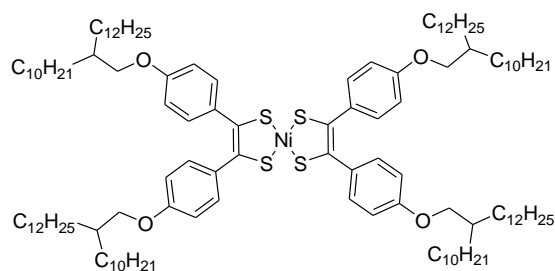
Black pasty powder (2.03 g, 49%). **Elemental Analysis:** found C, 73.75; H, 9.96; Ni, 3.58; S, 8.18. $\text{C}_{92}\text{H}_{148}\text{NiO}_4\text{S}_4$ requires C, 73.42; H, 9.91; Ni, 3.90; S, 8.52 %. δ_{H} (300 MHz, CD_2Cl_2) 7.38 (8 H, d, $J = 8.7$ Hz, aromatic H), 6.87 (8 H, d, $J = 8.7$ Hz, aromatic H), 3.91 (8 H, d, $J = 5.7$ Hz, $-\text{OCH}_2\text{CH}-$), 1.83-1.80 (4 H, m, $-\text{OCH}_2\text{CH}-$), 1.56-1.34 (96 H, m, $-\text{CH}_2-$), 0.93-0.91 (24 H, m, $-\text{CH}_3$). δ_{C} (75 MHz, CD_2Cl_2) 180.69, 160.32, 134.07, 130.29, 114.65, 114.33, 71.06, 37.94, 31.91, 31.86, 31.30, 30.00, 29.67, 29.58, 29.32, 26.81, 26.79, 22.68, 13.88. HRMS(CI- CH_4): found 1503.9624, $[\text{M}+\text{H}]^+$ requires 1503.9692.

Compound BT85: nickel bis[1,2-di(4-(2-octyldodecyloxy)phenyl)ethene-1,2-dithiolene] complex



Black pasty powder (2.28 g, 43%). **Elemental Analysis:** found C, 75.19; H, 10.64; Ni, 3.16; S, 6.72. $\text{C}_{108}\text{H}_{180}\text{NiO}_4\text{S}_4$ requires C, 75.00; H, 10.49; Ni, 3.39; S, 7.42 %. δ_{H} (400 MHz, CD_2Cl_2) 7.38 (8 H, d, $J = 8.8$ Hz, aromatic H), 6.87 (8 H, d, $J = 8.8$ Hz, aromatic H), 3.91 (8 H, d, $J = 5.2$ Hz, $-\text{OCH}_2\text{CH}-$), 1.84 (4 H, m, $-\text{OCH}_2\text{CH}-$), 1.50-1.34 (128 H, m, $-\text{CH}_2-$), 0.95 (24 H, m, $-\text{CH}_3$). δ_{C} (100 MHz, CD_2Cl_2) 180.60, 160.31, 134.11, 130.32, 114.33, 71.09, 37.97, 31.95, 31.32, 30.03, 29.70, 29.67, 29.66, 29.61, 29.38, 29.36, 26.85, 22.71, 13.92. **MS**(MALDI: dithranol): found 1729.10, $[\text{M}+\text{H}]^+$ requires 1729.21.

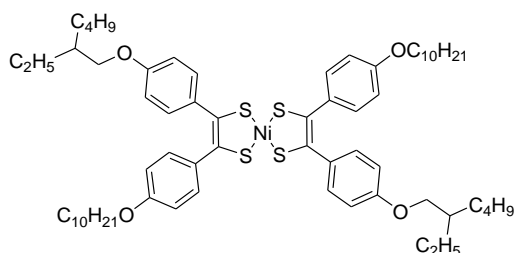
Compound BT86: nickel bis[1,2-di(4-(2-decyltetradecyloxy)phenyl)ethene-1,2-dithiolene] complex



Black pasty powder (3.74 g, 57%). **Elemental Analysis:** found C, 76.79; H, 11.11; Ni, 2.86; S, 6.91. $\text{C}_{124}\text{H}_{212}\text{NiO}_4\text{S}_4$ requires C, 76.22; H, 10.94; Ni, 3.00; S, 6.56. δ_{H} (300 MHz, CD_2Cl_2) 7.38 (8 H,

d, $J = 8.7$ Hz, aromatic H), 6.87 (8 H, d, $J = 8.7$ Hz, aromatic H), 3.90 (8 H, d, $J = 5.7$ Hz, -OCH₂CH-), 1.82 (4 H, m, -OCH₂CH-), 1.56-1.30 (160 H, m, -CH₂-), 0.94-0.85 (24 H, m, -CH₃), δ_C (75 MHz, CD₂Cl₂) 180.72, 160.32, 134.07, 130.28, 114.33, 71.07, 37.91, 31.92, 31.27, 29.99, 29.66, 29.62, 29.35, 26.80, 22.69, 13.88. **MS** (MALDI: dithranol): found 1953.57, $[M+H]^+$ requires 1953.47.

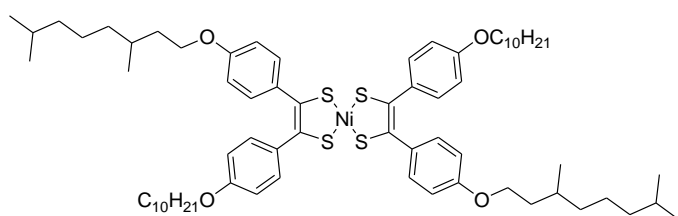
Compound BT81: nickel bis[1-(4-(2-ethylhexyloxy)phenyl)-2-(4-decyloxyphenyl)ethene-1,2-dithiolene] complex



Black powder (1.24 g, 73%, mp 153.2 °C). **Elemental Analysis:** found C, 68.80; H, 8.23; Ni, 5.06; S, 11.57. C₆₄H₉₂NiO₄S₄ requires C, 69.10; H, 8.34; Ni, 5.28; S, 11.53 %. δ_H (400 MHz, CD₂Cl₂) 7.37 (8 H, d, $J = 8.4$ Hz, aromatic H), 6.86 (8 H, m, aromatic H), 4.02 (4

H, t, $J = 6.4$ Hz, -OCH₂CH₂-), 3.92 (4 H, d, $J = 5.2$ Hz, -OCH₂CH-), 1.84-1.75 (6 H, m), 1.57-1.34 (44 H, m), 1.00-0.92 (18 H, m, -CH₃). δ_C (100 MHz, CD₂Cl₂) 180.59, 180.55, 160.29, 160.05, 134.16, 134.10, 130.35, 114.32, 114.28, 70.65, 68.20, 39.40, 31.92, 30.48, 29.60, 29.58, 29.41, 29.34, 29.23, 29.08, 26.02, 23.84, 23.06, 22.70, 13.89, 13.87, 10.90. HRMS(CI-CH₄): found 1111.5359, $[M+H]^+$ requires 1111.5310.

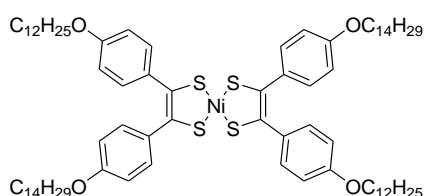
Compound BT84: nickel bis[1-(4-(3,7-dimethyloctyloxy)phenyl)-2-(4-decyloxyphenyl)ethene-1,2-dithiolene] complex



Black powder (1.7 g, 59%, mp 158.5 °C). **Elemental Analysis:** found C, 70.04; H, 8.68; Ni, 4.94; S, 11.11. C₆₈H₁₀₀NiO₄S₄ requires C, 69.90; H, 8.63; Ni, 5.02; S, 10.98 %.

δ_H (300 MHz, CD₂Cl₂) 7.37 (8 H, m, aromatic H), 6.86 (8 H, m, aromatic H), 4.04 (8 H, m, -OCH₂CH₂-), 1.90-1.20 (52 H, m), 1.00-0.90 (24 H, m, -CH₃). δ_C (75 MHz, CD₂Cl₂) 180.61, 160.05, 134.12, 130.34, 114.28, 68.20, 66.54, 39.23, 37.25, 36.12, 31.91, 29.87, 29.59, 29.57, 29.39, 29.33, 29.21, 27.99, 26.01, 24.65, 22.69, 22.45, 22.35, 19.41, 13.89. **HRMS**(CI-CH₄): found 1167.5985, $[M+H]^+$ requires 1167.5936.

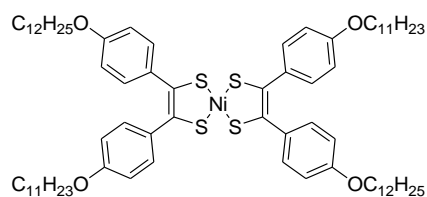
Compound BT114: nickel bis[1-(4-dodecyloxyphenyl)-2-(4-tetradecyloxyphenyl)ethene-1,2-dithiolene] complex



Brown powder (0.67 g, 52%, Mp 163.7 °C). **Elemental Analysis:** found C, 71.82; H, 9.42; Ni, 4.21; S, 8.68.

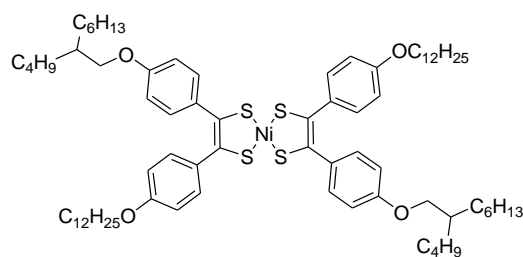
$C_{80}H_{124}NiO_4S_4$ requires C, 71.88; H, 9.35; Ni, 4.39; S, 9.59 %. δ_H (300 MHz, CD_2Cl_2) 7.37 (8 H, dd, $J = 2.0$ - 9.0 Hz, aromatic H), 6.86 (8 H, dd, $J = 2.0$ - 9.0 Hz, aromatic H), 4.00 (8 H, t, $J = 6.6$ Hz, $-OCH_2CH_2-$), 1.88-1.75 (8 H, m, $-OCH_2CH_2-$), 1.54-1.31 (80 H, m), 0.92 (12 H, t, $J = 6.3$ Hz, $-CH_3$). δ_C (75 MHz, CD_2Cl_2) 180.98, 160.08, 134.10, 130.31, 114.28, 68.20, 31.92, 29.65, 29.59, 29.57, 29.37, 29.34, 29.19, 25.98, 22.68, 13.86. **HRMS**(CI- CH_4): found 1335.7930, $[M+H]^+$ requires 1335.7814.

Compound BT117: nickel bis[1-(4-dodecyloxyphenyl)-2-(4-undecyloxyphenyl)ethene-1,2-dithiolene] complex



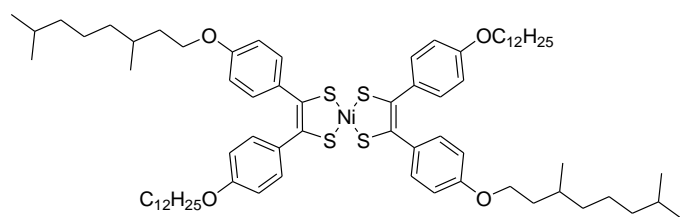
Brown powder (0.79 g, 68%, mp 171.9 °C). **Elemental Analysis:** found C, 70.68; H, 9.12; Ni, 4.52; S, 9.06. $C_{74}H_{112}NiO_4S_4$ requires C, 70.95; H, 9.01; Ni, 4.69; S, 10.24 %. δ_H (300 MHz, CD_2Cl_2) 7.38 (8 H, dd, $J = 2.0$ - 9.0 Hz, aromatic H), 6.86 (8 H, dd, $J = 2.0$ - 9.0 Hz, aromatic H), 4.00 (8 H, t, $J = 6.6$ Hz, $-OCH_2CH_2-$), 1.84-1.77 (8 H, m, $-OCH_2CH_2-$), 1.56-1.32 (68 H, m), 0.92 (12 H, t, $J = 6.6$ Hz, $-CH_3$). δ_C (75 MHz, CD_2Cl_2) 180.72, 160.08, 134.10, 130.31, 114.28, 68.20, 31.91, 29.65, 29.63, 29.60, 29.57, 29.38, 29.34, 29.19, 25.99, 22.68, 13.87. **HRMS**(CI- CH_4): found 1251.6968, $[M+H]^+$ requires 1251.6875.

Compound BT116: nickel bis[1-(4-(2-butyloctyloxy)phenyl)-2-(4-dodecyloxyphenyl)ethene-1,2-dithiolene] complex



Black powder (1.48 g, 71%, mp 99.0 °C). **Elemental Analysis:** found C, 70.98; H, 9.17; Ni, 4.33; S, 9.59. $C_{76}H_{116}NiO_4S_4$ requires C, 71.28; H, 9.13; Ni, 4.58; S, 10.01 %. δ_H (300 MHz, CD_2Cl_2) 7.38 (8 H, d, $J = 8.7$ Hz, aromatic H), 6.87 (8 H, dd, $J = 1.5$ - 8.7 Hz, aromatic H), 4.00 (4 H, t, $J = 6.6$ Hz, $-OCH_2CH_2-$), 3.90 (4 H, d, $J = 5.7$ Hz, $-CH_2CH-$), 1.87-1.78 (6 H, m), 1.57-1.32 (68 H, m), 0.97-0.90 (18 H, m, $-CH_3$). δ_C (75 MHz, CD_2Cl_2) 180.71, 180.65, 160.31, 160.07, 134.13, 134.05, 130.32, 130.30, 114.32, 114.28, 71.05, 68.20, 37.91, 31.92, 31.86, 31.30, 31.00, 29.67, 29.64, 29.60, 29.58, 29.39, 29.35, 29.21, 29.05, 26.79, 26.00, 23.05, 22.69, 22.67, 13.88, 13.86. **HRMS**(CI- CH_4): found 1279.7188, $[M+H]^+$ requires 1279.7188.

Compound BT115: nickel bis[1-(4-(3,7-dimethyloctyloxy)phenyl)-2-(4-dodecyloxyphenyl)ethene-1,2-dithiolene] complex

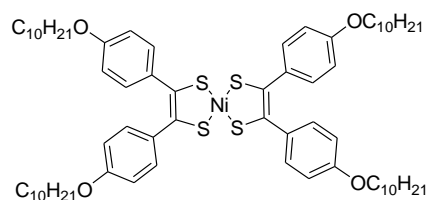


Brown powder (1.13 g, 55%, mp 149.7 °C). **Elemental Analysis:** found C,

70.80; H, 8.88; Ni, 4.64; S, 10.20.

$C_{72}H_{108}NiO_4S_4$ requires C, 70.62; H, 8.89; Ni, 4.79; S, 10.47 %. δ_H (300 MHz, CD_2Cl_2) 7.38 (8 H, d, $J = 9.0$ Hz, aromatic H), 6.87 (8 H, dd, $J = 1.5-9.0$ Hz, aromatic H), 4.08-3.99 (8 H, m, $-OCH_2-$), 1.85-1.20 (60 H, m), 1.00-0.90 (24 H, m, $-CH_3$). δ_C (75 MHz, CD_2Cl_2) 180.71, 160.07, 134.10, 130.31, 114.29, 68.20, 66.54, 39.22, 37.23, 36.10, 31.92, 29.86, 29.65, 29.63, 29.59, 29.57, 29.38, 29.34, 29.19, 27.98, 25.99, 24.64, 22.68, 22.43, 22.34, 19.39, 13.89. **HRMS**(CI- CH_4): found 1223.6636, $[M+H]^+$ requires 1223.6562.

Compound BT163: nickel bis[1,2-di(4-decyloxyphenyl)ethene-1,2-dithiolene] complex



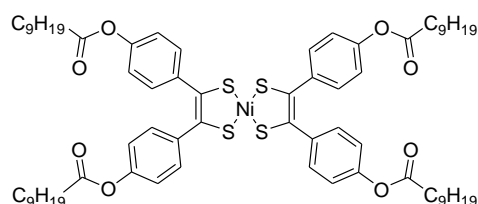
Brown solid (1.6 g, yield 70%); Elemental Analysis: found C,

69.22; H, 8.72; S, 10.62; $C_{68}H_{100}NiO_4S_4$ requires C, 69.90; H,

8.63; S, 10.98 %; δ_H (300 MHz, CD_2Cl_2) 7.37 (8 H, dt, $J = 3.0-$

9.6 Hz, aromatic H), 6.86 (8 H, dt, $J = 3.0-9.6$ Hz, aromatic H), 4.00 (8 H, t, $J = 6.6$ Hz, $-OCH_2-$), 1.82 (8 H, quint, $J = 6.6$ Hz, $-OCH_2CH_2-$), 1.51-1.33 (56 H, m), 0.92 (12 H, t, $J = 6.6$ Hz, $-CH_3$); δ_C (75 MHz, CD_2Cl_2) 180.73, 160.08, 134.10, 130.31, 114.28, 68.20, 31.89, 29.57, 29.55, 29.37, 29.31, 29.19, 25.97, 22.67, 13.86; **HRMS**(CI- CH_4): found 1166.5695, $[M]^+$ requires 1166.5858

Compound BT153F2: nickel bis[1,2-di(4-decanoylphenyl)ethene-1,2-dithiolene] complex



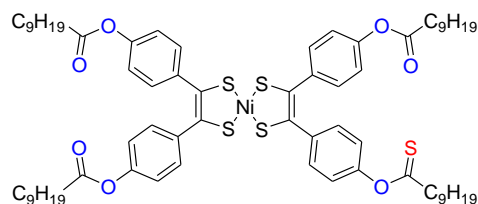
Green solid (0.4 g, yield 10%); Elemental Analysis: found

C, 66.28; H, 7.88; S, 10.74; $C_{68}H_{92}NiO_8S_4$ requires C,

66.70; H, 7.57; S, 10.48 %; δ_H (400 MHz, CD_2Cl_2) 7.45 (8

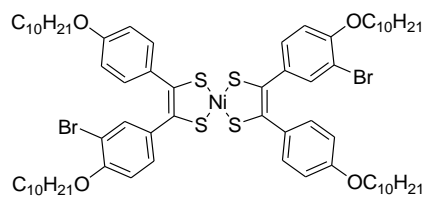
H, dt, $J = 2.8-9.6$ Hz, aromatic H), 7.09 (8 H, dt, $J = 2.8-9.6$ Hz, aromatic H), 2.60 (8 H, t, $J = 7.2$ Hz, $-OC(=O)CH_2-$), 1.77 (8 H, quint, $J = 7.60$ Hz, $OC(=O)CH_2CH_2-$), 1.49-1.33 (48 H, m), 0.93 (12 H, t, $J = 6.8$ Hz, $-CH_3$); δ_C (100 MHz, CD_2Cl_2) 180.78, 171.77, 151.60, 138.43, 130.00, 121.81, 34.30, 31.86, 29.41, 29.25, 29.06, 24.83, 22.67, 13.86. **HRMS**(CI- CH_4): found 1223.5134, $[M+H]^+$ requires 1223.5107

Compound BT153F1: nickel [1,2-di(4-decanoylphenyl)ethene-1,2-dithiolene] [1-(4-decanoylphenyl)-2-(4-thiodecanoatephenyl)ethene-1,2-dithiolene] complex (*isolated in the synthesis of BT153F2*)



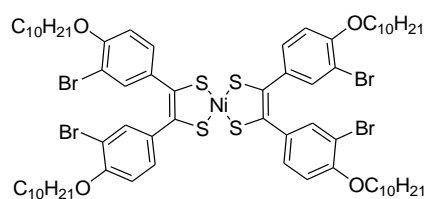
Green solid (70 mg); **Elemental Analysis:** found C, 65.32; H, 7.73; S, 13.94; $C_{68}H_{92}NiO_7S_5$ requires C, 65.84; H, 7.48; S, 12.92 %; δ_H (300 MHz, CD_2Cl_2) 7.46 (8 H, m, aromatic H), 7.05 (8 H, m, aromatic H), 3.00 (2 H, t, $J = 7.5$ Hz, $-OC(=S)CH_2-$), 2.59 (6 H, t, $J = 7.5$ Hz, $-OC(=O)CH_2-$), 1.94 (2 H, quint, $J = 7.5$ Hz, $-OC(=S)CH_2CH_2-$), 1.75 (6 H, quint, $J = 7.8$ Hz, $-OC(=O)CH_2CH_2-$), 1.47-1.33 (48 H, m), 0.94 (12 H, m, $-CH_3$); δ_C (75 MHz, CD_2Cl_2) 181.03, 180.81, 180.42, 171.78, 155.12, 151.62, 139.13, 138.42, 138.31, 130.20, 130.06, 130.00, 122.34, 121.84, 46.77, 34.31, 31.88, 29.43, 29.27, 29.07, 24.84, 22.69, 13.88; HRMS(CI- CH_4): found 1239.4738, $[M+H]^+$ requires 1239.4878

Compound BT167: nickel bis[1-(4-decyloxy-3-bromophenyl)-2-(4-decyloxyphenyl)ethene-1,2-dithiolene] complex



Black solid (0.5 g, yield 76 %); **Elemental Analysis:** found C, 61.81; H, 7.46; S, 10.89; Br, 11.94; $C_{68}H_{98}Br_2NiO_4S_4$ requires C, 61.58; H, 7.45; S, 9.67; Br, 12.05 %; δ_H (400 MHz, CD_2Cl_2) 7.72 (2 H, d, $J = 2.4$ Hz, aromatic H), 7.36 (4 H, dt, $J = 3.2-10$ Hz, aromatic H), 7.26 (2 H, dd, $J = 2.4-8.8$ Hz, aromatic H), 6.86 (6 H, m, aromatic H), 4.07 (4 H, t, $J = 6.4$ Hz, $-OCH_2-$), 4.07 (4 H, t, $J = 6.8$ Hz, $-OCH_2-$), 1.85 (8 H, m, $-OCH_2CH_2-$), 1.56-1.33 (56 H, m), 0.93 (12 H, t, $J = 6.8$ Hz, $-CH_3$); δ_C (100 MHz, CD_2Cl_2) 181.37, 178.57, 160.26, 156.12, 135.07, 133.64, 133.53, 130.37, 129.20, 114.43, 112.41, 111.90, 69.39, 68.27, 31.91, 29.58, 29.56, 29.39, 29.32, 29.18, 29.02, 25.99, 25.95, 22.68, 13.87; HRMS(CI- CH_4): found 1326.4076, $[M]^+$ requires 1326.4039

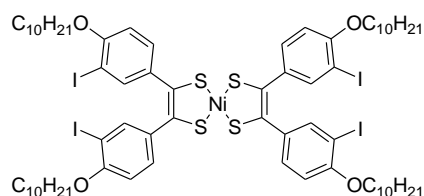
Compound BT159: nickel bis[1,2-(4-decyloxy-3-bromophenyl)ethene-1,2-dithiolene] complex



Black solid (1.1 g, yield 65%); **Elemental Analysis:** found C, 54.80; H, 6.59; S, 8.41; Br, 21.57; $C_{68}H_{96}Br_4NiO_4S_4$ requires C, 55.03; H, 6.52; S, 8.64; Br, 21.54 %; δ_H (300 MHz, CD_2Cl_2) 7.71 (4 H, d, $J = 2.7$ Hz, aromatic H), 7.18 (4 H, dd, $J = 2.4-8.7$ Hz, aromatic H), 6.76 (4 H, d, $J = 8.7$ Hz, aromatic H), 4.06 (8 H, t, $J = 6.3$ Hz, $-OCH_2-$), 1.88 (8 H, quint, $J = 6.6$ Hz, $-OCH_2CH_2-$), 1.57-1.37 (56 H, m), 0.93 (12 H, $J = 6.6$ Hz, $-CH_3$);

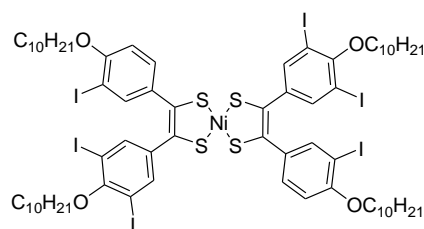
δ_c (75 MHz, CD_2Cl_2) 178.77, 156.17, 134.60, 133.53, 129.36, 112.39, 111.96, 69.41, 31.93, 29.58, 29.36, 29.35, 29.04, 25.97, 22.70, 13.90; MS(CI- CH_4): found 1483.43 ($[M]^+$)

Compound BT166 : nickel bis[1,2-(4-decyloxy-3-iodophenyl)ethene-1,2-dithiolene] complex



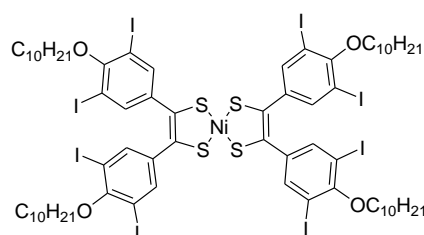
Black solid (2.16 g, yield 81 %). Elemental Analysis: found C, 48.91; H, 5.67; S, 8.35; I, 29.73; $C_{68}H_{96}I_4NiO_4S_4$ requires C, 48.85; H, 5.79; S, 7.67; I, 30.36 %; δ_H (300 MHz, CD_2Cl_2) 7.96 (4 H, d, $J = 2.4$ Hz, aromatic H), 7.22 (4 H, dd, $J = 2.4-8.7$ Hz, aromatic H), 6.72 (4 H, d, $J = 8.7$ Hz, aromatic H), 4.06 (8 H, t, $J = 6.3$ Hz, $-OCH_2-$), 1.88 (8 H, quint, $J = 6.6$ Hz, $-OCH_2CH_2-$), 1.58-1.33 (56 H, m), 0.93 (12 H, m, $-CH_3$); δ_c (75 MHz, CD_2Cl_2) 178.81, 158.42, 139.66, 135.26, 130.28, 111.27, 86.29, 69.55, 31.93, 29.58, 29.35, 29.33, 29.03, 26.05, 22.70, 13.90; HRMS(CI- CH_4): found 1671.1726, $[M+H]^+$ requires 1671.1802

Compound BT165: nickel bis[1-(4-decyloxy-3,5-diiodophenyl)-2-(4-decyloxy-3-iodophenyl)ethene-1,2-dithiolene] complex



Black solid (0.85 g, yield 55%); Elemental Analysis: found C, 42.67; H, 4.90; S, 6.43; I, 38.00; $C_{68}H_{94}I_6NiO_4S_4$ requires C, 42.45; H, 4.92; S, 6.67; I, 39.58 %; δ_H (400 MHz, $CDCl_3$) 7.88 (2 H, $J = 2.0$ Hz, aromatic H), 7.77 (4 H, s, aromatic H), 7.20 (2 H, dd, $J = 2.4-8.8$ Hz, aromatic H), 6.68 (2 H, d, $J = 8.8$ Hz, aromatic H), 4.05 (4 H, t, $J = 6.4$ Hz, $-OCH_2-$), 4.02 (4 H, t, $J = 6.8$ Hz, $-OCH_2-$), 1.93 (4 H, quint, $J = 6.8$ Hz, $-OCH_2CH_2-$), 1.86 (4 H, quint, $J = 6.8$ Hz, $-OCH_2CH_2-$), 1.59-1.28 (56 H, m), 0.89 (12 H, m, $-CH_3$); δ_c (100 MHz, $CDCl_3$) 180.19, 176.12, 158.75, 158.68, 140.01, 139.89, 139.82, 134.37, 130.17, 111.36, 90.77, 86.73, 69.59, 31.93, 30.08, 29.63, 29.60, 29.54, 29.51, 29.36, 29.32, 28.97, 26.04, 25.98, 22.72, 14.14; MS(CI- CH_4): found 1923.8342 ($[M]^+$)

Compound BT164: nickel bis[1,2-(4-decyloxy-3,5-diiodophenyl)ethene-1,2-dithiolene] complex

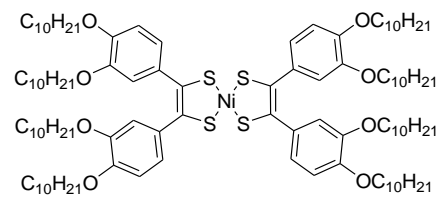


Black solid (0.66 g, yield 30 %); Elemental Analysis: found C, 37.94; H, 4.34; S, 5.00; I, 45.56; $C_{68}H_{92}I_8NiO_4S_4$ requires C, 37.54; H, 4.26; S, 5.90; I, 46.66; δ_H (400 MHz, CD_2Cl_2) 7.80 (8 H, s, aromatic H), 4.07 (8 H, t, $J = 6.8$ Hz, $-OCH_2-$), 1.97 (8 H, quint, $J = 6.4$ Hz, $-OCH_2CH_2-$), 1.63-1.34 (56 H, m), 0.93

(12 H, t, $J = 6.8$ Hz, $-CH_3$); δ_C (100 MHz, CD_2Cl_2) 177.70, 159.19, 140.10, 139.06, 90.70, 73.88, 31.93, 30.06, 29.62, 29.51, 29.36, 25.95, 22.71, 13.89

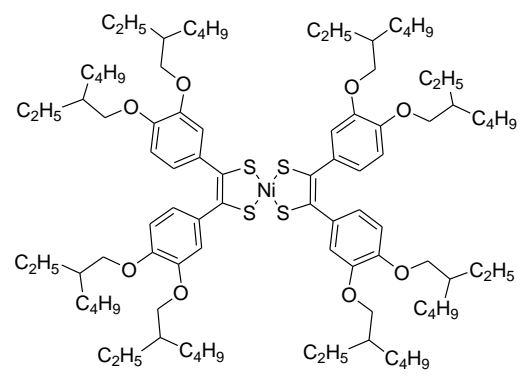
Compound BT22: nickel bis[1,2-di(3,4-di-*n*-decyloxyphenyl)ethene-1,2-dithiolene]

complex

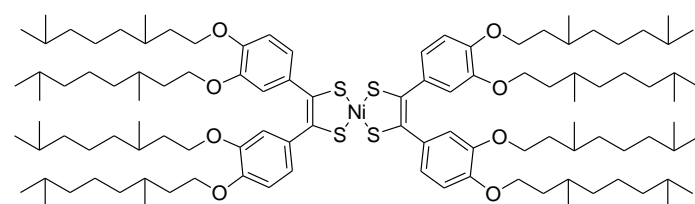
 Black green powder (0.1 g, yield 30%); **Elemental Analysis:** found C, 72.70; H, 10.16 %; $C_{108}H_{180}NiO_8S_4$ requires C, 72.32; H, 10.12 %. δ_H (300 MHz, CD_2Cl_2) 7.12 (4 H, dd, $J = 2.1-8.4$ Hz, aromatic H), 6.87 (4 H, s, aromatic H), 6.85 (4 H, d, $J = 2.1$ Hz, aromatic H), 4.04 (8 H, t, $J = 6.6$ Hz, $-OCH_2-$), 3.80 (8 H, t, $J = 6.6$ Hz, $-OCH_2-$), 1.84 (8 H, m, $-OCH_2CH_2-$), 1.69 (8 H, m, $-OCH_2CH_2-$), 1.56-1.32 (112 H, m), 0.92 (24 H, m, $-CH_3$). δ_C (75 MHz, CD_2Cl_2) 180.84, 150.24, 148.58, 134.36, 121.96, 114.40, 112.84, 69.17, 69.07, 31.94, 31.92, 29.70, 29.62, 29.60, 29.43, 29.39, 29.35, 29.26, 29.09, 26.03, 25.99, 22.69, 13.87. MS(FAB): found 1792 ($[M]^+$)

Compound BT132: nickel bis[1,2-di(3',4'-di(2-ethylhexyloxy)phenyl)ethene-1,2-dithiolene]

complex

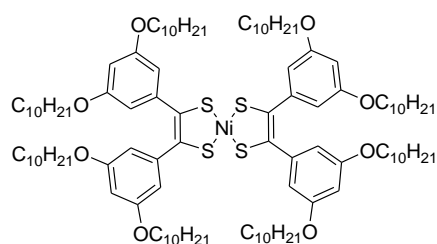
 Black pasty powder (0.56 g, yield 41%). **Elemental Analysis:** found C, 70.77; H, 9.56 %; $C_{92}H_{148}NiO_8S_4$ requires C, 70.42; H, 9.51 %. δ_H (300 MHz, CD_2Cl_2) 7.10 (4 H, dd, $J = 2.1-8.4$ Hz, aromatic H), 6.86 (8 H, dd, $J = 2.1-8.4$ Hz, aromatic H), 3.90 (8 H, d, $J = 5.7$ Hz, $-OCH_2-$), 3.64 (8 H, d, $J = 5.7$ Hz, $-OCH_2-$), 1.81-0.88 (120 H, m). δ_C (75 MHz, CD_2Cl_2) 180.89, 150.60, 148.97, 134.28, 121.83, 114.21, 112.55, 71.53, 71.37, 39.59, 39.33, 30.58, 30.52, 29.13, 29.01, 23.92, 23.81, 23.06, 13.85, 10.98, 10.88. HRMS(CI- CH_4): found 1566.9460, $[M]^+$ requires 1566.9563

Compound BT128: nickel bis[1,2-di(3',4'-di(3,7-dimethyloctyloxy)phenyl)ethene-1,2-dithiolene] complex

 Black pasty powder (0.44 g, yield 28%). **Elemental Analysis:** found C, 72.40, H, 10.18 %; $C_{108}H_{180}NiO_8S_4$ requires C, 72.32; H, 10.12 %. δ_H (300 MHz, CD_2Cl_2) 7.13 (4 H, dd, $J = 2.0$ Hz, aromatic H), 6.87 (8 H, dd, $J = 2.0-8.4$ Hz, aromatic H), 4.06

(8 H, m, $-\text{OCH}_2-$), 3.80 (8 H, m, $-\text{OCH}_2-$), 1.95-0.90 (152 H, m). δ_{C} (75 MHz, CD_2Cl_2) 180.83, 150.23, 148.60, 134.34, 121.92, 114.23, 112.67, 67.47, 67.39, 39.25, 37.35, 36.18, 36.05, 29.98, 29.96, 28.00, 24.75, 24.71, 22.46, 22.37, 19.45, 19.32. HRMS(CI- CH_4): found 1792.1937, $[\text{M}+\text{H}]^+$ requires 1792.1993

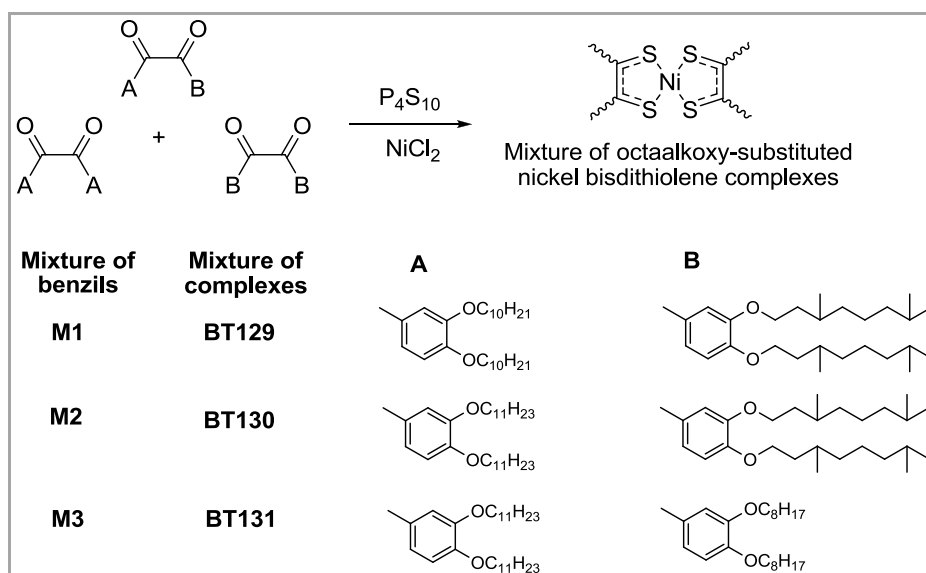
Compound BT152: nickel bis[1,2-di(3,5-di-*n*-decyloxyphenyl)ethene-1,2-dithiolene] complex



Black powder (0.36 g, yield 28 %). Elemental Analysis: found C, 72.08; H, 10.28; S, 7.17; $\text{C}_{108}\text{H}_{180}\text{NiO}_8\text{S}_4$ requires C, 72.32; H, 10.12; S, 7.15 %; δ_{H} (400 MHz, CD_2Cl_2) 6.53 (4 H, d, $J = 2.0$ Hz, aromatic H), 6.47 (2 H, t, $J = 2.0$ Hz, aromatic H), 3.82 (8 H, t, $J = 6.8$ Hz, $-\text{OCH}_2-$), 1.68 (8 H, quint, $J = 6.4$ Hz, $-\text{OCH}_2\text{CH}_2-$), 1.41-1.29 (56 H, m), 0.88 (12 H, t, $J = 6.8$ Hz, $-\text{CH}_3$). δ_{C} (100 MHz, CD_2Cl_2) 181.73, 160.09, 159.50, 142.68, 107.31, 106.72, 102.63, 68.30, 67.71, 31.92, 31.33, 29.62, 29.58, 29.35, 29.06, 29.03, 28.99, 28.76, 28.47, 25.96, 25.37, 22.69, 22.10, 13.89, 13.30. HRMS(CI- CH_4): found 1792.0989, $[\text{M}+\text{H}]^+$ requires 1792.1993

Mixture of octaalkoxy-substituted nickel bisdithiolene complexes

BT129: 0.77 g (black pasty powder), **BT130:** 0.66 g (black pasty powder), **BT131:** 1.75 g (black pasty powder).



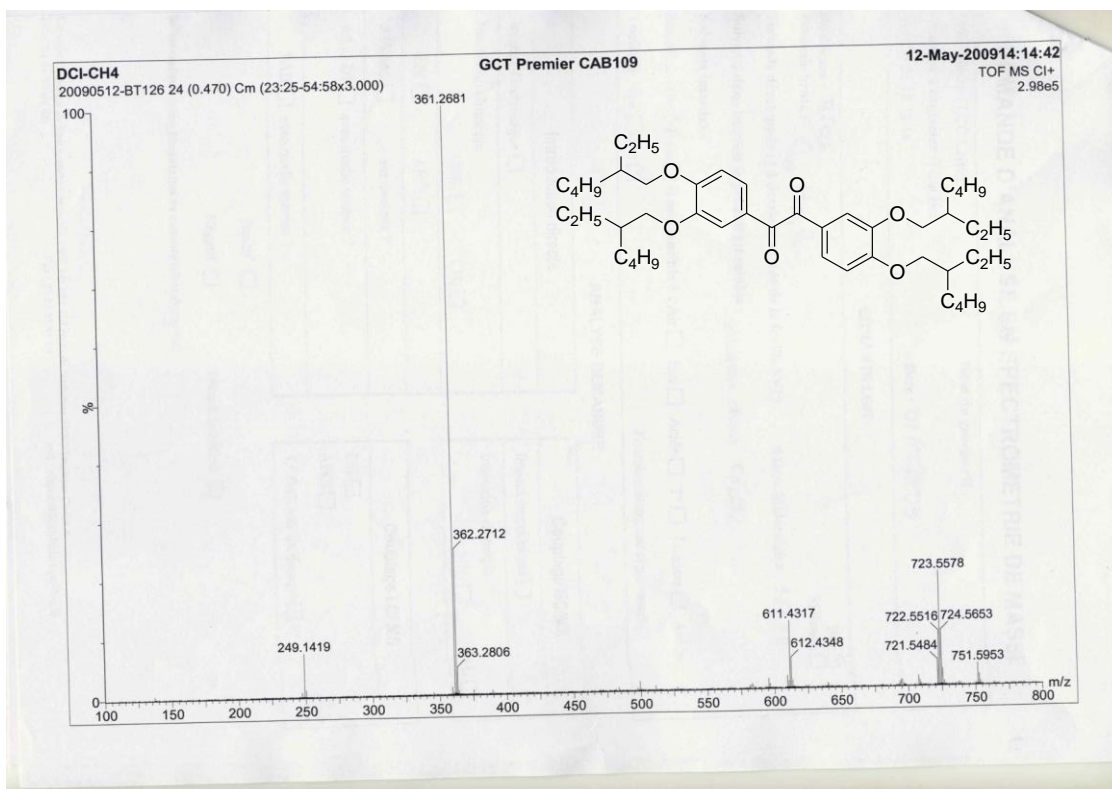


Figure 83 MS of **5b**

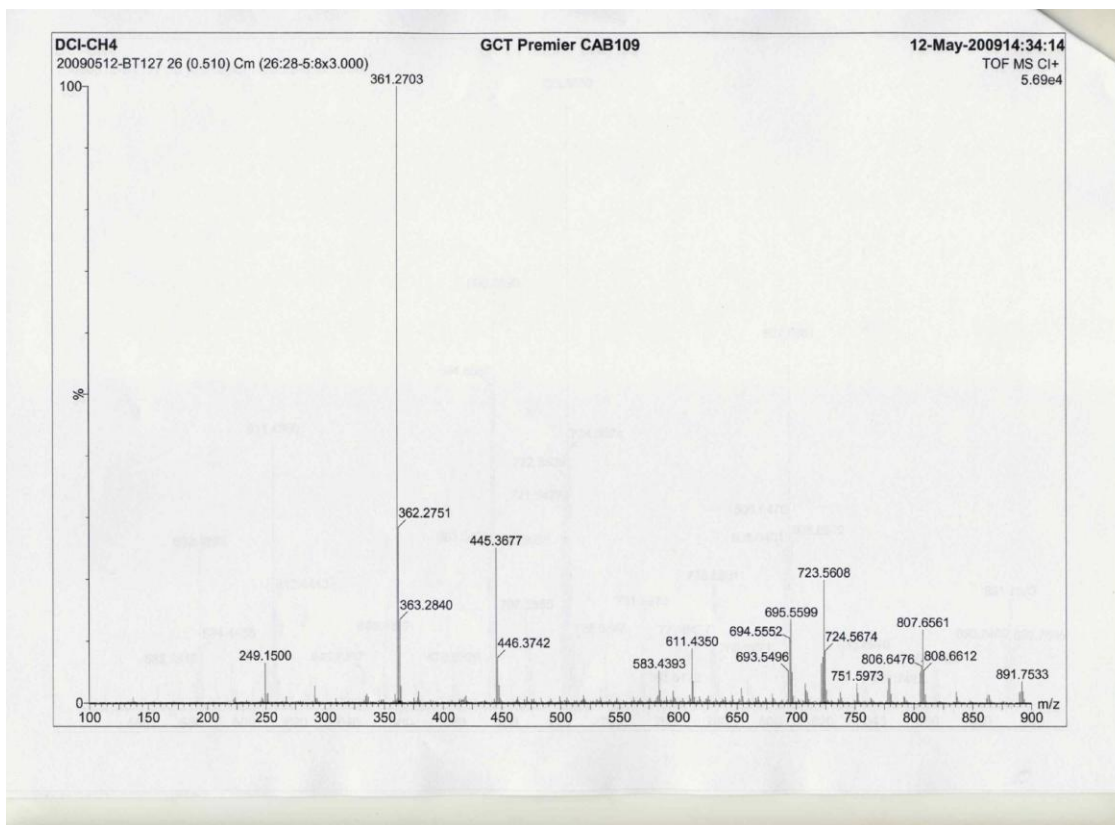


Figure 84 MS of **M3**

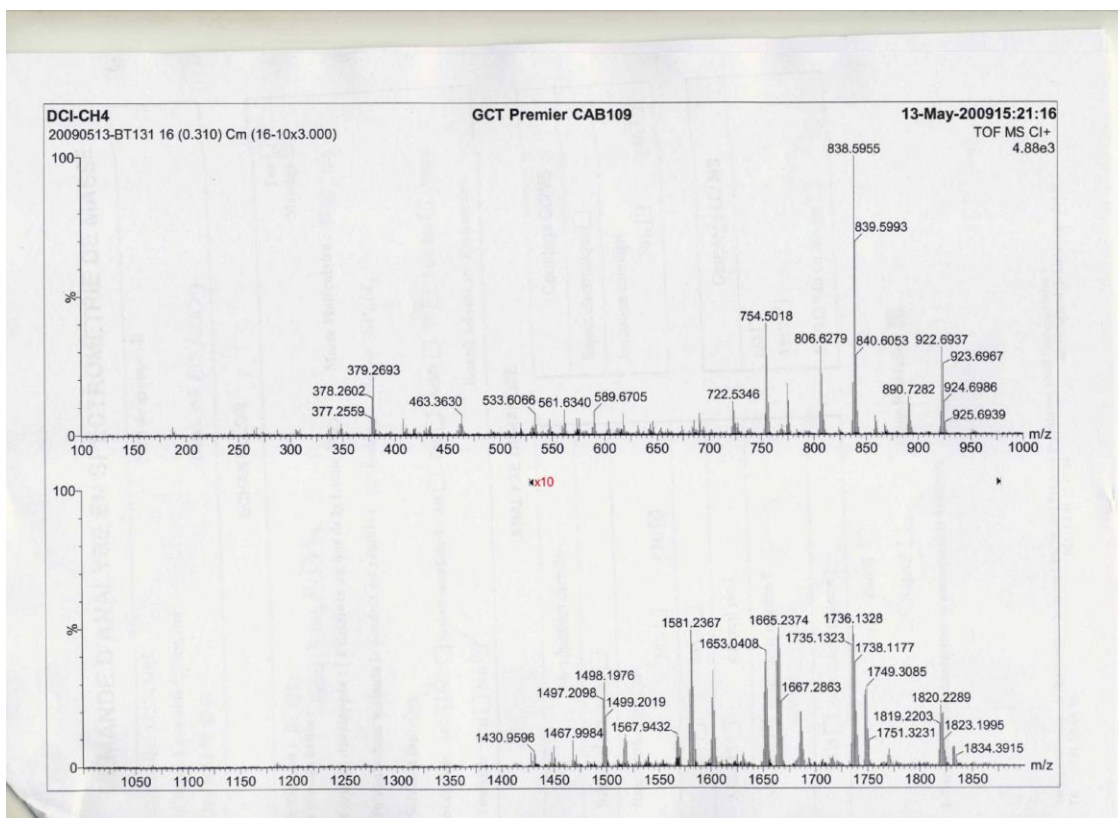


Figure 85 MS of BT131

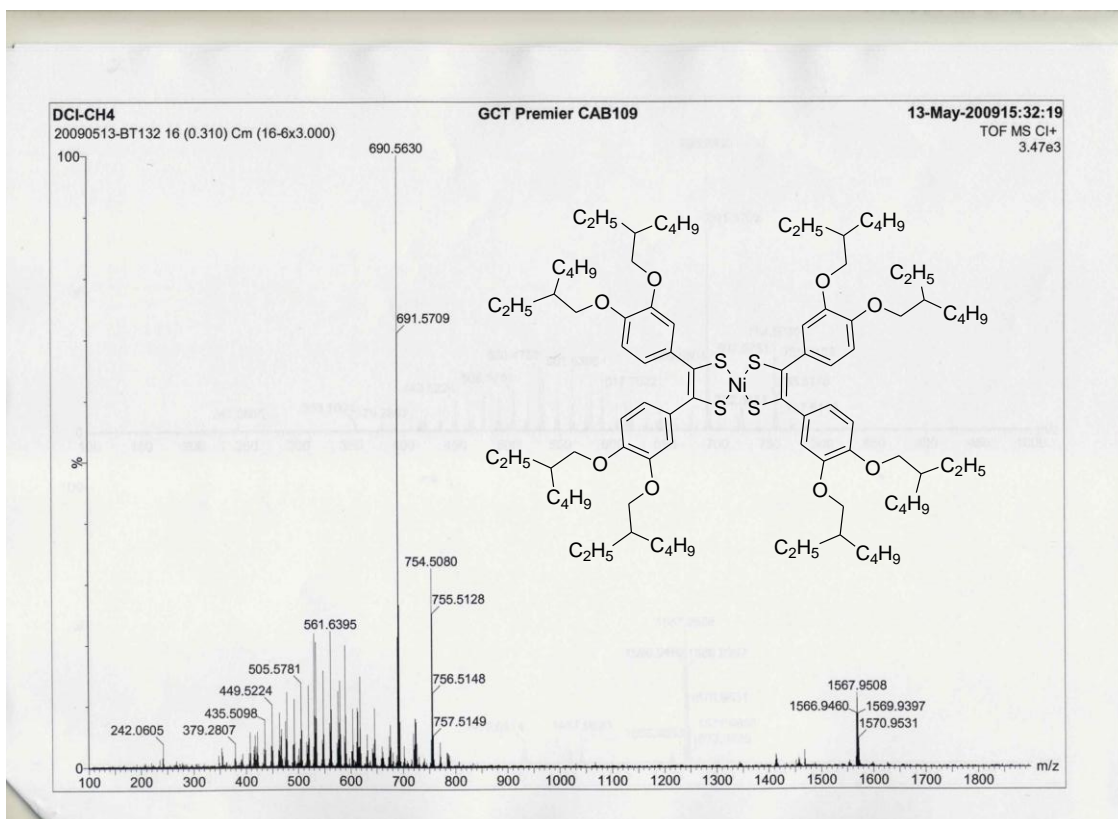


Figure 86 MS of BT132

5.2. References

- [1] N. Armaroli, V. Balzani, *Angew. Chem. Int. Ed.* **2007**, *46*, 52-66.
- [2] J.-L. Bobin, E. Huffer, H. Nifenecker, *L'énergie de demain : Techniques - environnement - économie*, EDP Sciences, **2005**.
- [3] P. Hoffmann, *Tomorrow's Energy: Hydrogen, Fuel Cells, and the Prospects for a Cleaner Planet*, The MIT Press, **2001**.
- [4] S.-S. Sun, N. S. Sariciftci, *Organic Photovoltaics: Mechanisms, Materials, and Devices*, CRC Press, Taylor & Francis Group, **2005**.
- [5] C. Brabec, U. Scherf, V. Dyakonov, *Organic Photovoltaics: Materials, Device Physics, and Manufacturing Technologies*, Wiley-VCH Verlag GmbH & Co. KGaA, Weinheim, **2008**.
- [6] G. Vériot, M. Firon, *CLEFS CEA 2004-2005*, *50/51*, 122-123.
- [7] E. I. Stiefel, *Dithiolene Chemistry: Synthesis, Properties and Applications (Progress in Inorganic Chemistry, Volume 52)*, John Wiley and Sons, Hoboken, New Jersey, **2004**.
- [8] B. Garreau-de Bonneval, K. Moineau-Chane Ching, F. Alary, T.-T. Bui, L. Valade, *Coord. Chem. Rev.* **2010**, *254*, 1457-1467.
- [9] T.-T. Bui, B. Garreau-de Bonneval, K. Moineau-Chane Ching, *New J. Chem.* **2010**, *34*, 337-347.
- [10] P. Destruel, I. Seguy, *Techniques de l'Ingénieur* **2004**, RE25.
- [11] J.-L. Bobin, E. Huffer, H. Nifenecker, *L'énergie de demain: Techniques - environnement - économie*, EDP Sciences, **2005**.
- [12] A. W. Copeland, O. D. Black, A. B. Garrett, *Chem. Rev.* **1942**, *31*, 177-226.
- [13] A.-E. Becquerel, *Comptes Rendus de l'Académie des Sciences* **1839**, *9*, 561-567.
- [14] W. Smith, *Nature* **1873**, *7*, 303.
- [15] W. G. Adams, R. E. Day, *Proceedings of the Royal Society of London* **1876**, *25*, 113-117.
- [16] A. Pochettino, *Atti della Accademia Nazionale dei Lincei, Classe di Scienze Fisiche, Matematiche e Naturali, Rendiconti* **1906**, *15*, 355-363.
- [17] M. Volmer, *Annalen der Physik* **1913**, *345*, 775-796.
- [18] J. Perlin, in *Organic Photovoltaics: Mechanisms, Materials, and Devices* (Eds.: S.-S. Sun and N. S. Sariciftci), CRC Press, Taylor & Francis Group, Boca Raton, FL, **2005**, pp. 3-17.
- [19] D. M. Chapin, C. S. Fuller, G. L. Pearson, *J. Appl. Phys.* **1954**, *25*, 676-677.
- [20] M. A. Green, K. Emery, Y. Hishikawa, W. Warta, *Prog. Photovolt: Res. Appl.* **2010**, *18*, 144-150.
- [21] H. Kallmann, M. Pope, *J. Chem. Phys.* **1959**, *30*, 585.
- [22] V. Y. Merritt, *IBM J. Res. Develop.* **1978**, *22*, 353-371.
- [23] C. W. Tang, *Appl. Phys. Lett.* **1986**, *48*, 183-185.
- [24] P. Peumans, S. R. Forrest, *Appl. Phys. Lett.* **2001**, *79*, 126-128.
- [25] J. Xue, S. Uchida, B. P. Rand, S. R. Forrest, *Appl. Phys. Lett.* **2004**, *84*, 3013-3015.
- [26] J. Y. Kim, K. Lee, N. E. Coates, D. Moses, T.-Q. Nguyen, M. Dante, A. J. Heeger, *Science* **2007**, *317*, 222-225.
- [27] H.-Y. Chen, J. Hou, S. Zhang, Y. Liang, G. Yang, Y. Yang, L. Yu, Y. Wu, G. Li, *Nat. Photonics* **2009**, *3*, 649-653.
- [28] S. H. Park, A. Roy, S. Beaupre, S. Cho, N. Coates, J. S. Moon, D. Moses, M. Leclerc, K. Lee, A. J. Heeger, *Nat. Photonics* **2009**, *3*, 297-302.
- [29] F. C. Krebs, *Sol. Energy Mater. Sol. Cells* **2009**, *93*, 394-412.
- [30] B. O'Regan, M. Gratzel, *Nature* **1991**, *353*, 737-740.
- [31] F.-T. Kong, S.-Y. Dai, K.-J. Wang, *Advances in OptoElectronics* **2007**, Article ID 75384. Doi:75310.71155/72007/75384.
- [32] H. Im, S. Kim, C. Park, S.-H. Jang, C.-J. Kim, K. Kim, N.-G. Park, C. Kim, *Chem. Commun.* **2010**, *46*, 1335-1337.

- [33] H. Choi, H. Choi, S. Paek, K. Song, M.-s. Kang, J. Ko, *Bull. Korean Chem. Soc.* **2010**, *31*, 125-132.
- [34] H. Imahori, T. Umeyama, S. Ito, *Acc. Chem. Res.* **2009**, *42*, 1809-1818.
- [35] L. Spiccia, G. B. Deacon, C. M. Kepert, *Coord. Chem. Rev.* **2004**, *248*, 1329-1341.
- [36] Y. Saito, T. Azechi, T. Kitamura, Y. Hasegawa, Y. Wada, S. Yanagida, *Coord. Chem. Rev.* **2004**, *248*, 1469-1478.
- [37] Z.-S. Wang, H. Kawauchi, T. Kashima, H. Arakawa, *Coord. Chem. Rev.* **2004**, *248*, 1381-1389.
- [38] K. M. P. Bandaranayake, M. K. Indika Senevirathna, P. M. G. M. Prasad Weligamuwa, K. Tennakone, *Coord. Chem. Rev.* **2004**, *248*, 1277-1281.
- [39] B. Peng, G. Jungmann, C. Jäger, D. Haarer, H.-W. Schmidt, M. Thelakkat, *Coord. Chem. Rev.* **2004**, *248*, 1479-1489.
- [40] Q. Zhang, C. S. Dandeneau, X. Zhou, G. Cao, *Adv. Mater.* **2009**, *21*, 4087-4108.
- [41] I. Gonzalez-Valls, M. Lira-Cantu, *Energy Environ. Sci.* **2009**, *2*, 19-34.
- [42] J. Boucle, P. Ravirajan, J. Nelson, *J. Mater. Chem.* **2007**, *17*, 3141-3153.
- [43] S. Günes, N. S. Sariciftci, *Inorg. Chim. Acta* **2008**, *361*, 581-588.
- [44] M. D. McGehee, *MRS Bulletin* **2009**, *34*, 95-100.
- [45] M. Skompska, *Synth. Met.* **2010**, *160*, 1-15.
- [46] Y. Zhou, F. S. Riehle, Y. Yuan, H.-F. Schleiermacher, M. Niggemann, G. A. Urban, M. Krüger, *Appl. Phys. Lett.* **2010**, *96*, 013304.
- [47] S. Guenes, H. Neugebauer, N. S. Sariciftci, *Chem. Rev.* **2007**, *107*, 1324-1338.
- [48] B. Walker, A. B. Tamayo, X.-D. Dang, P. Zalar, J. H. Seo, A. Garcia, M. Tantiwiwat, T.-Q. Nguyen, *Adv. Funct. Mater.* **2009**, *19*, 3063-3069.
- [49] P. Peumans, S. Uchida, S. R. Forrest, *Nature* **2003**, *425*, 158-162.
- [50] V. V. N. Ravi Kishore, A. Aziz, K. L. Narasimhan, N. Periasamy, P. S. Meenakshi, S. Wategaonkar, *Synth. Met.* **2002**, *126*, 199-205.
- [51] Y. Nagamune, H. Watabe, F. Sogawa, Y. Arakawa, *Appl. Phys. Lett.* **1995**, *67*, 1535-1537.
- [52] T. A. Beierlein, B. Ruhstaller, D. J. Gundlach, H. Riel, S. Karg, C. Rost, W. Rieß, *Synth. Met.* **2003**, *138*, 213-221.
- [53] V. Bulovic, S. R. Forrest, *Chem. Phys. Lett.* **1995**, *238*, 88-92.
- [54] P. Peumans, A. Yakimov, S. R. Forrest, *J. Appl. Phys.* **2003**, *93*, 3693-3723.
- [55] R. G. Kepler, P. M. Beeson, S. J. Jacobs, R. A. Anderson, M. B. Sinclair, V. S. Valencia, P. A. Cahill, *Appl. Phys. Lett.* **1995**, *66*, 3618.
- [56] O. D. Jurchescu, J. Baas, T. T. M. Palstra, *Appl. Phys. Lett.* **2004**, *84*, 3061.
- [57] J. E. Anthony, *Angew. Chem. Int. Ed.* **2008**, *47*, 452-483.
- [58] J. E. Anthony, *Chem. Rev.* **2006**, *106*, 5028-5048.
- [59] A. Mishra, C.-Q. Ma, P. Bauerle, *Chem. Rev.* **2009**, *109*, 1141-1276.
- [60] J. Roncali, P. Leriche, A. Cravino, *Adv. Mater.* **2007**, *19*, 2045-2060.
- [61] V. Coropceanu, J. Cornil, D. A. da Silva Filho, Y. Olivier, R. Silbey, J.-L. Bredas, *Chem. Rev.* **2007**, *107*, 926-952.
- [62] W. Pisula, M. Zorn, J. Y. Chang, K. Müllen, R. Zentel, *Macromol. Rapid Commun.* **2009**, *30*, 1179-1202.
- [63] S. Braun, W. Osikowicz, Y. Wang, W. R. Salaneck, *Org. Electron.* **2007**, *8*, 14-20.
- [64] E. Bundgaard, F. C. Krebs, *Sol. Energy Mater. Sol. Cells* **2007**, *91*, 954-985.
- [65] R. Kroon, M. Lenes, J. C. Hummelen, P. W. M. Blom, B. de Boer, *Polymer Reviews* **2008**, *48*, 531-582.
- [66] M. Koppe, H.-J. Egelhaaf, G. Dennler, M. C. Scharber, C. J. Brabec, P. Schilinsky, C. N. Hoth, *Adv. Funct. Mater.* **2010**, *20*, 338-346.
- [67] E. H. Sargent, *Nat. Photonics* **2009**, *3*, 325-331.
- [68] F. G. Brunetti, X. Gong, M. Tong, A. J. Heeger, F. Wudl, *Angew. Chem. Int. Ed.* **2010**, *49*, 532-536.
- [69] S. Laschat, A. Baro, N. Steinke, F. Giesselmann, C. Hägele, G. Scalia, R. Judele, E. Kapatsina, S. Sauer, A. Schreivogel, M. Tosoni, *Angew. Chem. Int. Ed.* **2007**, *46*, 4832-4887.

- [70] S. Sergeyev, W. Pisula, Y. H. Geerts, *Chem. Soc. Rev.* **2007**, *36*, 1902-1929.
- [71] S. Kumar, *Chem. Soc. Rev.* **2006**, *35*, 83-109.
- [72] J.-Y. Cho, B. Domercq, S. C. Jones, J. Yu, X. Zhang, Z. An, M. Bishop, S. Barlow, S. R. Marder, B. Kippelen, *J. Mater. Chem.* **2007**, *17*, 2642-2647.
- [73] L. Schmidt-Mende, A. Fechtenkotter, K. Mullen, E. Moons, R. H. Friend, J. D. MacKenzie, *Science* **2001**, *293*, 1119-1122.
- [74] S. Singh, *Liquid crystals: Fundamentals*, World Scientific Publishing Co. Pte. Ltd., **2002**.
- [75] I.-C. Khoo, *Liquid Crystals*, 2nd ed., John Wiley & Sons, Inc., **2007**.
- [76] S. Chandrasekhar, *Liquid Crystals*, 2nd ed., Cambridge University Press, **1992**.
- [77] F. Reinitzer, *Monatshefte fur Chemie* **1888**, *9*, 421-441.
- [78] T. Kato, T. Yasuda, Y. Kamikawa, M. Yoshio, *Chem. Commun.* **2009**, 729-739.
- [79] H. K. Bisoyi, S. Kumar, *Chem. Soc. Rev.* **2010**, *39*, 264-285.
- [80] S. Kumar, *Liq. Cryst.* **2009**, *36*, 607-638.
- [81] S. Kumar, *Liq. Cryst.* **2004**, *31*, 1037 - 1059.
- [82] S. Chandrasekhar, G. S. Ranganath, *Rep. Prog. Phys.* **1990**, *53*, 57-84.
- [83] T. Niori, T. Sekine, J. Watanabe, T. Furukawa, H. Takezoe, *J. Mater. Chem.* **1996**, *6*, 1231-1233.
- [84] S. Chandrasekhar, B. K. Sadashiva, K. A. Suresh, *Pranama* **1977**, *9*, 471-480.
- [85] Q. Li, L. Li, in *Thermotropic Liquid Crystals*, Springer Netherlands, **2007**, pp. 297-322.
- [86] K. Ohta, K. Hatsusaka, M. Sugibayashi, M. Ariyoshi, K. Ban, F. Maeda, R. Naito, K. Nishizawa, A. M. van de Craats, J. M. Warman, *Mol. Cryst. Liq. Cryst.* **2003**, *397*, 325-345.
- [87] G. Heppke, D. Kruerke, C. Lohning, D. Lotzsch, D. Moro, M. Muller, H. Sawade, *J. Mater. Chem.* **2000**, *10*, 2657-2661.
- [88] B. Glusen, W. Heitz, A. Kettner, J. H. Wendorff, *Liq. Cryst.* **1996**, *20*, 627-633.
- [89] E. Fontes, P. A. Heiney, W. H. de Jeu, *Phys. Rev. Lett.* **1988**, *61*, 1202-1205.
- [90] A. M. Giroud-godquin, J. Billard, *Mol. Cryst. Liq. Cryst.* **1981**, *66*, 147-150.
- [91] H. Horie, A. Takagi, H. Hasebe, T. Ozawa, K. Ohta, *J. Mater. Chem.* **2001**, *11*, 1063-1071.
- [92] R. W. Date, E. F. Iglesias, K. E. Rowe, J. M. Elliott, D. W. Bruce, *Dalton Trans.* **2003**, *10*, 1914-1931.
- [93] B. Donnio, D. Guillon, R. Deschenaux, D. W. Bruce, in *Comprehensive Coordination Chemistry II, Vol. 7* (Eds.: J. A. McCleverty and T. J. Meyer), Pergamon, Oxford, **2003**, pp. 357-627.
- [94] J. M. Warman, J. Piris, W. Pisula, M. Kastler, D. Wasserfallen, K. Mullen, *J. Am. Chem. Soc.* **2005**, *127*, 14257-14262.
- [95] S. Tiwari, N. C. Greenham, *Optical and Quantum Electronics* **2009**, *41*, 69-89.
- [96] D. Adam, P. Schuhmacher, J. Simmerer, L. Haussling, K. Siemensmeyer, K. H. Eitzbachi, H. Ringsdorf, D. Haarer, *Nature* **1994**, *371*, 141-143.
- [97] H. Iino, Y. Takayashiki, J.-i. Hanna, R. J. Bushby, D. Haarer, *Appl. Phys. Lett.* **2005**, *87*, 192105.
- [98] H. Iino, J.-i. Hanna, D. Haarer, *Phys. Rev. B* **2005**, *72*, 193203.
- [99] H. Iino, Y. Takayashiki, J.-i. Hanna, R. J. Bushby, *Jpn. J. Appl. Phys., Part 2* **2005**, *44*, L1310-L1312.
- [100] H. Iino, J.-i. Hanna, R. J. Bushby, B. Movaghar, B. J. Whitaker, M. J. Cook, *Appl. Phys. Lett.* **2005**, *87*, 132102.
- [101] A. M. Van de Craats, J. M. Warman, A. Fechtenkötter, J. D. Brand, M. A. Harbison, K. Müllen, *Adv. Mater.* **1999**, *11*, 1469-1472.
- [102] Z. An, J. Yu, B. Domercq, S. C. Jones, S. Barlow, B. Kippelen, S. R. Marder, *J. Mater. Chem.* **2009**, *19*, 6688-6698.
- [103] E. Grelet, H. Bock, *Europhys. Lett.* **2006**, *73*, 712-718.
- [104] E. Charlet, E. Grelet, P. Brettes, H. Bock, H. Saadaoui, L. Cisse, P. Destruel, N. Gherardi, I. Seguy, *Appl. Phys. Lett.* **2008**, *92*, 024107.
- [105] L. Li, S.-W. Kang, J. Harden, Q. Sun, X. Zhou, L. Dai, A. Jakli, S. Kumar, Q. Li, *Liq. Cryst.* **2008**, *35*, 233-239.

- [106] H. C. Hesse, J. Weickert, M. Al-Hussein, L. Dössel, X. Feng, K. Müllen, L. Schmidt-Mende, *Sol. Energy Mater. Sol. Cells* **2010**, *94*, 560-567.
- [107] K. Hirota, K. Tajima, K. Hashimoto, *Synth. Met.* **2007**, *157*, 290-296.
- [108] L. Schmidt-Mende, A. Fechtenkötter, K. Müllen, R. H. Friend, J. D. MacKenzie, *Physica E* **2002**, *14*, 263-267.
- [109] Q. Sun, L. Dai, X. Zhou, L. Li, Q. Li, *Appl. Phys. Lett.* **2007**, *91*, 253505.
- [110] T. Hassheider, S. A. Benning, M. W. Lauhof, H.-S. Kitzerow, H. Bock, M. D. Watson, K. Müllen, *Mol. Cryst. Liq. Cryst.* **2004**, *413*, 461-472.
- [111] H. Bock, N. Buffet, E. Grelet, I. Seguy, J. Navarro, P. Destruel, in *Emerging Liquid Crystal Technologies III, Vol. 6911* (Ed.: L.-C. Chien), SPIE, San Jose, CA, USA, **2008**, pp. 69110N-69118.
- [112] I. A. Levitsky, W. B. Euler, N. Tokranova, B. Xu, J. Castracane, *Appl. Phys. Lett.* **2004**, *85*, 6245-6247.
- [113] J. A. McCleverty, in *Prog. Inorg. Chem., Vol. 10* (Ed.: F. A. Cotton), Interscience Publishers New York, **1968**, pp. 49-221.
- [114] U. T. Mueller-Westerhoff, B. Vance, in *Comprehensive Coordination Chemistry, Vol. 2* (Ed.: G. Wilkinson), Pergamon Press, **1987**, pp. 595-631.
- [115] R.-M. Olk, B. Olk, W. Dietzsch, R. Kirmse, E. Hoyer, *Coord. Chem. Rev.* **1992**, *117*, 99-131.
- [116] P. Cassoux, *Coord. Chem. Rev.* **1999**, *185-186*, 213-232.
- [117] A. E. Pullen, R.-M. Olk, *Coord. Chem. Rev.* **1999**, *188*, 211-262.
- [118] N. Robertson, L. Cronin, *Coord. Chem. Rev.* **2002**, *227*, 93-127.
- [119] R. Kato, *Chem. Rev.* **2004**, *104*, 5319-5346.
- [120] A. Kobayashi, E. Fujiwara, H. Kobayashi, *Chem. Rev.* **2004**, *104*, 5243-5264.
- [121] U. T. Mueller-Westerhoff, B. Vance, D. Ihl Yoon, *Tetrahedron* **1991**, *47*, 909-932.
- [122] P. Deplano, M. L. Mercuri, A. Serpe, L. Pilia, in *The chemistry of metal enolates* (Ed.: J. Zabicky), John Wiley & Sons, Ltd, **2009**, pp. 879-928.
- [123] D. Belo, M. Almeida, *Coord. Chem. Rev.* **2010**, doi:10.1016/j.ccr.2009.1012.1011.
- [124] M. Arca, M. C. Aragoni, in *Handbook of Chalcogen Chemistry New Perspectives in Sulfur, Selenium and Tellurium* (Ed.: F. A. Devillanova), The Royal Society of Chemistry, Cambridge, **2007**, pp. 797-830.
- [125] S. Dalglish, N. Robertson, *Coordination Chemistry Reviews* **2009**, doi:10.1016/j.ccr.2009.1010.1022.
- [126] L. Valade, H. Tanaka, in *Molecular Materials* (Eds.: D. W. Bruce, D. O'Hare and R. I. Walton), John Wiley & Sons Ltd, **2010**, pp. 215-290.
- [127] T. B. Rauchfuss, in *Prog. Inorg. Chem., Vol. 52* (Ed.: E. I. Stiefel), John Wiley & Sons, Inc., Hoboken, New Jersey, **2004**, pp. 1-54.
- [128] G. N. Schrauzer, V. Mayweg, *J. Am. Chem. Soc.* **1962**, *84*, 3221-3221.
- [129] G. N. Schrauzer, V. P. Mayweg, *J. Am. Chem. Soc.* **1965**, *87*, 1483-1489.
- [130] G. N. Schrauzer, H. W. Finck, *Angew. Chem. Int. Ed.* **1964**, *3*, 133.
- [131] G. N. Schrauzer, H. W. Finck, V. Mayweg, *Angew. Chem. Int. Ed.* **1964**, *3*, 639-640.
- [132] G. N. Schrauzer, V. Mayweg, H. W. Finck, U. Müller-Westerhoff, W. Heinrich, *Angew. Chem. Int. Ed.* **1964**, *3*, 381.
- [133] G. N. Schrauzer, V. Mayweg, *Zeitschrift für Naturforschung B - A Journal of Chemical Sciences* **1964**, *19b*, 192.
- [134] P. Y. Bie, H. Wang, C. L. Zhang, X. F. Pan, T. K. Yang, *Chin. Chem. Lett.* **2002**, *13*, 167-170.
- [135] N. Kuramoto, K. Asao, *Dyes Pigm.* **1990**, *12*, 65-76.
- [136] K. Ohta, A. Takagi, H. Muroki, I. Yamamoto, K. Matsuzaki, T. Inabe, Y. Maruyama, *J. Chem. Soc., Chem. Commun.* **1986**, 883-885.
- [137] K. Ohta, A. Takagi, H. Muroki, I. Yamamoto, K. Matsuzaki, T. Inabe, Y. Maruyama, *Mol. Cryst. Liq. Cryst.* **1987**, *147*, 15-24.

- [138] K. Ohta, H. Hasebe, H. Ema, T. Fujimoto, I. Yamamoto, *J. Chem. Soc., Chem. Commun.* **1989**, 1610-1611.
- [139] K. Ohta, H. Hasebe, H. Ema, M. Moriya, T. Fujimoto, I. Yamamoto, *Mol. Cryst. Liq. Cryst.* **1991**, *208*, 21-32.
- [140] K. Ohta, H. Hasebe, M. Moriya, T. Fujimoto, I. Yamamoto, *Mol. Cryst. Liq. Cryst.* **1991**, *208*, 33-41.
- [141] K. Ohta, Y. Inagaki-Oka, H. Hasebe, I. Yamamoto, *Polyhedron* **2000**, *19*, 267-274.
- [142] K. Arumugam, J. E. Bollinger, M. Fink, J. P. Donahue, *Inorg. Chem.* **2007**, *46*, 3283-3288.
- [143] J. U. Im, C. Y. Yu, J. Y. Yoo, S. M. Son, G. D. Lee, S. S. Park, *Mater. Sci. Forum* **2006**, *510-511*, 702-705.
- [144] R. Perochon, L. Piekara-Sady, W. Jurga, R. Clerac, M. Fourmigue, *Dalton Trans.* **2009**, 3052-3061.
- [145] K. Takuma, Y. Irizato, K. Katho, *United States Patent 5182409* **1990**.
- [146] O. Mitsunobu, M. Yamada, T. Mukaiyama, *Bull. Chem. Soc. Japan* **1967**, *40*, 935-939.
- [147] O. Mitsunobu, M. Yamada, *Bull. Chem. Soc. Japan* **1967**, *40*, 2380-2382.
- [148] T. Y. S. But, P. H. Toy, *Chem. Asian J.* **2007**, *2*, 1340-1355.
- [149] K. C. K. Swamy, N. N. B. Kumar, E. Balaraman, K. V. P. P. Kumar, *Chem. Rev.* **2009**, *109*, 2551-2651.
- [150] D. Sartain, M. R. Truter, *J. Chem. Soc. A* **1967**, 1264-1272.
- [151] M. C. Aragoni, M. Arca, F. A. Devillanova, F. Isaia, V. Lippolis, A. Mancini, L. Pala, G. Verani, T. Agostinelli, M. Caironi, D. Natali, M. Sampietro, *Inorg. Chem. Commun.* **2007**, *10*, 191-194.
- [152] S. Oliver, C. Winter, *Adv. Mater.* **1992**, *4*, 119-121.
- [153] C. S. Winter, S. N. Oliver, J. D. Rush, C. A. S. Hill, A. E. Underhill, *Mol. Cryst. Liq. Cryst.* **1993**, *235*, 181-189.
- [154] J.-Y. Cho, S. Barlow, S. R. Marder, J. Fu, L. A. Padilha, E. W. Van Stryland, D. J. Hagan, M. Bishop, *Opt. Lett.* **2007**, *32*, 671-673.
- [155] G. C. Anyfantis, G. C. Papavassiliou, N. Assimomytis, A. Terzis, V. Psycharis, C. P. Raptopoulou, P. Kyritsis, V. Thoma, I. B. Koutselas, *Solid State Sci.* **2008**, *10*, 1729-1733.
- [156] T. D. Anthopoulos, G. C. Anyfantis, G. C. Papavassiliou, D. M. de Leeuw, *Appl. Phys. Lett.* **2007**, *90*, 122105.
- [157] T. D. Anthopoulos, S. Setayesh, E. Smits, M. Cölle, E. Cantatore, B. de Boer, P. W. M. Blom, D. M. de Leeuw, *Adv. Mater.* **2006**, *18*, 1900-1904.
- [158] T. Taguchi, H. Wada, T. Kambayashi, B. Noda, M. Goto, T. Mori, K. Ishikawa, H. Takezoe, *Chem. Phys. Lett.* **2006**, *421*, 395-398.
- [159] H. Wada, T. Taguchi, B. Noda, T. Kambayashi, T. Mori, K. Ishikawa, H. Takezoe, *Org. Electron.* **2007**, *8*, 759-766.
- [160] C. L. Kean, D. O. Miller, P. G. Pickup, *Journal of Materials Chemistry* **2002**, *12*, 2949-2956.
- [161] K. Ohta, A. Takagi, H. Muroki, I. Yamamoto, K. Matsuzaki, T. Inabe, Y. Maruyama, *Molecular Crystals and Liquid Crystals* **1987**, *147*, 15-24.
- [162] K. Ohta, H. Hasebe, H. Ema, M. Moriya, T. Fujimoto, I. Yamamoto, *Mol. Cryst. Liq. Cryst.* **1991**, *208*, 21-32.
- [163] T. T. Bui, B. Garreau-de Bonneval, K. I. Moineau-Chane Ching, *New Journal of Chemistry* **2010**, DOI: 10.1039/b1039nj00519f.
- [164] K. H. Drexhage, Mullerwe.Ut, *Ieee Journal of Quantum Electronics* **1972**, *QE 8*, 759.
- [165] C. L. Kean, D. O. Miller, P. G. Pickup, *J. Mater. Chem.* **2002**, *12*, 2949-2956.
- [166] E. C. P. Smits, T. D. Anthopoulos, S. Setayesh, E. van Veenendaal, R. Coehoorn, P. W. M. Blom, B. de Boer, D. M. de Leeuw, *Phys. Rev. B* **2006**, *73*, 205316.
- [167] N. Derevyanko, A. Ishchenko, A. Verbitsky, *Materials Science-Poland* **2002**, *20*, 13-18.
- [168] M. Veber, R. Fugnitto, H. Strzelecka, *Mol. Cryst. Liq. Cryst.* **1983**, *96*, 221-227.
- [169] J.-Y. Cho, J. Fu, L. A. Padilha, S. Barlow, E. W. Van Stryland, D. J. Hagan, M. Bishop, S. R. Marder, *Mol. Cryst. Liq. Cryst.* **2008**, *485*, 915-927.

- [170] T. Hassheider, S. A. Benning, H.-S. Kitzerow, M.-F. Achard, H. Bock, *Angew. Chem. Int. Ed.* **2001**, *40*, 2060-2063.
- [171] H. Bock, M. Rajaoarivelo, S. Clavaguera, É. Grelet, *Eur. J. Org. Chem.* **2006**, *2006*, 2889-2893.
- [172] S. Alibert-Fouet, I. Seguy, J.-F. Bobo, P. Destruel, H. Bock, *Chem. Eur. J.* **2007**, *13*, 1746-1753.
- [173] S. Alibert-Fouet, S. Dardel, H. Bock, M. Oukachmih, S. Archambeau, I. Seguy, P. Jolinat, P. Destruel, *ChemPhysChem* **2003**, *4*, 983-985.
- [174] S. Sergeev, O. Debever, E. Pouzet, Y. H. Geerts, *J. Mater. Chem.* **2007**, *17*, 3002-3007.
- [175] S. Sergeev, E. Pouzet, O. Debever, J. Levin, J. Gierschner, J. Cornil, R. G. Aspe, Y. H. Geerts, *J. Mater. Chem.* **2007**, *17*, 1777-1784.
- [176] E. Voisin, E. J. Foster, M. Rakotomalala, V. E. Williams, *Chem. Mater.* **2009**, *21*, 3251-3261.
- [177] C. W. Ong, C.-Y. Hwang, S.-C. Liao, C.-H. Pan, T.-H. Chang, *J. Mater. Chem.* **2009**, *19*, 5149-5154.
- [178] M. L. Tang, J. H. Oh, A. D. Reichardt, Z. Bao, *J. Am. Chem. Soc.* **2009**, *131*, 3733-3740.
- [179] S. Saïdi-Besbes, É. Grelet, H. Bock, *Angew. Chem. Int. Ed.* **2006**, *45*, 1783-1786.
- [180] U. T. Mueller-Westerhoff, D. I. Yoon, K. Plourde, *Mol. Cryst. Liq. Cryst.* **1990**, *183*, 291-302.
- [181] C. Giansante, P. Ceroni, V. Balzani, M. Maestri, S.-K. Lee, F. Vogtle, *New J. Chem.* **2007**, *31*, 1250-1258.
- [182] O. Mitsunobu, M. Yamada, T. Mukaiyama, *Bull. Chem. Soc. Jpn.* **1967**, *40*, 935-939.
- [183] O. Mitsunobu, M. Yamada, *Bull. Chem. Soc. Jpn.* **1967**, *40*, 2380-2382.
- [184] P. Secondo, F. Fages, *Organic Letters* **2006**, *8*, 1311-1314.
- [185] E. J. Foster, J. Babuin, N. Nguyen, V. E. Williams, *Chem. Commun.* **2004**, 2052-2053.
- [186] Y. Shirai, A. J. Osgood, Y. Zhao, Y. Yao, L. Saudan, H. Yang, C. Yu-Hung, L. B. Alemany, T. Sasaki, J.-F. Morin, J. M. Guerrero, K. F. Kelly, J. M. Tour, *J. Am. Chem. Soc.* **2006**, *128*, 4854-4864.
- [187] B. N. Boden, A. Abdolmaleki, C. T.-Z. Ma, M. J. MacLachlan, *Can. J. Chem.* **2008**, *86*, 50-64.
- [188] N. O. Calloway, *Chem. Rev.* **1955**, *17*, 327-392.
- [189] P. H. Gore, *Chem. Rev.* **2002**, *55*, 229-281.
- [190] J. K. Groves, *Chem. Soc. Rev.* **1972**, *1*, 73-97.
- [191] T. B. Poulsen, K. A. Jorgensen, *Chem. Rev.* **2008**, *108*, 2903-2915.
- [192] G. Sartori, R. Maggi, *Chem. Rev.* **2006**, *106*, 1077-1104.
- [193] S.-L. You, Q. Cai, M. Zeng, *Chem. Soc. Rev.* **2009**, *38*, 2190-2201.
- [194] B. Mohr, V. Enkelmann, G. Wegner, *J. Org. Chem.* **1994**, *59*, 635-638.
- [195] T.-T. Bui, *Synlett* **2009**, Submitted.
- [196] G. Wenz, *Makromol. Chem., Rapid Commun.* **1985**, *6*, 577-584.
- [197] M. Weiss, M. Appel, *J. Am. Chem. Soc.* **1948**, *70*, 3666-3667.
- [198] K. Ohta, A. Takagi, H. Muroki, I. Yamamoto, K. Matsuzaki, T. Inable, Y. Maruyama, *J. Chem. Soc., Chem. Commun.* **1986**, 883-885.
- [199] A. Sournia-Saquet, B. Garreau-de Bonneval, K. I. Chane-Ching, L. Valade, *J. Electroanal. Chem.* **2008**, *624*, 84-90.
- [200] D. Sartain, M. R. Truter, *Chemical Communications (London)* **1966**, 382-383.
- [201] T. Anjos, S. J. Roberts-Bleming, A. Charlton, N. Robertson, A. R. Mount, S. J. Coles, M. B. Hursthouse, M. Kalaji, P. J. Murphy, *J. Mater. Chem.* **2008**, *18*, 475-483.
- [202] J. L. Bredas, R. Silbey, D. S. Boudreaux, R. R. Chance, *J. Am. Chem. Soc.* **1983**, *105*, 6555-6559.
- [203] S. Janietz, D. D. C. Bradley, M. Grell, C. Giebeler, M. Inbasekaran, E. P. Woo, *Appl. Phys. Lett.* **1998**, *73*, 2453.
- [204] J. Tauc, R. Grigorovici, A. Vancu, *Phys. Stat. Sol.* **1966**, *15*, 627-637.
- [205] E. M. Stuve, A. Krasnopoler, D. E. Sauer, *Surf. Sci.* **1995**, *335*, 177-185.

- [206] G. Dennler, M. C. Scharber, T. Ameri, P. Denk, K. Forberich, C. Waldauf, C. J. Brabec, *Adv. Mater.* **2008**, *20*, 579-583.
- [207] D. Mühlbacher, M. Scharber, M. Morana, Z. Zhu, D. Waller, R. Gaudiana, C. Brabec, *Adv. Mater.* **2006**, *18*, 2884-2889.
- [208] M. C. Scharber, D. Mühlbacher, M. Koppe, P. Denk, C. Waldauf, A. J. Heeger, C. J. Brabec, *Adv. Mater.* **2006**, *18*, 789-794.
- [209] M. Al-Ibrahim, O. Ambacher, S. Sensfuss, G. Gobsch, *Applied Physics Letters* **2005**, *86*, 201120.
- [210] C. Winder, N. S. Sariciftci, *J. Mater. Chem.* **2004**, *14*, 1077-1086.
- [211] D. M. de Leeuw, M. M. J. Simenon, A. R. Brown, R. E. F. Einerhand, *Synth. Met.* **1997**, *87*, 53-59.
- [212] M. Knupfer, H. Peisert, T. Schwieger, *Phys. Rev. B* **2001**, *65*, 033204.
- [213] I. G. Hill, A. Kahn, Z. G. Soos, J. Pascal, R. A., *Chem. Phys. Lett.* **2000**, *327*, 181-188.
- [214] S. Barth, H. Bässler, *Phys. Rev. Lett.* **1997**, *79*, 4445-4448.
- [215] S. F. Alvarado, P. F. Seidler, D. G. Lidzey, D. D. C. Bradley, *Phys. Rev. Lett.* **1998**, *81*, 1082-1085.
- [216] C.-T. Chou, Y.-F. Pai, C.-C. Lin, T. K. Misra, C.-Y. Liu, *Journal of Chromatography A* **2004**, *1043*, 255-263.
- [217] M. Veber, P. Davidson, C. Jallabert, A. M. Levelut, H. Strzelecka, *Molecular Crystals and Liquid Crystals, Letters Section* **1987**, *5*, 1-7.
- [218] A. Tracz, J. Ulanski, T. Pakula, M. Kryszewski, *Polish Patent P-131986* **1986**.
- [219] L. Burda, A. Tracz, T. Pakula, J. Ulanski, M. Kryszewski, *J. Phys. D: Appl. Phys.* **1983**, *16*, 1737.
- [220] A. Tracz, E. El Shafee, J. Ulanski, J. K. Jeszka, M. Kryszewski, *Mater. Sci.* **1988**, *14*, 181.
- [221] A. Tracz, E. El Shafee, J. Ulanski, J. K. Jeszka, M. Kryszewski, in *Electronic Properties of Conjugated Polymers* (Eds.: H. Kutzmany, M. Mehring and S. Roth), Springer-Verlag, Berlin, **1989**, pp. 442-447.
- [222] A. Tracz, E. El Shafee, J. Ulanski, J. K. Jeszka, M. Kryszewski, *Synth. Met.* **1990**, *37*, 175.
- [223] W. Pisula, Z. Tomovic, M. Stepputat, U. Kolb, T. Pakula, K. Mullen, *Chem. Mater.* **2005**, *17*, 2641-2647.
- [224] A. Tracz, J. K. Jeszka, M. D. Watson, W. Pisula, K. Mullen, T. Pakula, *J. Am. Chem. Soc.* **2003**, *125*, 1682-1683.
- [225] A. Tracz, T. Makowski, S. Masirek, W. Pisula, Y. H. Geerts, *Nanotechnology* **2007**, *18*, 485303.
- [226] J. Piris, W. Pisula, A. Tracz, T. Pakula, K. Mullen, J. M. Warman, *Liq. Cryst.* **2004**, *31*, 993-996.
- [227] W. Pisula, A. Menon, M. Stepputat, I. Lieberwirth, U. Kolb, A. Tracz, H. Siringhaus, T. Pakula, K. Müllen, *Adv. Mater.* **2005**, *17*, 684-689.
- [228] P. Miskiewicz, S. Kotarba, J. Jung, T. Marszalek, M. Mas-Torrent, E. Gomar-Nadal, D. B. Amabilino, C. Rovira, J. Veciana, W. Maniukiewicz, J. Ulanski, *J. Appl. Phys.* **2008**, *104*, 054509.
- [229] P. Miskiewicz, A. Rybak, J. Jung, I. Glowacki, W. Maniukiewicz, A. Tracz, J. Pfleger, J. Ulanski, K. Mullen, *Nonlinear Optics, Quantum Optics* **2007**, *37*, 207-218.
- [230] P. Miskiewicz, M. Mas-Torrent, J. Jung, S. Kotarba, I. Glowacki, E. Gomar-Nadal, D. B. Amabilino, J. Veciana, B. Krause, D. Carbone, C. Rovira, J. Ulanski, *Chem. Mater.* **2006**, *18*, 4724-4729.
- [231] P. Miskiewicz, A. Rybak, J. Jung, I. Glowacki, J. Ulanski, Y. Geerts, M. Watson, K. Mullen, *Synth. Met.* **2003**, *137*, 905-906.
- [232] M. Mas-Torrent, S. Masirek, P. Hadley, N. Crivillers, N. S. Oxtoby, P. Reuter, J. Veciana, C. Rovira, A. Tracz, *Org. Electron.* **2008**, *9*, 143-148.
- [233] C. M. Duffy, J. W. Andreasen, D. W. Breiby, M. M. Nielsen, M. Ando, T. Minakata, H. Siringhaus, *Chem. Mater.* **2008**, *20*, 7252-7259.

- [234] F. Alary, J.-L. Heully, A. Scemama, B. Garreau-de Bonneval, K. Chane-Ching, M. Caffarel, *Theor. Chem. Acc.* **2009**, DOI 10.1007/s00214-00009-00679-00219.
- [235] D. W. Breiby, O. Bunk, W. Pisula, T. I. Solling, A. Tracz, T. Pakula, K. Mullen, M. M. Nielsen, *J. Am. Chem. Soc.* **2005**, *127*, 11288-11293.
- [236] H. Takezoe, K. Kishikawa, E. Gorecka, *J. Mater. Chem.* **2006**, *16*, 2412-2416.
- [237] P. Stallinga, A. R. V. Benvenho, E. C. P. Smits, S. G. J. Mathijssen, M. Cölle, H. L. Gomes, D. M. de Leeuw, *Org. Electron.* **2008**, *9*, 735-739.
- [238] R. I. Gearba, M. Lehmann, J. Levin, D. A. Ivanov, M. H. J. Koch, J. Barberá, M. G. Debije, J. Piris, Y. H. Geerts, *Adv. Mater.* **2003**, *15*, 1614-1618.
- [239] O. Thiebaut, H. Bock, E. Grelet, *J. Am. Chem. Soc.* **2010**, ASAP Article, Available online, DOI: 10.1021/ja1012596.

Résumé

Synthèse et étude de matériaux moléculaire pour application photovoltaïque organique

Ce travail fait partie d'un projet financé par l'ANR dédié à la conception d'un nouveau type de cellule photovoltaïque organique. Le but est de concevoir un nouveau dispositif de type bicouche ou multicouche, et composé de deux matériaux (donneur et accepteur d'électrons) moléculaires cristaux liquides colonnaires.

Ce mémoire de thèse décrit la synthèse et la caractérisation de nouveaux matériaux accepteurs combinant plusieurs propriétés : stabilité en température et à l'air, capacité à s'auto-organiser en cristaux liquides colonnaires, absorption forte dans le domaine proche infrarouge et infrarouge.

Le choix s'est porté sur des complexes de nickel bisdithiolenes neutres. Plusieurs séries de complexes ont été synthétisées avec des ligands de type dpedt (diphenyl-ethylenedithiolate). Leurs comportements physico-chimiques ont été caractérisés par utilisation de différentes techniques : analyse thermique différentielle et thermogravimétrique, microscopie optique en lumière polarisée, voltammétrie cyclique et voltammétrie à vague carrée, spectrométrie d'absorption.

Les résultats montrent qu'ils sont tous très stables à l'air et thermiquement jusqu'à 300°C, qu'ils absorbent fortement entre 750 nm à 1100 nm et qu'ils possèdent une haute affinité électronique. De plus, certains de ces composés présentent en phase condensée une phase cristalline liquide colonnaire autour de 80 à 110°C, métastable à température ambiante. En particulier, il est montré que le gap énergétique entre les niveaux HOMO et LUMO de tels complexes peut être modulé en fonction des groupements fonctionnels portés par les ligands. L'ensemble de ces propriétés rendent ces composés très intéressants pour une application photovoltaïque.

Mots clés : chimie de coordination, chimie organique, matériaux moléculaires, photovoltaïque organique, complexe métal bisdithiolene, cristal liquide, proche infrarouge

Abstract

Synthesis and characterization of molecular materials for organic photovoltaic application

This work is part of a project funded by the ANR dedicated to the design of a new type of organic photovoltaic cell. The goal is to design a new device architecture, bilayer or multilayer, composed of two columnar liquid crystalline molecular materials (electron donor and electron acceptor).

This thesis describes the synthesis and characterization of new electron acceptor materials combining several properties: thermal stability and stability in air, capability of self-organize into columnar liquid crystals, strong absorption in near infrared and infrared spectral domain.

The choice is the neutral nickel bisdithiolene complexes. Several series of complexes have been synthesized with dpedt (diphenyl-ethylenedithiolate) ligands. Their physicochemical behaviors were characterized by using different techniques: differential thermal analysis and thermogravimetric, polarized light microscopy, cyclic voltammetry and square wave voltammetry, absorption spectroscopy.

The results show that they are all very stable in air and heat until 300 °C, they absorb strongly between 750 nm to 1100 nm and they have high electron affinity. In addition, some of these compounds show columnar liquid crystalline phase around 80 to 110 °C, metastable at room temperature in the condensed state. In particular, it is shown that the HOMO-LUMO energy gap of such complexes can be modulated as a function of functional groups grafted on the dpedt ligands. All these properties make these compounds very interesting for photovoltaic application.

Keywords: coordination chemistry, organic chemistry, molecular materials, organic photovoltaics, metal bisdithiolenes, liquid crystal, near infrared dye.